UNIVERSITY OF GENOA

PHD PROGRAM IN BIOENGINEERING AND ROBOTICS

Position sense and force control: assessment in unimanual and bimanual tasks

by

Elisa Galofaro

Thesis submitted for the degree of Doctor of Philosophy (33° cycle)

April 2021

Prof. Dr. Maura Casadio	*Supervisor*
Prof. Dr. Lorenzo Masia	*Co-supervisor*

Thesis Jury:

Prof. Dr. Angelo Basteris, University of Southern Denmark	External examiner
Prof. Dr. Ilana Nisky, Ben Gurion University of the Negev	External examiner
Dr. Andrea Canessa	Internal examiner

Dibris

Department of Informatics, Bioengineering, Robotics and Systems Engineering

Declaration

I hereby declare that except where specific reference is made to the work of others, the contents of this dissertation are original and have not been submitted in whole or in part for consideration for any other degree or qualification in this, or any other university. This dissertation is my own work and contains nothing which is the outcome of work done in collaboration with others, except as specified in the text.

Elisa Galofaro

April 2021

“Above all, don’t fear difficult moments. The best comes from them.”

Rita Levi Montalcini

Abstract

Human-environment interactions are common natural occurrences affecting every action. The environment includes objects whose manipulation requires careful *somatosensory integration*. For successful manipulation, the nervous system must be able to represent and predict the *geometrical* and *mechanical* features of sensory stimuli arising from the interaction with objects. These interactions involve sensory perturbations that must be predicted and compensated by the nervous system. Despite the importance of *somatosensory integration*, a comprehensive understanding of how the unimpaired sensory-motor system integrates information on *force* and *position* remains elusive.

Over the last decades, the evolution of technology has allowed researchers to develop highly controllable settings for evaluating sensory-motor integration and delivering haptic feedback. However, most of the existing haptic setups consist of systems with *limited workspace* and reduced-force capabilities. Recent advancements in *exoskeleton devices* provide a framework for developing haptic setups adequate to cover the *full-human* range of motion and offer a wide range of force and torque. Moreover, considering the prevalence of real-life activities involving two hands, *bimanual control* should be implemented and integrated in virtual reality and haptic interfaces.

The aim of my thesis project was to understand *proprioception* and *force control* in *unimanual* tasks and extend from that to *bimanual* and *multi-joint tasks*. To do this, I developed six setups (three *unimanual* and three *bimanual*), which progressively increased the complexity of the technologies employed and the human movements examined, to investigate motor strategies in unimpaired subjects. In the *first unimanual setup*, I enrolled 36 subjects to study with a planar manipulandum how subjects control the contact *force* exerted by their dominant arm in predictable (known arm position) and unpredictable (unknown arm position) environments. I was surprised to observe that contact forces can be precisely controlled with variable contact impedance, that is, without a persistent relation between applied force and resulting motion. In the *second unimanual task*, I investigated how proprioception of wrist position is affected by different types of kinesthetic perturbations of multi-joint arm movements. I enrolled 18 healthy subjects employing a 3-DoFs wrist device. Results evidenced important findings that should also be considered in the clinical evaluation of neurological patients: testing patients'

proprioception in a configuration that is close to the joints' physiological workspace limits may increase mechanoreceptors excitation and provide a fine measurement of sensory acuity. Finally, in the *third unimanual setup*, since the proprioception involving the concurrent evaluation of *proximal* and *distal multi-joint* (more than a single DoF) upper limbs movements remained an open question, I evaluated 18 healthy participants wearing a robotic exoskeleton. Even in this application, results have relevance to common clinical practice: standard proprioceptive tests are manually dispensed by the therapists, the use of similar wearable technologies that contemplate a multi-joint and 3D-space evaluation could drastically improve measurement accuracy and reliability.

Regarding the *bimanual studies*, in the *first* one, I evaluated 12 young participants controlling *position* and *force* while orienting an object with both hands. To approximate a scenario common to daily living activities, I designed an instrumented stand-alone device and implemented a *coupled* task oriented to assess bimanual proprioception. Results showed how much the perception of one's body in space affects the proprioceptive acuity for targets near to or far from the body. Proper changes in the evaluation protocol suggest the possible use in the clinical practice of such low-cost instrumentation. The same device was employed even in the *second setup*. In this case, it was opportunely fixed to make the task *decoupled* and used to evaluate the bimanual coordination in isometric force control. Compared to other studies, investigating the sole fingers' contribution, here I considered the full arm by involving both proximal and distal muscles. Two populations were evaluated: young and elderly subjects. The inclusion of elderly subjects introduces insights about the deterioration of human abilities including higher asymmetry, lower accuracy, and more variable performance. Even this setup, appropriately modulated, may be adopted by therapists to evaluate neurological patients. Finally, with the *third* setup, I designed a task in which subjects performed *multi-joint* upper limb *reaching movements* in *3D-space* while manipulating a *virtual object* with *variable compliances*, i.e., that should handle with less/more care. I re-programmed a bimanual robotic exoskeleton to provide several forms of *haptic feedback*. I tested the potentiality and the system stability on 15 healthy subjects of this new technology to evaluate motor strategies in the presence of simulated objects capable of reproducing more or less deformable materials. This last application provides a fully-customized environment that should be introduced even in rehabilitative applications requiring the bimanual control of concurrent *position* and *force sense* while *haptic feedback* is provided.

Accurately assessing proprioceptive deficits can complement regular therapy to better predict the recovery path. Moreover, bimanual haptic interfaces could provide solutions to clinical evaluation or motor recovery treatment of patients with neurological damages, increasing the efficiency of training and reducing the amount of individual attention needed from the clinician.

My outcomes on healthy subjects denote the potentialities of the designed and/or implemented device, tasks, and haptic interface. In particular, they denote a starting point for fully customized environments which could have implications for several assessment or rehabilitative interventions in patients with neurological diseases.

Table of contents

1. Introduction

The use of upper limbs robotic devices for *rehabilitative purposes* has considerably increased over the last two decades (Basteris et al., 2014), both in research and clinical settings. However, such technologies are not entirely exploited to their full potential. In fact, in clinical practice, the most common methods still rely on rating scales (Suetterlin and Sayer, 2014), which, unlike robotic or technology-based approaches, suffer from the subjective therapist's evaluation. Despite robots' accuracy in recording human performance and replicating specific tasks, they are not often adopted in clinical practice due to the difficulty of implementing personalized treatments on commercial solutions (Micera et al., 2020). In particular, they are primarily oriented to provide the therapist with a *rehabilitation tool* more than an instrument for *assessing* the patient's current state (Norouzi-Gheidari et al., 2012; Brihmat et al., 2020). The importance of this latter aspect is mainly underestimated, although patients' deficits need to be thoroughly investigated to improve the diagnosis and the rehabilitation intervention planning. The altered proprioception and, therefore, the lack of ascending afferent information on the perception of the current position leads to severe consequences such as problems in maintaining posture (Jamali et al., 2017), difficulties during the generation of upper limbs coordinated movements (Lewis and Perreault, 2009), complications in the modulation of force during grasping tasks (Quaney et al., 2005) and in general to accomplish daily living activities.

The execution of daily activities engages the entire kinematic chain and therefore involves *multi-joint* movements. To perform movements correctly is necessary to build an accurate internal body model about the external world. A functional *internal model* allows for converting motor commands into sensory consequences to produce efficient movements (Shadmehr et al., 2010). This capacity strongly depends on forming musculoskeletal dynamics internal models (Shadmehr and Mussa-Ivaldi, 1994b; Sainburg et al., 1999). One of the critical elements required for developing these robust dynamical models is ***proprioceptive feedback***. Neurological pathologies, such as stroke (Carey, 1995) or Parkinson's disease (Konczak et al., 2012), may deprive the brain of its primary sources of information from the skin and muscles (Debert et al., 2012), resulting in the compromised encoding of limb's state information, with negative consequences on motor control and associated recovery progress (Schabrun and Hillier, 2009). Despite the

importance of contextualizing clinical assessment in a practical setting (multi-joint and 3D-workspace), most of the studies proposed in the literature consider methods for evaluating patients' sensorimotor abilities which focus only on one specific joint (Marini et al., 2016b; Basteris et al., 2018; Rinderknecht et al., 2018; Kenzie et al., 2019). For example, several robotic devices and related protocols (Dukelow et al., 2012; Contu et al., 2017; Casadio et al., 2018) evaluated the sense of position at the shoulder (Janwantanakul et al., 2001), the elbow (Ozkul et al., 2011) and the wrist joint (Cappello et al., 2015; Marini et al., 2016b; Basteris et al., 2018). Moreover, a thorough search of the relevant literature has not produced any study that, in a 3D-workspace setting, investigated how sensory signals are processed when the *proximal* and *distal* joints of the body are evaluated concurrently. Given the previous insights, it would be essential to have a customized tool for evaluating proprioception during a complex task involving multiple joints, as typically happens in everyday daily living activities (Galofaro et al., 2019; Valdés et al., 2019), especially in people with neurological diseases.

Every year, the new incidence of stroke affects about 15 million people worldwide, and the incidence rate doubles every decade after 55 years of age (Virani et al., 2020). For almost 80% of cases, the leading disability is reflected on *upper limbs*, leading to severe limitations in daily living activities (ADLs) (Johansen-Berg et al., 2002; Murphy et al., 2011). These deficits are identified in patients with reduced personal care activities such as washing, dressing, eating, and more complex ones (Anderson, 2006). Many patients often present hemiparesis after a stroke event and cannot use *both upper limbs* to perform *bimanual functions*, relying on compensatory strategies with the unimpaired limb and the trunk. This fact is very disabling for patients since healthy individuals conduct most functional activities using *both limbs* in a coordinated and efficient manner (Kilbreath and Heard, 2005; Bailey et al., 2015). In the literature, exist two different methods for upper limb rehabilitation concerning the neurorehabilitation principles: *unilateral* and *bilateral* upper limb training (Wu et al., 2013; Chen et al., 2019). The *unilateral* (unilateral upper limb training - *UULT*) approach represents the traditional constraint-induced therapy, which accentuates an extensive training of the paretic arm and locks the healthy arm to restrict neural compensation at the same time (Krebs et al., 1998; Wolf et al., 2006). Although these studies focus on isolated limb movements, patients are also concerned about completing the functional process with adequate coordination of both arms (Rose and Winstein, 2004). The *bilateral* (bilateral upper limb training - *BULT*) mode has been

adopted more recently and has highlighted how bimanual re-training is essential and encouraging for severe arm impairment (Yu et al., 2016; Abdollahi et al., 2018; Itkonen et al., 2019). Compared to *UULT*, the *BULT* method returned more remarkable progress in improving motor impairment of people with stroke, as measured by the FMA-UE (Fugl-Meyer Assessment of Upper Extremity), (Chen et al., 2019). In this approach, the unimpaired limb is treated in order to boost the functional recovery of the impaired limb by facilitating the physiological *coupling* effects between the two upper limbs (Cauraugh and Summers, 2005). Several studies have indicated the superiority of *BULT* with respect to conventional therapies (e.g., unilateral robotic-assisted training) for improving the standard evaluation test results (FMA-UE, WMFT (Wolf Motor Function Test), ARAT (Action Research Arm Test), and MAL (Motor Activity Log)) and the ranges of motion (ROM) of proximal and distal joints in people with stroke (Lin et al., 2010; Kim et al., 2013; van Delden et al., 2013; Lee et al., 2017). Bilateral skills need more complex neuromotor control mechanisms (Whitall et al., 2011; van Delden et al., 2013), consequently, their recovery is most challenging and requires adopting a specific approach. Moreover, *bimanual* control involves an interaction between the same person's hands and consists of two submodalities: *uncoupled* or *coupled* tasks. The term *uncoupled* is related to a task in which hands act separately without a common objective and on separate workspaces (Tcheang et al., 2007; Nozaki and Scott, 2009), such as a task in which each hand moves independently to manipulate two (or more) separate objects. The term c*oupled* refers to a task in which the hands mutually interact with a common objective, i.e., by manipulating the same object simultaneously (Mutalib et al., 2019), such as squeezing a rubber ball with both hands. Since each hand can perceive the contralateral hand's force, coupled tasks introduce additional sensorimotor information that patients could exploit during retraining.

For the reasons mentioned above, a bimanual sensorimotor assessment and, as a consequence, a bimanual recovery treatment would be suitable. However, the literature still missing univocal evidence on how bimanual coordination policies are established during complex activities - even in healthy individuals. The findings that can be found regarding the functional specialization of the two cerebral hemispheres and, consequently, the motor one, are highly *task- and body-district dependent*. For example, there are typical features (sensor-motor, spatial, temporal, or attentional) that result in different levels of coordination complexity (Sleimen-Malkoun et al., 2011; Maes et al., 2017). When clapping hands, i.e., performing a rhythmic task, synchronized hand movements are

recognized as patterns of "spontaneous" coordination, i.e., relying on default central nervous system (CNS) organization (Kelso, 1984). Conversely, when performing more complex actions, such as typing on a keyboard, other interlimb coordination patterns take over, necessitating learning and prolonged training (Sisti et al., 2011; Salimpour and Shadmehr, 2014). The repetition of a given bimanual task promotes improvements that ensure synchronization of movements in both spatial and temporal terms in healthy subjects (Shmuelof and Krakauer, 2011; Shmuelof et al., 2012): successful performance is reflected in a decrease in the inter-trial variability. When familiarity with the task is achieved, the skills become " automatized" to leave the subject with cognitive resources for new tasks (Willingham, 1998). In fact, exist changes of interhemispheric coupling associated with different stages of bimanual learning: for example, dynamic changes in interhemispheric interaction may take over to create efficient bimanual *motor routines* (Gerloff and Andres, 2002). For instance, a study on bimanual coordination of skilled finger movements, reports that interhemispheric interaction between human premotor, sensorimotor and posterior parietal areas is augmented while learning a new bimanual task and returns to a baseline level as soon as performance has stabilized. This study suggests that the modulation of the so-called “interhemispheric coupling” is correlate to the current bimanual learning stage (Andres et al., 1999). Another study sheds light on how the brain switch from the *unimanual* to the *bimanual* operation mode. In particular, authors have shown that the fundamental points of bimanual coordination are not the simple sum of those found for unimanual tasks (Swinnen, 2002). Performing bimanual skills is more complex than unimanual skills because interlimb coordination control must be acquired to synchronize movement sequences.

However, the mentioned studies provide such general understandings while employing instrumentation that limits the naturalness typical of the "*outside*" environment (flexion/extension fingers, handgrip). The need to generalize previous results regarding bimanual coordination and highlight new ones guided my research in a more realistic context.

In particular, in this Ph.D. project, particular importance has been given to: (i) the study of *proprioception*, considering both *position* sense and *force* sense evaluated individually or concurrently in *unimanual configuration*; (ii) the assessment of complex movements involving *multi-joint* recruitment of both *proximal* and *distal* body part, investigating *bimanual movements* to be included in future *therapeutic approaches*. Overall, this thesis investigates *different methodologies* for assessing *proprioception* and

motor coordination strategies in different conditions and settings. In particular, I investigated *proprioception* and *force control* in *unimanual* tasks and then extended the study to *bimanual* and *multi-joint tasks*. Moreover, the implementation of several haptic modalities allows studying how bimanual motor coordination is influenced by proprioception during the execution of bimanual tasks involving complex *multi-joint* movements. All presented setups represent an attempt to develop future scenarios for rehabilitation.

1.1. Aims and outline of the thesis

The objective of my Ph.D. project is to understand proprioception and its contribution to force and motion control during *unimanual* and *bimanual* tasks.

Specifically, after a careful review of the literature (Chapter 2), I studied:

1. ***In unimanual tasks*** (*Part I* - Chapter 3)***:***
    - The control of contact force in predictable and unpredictable environments, where the available force and position information were either coupled or uncoupled (Chapter 3.1).
    - The position sense at the wrist joint and its changes induced by different kinaesthetic perturbations (Chapter 3.2).
    - The processing and integration of proprioceptive information when estimating separately or jointly the position of *proximal* and *distal* arm joints (Chapter 3.3).

2. ***In bimanual tasks*** (*Part II* - Chapter 4)***:***
    - The control of position and force when matching a specific orientation of an object (box) hold with both hands (*coupled task*), without relying on visual feedback (Chapter 4.1).
    - The bimanual isometric force control when simultaneously applying the same amount of isometric force pushing with the palm and fingers on two decoupled plates (*uncoupled* tasks). I focus on differences in performance between young and older subjects (Chapter 4.2).

- The influence of object impedance on the control of *multi-joint* forces and movements in the *3D-space,* while manipulating various *virtual* objects with both hands (coupled task), (Chapter 4.3).

All these studies were performed in unimpaired subjects. To reach these goals I used different devices: a 2-DoFs planar robotic device (Casadio et al., 2006), a 3-DoFs wrist robotic device (Masia et al., 2009), a 6-DoFs robotic exoskeleton (Pirondini et al., 2016) and a custom-made sensorized box (Galofaro et al., 2019).

The last part of the thesis (Chapter 5) draws the general discussion of the work, highlights my significant contributions, and elaborates on the open questions and future work paths.

2. Background

This chapter presents an *overview* of the key topics included in the next *Part I* and *Part II* of the thesis. At the beginning of this chapter, there is an introduction to the ***submodalities of sensory perception***. This brief overview will be essential in view of the different perceptions that have been evaluated in the designed setups. Next, the ***receptors*** that detect possible external stimuli will be mentioned, stating their main characteristics and functionalities for each of them. It will be followed by a summary of the ***methodologies of position and force sense assessment*** that have been employed and used in the past or are currently used in clinical or research settings. The main advantages and disadvantages of each will be highlighted to contextualize the choices that have been addressed during my research path. Then, there will be a transition about the ***haptic perception:*** more in detail, what is meant by this term, giving some examples to facilitate its understanding. This topic is fundamental because of the last issue treated in this thesis (*Section 4.3*). The next part of this brief review will focus on the various ***technologies*** currently available to provide subjects with ***haptic feedback***. To conclude, an overview of the types of ***bimanual tasks*** that have been implemented and employed in the different years will be presented, highlighting differences between them. This last part will be crucial to contextualize my bimanual studies (*Part II*) in the current state of the art.

2.1. Submodalities of sensory perception

During the daily interaction with objects in the environment, it is essential to sense and control continuously and concurrently the generated position/movement and force to estimate the items' mechanical properties and form an internal representation to predict imminent stimulus. In the statement mentioned above, we automatically hint at movement when we refer to the term position. These two submodalities can be enclosed in the term *proprioception*. In the past century, different researchers provided several conceptualizations and definitions of this term (Bell, 1826; Bastian, 1887; Sherrington, 1907, 1952). In 1826, Charles Bells wrote: *"Between the brain and the muscles there is a circle of nerve; one nerve (ventral roots) conveys the influence from the brain to the muscle, another (dorsal roots) gives the sense of the condition of the muscle to the brain."* This was the first attempt to consider proprioception as a closed loop between the brain

and the muscles. Later, in 1887, Henry Bastian introduced, for the first time, the term *kinaesthesia*, in which he referred to the sensations that we receive following body movements. Then, in 1907, Sherrington adopted the term *proprioception* that he considered "*the perception of joint and body movement as well as position of the body, or body segments, in space*". Actually, both the terms "*proprioception*" and "*kinaesthesia*" are adopted in the published literature. However, the second term - *kinaesthesia* - is common to include both *proprioception* and *force sensing*. In fact, it is a sort of set consisting of three sub-senses: the sense of orientation and position of a single joint and body, the sense that enables us to perceive the movement of the limbs, and the sense that permits us to perceive the force produced by our muscles and an experienced effort (Proske, 2006; Proske and Gandevia, 2009). Among the sense of force, two principal modalities collectively refer to the term *haptics*: *kinaesthetic* and *tactile*. *Kinesthetic* information is perceived by the tension of the muscles and Golgi tendon organs, while tactile one is sensed at the contact points with handled objects by mechanoreceptors located in the skin (Kandel et al., 2000).

2.2. **Receptors for proprioception and haptics**

The proprioception process needs the stimulation of the *mechanoreceptors* that are embedded in the joints, tendons, muscles, and skin. These must be stimulated to exceed a certain threshold due to changes in body position or pressure.

In particular, *mechanoreceptors* detect from the external environment stimuli like pressure, vibration, and touch. They contain neurons that respond to displacement variations, usually in a localized area.

There are four classes of the *cutaneous mechanoreceptive* afferent neuron that innervate the skin: slowly adapting type 1 (*SA1*) afferents that end in Merkel cells, rapidly adapting (*RA*) afferents that end in Meissner corpuscles, Pacinian (*PC*) afferents that end in PC corpuscles, and slowly adapting type 2 (*SA2*) afferents that are thought to terminate in Ruffini corpuscles (Johnson, 2001), Figure 1.

Each of these receptors responds differently to a given stimulus (motion or skin deformation), (Molnar and Gair, 2013).

The first type, namely the *SA1,* responds to a sustained stimulus giving a prolonged discharge, which adapts slowly and linearly correlated to the stimulus's depth. The *SA1* population transmits an acute spatial neural image of a tactile stimulus (Goodwin and

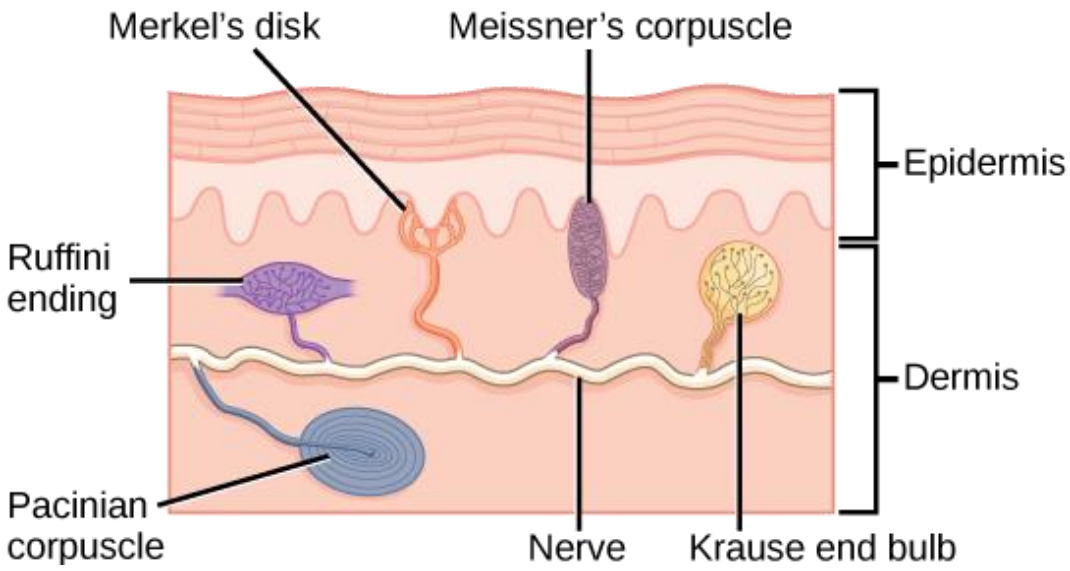

Figure 1: Four of the primary *mechanoreceptors* in human skin. *Merkel's disks*, which are unencapsulated, respond to light touch. *Meissner's corpuscles*, *Ruffini endings*, *Pacinian corpuscles*, and *Krause end bulbs* are all encapsulated. (Molnar, C., & Gair, J. (2013). 17.2 Somatosensation. Concepts of Biology-1st Canadian Edition).

Wheat, 1999). It has been demonstrated that it is responsible for form and texture perception (Johnson et al., 2000).

Instead, the *RA* afferents innervate the skin more densely than the SA1, but they are insensitive to static skin deformation while strongly sensitive to dynamic skin deformation compared to *SA1*. Then, *RA* afferents are responsible for transmitting a robust neural image of skin motion. Moreover, they are the most effective at signaling forces that act when objects are held in hand (Macefield et al., 1996).

Regarding *PC* afferents, they are located throughout the palm and fingers, and they present three unique properties. First, their extreme sensitivity, in fact, they respond to 10 nm of skin motion or less at 200 Hz (Brisben et al., 1999); second, their intense filtering of low-frequency stimuli that would otherwise overwhelm the sensitive *PC* receptors; third, they respond to stimuli less than 100–150 Hz with a phase-locked (Freeman and Johnson, 1982). Thanks to these properties, the *PC* afferents produce a high-fidelity neural image of transient and vibratory stimuli (high-frequency stimuli) transmitted to the hand by objects held in hand.

Finally, the *SA2* afferents are less dense on the skin compared to *SA1* or *RA* afferents. The receptive fields are larger, less sensitive to skin pressure, and more sensitive to skin stretch than *SA1* afferents. Accordingly, the SA2 afferents transmit a neural image of skin stretch. Their importance is known for (i) the ability to perceive the direction of object

motion or force when the motion or direction of force produces skin stretch (Olausson et al., 2000); (ii) the perception, with muscle spindles, of hand shape and finger position through the pattern of skin stretch produced by each hand and finger conformation (Collins and Prochazka, 1996), (Collins et al., 2000). Two different studies have demonstrated that if *SA2* afferents are activated by stretching the skin properly, an illusion of finger flexion is provided to the subject (Edin and Johansson, 1995), (Collins and Prochazka, 1996).

The motor system needs sensory input to work properly: in combination with sensory information from the outside world, it also requires sensory information about the current state of the muscles and limbs. The *Muscle spindles* are enclosed in the muscle tissue, recognized as the primary sensory organs, and signals the length of a muscle and relative changes. The *Golgi tendon organ* signals the tendon tension by force being applied to a muscle (Fallon and Macefield, 2007).

In particular, the *Muscle spindles* are a collection of 6-8 specialized muscle fibers located in the muscle mass itself. They specialize in signaling length and the rate of change of length in terms of speed. They have a *fusiform shape*, hence the terminology *intrafusal fibers*. Each muscle internally has a large number of fibers, and they are essential for detecting posture. There are three types of muscle spindles (divided by shape and type of information): *Nuclear Chain fibers* (single chain and information about the muscle static length), *Static Nuclear Bag fibers* (collected in a bundle and information about the static length of the muscle) and *Dynamic Nuclear Bag fibers* (similar to the static nuclear bag fibers but information about the rate of change of muscle length). The muscle spindle signals are sent to the CNS through two types of specialized sensory fibers that innervate the intrafusal fibers: *Group Ia afferents* (also called *primary afferents*) and *Group II afferents* (also called *secondary afferents*). Regarding instead, the *Golgi tendon organ* is located between the muscle and the tendon, in series with the muscle and signals information about the load or force applied to the muscle. A Golgi tendon organ consists of a capsule containing numerous collagen fibers, and it is innervated by primary afferents (*Group Ib fibers*). When force is put into a muscle, the organ is stretched, causing subsequent compression of collagen fibers. At this point, the afferent is depolarized and fires action potentials that encode the amount of force (Macefield and Knellwolf, 2018).

From this brief summary, it is clear how there is an optimal division of functions between the afferent systems that innervate the human body, allowing the optimal encoding of the internal sensory stimuli as well as those that surrounding ourselves in the external environment.

2.3. **Methods to characterize force and position sense**

The proprioceptive information has a leading role in processing human movement control (Riemann and Lephart, 2002a, 2002b). The onset of neurological diseases leads to severe proprioceptive alterations. It is crucial to quantify, after neurological diseases or injuries, the actual level of sensorimotor deficit. An accurate evaluation ensures a customized rehabilitative treatment.

Since a technical supporting staff is not always available on the hospital site, the assessment tools should be objective and easily usable by physical therapists (PTs), (Haryani et al., 2017). In standard clinical practice exist three different methodologies that are adopted by sports sciences and researcher to assess proprioceptive acuity: (i) Threshold to Detection of Passive Motion (TTDPM), (ii) Joint Position Reproduction or Joint Position Matching (JPM), and (iii) Active Movement Extent Discrimination (AMEDA), (Han et al., 2016), Figure 2.

In the TTDPM technique is adopted the *passive movement criterion*: subjects' body site is isolated and is moved to a predetermined position. The subject has to stop the movement as soon as she/he perceives the movement's direction. This method is in accordance with Gibson (Gibson, 1966), which assumed that proprioception arises when an external movement acts on the subject.

Instead, the JPM method could be conducted in *active* and *passive* ways for *criterion* and *reproduction* movement. Moreover, it could include Ipsilateral (I-JPM) or

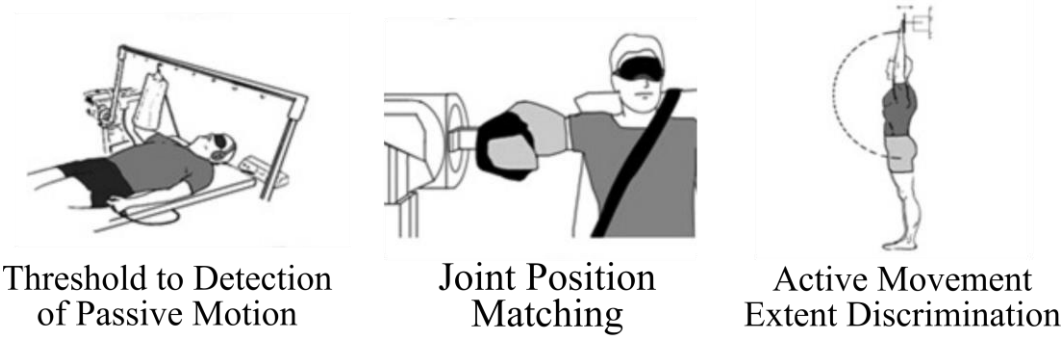

Figure 2: Comparison among different apparatus employed in TTDPM (Threshold to Detection of Passive Movements), JPM (Joint Position Matching), and AMEDA (Active Movement Extent Discrimination) proprioception tests, exemplified at the *shoulder joint*.

Contralateral (C-JPM) movements. Regarding the I-JPM condition, participants have to reproduce the target position, presented actively or passively on the limb, with the same limb. Namely, they need to remember the experienced target position. In the C-JPM, instead, the procedure is analogous to the I-JPM one, but, in this case, participants have to match the target position with the contralateral limb. In this case, the test does not include the memory factor: subjects can exploit online information.

Finally, the AMEDA test, that is managed exclusively using *active* movements. Subjects are provided with a long familiarization phase in which they experience, for example, four-movement displacements of increasing amplitude (where 1 is the smallest and 4 is the largest). The familiarization required at least ten trials for each amplitude. Then, during the test, only one ballistic active movement out to the stop at a steady place is allowed: a physical constraint interrupts the movement to one of the designated positions, followed by a return to the initial position. The following step is to demand the subjects their choice among the four possible positions without providing feedback on their judgment's correctness. In this task, it is again required an appeal to the subject's memory.

Of course, each of the previous methods presents positive and negative aspects. For instance, Goble (Goble, 2010) adopted a contralateral method – C-JPM – that involved active movement for matching the contralateral limb position passively moved on its target position. Employing an active matching movement is an excellent trade-off to avoid using many trials required, for example, in psychophysical methods. Moreover, in this study is evidenced the advantage of employing a contralateral reproduction task: it involves matching a joint angle with the opposite limb exploiting it as an "online reference" to aid participants during matching. Indeed, it represents an essential advantage because it is unnecessary to use memory – then a good deal, especially for elderly subjects and patients. However, a negative aspect could be related to the necessity of *interhemispheric communication* and the transfer of sensory information between the hemispheres, that, for sure must be preserved, but in some clinical conditions could be compromised (Zeitlin et al., 1989), (Zhao et al., 2017).

The passive mode is definitely accurate for the fact that it represents a pure sensory measure not influenced by i) the elaboration of afferent sensory information of the active limb, ii) the internal predicted sensory information for the matching movement, and iii) their integration to generate a perception of the limb position (von Holst, 1954), (Blakemore et al., 2001). However, the negative side is represented by not having a complete proprioceptive view (position and movement). Is not the proprioception

constituted by the sense of position and the sense of movement? Thus, completely removing a sensory afference is perhaps not a guarantee of an accurate evaluation but instead of a specific one.

Even the *force sense* plays a fundamental role during the execution of tasks that required manipulating objects (Proske and Gandevia, 2012). The *sense* of *force* has also been used to measure proprioception (Gandevia and Kilbreath, 1990; Jones, 1994). Traditionally it is evaluated adopting *Force Reproduction* tests (Stevens and Cain, 1970; Dover and Powers, 2003; Trousset et al., 2018). In literature, exist several methods and instruments able to investigate humans' ability to matching forces.

A possible example is the *contralateral limb-matching* procedure that requires subjects to generate a specific force range with a particular body district and then to reproduce it with the same perceived intensity through their contralateral joint after achieving it (Jones, 1989) – hence examining one body part at a time. It is usually implemented to evaluate elbow or shoulder muscles force exertion and commonly adopts instruments consisting of customized devices containing strain-gauge force transducers on their surface.

Further typologies of *Force Reproduction* tests investigate the paradigm of *isometric force reproduction*. In such typology, the user must control a moving cursor depicted on the computer screen and following a specific force trajectory by modulating the applied force with the involved body district, usually with the fingers. In the literature, exist two types of approaches: the *single-* and the *bimanual- effector isometric force tasks*. The rationale behind investigating *bimanual* procedure reflects the concept that the two effectors (hands) should act in a coordinated manner to realize a common task goal (Hu et al., 2011). Furthermore, this methodology includes motor control representation as the force's total output applied with both hands during the task (visual feedback). The visual feedback can be provided in various modalities: visual gain (number of pixels on the screen per unit of force) (Newell and McDonald, 1994), intermittency of feedback (Slifkin et al., 2000), and visual manipulation of the frequency of the force output (Hu and Newell, 2010). From these previous authors has been shown that different feedback typology could modulate the performance outcome.

A further evaluation regards the *handgrip strength test*, which adopts the handgrip dynamometer to measure the hand, forearm, and surrounding musculature strength.

This digression evidences the possible modalities to investigate *force* and *position* senses, however, always considering them separately in such a way that they could not be

evaluated *concurrently*. Moreover, the evidenced aspects and characteristics of all the mentioned methods highlight the necessity to design setups following the final user necessity carefully.

2.4. Haptic perception and technological approaches

Traditionally, when referring to the term *somatosensation*, we imagine an ensemble of different sensory modalities, including all the sensations received from the skin, the limbs, and the joints, that do not interact with each other. However, the *sense of touch*, the *kinaesthesia*, and the *temperature sensation* are all *carefully integrated* by our nervous system to provide the external environmental perception we usually interact (Rincon-Gonzalez et al., 2011b).

We can intend this process as the *haptics*. Rincon-Gonzalez et al. demonstrated that signals that are typically assigned separately to cutaneous and proprioceptive modalities –

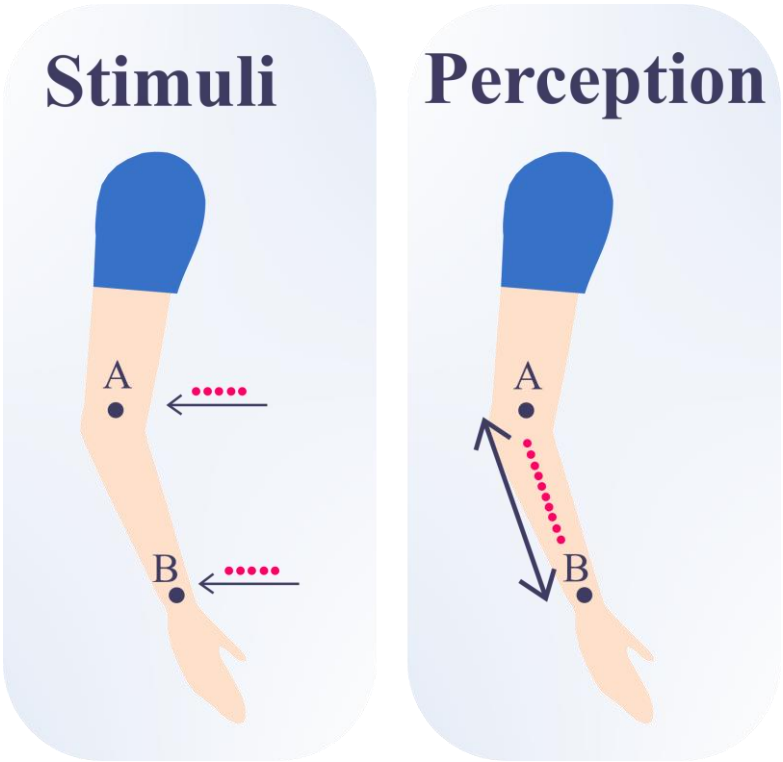

Figure 3: The *Cutaneous Rabbit Illusion* or *Cutaneous Saltation* example; stimuli of 5 consecutive and rapid taps (magenta points) are given at 2 locations (elbow (A) and wrist (B)) but are perceived at 10 taps distributed evenly in the region between the 2 locations.

tactile sensations and self-position – interact in a way that complicates the signal processing of haptics. To demonstrate this evidence, namely, to examine the relationship between tactile and kinaesthetic modalities, they adopted a tactile illusion: the *Cutaneous Rabbit Effect* (Geldard and Sherrick, 1972), and they demonstrated that body posture variations could considerably impact the sense of touch. The *cutaneous rabbit effect* or *cutaneous saltation* is evoked when two - or more - skin locations/regions are stimulated (by a sequence of taps) in rapid succession. The rapid sequence of taps generates the sensation of sequential taps from skin region 1 to region 2 even if no actual stimulation has been delivered, Figure 3. This insight shows how in healthy human subjects' different sensory signals are combined into complex information managed by our brains to interface with the complex and anisotropic external environment successfully.

The typical development of haptic function in humans requires active touch and the inclusion of multiple sensory modalities. The neural mechanisms and pathways associated with haptics are the first to develop and are the most mature of humans' sensory systems (Weiss, 2005). For this reason, haptics is crucial for our daily activities. Trying to imagine a life without it is quite impossible. Every dexterous action requires simultaneous sensory feedback encoding kinaesthetic intervention – for example, the actual hand opening and location - and haptic information.

Kinaesthetic and haptics represent the two sensory modalities crucial, for example, in *prosthetics* (Antfolk et al., 2013), (Stephens-Fripp et al., 2018). In the literature, there are several attempts for restoring *kinaesthetic feedback* using non-invasive methods such as vibrotactile feedback system with several kinds of spatiotemporal pattern (Sagastegui Alva et al., 2020) and cutaneous electro-tactile (Dosen et al., 2016) that involve different sensations, thanks to the activation of skin receptors. However, a unique approach that is perfectly tolerated by every subject and universal in his coding is still out of technical currents. Nevertheless, all previously mentioned studies evidence how *haptic feedback* is effective for *improving kinaesthetic*. The actual issue is understanding which approach is the most suitable considering aspects such as invasiveness, tolerability, and ease of use.

Another exciting application of haptics regards electrical stimulation to improve *the upper extremity's motor control and functional abilities* after stroke (Laufer and Elboim-Gabyzon, 2011). Sensory Transcutaneous Electrical Stimulation (TENS) is a relatively risk-free and easy-to-implement modality for rehabilitation adopted recently in various clinical studies. This technique is a modality that can provide sensory input by peripheral nerve stimulation via electrodes placed on the skin. This kind of approach is frequently

adopted in rehabilitation to reduce pain, more recently even for enhancing motor recovery following a stroke (Castel-Lacanal et al., 2009).

Since the various modalities in which haptics can be evoked, there are also other ways in which haptic sensations can be administered, namely through robotic devices capable of opportunely *simulating* environments with different physical characteristics. In our daily living activities, we usually interact with soft, compliant, and deformable objects, or in more specialized environments, like in surgery, physicians may need to distinguish tissues or perceive abnormalities. Such interactions necessitate judging and recognition among individual objects. In literature, many ongoing efforts try to understand the physical and perceptual cues that ensure our sense of stiffness. Many of them considered skin deformation and spatial distribution of pressure (Tiest and Kappers, 2009; Hauser and Gerling, 2017; Farajian et al., 2020, 2021). It is highly expected that strategies vary between individual, task typology, and compliance range. On the other side, a remarkable number of current studies about compliance interactions adopt engineered materials, such as silicone-elastomers and foams (Norman et al., 2004; Weber et al., 2013; Cavdan et al., 2019). Other research groups adopt robotic devices to simulate and sense differences in real objects' properties to sort, grasp, and manipulate them (Xu et al., 2013, 2019; Zujevs et al., 2015). Even in this research field, it is still challenging to identify specific exploratory strategies that establish which perceptual cues most optimally encode ecologically relevant objects' stiffness.

Simulated experiences such as virtual reality (*VR*) and augmented reality (*AR*), provided by means of VR headsets consisting of a head-mounted display and hand-held controllers, have recently attracted attention for their improved availability, functionality, and affordability (Bohil et al., 2011; Sacks et al., 2013; Tieri et al., 2018). These systems mainly provide immersion by *visual* and *auditory* feedback modalities while simulating a specific desired experience (teleoperation, immersive entertainment, physical therapy, work simulations). Further external devices that currently interface with these technologies and provide interactive haptic feedback are mostly desktop systems with limited workspace and low force capabilities that make their use still rather limited. In the future, the development of flexible and elastic materials that could be easily embedded into the existing robotic devices or the employment of wearable robotic exoskeletons may allow the implementation of experiences that are even more natural to human movements, Figure 4.

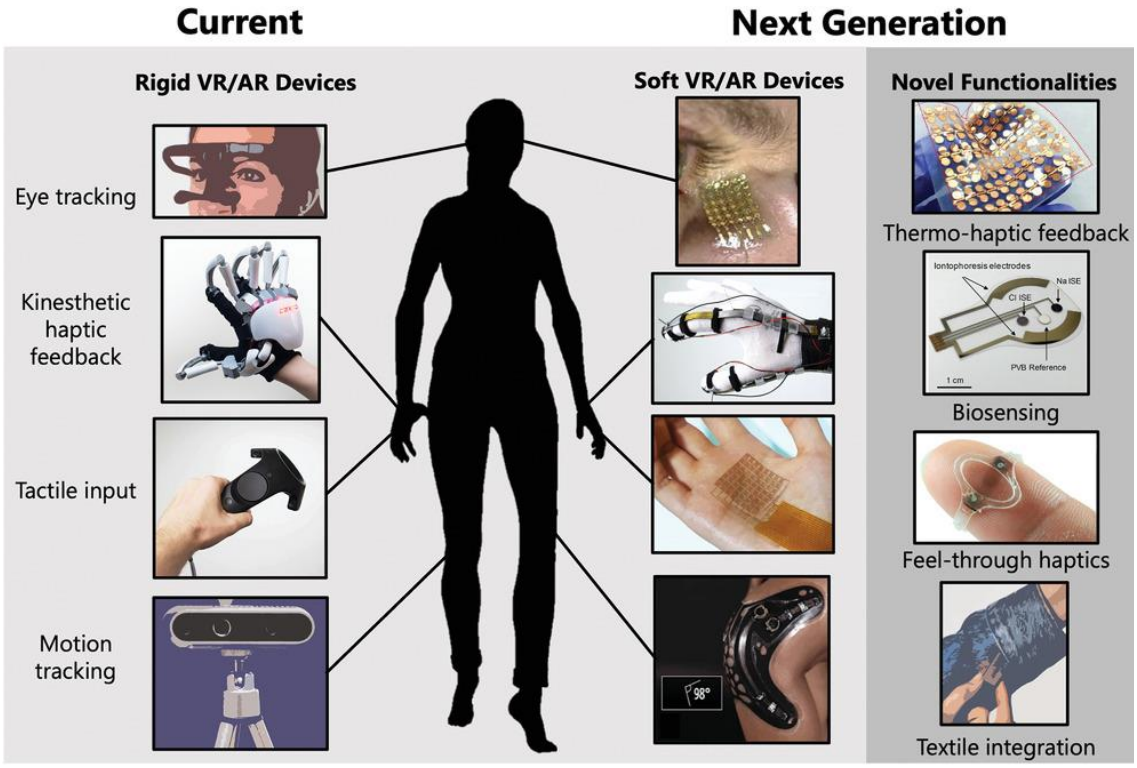

Figure 4: Current (rigid) VR/AR technologies and the next generation of soft VR/AR ones. *Left column*, from top: eye-tracking headset, kinesthetic haptic feedback glove, handheld VR controller, and motion capture. *Middle column*, from top: wearable eye-tracking sensor, haptic glove with electrostatic clutches, tactile sensing skin and wearable sensor measuring knee angle. *Right column*, from top: thermo-haptic feedback electronic skin, wearable biosensor, feel-through haptic sensor on fingertip, and electronic device in jacket sleeve. Figure from: Yin, J., Hinchet, R., Shea, H., & Majidi, C. (2020). "Wearable Soft Technologies for Haptic Sensing and Feedback", *Advanced Functional Materials*, 2007428. All the copyrights are declared in the mentioned paper.

In many *VR* applications is required to achieve a reasonable degree of immersion to allow the user to interact in real-time with virtual objects able to simulate stimuli provided by the real environment (Rose et al., 2018b). Typical employment of *VR* technologies covers various fields such as education, surgical training, entertainment, public safety, rehabilitation, and athletics (Li et al., 2018; Radianti et al., 2020).

In general, *VR* applications have most used the *visual* and *auditive* modalities to deliver feedback from the (virtual environment) *VE* to the user. When the experience does not require direct interaction with the *VE*, such as in the virtual tours, the modalities mentioned above may prove a sufficient immersion.

However, these sensorial modes alone may be weak when actual interaction between the user's hands and virtual objects is involved, such as in manipulation simulation.

When we interact directly with objects in real life, a further sense is heavily involved in the perception of that interaction: the *haptic sense*, as described above.

Over the last decades, haptic interaction has gained increasing attention since its importance for interactive applications (O'malley and Gupta, 2008; Contu et al., 2016;

Loch et al., 2018; Corrêa et al., 2019; Voutsakelis et al., 2020). Its inclusion in *VR* systems was possible through the use of the so-called *haptic devices*, which can be considered as human-machine interfaces designed to detect the user's position to stimulate the haptic perception.

Haptic devices entail peripheral devices equipped with special motors and sensors (e.g., force feedback joysticks and steering wheels) (Shakeri et al., 2018; San Vito et al., 2019) and more sophisticated devices adopted for several applications (Laycock and Day, 2003; Choi et al., 2016; Gabardi et al., 2016; Papini et al., 2016; Guo et al., 2017), Figure 5. The classical approach to control forces during the interaction between the user and the *haptic device* exploits the *closed-loop* (Carignan and Cleary, 2000). Two main classes of *closed-loop* rendering structures exist: impedance and admittance. The *impedance control* generates the forces from the user's motions applied from the user to the device. Conversely, the *admittance control* measures the user's forces and controls the position and the velocity of the device's end-effector. However, such kind approaches could introduce instabilities that provoke oscillations amplified over time.

Figure 5: Haptic devices. **(A)** Some examples of commercial haptic devices *for gaming*: a steering wheel (Logitech), gaming foot pedals (Logitech), a gaming mouse (Logitech), a wireless controller (Sony), and a force feedback joystick (Logitech). **(B)** Other examples of commercial haptic devices *for surgical simulation, teaching, and education*. From top to low: Touch X®, 3D systems™; Phantom®; Omni™; Novint Falcon®, Geomagic Touch™.

2.5. **Haptic feedback rendering**

The haptic feedback could be implemented by joining the end-effector device to the virtual representations of the user inside the *VE* through the virtual proxies, which replicate the user's motions and send back the interaction forces.

The existing haptic rendering techniques refer to the methods used to generate and render haptic feedback to users, notably resulting from interaction with a VE. An established technique for haptic interaction and rendering is the *god-object algorithm* (Zilles and Salisbury, 1995), which uses a single-point representation of the haptic device element (end-effector) in the simulation that will respond to physical constraints (simulated wall or surfaces) in the *VE*. Ruspini et al. proposed using virtual proxies, i.e., virtual representations of the haptic devices with an *object* (like a sphere) instead of a point, and introduced the smoothing of object surfaces and the friction (Ruspini et al., 1997). Ortega et al. proposed a further generalization of the *god-object* method, with rigid proxies, that could perform well with high-complexity objects (Ortega et al., 2007).

Thus, to stabilize the *control-loop* has been introduced the *Virtual Coupling method* which consists of applying a spring-damper link between the haptic device and its virtual counterpart (Colgate et al., 1995). In the literature several *virtual coupling* schemes exist that guarantee the overall system stability. For example, the *god-object* method by Ortega et al. (Ortega et al., 2007) iterated on the *virtual coupling* approach by separating the computation of the motion of the proxy and that of force feedback. In conclusion, the same approach could not be suitable for all possible applications, and an appropriate design must be developed.

Finally, in a perfect scenario, users would interact with simulated items with both their hands by grasping and moving them around the space. Moreover, both hands could be involved during these interactions in different ways depending on the simulation necessity: *coupled* or *uncoupled*. This last aspect is treated in the next section.

2.6. **Bimanual tasks typologies**

In our daily lives, we commonly use both hands to perform all sorts of tasks: *bimanual tasks* specifically refer to a type of interaction between the same person's hands. Such aspect is often categorized into two distinct types of approaches: (i) *uncoupled independent control*, where hands separately act without a common objective and on separate workspaces, (ii) *coupled control* in which they mutually interact with a common goal, by manipulating the same object simultaneously, Figure 6.

Mechanisms underlying the control of bimanual actions have been extensively investigated for *uncoupled* tasks (Tcheang et al., 2007; Nozaki and Scott, 2009; Casadio et al., 2010), while few contributions specifically focused on bimanual tasks in *coupled* settings (Johansson et al., 2006; Mutalib et al., 2019).

Predominantly, the research focuses on investigating *uncoupled tasks* in which various artificially generated force fields interact with the user. Harley et al. (Harley and Prilutsky, 2012) examined the separated effects on arms in motor adaptation during a bimanual reaching task in a viscous force field. More specifically, the bimanual planar task was designed to perform reaching in four different conditions by using (i) the right dominant arm, (ii) the left non-dominant arm, (iii) both arms receiving a force field on the right dominant arm, (iv) both arms experiencing a force field on the left non-dominant one. The authors found that the motor adaptation rate was higher during the bimanual task when the right dominant arm experienced the force field. At the same time, performance

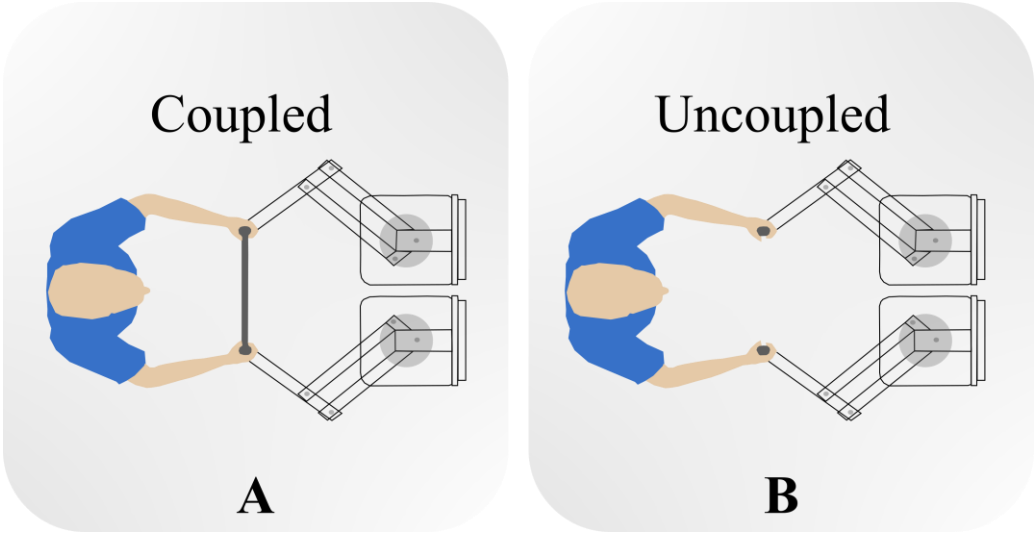

Figure 6: Example of bimanual tasks. **(A)** *Coupled control*, in which subject' hands are constrained by a bar. **(B)** *Uncoupled control*, in which subject' hands work independently.

drastically drops during the bimanual task in a specular condition when the field was imposed on the left non-dominant limb.

Moreover, Hayashi et al. (Hayashi and Nozaki, 2016) have proven that training on a single hand (unimanual) is expected to improve the bimanual performance: in particular, authors have shown that, when a particular bimanual ability is almost entirely developed, further unimanual training can be beneficial and boost bimanual skills. In a previous study (Nozaki et al., 2006), the same group had already pointed out how a transfer of skills is possible from unimanual to bimanual when a force field is applied on the left non-dominant arm. These representative studies show that motor abilities can be categorized exclusively in unimanual-specific and bimanual-specific control mechanisms.

On the other hand, the reduced number of investigations on *coupled bimanual* tasks followed a different approach by focusing on the brain´s hemispheres' role and their specialization motor control manifolds. In a study involving bimanual object manipulation employing a dual-wrist robotic interface, Takagi et al. (Takagi et al., 2020) tried to characterize the role of each limb: conversely to the dynamic-dominance theory (Sainburg, 2002), whereby the left non-dominant hand is specialized in the task stabilization while the right dominant one is required for fine control, the authors found that subjects preferred to stabilize the manipulated object with the right dominant hand.

There is a substantial difference between the two previously introduced conditions (*uncoupled* or *coupled*), especially from a neurophysiological point of view: many studies have highlighted how bimanual manipulation is computed in specific dedicated brain areas where unique synapse develop (Donchin et al., 1998; Steinberg et al., 2002; Rokni et al., 2003; Ifft et al., 2013). Literature suggests that the central nervous system does not exploit bimanual manipulation by simply delegating neuronal activities to two independent single-arm representations but rather to dedicated areas exhibiting specific neural patterns for *bimanual control* (Donchin et al., 1998; Steinberg et al., 2002; Rokni et al., 2003; Ifft et al., 2013). For these reasons, the study of specific strategies adopted during bimanual tasks results interesting because of the different signal coding that is done compared to unimanual tasks.

Finally, *coupled tasks* have the further advantage of providing continuous extra sensorimotor information, compared to *uncoupled* ones: each hand can perceive the force or the movement generated by the other hand through a coordinated interaction with the manipulated item (Galofaro et al., 2019; Mutalib et al., 2019).

Part I

Proprioception and force control in unimanual tasks

3. Proprioception and force control in *unimanual tasks*

The assessment of proprioception, in terms of position and force sense, is mainly performed by separate evaluations of these two aspects. Typically, in a clinical scenario, the evaluation is achieved using standard scales that do not accurately picture the patient's sensorimotor status, making it challenging to identify a targeted rehabilitation treatment. Consequently, contrasting results could be obtained in the quantification of proprioceptive deficits in subjects with neurological diseases. In order to gain a better comprehension of such proprioceptive deficits and their impact on motor functions, different quantitative assessment routines have been proposed in recent years using various technological solutions.

Hence, the first part of this thesis describes three different types of setups, all *unimanual* (right–dominant hand), which will contemplate the co-investigation of proximal and distal districts. First, I developed a “concurrent” task that simultaneously encompasses both the sense of force and position on a planar manipulandum by engaging participants in a task whose success depends on perceiving a specific force when interacting against different virtually simulated springs. Second, I study proprioception involving *distal multi-joint movements* through a robotic wrist device since it is still a poorly investigated domain, and there is, to our knowledge, little evidence in the literature on how multiple information streaming from different muscles are decoded and integrated. Finally, I proposed a novel 3D and multi-joint paradigm investigating proprioceptive acuity in coordinated multi-joint environments since they are still limited to single-joint or confined in the execution of tests involving planar workspace.

3.1. Control of Contact Force in Predictable and Unpredictable Environments [1]

3.1.1. Introduction

Knowledge about the spatial location of our limbs and about the forces that we are exerting on a fixture derives from the central processing of proprioceptive information. When body posture changes or when pressure is exerted upon or by the environment, different *mechanoreceptors,* localized within the joints, tendons, muscles, and skin, may be stimulated in excess of the threshold for response. They respond to such kinds of variations and are responsible for conscious sensations that include limb position and movement, the sensation of tension or force, the sense of effort, and the sense of balance (McCloskey, 1978a). As we move, we are unaware of the proprioception's fundamental role for all aspects concerning motor control. Since birth, the proprioceptive awareness of the body in the space plays a crucial role in the learning process of new skills (Goble et al., 2005). Then, as the learning proceeds and the movements are refined, afferent feedback signals from the participating body segments are systematically stored in the brain as templates of properly executed movement. Consistent evidence has been obtained through research employing functional magnetic resonance imaging (fMRI) and positron emission tomography (PET), suggesting that the cerebellum and pre-frontal cerebral cortex are the primary sites for this learning process (Jenkins et al., 1994; Flament, D., Ellermann, J. M., Kim, S. G., Uğurbil, K., & Ebner, 1996).

All daily gestures are processed by the central nervous system (CNS), managing somatosensory feedbacks and allowing for the correct processing of the actions performed upon the environment (Riemann and Lephart, 2002a, 2002b). Sensory feedback refers to somatosensory information associated with the acquisition, maintenance, and update of internal models related to the physical properties of the objects being manipulated (Haggard and Flanagan, 1996). Sensory experience continuously updates these internal models, and feedback control is based on the ongoing comparison between actual and predicted somatosensory information. External "noise" during the execution of actions, such as lifting a bottle thinking it is full of water, could produce a mismatch

[1] Part of this Chapter has been published as: E. Galofaro, R.A. Scheidt, F.A. Mussa-Ivaldi and M. Casadio. "*Testing the ability to represent and control a contact force"*, ICNR 2018.

between the predicted and the actual sensory input. However, detection of this mismatch leads to updating the internal model and correcting the prediction (Johansson, 1996; Wolpert and Flanagan, 2001; Shadmehr et al., 2010). Different studies investigate the importance and the existence of an internal model that is continuously updated by sensory feedback and how the long-term deprivation of cutaneous and proprioceptive feedback results in imprecision in both the force scaling and the temporal relationship between grip and load force profiles (Babin-Ratté et al., 1999; Nowak et al., 2002, 2004). The internal models that human subjects form enable the prediction of state-dependent force perturbations applied to the arm during movement and lead to the generation of compensatory forces that restore the desired motions (Lackner and Dizio, 1994; Shadmehr and Mussa-Ivaldi, 1994a; Sainburg et al., 1999). These models are successfully applied to the manipulation of objects that required, for example, to be balanced during the transport or to be wielded with moderate grasping force (Wolpert and Kawato, 1998; Haaland, Kathleen Y., Deborah L. Harrington, 2000; Imamizu, H., 2000).

Our senses and, specifically, *Force Sense* (***FS***) and *Position Sense* (***PS***) play a fundamental role during the execution of tasks involving the manipulation of objects (Proske and Gandevia, 2012). Different studies (Dover and Powers, 2003; Proske and Gandevia, 2012; Niespodziński et al., 2018), investigated their relationship, however, always considering them separately in such a way that they could not be evaluated *concurrently*. Traditionally force and position sense are evaluated adopting two or more testing modalities: Force Reproduction tests (FR) to assess ***FS*** (Stevens and Cain, 1970; Jones, 1989; Dover and Powers, 2003; Trousset et al., 2018) and Joint Position Matching tasks (JPM or similar approaches) to assess ***PS*** (Dukelow et al., 2009; Aman et al., 2015; Contu et al., 2017).

Here, we developed a *concurrent* evaluation method (***FS***+***PS***), employing a unimanual-robotic planar manipulandum, by engaging participants in a task whose success depends critically upon perceiving a specific force when they interact against different virtually-simulated springs, which establish predefined relations between force and position.

The purpose of this study was (i) to determine if subjects are able to learn to exert a specific amount of force (10 N) with their right arm in a way that is *independent* of the effects of applying such force at different positions, i.e., by decoupling ***FS*** and ***PS***. To address this point, we engaged two groups of subjects (12 in each group, which were instructed to apply force in different directions) in a task whose success depends critically

on exerting a fixed contact force against simulated springs with randomly ***variable coefficients of stiffness***.

This study's second purpose was (ii) to compare the effect of uncoupled force and position feedback against a condition in which the coupling is constant and therefore predictable. To this end, an additional third group of subjects was required to perform the same task, but against simulated spring with a ***constant stiffness coefficient***, i.e., the amount of displacement of the spring was always linearly related to the applied force by a fixed stiffness coefficient. Part of this study was presented in abstract form (Galofaro et al., 2018).

3.1.2. Experimental Setup, Task and Participants

Subjects grasped with their right hand the instrumented handle of a planar manipulandum with two degrees of freedom (Casadio et al., 2006). The torso was restrained to the back of the customized chair. The arm was maintained parallel to the floor, with the forearm secured to custom-made support attached to the handle that provided support against gravity. At the beginning of each trial, the seat position was adjusted so that the subjects had the elbow and shoulder joints flexed by about 65˚ and

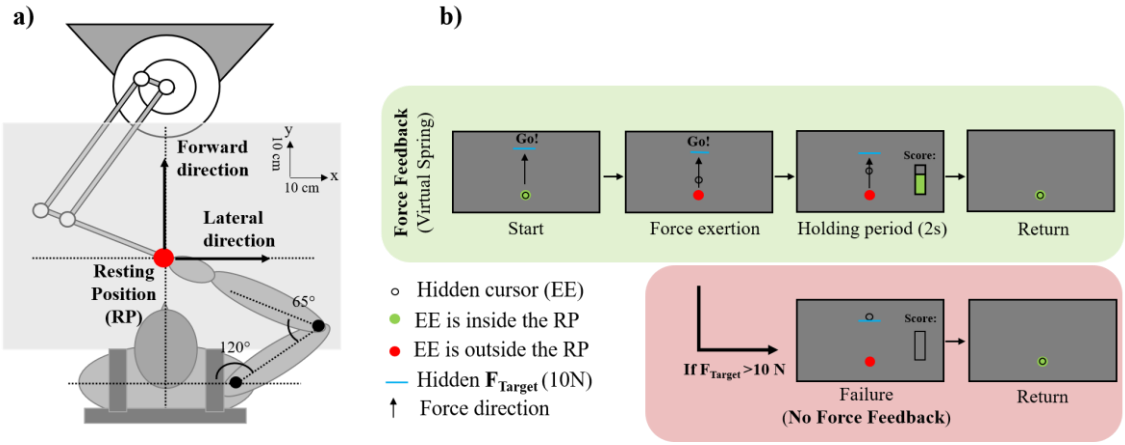

Figure 7: *Experimental Setup and Task.* Panel **(A)** shows the subject that holds the end-effector (EE) of the planar manipulandum with his right hand located in the *Resting Position* (*RP*, black target). Elbow and shoulder joints are flexed at about 65° and 120°, respectively. An opaque screen hides the arm and the hand for the entire experimental session (opaque grey rectangle). Panel **(B)** displays a single trial's temporal sequence, exemplified for the Forward direction (top sequence, green – Force feedback). Start: the *Hidden Cursor*, namely the device' end-effector (*EE*, little empty circle) is inside the *RP*, which remains green as long as the subject stays inside it. Then, a message (Go!) appears along the direction that the subject must follow (frontal in this case). Force exertion: as soon as the subject leaves the RP, for moving against the virtual spring, it switches color into red. Holding period: subjects decide to stop their hand when they believe that the target force has been achieved and maintains the steady force for 2 seconds. Only after this period, the score is shown. Return: the device brings back the EE inside the RP. If the participant exceeds the target force (F_{Target} > 10N), the force feedback is turned off (bottom sequence, red – No Force feedback). Failure: subjects receive a score equal to zero. Return: the device brings back the subject's hand into the RP.

120˚respectively (*Resting Position - RP*). Consequently, the initial hand position was in front of them, on the sagittal plane (Figure 7A).

During the entire experiment, the hand, the elbow, and the shoulder were on the same plane parallel to the floor. An opaque curtain hid the subjects' whole arm and the robot arm. A 32" monitor mounted vertically in front of the subjects at their eyes' level showed the written information necessary to correctly perform the experiment. The manipulandum had a large workspace (0.8 x 0.4 m ellipse) and was actuated by a direct-drive brushless motor resulting in a low intrinsic mechanical impedance. Two encoders measured the joint angles and allowed estimating the end effector's trajectory with high-resolution (< 0.1 mm). The control loop was closed at 1 kHz. Hand position and contact forces were recorded at a rate of 100 Hz. The task was implemented in Simulink/MATLAB® and based on the Real-Time Windows Target toolset.

In this experiment, the robot generated an elastic force (*Force Feedback*) that opposed the subject's hand motion:

$$F = -K_i(x - x_0) \quad (1)$$

Where x is the hand displacement from the initial position x_0 and K_i is the stiffness of the robot on trial i^{th}.

Subjects were required to move their hand in one specified direction - either *forward* or *laterally* - until they perceived that the robot opposed a force of 10 N ($\boldsymbol{F_{Target}}$), then to hold that position for 2 seconds. If subjects exceeded the $\boldsymbol{F_{Target}}$, the robot turned off the interaction force (*No Force Feedback*).

Thus, subjects were instructed to arrive as close as possible to the target force but to not exceeding it, otherwise, they failed the trial (Figure 7B).

Each trial started with the hand in the *Resting Position* (*RP*) as described above, corresponding to 0 force, i.e., the length of the virtual spring was equal to its resting length x_0. No visual feedback of the arm, both of the subject and the robot, was provided during the trials. To ensure that subjects always started from the same position, a fixed home target of 1 cm diameter was always visible on the screen. If the hand subjects' position, namely the hidden end-effector (EE *Hidden Cursor*), was outside the *RP*, the target remains red. Otherwise, if the *EE* was inside it, its color becomes green, and the new trial could start. At the end of each trial, subjects had to go back in the *RP*, corresponding to 0 interaction force. In the trials in which they failed, namely, they exceeded the $\boldsymbol{F_{Target}}$, the

subject's hand was brought back on the *RP* by the device. In each trial, subjects had to apply the force along a required direction avoiding lateral deviations. If subjects made a lateral deviation error $\geq \pm 1$ cm with respect to the nominal direction, the trial was discharged and presented again later in the experiment.

The experimental session included a *Training Phase* consisting of 300 trials, divided into 10 *blocks* ($\mathbf{T_1}, \ldots, \mathbf{T_{10}}$) of 30 trials each, alternated with brief pauses to avoid fatigue. Then, subjects performed a *Generalization Phase* consisting of one *block* with 30 trials (**G**).

Subjects were divided into three groups, differing for the force direction (*forward* or *lateral*) and the implicit availability of position information, i.e., the *variable* or *constant* virtual spring stiffness coefficient.

During the *Training Phase*:

- Group *Forward Variable* (***FV***) the force was exerted along with the *forward* direction, and at any trial, the stiffness coefficient of the virtual spring K_i could take randomly one of 6 different stiffness values: 67 N/m, 77 N/m, 91 N/m, 111 N/m, 142 N/m, 200 N/m.
- Group *Lateral Variable* (***LV***) exerted a force along the *lateral* direction and at any given trial K_i changed as for ***FV***.
- Group *Forward Constant* (***FC***) exerted a force in the *forward* direction, and the spring stiffness K_i was maintained constant (67 N/m).

Note that for group ***FV*** and ***LV,*** the $\boldsymbol{F_{Target}}$ equal to 10 N was decupled from the position, forcing the subjects to focus on force perception to solve the task, while for group ***FC,*** the level of the force was always associated with the same displacement.

During the *Generalization Phase,* subjects exerted the required force orthogonal to the direction assumed during the *Training Phase*, namely group ***FV*** and ***FC*** pushed along the *lateral* direction while group ***LV*** along the *forward* direction. In this phase, for all groups, K_i assumed the previous 6 *variable* stiffness values. Figure 8A shown a schematic overview of group conditions.

During each trial, if the subjects exceed $\boldsymbol{F_{Target}}$, the robot simulated the "breaking of the virtual spring", suddenly turning off the force feedback. This feedback was identical in both phases. No other feedback was provided during the *Generalization Phase.*

Only during the *Training Phase,* additional information was provided to the subjects as knowledge of results. After each trial, subjects received a score based on their performance. If the subjects exerted more than 10 N, they failed the trial, and their score

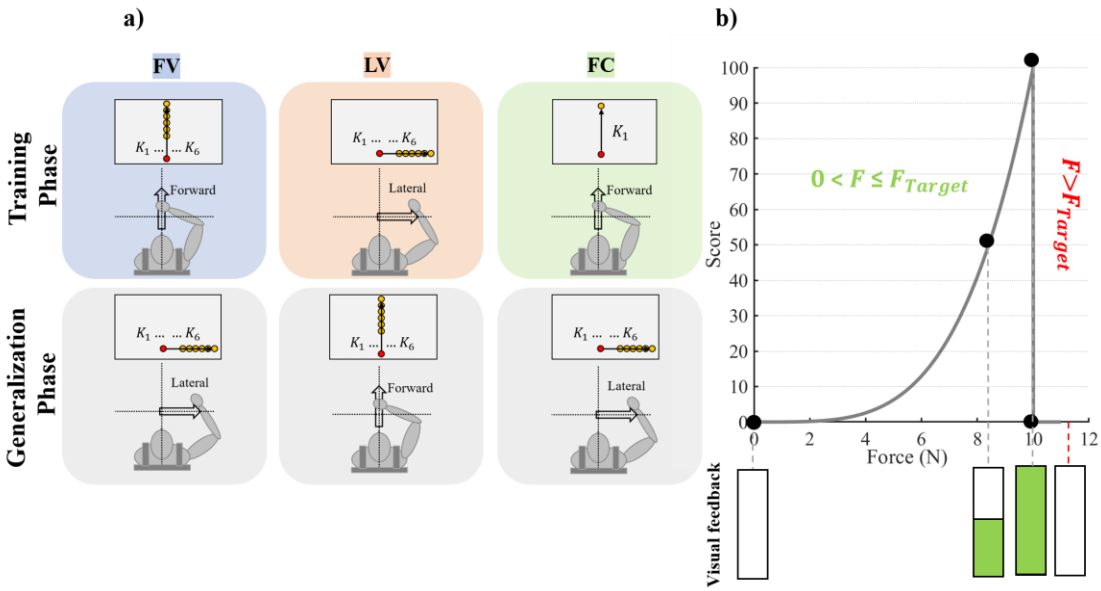

Figure 8: *Protocol and Score feedback.* In panel **(A)** a schematic overview of groups' conditions: *FV* (blue), *LV* (orange) and *FC* (green). The *direction* in which they must exert the force is evidenced by the sketch (*forward* or *lateral*). The relationship between position and force – *constant (1 stiffness coefficient – K_1)* or *variable (6 stiffness coefficients – $K_1 \dots K_6$)* robot stiffness coefficients – is showed in every panel. The first row depicts the *Training Phase* (number of trials: 300), while the second row shows the *Generalization Phase* (number of trials: 30) for each group. Panel **(B)** describes the relationship between the steady-hand force applied by subjects (averaged during the 2-sec holding period) and the score provided as visual feedback. Below the graph is depicted the correspondent visual feedback that was presented to subjects during the *Training Phase*.

was set to 0. If they were able to apply a force below 10 N, they received a trial score that depended on the average valued of the last 2 s of steady hand force (i.e., during the holding period).

The score was a quadratic function of this force ranging from 0 to 100 according to the following equation:

$$S = c * F^4 \qquad (2)$$

F is the average value of the last 2 s of steady hand force, c is the constant equal to 0.01, and S is the resulting score shown as visual feedback (Figure 8B).

The score function was strongly asymmetric with a sudden breakdown at the target force, and an increasing quadratic component as the force approached the target level. The latter was designed to encourage subjects to take risks by increasing the reward more rapidly than a linear function of the applied force's distance from the desired value.

Subjects: Thirty-six healthy young subjects (24.2 ± 2 (mean±std) years old, 21 females) participated in this experiment. Inclusion criteria were (i) no evidence or known history of neurological disease or injury (ii) normal upper limb joint range of motion and muscle strength (iii) being right-handed (iv) absence of problems of visual integrity that could not be corrected with glasses or contact lenses. Subjects were divided in the 3 matched groups of 12 subjects each: group ***FV*** (25.2 ± 2 (mean±std), 7 female), group ***LV*** (24.2 ± 2 (mean±std, 7 female) and group ***FC*** (23.3 ± 2 (mean±std), 7 female).

3.1.3. Data Analysis and Outcome Measures

For each trial, to evaluate the subjects' ability to modulate a specific amount of force depending on the above-mentioned different conditions, we computed the following metrics:

- *Score* (0-100): score computed as in (2).
- *Rate of Failure, RF* (%): percentage of trials where subjects failed, over the total number of trials for each block (30 trials).

For the successful trials, i.e., the trials in which the steady force exerted by the subject did not exceed $\boldsymbol{F_{Target}}$, we computed:

- *Force* (N): the average value of the steady-state hand force maintained during the holding time.
- *Force error, FE* (%): the error between the desired force and the applied force, expressed as a percentage of the target force.

For the 'failed' trials, when the haptic feedback was turned off, we considered the difference between the applied force and the trial's target force *before* and *after* the *Failure*. We computed respectively the Error_{Pre} and the $Error_{Post}$, expressed as the percentage of the target force:

$$Error_{pre}\ (\%) = \frac{F_{Target} - F_{n-1}}{F_{Target}} * 100 \quad (3)$$

$$Error_{post}(\%) = \frac{F_{Target} - F_{n+1}}{F_{Target}} * 100; \quad (4)$$

where n is the failure trial, F_{n-1} and F_{n+1} are respectively the amount of force applied at the preceding and the subsequent trials, respectively.

Statistical Analysis: For each group, to test learning, we compared subjects' performance between block 1 (***T1***) and block 10 (***T10***) of the *Training Phase*. We further tested if subjects with variable stiffness conditions (***FV*** and ***LV*** group) were able to generalize their performance across a direction orthogonal to that adopted during the training by comparing the performance in the block ***T10*** versus ***G.***

Moreover, we compared the ***FC*** group's performance in ***G*** with the ***LV*** group's performance in ***T1***, i.e., we compared subjects that experimented with the same conditions (*lateral* direction and *variable* stiffness), but with a different degree of experience (post - Training Phase versus pre - Training Phase). This last analysis was run to understand if there was some performance retention for the ***FC*** group, despite the exploitation of position information during the *Training Phase*. We used a non-parametric test (Wilcoxon signed-rank test) since the number of participants for each group was small and the performance variables were not normally distributed.

3.1.4. Results

All subjects successfully participated in this study and did not report any adverse event or muscle fatigue.

Learning to control a contact force is possible when force sense and position feedback are mutually independent (FV and LV groups).

Figure 9A displays subjects' *Score* (left axis) in relation to the *Force* (right axis): data were divided into the above-described blocks, and in each block are evidence 5 bins of 6 trials each. Figure 9A (top) illustrated ***FV*** and ***LV*** groups' performance, the two ones belonging to the variable stiffness condition (*FS* and *PS* independent).

Subjects were able to learn across the *Training Phase*, despite the lack of relationship between force and displacement, as evidenced by comparing ***T1*** with ***T10*** ($p=0.0022$, $z=-3.0594$ for both groups). Their learning curves plotted during the *Training Phase* (T1-T10: 300 trials) were similar, Figure 9B, with a predictably higher learning rate at constant stiffness (***FC***). The coefficients reported in *Table 1* quantify this aspect deeply.

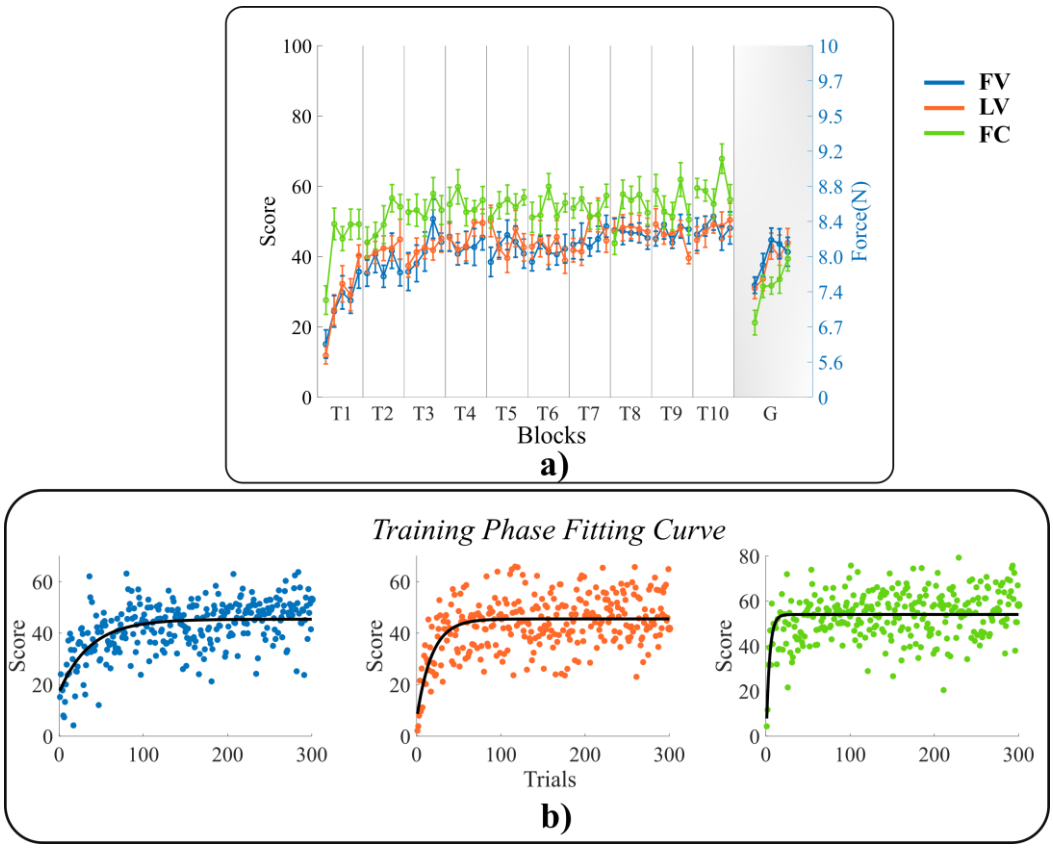

Figure 9: *Performance results.* Panel **(A)** depicts on the top row score performance (with the corresponding amount of force on the right axis) for *FV* (blue line) and *LV* (orange line) groups. On the bottom row *FV* (blue) and *FC* (green) groups. The indicators score and force were averaged across 5 bins, each bin corresponding to 6 trials, including all six stiffness coefficients. Panel **(B)** shows the exponential fits (black lines) obtained on averaged performance for each group (colored dots).

Fitting Coefficients	**FV group**	**LV group**	**FC group**
a	**45.4** (44.1, 46.7)	**45.5** (44.3, 46.7)	**54.0** (52.8, 55.2)
b	**28.5** (22.9, 34.0)	**38.9** (29.8, 48.2)	**59.3** (33.5, 85.1)
λ	**0.02** (0.018, 0.036) (=**70 trials**)	**0.04** (0.036, 0.075) (=**36 trials**)	**0.25** (0.112, 0.387) (=**6 trials**)

Table 1: Fitting coefficients (95% confidence bounds). Where a is the constant term, b is the initial quantity, and λ is the learning rate.

These latter were obtained by fitting data with an exponential curve, as in the following equation:

$$y(x) = a - b * e^{-\lambda x}, \qquad (5)$$

in which *a* is the constant term, *b* is the initial quantity, and λ is the learning rate, and y(x) is the resulting curve.

Comparing ***FV*** and ***LV*** groups' coefficient λ (0.02 and 0.04 respectively), we could denote that they have the same order of magnitude. This allows us to state that the different *movement's direction* (*forward* or *lateral*, respectively) adopted among groups during the *Training Phase*, and consequently the different *arm geometry*, does not affect force perception and force learning.

Learning retention is partial when changing one feature (direction).

We compared the performance of both the ***FV*** group and the ***LV*** group during the G*eneralization Phase* ***G*** with (i) the performance in ***T1*** to assess if they returned to a naïve level and (ii) the performance in ***T10*** to assess if they were able to maintain the acquired skill entirely or if they had a slacking in the performance. Subjects did not return to a naïve level; in fact, we found a significant difference between ***T1*** and ***G*** blocks for both groups (***FV*** group: p=0.01, z=-2.5887; ***LV*** group p=0.02, z=-2.3534). However, when comparing the performance of the last block of training ***T10*** with the generalization phase block ***G***, we obtained a significant difference in both cases (***FV*** group: p=0.0229, z=2.2749; ***LV*** group p=0.022, z=3.0594) due to the new task solving direction. The level of performance reached at the end of the training was recovered after two bins (12 trials) in both groups (***FV*** group: p=0.25, z=-1.1968; ***LV*** group p=0.29, z=-1.2124), A (top).

Training performance is better when force and position information (FC Group) are coupled, but the performance improvement is not retained when position information was not available.

FC group could exploit hand position information, since perceived force and position of the hand were coupled during the *Training Phase*. This group learned to apply a force of 10 N that corresponded to a forward displacement of 0.15 m. A significant improvement was evident during the *Training Phase* (***T1-T10***: p=0.0022, z=-3.0594). Subjects showed a faster learning rate (λ=0.25) compared to the other two groups (λ=0.02 and λ=0.04), and the final performance was higher, as also demonstrated by the higher constant *a* shown in *Table 1*.

However, the performance was remarkably worse during the *Generalization Phase*: we compared the performance in ***G*** with ***T10***, and the performance was significantly lower

(p=0.0022, z=3.0594). Then, we compared the ***FC*** group's performance in ***G*** (namely after training) with the performance of the ***LV*** group in ***T1***, i.e., with subjects practicing the task for the first time (same conditions: *forward* direction and *variable* stiffness coefficient). We found no significant difference between the two groups (p=0.23, z=-1.1767). Subjects that learned to exert the force in a given direction with a *constant* level of impedance (***FC*** Group), when tested with *variable* impedance, returned to a complete naïve level, without partial retention of the learned skill, Figure 9A (bottom).

Score distribution over stiffness values.

We qualitatively investigated the subject's performance during ***T1***, ***T10,*** and ***G***, in terms of *Score*, considering how it varied depending on the virtual spring's different stiffness values (Figure 14). Independent of the impedance, score values were higher for ***T10*** for all groups than ***T1***, as previously observed on stiffness average (Figure 10). Moreover, observing score metrics on ***T1***, we denoted lower performance, both for ***FV*** and ***LV*** groups, when the virtual spring was stiffer, namely for K_6=200 N/m. This difference was not maintained during ***T10***, in which performance was almost comparable between all the impedance values (distribution around the red line).

Relationship between $Error_{pre}$ and $Error_{post}$: what happens when subjects failed the trial.

The $Error_{pre}$ distribution was fundamental to explore how close the subjects were to the target force of the *trial before* failing. The $Error_{post}$ compared to $Error_{pre}$ provides an estimate of risk acceptance/aversion caused by a recent failure.

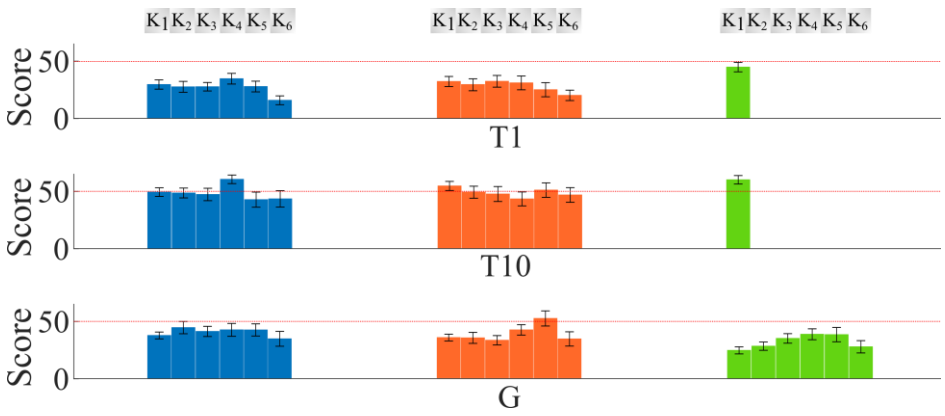

Figure 10: Score metrics evaluated separately for each value of the virtual spring stiffness (K_1=67 N/m, K_2=77 N/m, K_3=91 N/m, K_4=111 N/m, K_5=142 N/m, K_6=200 N/m) and for each group during T1, T10 and G.

In ***T1***, subjects belonging to ***FV*** and ***LV*** groups had values respectively of $Error_{pre}$ (mean ± se, express as % of the 10N target force) equal to 24.7±2.6 % and 22.3±1.9 % and $Error_{post}$ equal to 28.4±2.7 % and 28.9±1.7 %. Always in ***T1***, ***FC*** group, denoted significant smaller errors compared to the other two groups: $Error_{pre}$ equal to 10.2±1.2 % and $Error_{post}$ equal to 14.4±1.4 %, ($Error_{pre}$: ***FV*** versus ***FC*** p=0.0022, z=3.0594; ***LV*** versus ***FC*** p=0.0029, z=2.9810; $Error_{post}$: ***FV*** versus ***FC*** p=0.0029, z=2.9810; ***LV*** versus ***FC*** p=0.0022, z=3.0594), Figure 11 (top row).

During ***T10***, all the groups were able to reduce their errors' distribution compared to ***T1*** ($Error_{pre}$ (***T1-T10***): ***FV*** p= 0.0037, z= 2.9025; ***LV*** p= 0.0150, z=2.4318; ***FC*** p=0.0058, z=2.7562; $Error_{post}$: ***FV*** p=0.0029, z=2.9810; ***LV*** p=0.0047, z=2.8241; ***FC*** p=0.0076, z=2.6673). The $Error_{pre}$ was equal to 10.9±0.9 %, 10.3±2.1 % and 5.2±0.5 % while the $Error_{post}$ was equal to 18.7±2.25 %, 16.9±2.3 % and 9±1.1 % respectively for ***FV***, ***LV*** and ***FC*** group, Figure 11 (middle row).

Finally, in ***G***, subjects who were trained with *variable* impedance (***FV*** and ***LV***) showed no significant changes compared to ***T10*** regarding the $Error_{pre}$ (11.3±1.0% for ***FV***

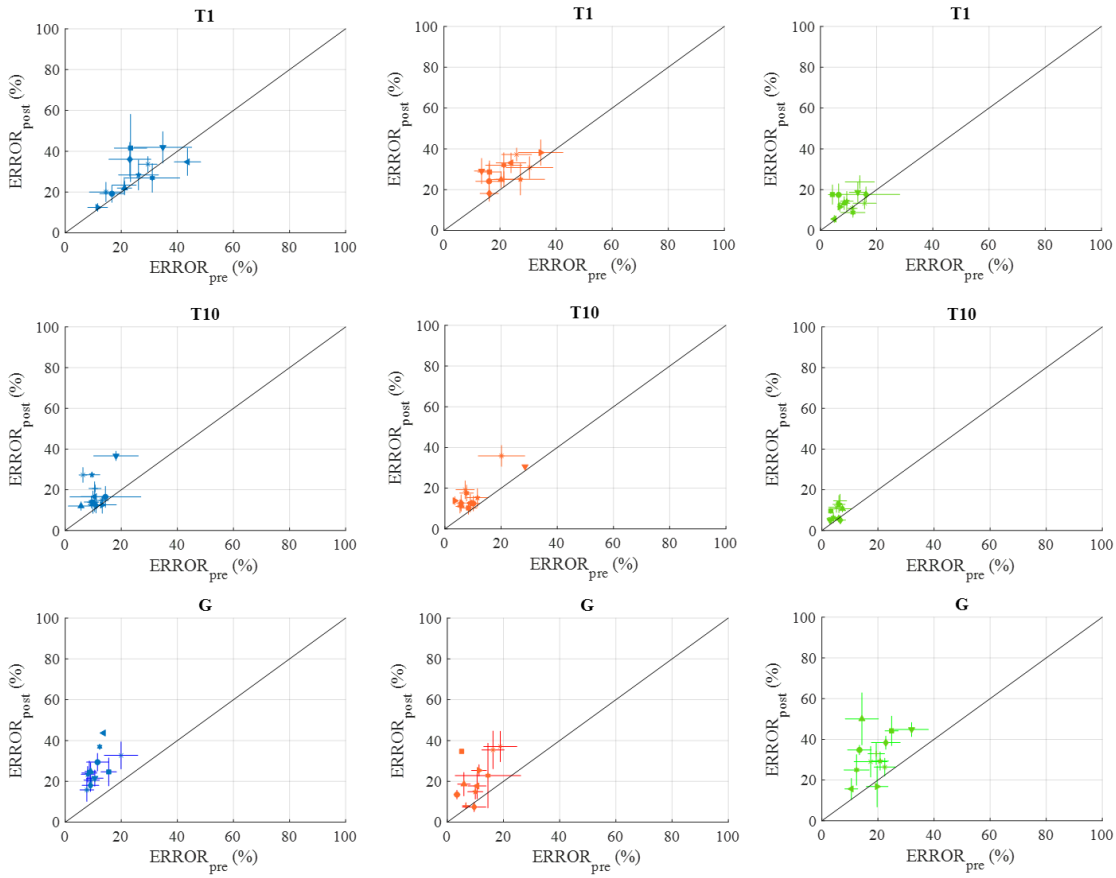

Figure 11: Comparison between $Error_{pre}$ and $Error_{post}$. Each point represents the average result for a single subject. The line through the origin (equality line) is represented by a continuous black line; if the subject' performance stays above this line the $Error_{post}$ is higher compared to the $Error_{pre}$, vice versa if it stays under the line.

and 10.2±1.4% ***LV***; p= 0.9375, z=-0.0784 and p=0.4236 z=-0.8002). From the same comparison, they significantly increased their $Error_{post}$ (26.3±2.3 % for ***FV*** and 23.5±3.6% for ***LV***; p=0.04, z=-1.9612 and p=0.0414, z=-2.0396). Interestingly, subjects belonging to the ***FC*** group, trained with a *constant* impedance, showed both significantly higher errors compared to the ones obtained in ***T10***: *Error-pre* equal to 19.2±1.8 % (p= 0.0033, z=-2.9341) and *Error-post* equal to 32.3±3.1 % (p= 0.0033, z=-2.9341), Figure 11 (bottom row).

3.1.5. Discussions and Conclusions

A well-investigated question about motor behavior is how we coordinate and control movements of the hand. Less attention has been dedicated to how we apply well-controlled forces to fixtures and objects in the environment. In this study, we focused on how the central nervous system attempts to apply a preset contact force upon an object with uncertain contact impedance. The uncertainty in the contact impedance limits the possibility to simply translate a desired contact force into a "virtual" displacement of the hand beyond the object boundary, as suggested by Hogan et al. (Hogan et al., 1987). In this study, we implemented a task requiring participants to exert with their hand a contact force of 10 N in one of two directions by interacting with a virtual spring with *variable* ***(FV*** and ***LV***) or *constant* (***FC***) stiffness. In this way, we investigated how reliance on *position* sense influences *force* control. Results showed that despite a randomly variable contact impedance, subjects learned slowly and gradually to approximate the desired level of contact force, albeit with a reduced accuracy compared to the group experiencing a constant contact impedance. In fact, both groups of subjects learned to maintain a steady-state level of contact force a few Newtons below the threshold for contact breaking; the subjects experiencing a variable stiffness tended to stay at a slightly more prudent distance from that critical point. Furthermore, they could generalize their learning even when using a different arm configuration. In contrast, subjects exposed to a constant (***FC***) contact impedance learned faster and had a higher final score than those dealing with variable impedance. But they had a reduced ability to generalize their learning when the position information was not available and when using a different arm configuration. This is consistent with other experiments suggesting that variable practice is more conducive to the consolidation of motor learning than constant practice (Kantak et al., 2010).

When subjects failed the trial exceeding the target force, they tended to perform with more prudence in the following trial. As a consequence, the error after failure exceeded the error (by default) before trial they encountered the event where the force feedback was removed. Therefore, the failure event, which constitutes a discontinuity in the subjects' practice, is also a transient hindrance in the process of learning.

Effects on participants' performance if they rely on or not on the position information.

The results suggest that as *constant position* information is presented through a proprioceptive channel, and visual feedback is not available, this is recognized and used as the primary information source to solve the task.

The estimation of contact stiffness is required to plan and perform successful interaction with objects in the environment (Kawato, 1999). A number of studies have investigated the effect of delayed force feedback in the perception of an object's rigidity (Ohnishi and Mochizuki, 2007; Pressman et al., 2007; Nisky et al., 2008, 2010, 2014; Leib et al., 2015; Kossowsky et al., 2021). While these studies revealed that these delays altered the perception of stiffness as reported by the subject, another experiment revealed that the subconscious processes that regulate the grasping force does not appear to be affected (Leib et al., 2018). In fact, Leib and coworkers found evidence that participants exposed to force feedback delays remained able to form an accurate *internal representation* of the load force (both in size and timing) and that this representation led to precise control of grip force, even when the force feedback was delayed.

In our study, it appeared that subjects generated a response pattern consistent with the estimate of the average stiffness based on the force and displacement experienced prior to the breaking of the virtual spring. If one assumes that in the late phases of training the subjects' internal representation of the commanded force corresponded to the required force of 10N – that is if they assumed to be closely approximating the desired level of contact force. Then the produced displacements would correspond to an overestimate of the contact stiffness by approximately 20%. Even assuming that after training the subjects adopted a substantial safety margin, this would still correspond to an overestimate of the stiffness caused by discontinuity in the contact behavior.

Future work: how error sensitivity affect performance.

Herzfeld et al. have observed that, in an environment where the perturbations are repeated without variation, learning is guided by a representation of errors, more so than when the perturbation is highly variable from trial to trial (Herzfeld et al., 2014). Here, unlike Hertzfeld, we considered a discontinuity in the error profile. On one hand, subjects can underestimate the target force by a variable amount. But on the other, the over-estimate by any amount results in complete and uncorrectable failure. A predictable effect of such failures is that they will induce some prudence in the following attempts, as it is observed in Figure 11, where the errors following failure tend to exceed the error accepted immediately before a failure. The analysis of the error sensitivity in our experiments is an upcoming development that will require considering how the action at the i^{th} trial depends upon the action performed and the error experienced in the previous trial. A specific challenge in our case is how to consider the "catastrophic error" which leads to the breaking of the boundary.

Limitations: This study's results should be interpreted with respect to the relatively small sample size tested per group, which, however, should be considered sufficient (Virzi, 1992). Moreover, all the subjects were right-handed; the inclusion of left-handed subjects could help to understand if the evidenced learning mechanisms are independent of handedness and/or hemispheric specialization. For the purposes of this study, the implemented *constant* condition alone (***FC***) might appear limited. However, we demonstrated in the *variable* conditions (***FV*** and ***LV***) that the learning process is similar in rate and final performance regardless of action direction. This fact allowed us to select a single-testing direction to verify our initial hypothesis - namely, the effect of coupled relationship between force and position on learning – during the experiment.

Conclusions: This study aims at providing a view of how contact forces can be precisely controlled independent of contact impedance, that is, independent of a persistent relation between applied force and ensuing motion. We designed a setup employing a unimanual-robotic planar manipulandum by engaging participants in a task in which success depends on perceiving a specific force when interacting against different virtually simulated springs. A critical element of the paradigm is the presence of a hard discontinuity, when a set level of required force is exceeded by any amount. Surprisingly, we observed that subjects learned to execute successfully the task in the presence of variable contact

stiffness, in which case the instructed contact force becomes effectively uncorrelated with the amount of contact displacement. Our findings demonstrated that this skill generalizes across directions, i.e., subjects could exert the practiced target force in a different arm configuration requiring different muscle activations. Our results suggest the possibility to use decoupled force and motion information in rehabilitative applications aimed at recovering the ability to manipulate fragile objects requiring the application of well-controlled contact forces. And similar skill demands are relevant to the performance of expert activities, such as surgery, where for instance, exerting controlled pressure on a tissue must be done with great precision. Understanding the factors that affect learning to control forces and motions is therefore critical both for clinical rehabilitation and professional training.

3.2. **Robotic assessment of wrist proprioception during kinaesthetic perturbations** [2]

3.2.1. Introduction

The term "proprioception", introduced in the early twentieth century, refers to the self-perception of position, motion and orientation of the body or body segments (Goldscheider, 1898; Sherrington, 1952; Evarts, 1981). Proprioceptive signals arise from mechanoreceptors embedded in our joints, muscles, and tendons such as muscle spindles or Golgi tendon organs (Proske and Gandevia, 2012). In general, two submodalities of proprioception are distinguished: (i) *kinaesthesia*, the sense of limb movement; (ii) *joint position sense*, the sense of limb position (Proske, 2006). These two senses constitute the sensory stream colloquially referred to as conscious proprioception.

Neurological pathologies, such as stroke (Carey, 1995) or Parkinson's disease (Konczak et al., 2012), can permanently deprive the brain of its main sources of dynamogenic information from skin and muscles (Debert et al., 2012), leading to a compromised coding of the proprioceptive information, with negative consequences in motor control and the associated recovery progress (Marchal-Crespo and Reinkensmeyer, 2009; Schabrun and Hillier, 2009). Accurate assessment and quantification of proprioceptive function becomes a leading factor in the diagnosis and treatment of neurological diseases.

Despite the paramount importance of proprioceptive feedback in motor coordination and recovery (Raspopovic et al., 2014), actually, there are no established methods capable of assessing multi-joint proprioceptive acuity in a reliable, objective fashion. Recent advancements in robotic and haptic technology (Yeong et al., 2009; Oblak et al., 2010) represent the starting point for the development of automated, repeatable robot-aided methodology for studying proprioception and potentially provide standardized, quantitative methodology to evaluate kinaesthetic and proprioceptive performance characterized by a continuous ratio scale (Simo et al., 2014; Deblock-Bellamy et al., 2018; Klein et al., 2018; Mochizuki et al., 2019). In addition, the use of robotic devices to study sensory motor control should be designed considering anthropometric and biomechanical

[2] The whole content of this Chapter has been published on *Frontiers in Neurorobotics* as: E. D'Antonio*, E. Galofaro*, J. Zenzeri, F. Patané, J. Konczak, M. Casadio and L. Masia. "*Robotic Assessment of Wrist Proprioception during Kinaesthetic Perturbations: a Neuroergonomic Approach"* (2021).

features, not only for what concerns the mechanical design but also for the implementation of the related control strategies. These complementary characteristics (design & control) are paramount to exploit the real potential of robotic technology in both neuroergonomics, addressing general motor behavioral aspects, and clinical environment where robustness and reliability of such devices can be only reached starting their conception from human factors.

Although it has been demonstrated that proprioception of distal joints is particularly involved in fine manipulation of daily living activities (Hoseini et al., 2015; Ponassi et al., 2018), scientific literature primarily reports contributions focused on proprioception at the level of proximal upper limb (shoulder and elbow). Few researches have been focused on distal joints, with particular emphasis on wrist's proprioceptive functions (Aman et al., 2015; Rose et al., 2018a). In particular, concerning our group, we extensively tested proprioceptive acuity using a device named WristBot (Masia et al., 2009), which allows for the implementation of a widely used test for the assessment of position sense (Cappello et al., 2015), the *Joint Position Matching* (JPM) paradigm (Goble, 2010): the test is run in absence of visual feedback and evaluates the proprioception by quantifying the accuracy in replicating a joint posture (proprioceptive target), previously imposed as angular displacement. Previous works investigated the wrist proprioception along a single degree of freedom (DoF) evaluating (Marini et al., 2016a) its anisotropy across wrist abduction/adduction (AA) and flexion/extension (FE) DoFs, as well as a gradual change of proprioceptive acuity during the developmental phase for individuals (Marini et al., 2017). However, proprioception for distal multi-joint movements, involving more than a single DoF, still remains an open question, and there is limited evidence in literature on the mechanism underlying the integration of proprioceptive sensory stream from multiple concurring anatomical joints (Sketch et al., 2018).

In daily manipulation tasks, the use of the wrist and hand requires a complex motion strategy between the fingers and the two distal DoFs corresponding to wrist FE and AA. Moreover, the forearm can rotate along its longitudinal axis by engaging a third wrist DoF, the pronation/supination (PS), which allows the hand to cover a wider workspace and exploit the arm's kinematic redundancy. The wrist biomechanics, almost unique among all human anatomical districts, allows an extremely efficient manipulation dexterity, as highlighted by the study of Kane et al. (Kane et al., 2014), which showed how the combination of FE and AA ROMs results in a workspace which is independent from the rotations around the PS axis, being its motion completely disconnected from the previous

wrist joints. Within the framework of the current study, we hypothesize that providing perturbations along the PS axis, consisting in rotational offset of variable amplitude along the forearm, will not lead to physical limitations on the remaining wrist DoFs and sensory conflicts in terms of proprioception acuity during joint position matching tasks. Despite wrist functionality is deeply known for what concerns its multi-joint biomechanics, it is a rather unexplored ground in terms of coordination and interpretation of different sensory streams arising from the multiple, concurring DoFs. Proprioceptive efferent signals are encoded in reference frames localized at the level of joints (Flanders and Soechting, 1995): in order to compute motor commands, the central nervous system must process such sensory information and project it into a spatial representation of motion (Colby, 1998). Yet, movement generation relies on information redundancy by merging both visual and proprioceptive feedback, continuously streamed during a general task execution, and consequently integrating both absolute spatial and local sensory streams respectively (Snyder et al., 1998). What happens if visual information is excluded from the integrative process and motion computation must rely on one sensory feedback? How, in such condition, an external disturbance, altering the encoding of proprioceptive information, influences the task performance? With this in mind, we designed an experiment to investigate if the sole proprioceptive information, can be robustly retained by the brain even in presence of a kinesthetic disturbance altering the geometric conditions between the presentation of the task and its execution.

How proprioceptive information is interpreted when complex wrist motions are performed, and whether multi-joint kinaesthetic sensory streams are encoded throughout the wrist workspace, are examples of unanswered questions crossing the domains of neurophysiology and clinical rehabilitation. Most studies involving multi-joint tasks, have primarily investigated distal arm goal directed movements towards visual targets: results suggest that the relative contributions of vision and proprioception to motor planning can change, depending on the modality in which task relevant information is represented (Sarlegna and Sainburg, 2007). Yet, all this extensive production of results has covered experimental paradigms deeply involving visual-feedback (Goble and Brown, 2009), while encoding of proprioceptive targets in coordinated tasks is still an open debate, especially for what concerns integration of proprioceptive information among the DoFs of a multi-joint articulation.

The goal of the present research is to investigate, using a neuroergonomic approach, the influence of wrist posture on proprioceptive acuity during multi-joint JPM tasks and

under different perturbations. By imposing angular offset rotations in different fashions of amplitude and sequence on the DoF which is not involved in the matching task (PS), we tested proprioceptive acuity on the remaining wrist joints, with the purpose of providing insights on how (i) proprioception is encoded in a complex biomechanical structure, (ii) sensory information are integrated and (iii) external disturbances are rejected.

3.2.2. Experimental Setup, Task and Participants

Eighteen young healthy subjects (age 27.4 ± 2.8 years (mean ± std), 9 females) were recruited for the study: participants self-reported no evidence or known history of neurological disease and exhibited normal joints range of motion and muscular strength. To be included in the study subjects had to be right-handed, according to the Edinburgh Handedness Inventory (Oldfield, 1971) (EHI score > 60; EHI score = 81.89 ± 13.07 (mean ± std)). The research was in accordance with the ethical principles of the 1964 Declaration of Helsinki, which protects research participants. Each subject signed a consent form conformed to these guidelines to participate in the study and to publish pseudonymized individual data. All the study procedures and documents were approved by the Heidelberg University Institutional Review Board (S-287/2020). Experiments were carried out at the Aries Lab (Assistive Robotics and Interactive Ergonomic Systems) of the Institute of Computer Engineering of Heidelberg University (Germany). The experimental design involved a task, where subjects were sitting in front of a screen, holding the handle of a haptic device (WristBot) with their right hand (Figure 12A). Subjects were blindfolded during the whole experiment, but during a phase of familiarization the visual feedback was provided to explain the task sequence and how to perform it correctly.

The employed device has three DoFs: FE (±62°); AA (+45/-40°); PS (±60°) and it allows almost the full range of motion of the human wrist. It is driven by 4 brushless motors dimensioned in order to compensate for weight and inertia and to provide sufficient haptic rendering at the level of wrist. Angular rotations on the three axes are acquired by means of incremental encoders, resulting in a resolution of 0.17°. The continuous torque ranges at the different wrist joints are 1.57 Nm on FE, 3.81 Nm on AA and 2.87 Nm on PS, Figure 12A. During the experiment, participants sat beside the robotic device with the frontal plane of their body aligned perpendicularly to the PS axis of the robotic device, Figure 12B. The position of each participant was carefully adjusted to ensure a 90° elbow angle and the correct alignment between the wrist and the robotic system axes, Figure 12B.

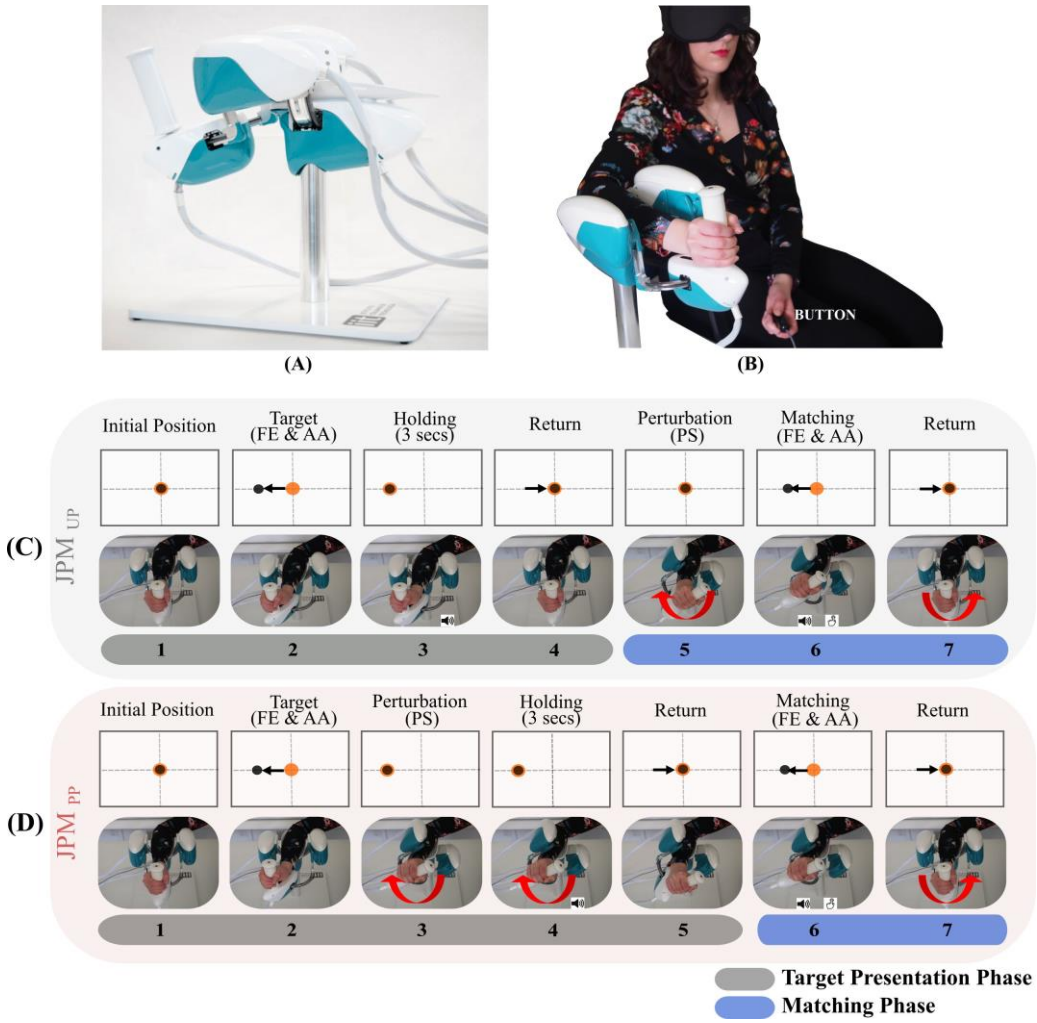

Figure 12: (A) Experimental setup. The subject is comfortably seated on a chair with the right forearm fixed on the Wristbot robotic device while holding its handle. In the contralateral hand the subject holds the button to press during the proprioceptive "Matching Phase". The subject wears a mask over his eyes to perform the experiment based only on his proprioceptive feedback. In the panel (B) and (C) are represented the temporal sequences for the two JPM conditions: *JPMUP* and *JPMPP*. From the initial position the wrist joint is passively moved towards the proprioceptive target (passive reaching) and then maintained for three seconds. An auditory cue marks that the proprioceptive target is reached. After returning to the resting position participants are asked to match the target, as accurate as possible (Matching Phase) by pressing the button with the contralateral hand. Another auditory cue signals to the subject the start of the Passive Matching Phase in which it is required to stop the robot once the same movement amplitude has been perceived. In different temporal moments, depending on the condition experienced, a perturbation is given (angular rotation along the PS axis of a certain random amplitude). This is evidenced by the red arrow in the figure. Orange dot represents the device end-effector position, while the black dot represents the proprioceptive target position.

Participants´ trunk was not constrained, yet the forearm was secured in such a way that backrest ensures a 90° elbow angle, while hand position on the device´s handle was kept constant over the course of the experiment and registered for each participant on her/his anthropometrics. Subjects' forearm was strapped to a mechanical support using anatomical references (i) to ensure repeatability of wrist positioning, thus trying to limit inter-trial variability, (ii) to avoid joints misalignment and (iii) involuntary relative movements between the device and the wrist during task execution. Moreover, the device's

handle was carefully designed to be opportunely adaptable to the different subjects' anthropometrics, by means of a sliding system that allows to secure the forearm on the device.

The protocol has been implemented in order to explore how angular perturbations can affect sensory acuity and consequently altering proprioceptive thresholds. A similar experimental design has been described in (Masia et al., 2009), where, in a point-to-point reaching task, rotational misalignments were applied between the visual (spatial) and the proprioceptive (local) frames, creating a visuo-proprioceptive miscalibration. We wanted to use a comparable paradigm applied to a single sensory feedback by using local rotations among the wrist degrees of freedom by changing the configurations between the presentation of the proprioceptive stimuli (target) and the matching task. In particular, we used the wrist rotation along the PS axis to provide the perturbation in the context of a passive JPM test, which was exploited using the remaining DoFs of the wrist (Goble, 2010; Marini et al., 2016a). The proprioceptive task consisted in an ipsilateral JPM along two DoFs of the wrist (FE and AA): from an initial rest position (0° of FE, 0° of AA and 0° of PS) a preset wrist stimulus or proprioceptive target, corresponding to about 50% of the total functional wrist ROM (Kim et al., 2014), was passively presented to a blindfolded participant, who was then asked to match it, as accurately as possible in a subsequent movement. In particular, these angles were: 32° for FE; 16° for AA (Marini et al., 2016a).
The perturbation delivered to participants during the JPM task consisted in seven pseudo randomized rotations along the PS axis (-45°, -20°, -5°, 0°, +5°, +20°, +45°), at speed equal to 12°/s and in two separate temporal fashions: depending on the time in which the perturbation was given, we distinguished two task conditions named JPM_{UP} (Unperceived Perturbation) and the JPM_{PP} (Perceived Perturbation), which will be explained in detail in the next paragraphs.

Each target set consisted of 48 repetitions (trials) for each of the two DoFs separately (FE and AA), for a total of 96 provided proprioceptive targets. It was divided into 2 sub-sets (20 min each), with a break of about 10 min, to avoid fatigue and loss of concentration.

Each single trial consisted in two separate phases indicated as "*Target Presentation Phase*" and "*Matching Phase*": seven blocks composed the aforementioned phases and are depicted as a breakdown in Figure 12 C-D (in the figure, only test on the FE is illustrated for sake of simplicity). From the initial wrist position (Block 1), the robot moved one DoF

to the preset angular position corresponding to the proprioceptive target or stimulus (Block 2). An *auditory cue* (high-frequency beep) was provided when the robot reached the proprioceptive target: from this block onward, the trial can follow a different order of presentation depending on the two disturbance conditions, as explained as follows.

1. Condition JPM_{UP} (Figure 12C): the current experimental condition is separated in three main events during each trial: *presentation of the proprioceptive target → PS perturbation → matching phase.*

In details, each single trial in such condition started with the wrist of the participant in the physiological neutral configuration (Block 1), then the robot moved the wrist to a *proprioceptive target* (Block 2) along FE (or AA) and maintains such configuration for three seconds (Block 3) (Fuentes and Bastian, 2010). Successively, the subject's wrist is moved back to the initial *rest* configuration (Block 4); At this point a pseudo random *perturbation* around the PS axis (Block 5) was provided. An *auditory cue* indicated the initiation of the *Matching Phase*, where the rotated subject's wrist was passively moved by the robot towards the same direction of the previously presented target (Block 6) on FE (or AA). During this block subjects were instructed to stop the robot motion by pushing a *button* with the contralateral hand as soon as they perceived to have reached a joint amplitude matching the one of the previously presented target. The robot speed was changed respect to the one experienced during the *proprioceptive target* presentation (Block 2), to prevent subjects from relying on the memory time factor during execution of the *matching phase*. At last, the robot drove back the subject's wrist to the initial position prior next trial initiation (Block 7).

2. Condition JPM_{PP} (Figure 12D): contrarily to the previous condition, we had 2 (and not 3) events: *presentation of the proprioceptive target including PS perturbation → matching phase.*

The presentation of the target along FE (or AA) was passively imposed by the robot starting from a rest position (Block 1-2). At this point, contrarily to the previous condition, the pseudo random PS perturbation (Block 3) was presented while maintaining the target presentation on FE (or AA), held for 3 s (Block 4) and successively repositioning FE (or AA) to the rest configuration (Block 5): this was the end of the *Target Presentation Phase*. The *Matching Phase* started with the *passive matching* (Block 6): after an *auditory cue*, subjects were required to stop the robot motion, by pressing the button in the contralateral hand once the same movement amplitude has been perceived. Immediately after pressing

the button, the robot brought the subjects wrist back again to the initial position for the next trial (Block 7).

Subjects were instructed to focus only on the location of the proprioceptive target and try to reject the effect of the perturbation along the PS axis during the *Matching Phase*. They did not receive any feedback about their performance, to eliminate a possible recalibration of the responses during the test. Across two days of testing (day 1 and day 2), participants were required to perform the task in a randomized order for the two conditions JPM_{UP} (day 1 or day 2) and JPM_{PP} (day 1 or day 2).

3.2.3. Data Analysis and Outcome Measures

Wrist joint rotations were recorded by means of the digital encoders of the WristBot (data collection frequency set at 100 Hz). Data were filtered offline using a 3rd order Savitzky–Golay low-pass filter (cut-off frequency of 10 Hz). For each condition, as a measure of the overall accuracy, we computed two indicators: the *error bias* and the *matching error* (Schmidt et al., 1988).

- The *error bias* ([°]), is the mean, over N repetitions for the same proprioceptive target (same DoF and disturbance condition), of the signed difference between the presented proprioceptive target location (ϑ_{target}) and the wrist position at the end of the matching task movement (ϑ_i). It indicates the subject's tendency to overshoot (positive *error bias*) or undershoot (negative *error bias*) the target after the *Matching Phase*. For a consistent interpretation, we transformed the signed *error bias* to a measure of a signed overshoot, $error\ bias_{\ OS}$ (Galofaro et al., 2019):

$$error\ bias_{\ OS} = \text{sign}(\vartheta_{target}) * \frac{\sum_{i=1}^{N}(\vartheta_i - \vartheta_{target})}{N} \quad (6)$$

where ϑ_i is the measured value at the end of the *i-th* trial, ϑ_{target} is the target position. In this metrics, negative values represent an undershoot, while positive values represent an overshoot independently of the sign of the target.

- The *matching error* ([°]), evaluates the accuracy during the *Matching Phase* and it is defined as the absolute value of the difference between the ϑ_i and the ϑ_{target} averaged over N repetitions of the same target in the same disturbance condition:

$$matching\ error = \frac{\sum_{i=1}^{N}|\vartheta_i - \vartheta_{target}|}{N} \quad (7)$$

Statistical Analysis

Data normality distribution was assessed using Shapiro-Wilk test, and sphericity condition for repeated measures analyses of variance (rANOVA) was assessed using the Mauchly test. The first test was always verified: when the second was violated, we applied the Greenhouse-Geisser correction. The three-way repeated measures ANOVA test was used to examine the effects, on the dependent variables (*error bias*, *matching error*) of the robot rotation around the PS axis, the DoF and the tasks condition, using three within-subject factors: (i) 'condition' (2 levels: JPM_{PP} and JPM_{UP}), (ii) 'PS perturbation' (7 levels: -45°,-20°, -5°, 0°, 5°, 20°, 45°), (iii) 'DoF' (2 levels: AA and FE) and their interaction. A post-hoc analysis was performed using Paired t-tests to evaluate the significant pairwise differences between each perturbation, DoF and condition. For all the tests, the level of statistical significance was set at 0.05, except for post-hoc analysis, where the significance level was chosen according to the Bonferroni correction for multiple comparisons. Statistical analysis was conducted by using IBM SPSS Statistics 23 (IBM, Armonk, New York, USA).

3.2.4. Results

Comparison between JPM_{UP} and JPM_{PP}.

Figure 13 shows the comparison between the two disturbance conditions (JPM_{UP} Vs JPM_{PP}) in terms of the *error bias* (A) and the *matching error* (B). As evidenced also by the rANOVA results, for both outcomes, we did not find any significant difference between the two conditions (JPM_{UP} Vs JPM_{PP}; *error bias:* F=0.986, p=0.329; *matching error*: F=1.424, p=0.211). *Error bias* and *Matching Error* indicated that the performance, averaged across all subjects and independently on the investigated DoF (FE and AA), it's closely distributed along the *equality line*, demonstrating that the process underlying encoding of proprioceptive target is not influenced by the order of rotation of the reference frames between *target presentation* and *matching movement*. Moreover, the same behavior persists across all the spanned values of the PS perturbation.

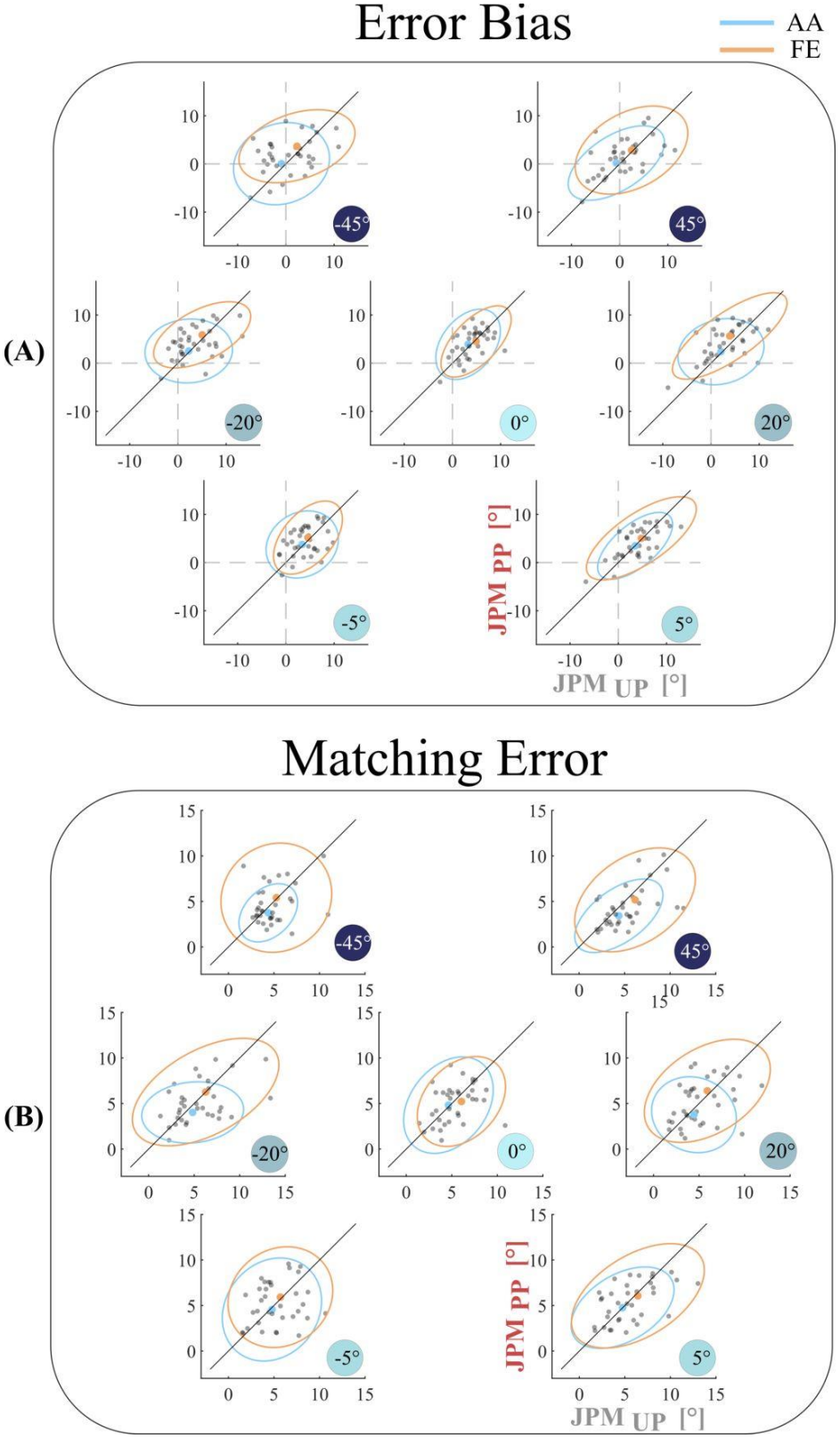

Figure 13: Comparison between the two experimental conditions (JPM_{UP} versus JPM_{PP}) for the (**A**) *Error Bias* and for the (**B**) *Matching Error* outcomes for AA (light blue) and FE (orange) DoFs. Each grey point represents the average result for a single subject. The mean result across the population is reported as light blue point for AA and orange point for FE joint. The line through the origin (equality line) is represented by a black line; if the subject performance stays above this line the error is higher for the JPM_{PP} task, vice versa if it stays under the line.

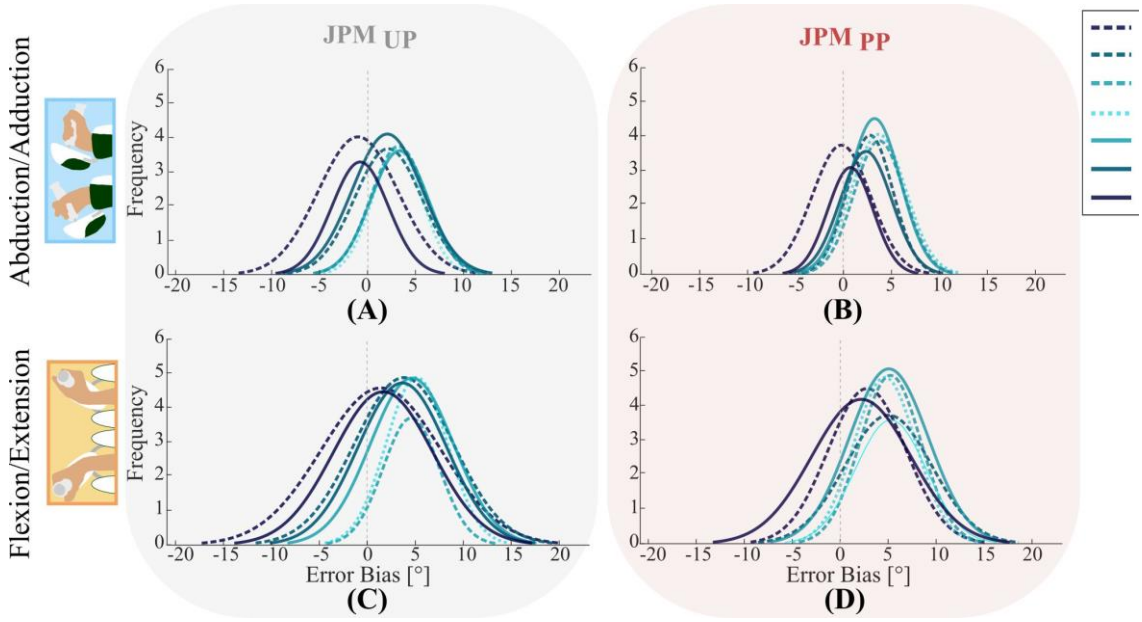

Figure 14: Probability density distributions for the Error Bias of the two DoFs AA (**A** and **B**) and FE (**C** and **D**) in both the JPM_{UP} (first column) and JPM_{PP} (second column) conditions. Coloured lines show the mean distribution for the specific perturbation denoted in the legend. The vertical dotted line highlights the error equal to zero, a distribution shifted to the left indicates error undershooting, while a distribution shifted to the right represents a tendency of target overshooting.

Effects of pronation/supination disturbance on over- and under-shooting the proprioceptive targets

The trend of the subjects to overshoot or undershoot the angular position of the proprioceptive target during the *Matching Phase* was examined by analyzing the probability density distribution of the *error bias* for across the two investigated DoFs FE and AA (Figure 14).

We evaluated the distribution for the 7 amplitude pseudo-random perturbations along PS and for both the JPM_{UP} and the JPM_{PP} conditions. The tendency to overshoot the proprioceptive target during the matching task was higher for low amplitude PS perturbations, rather than for the largest ones (-45° and +45°) in both tested DoFs (FE and AA). As previously reported, also in this metric the two conditions (JPM_{UP} and JPM_{PP}) did not influence the *error bias*. Task execution along the AA axis (Figure 14A-B) shows a tall narrow distribution mainly shifted to the right side for the perturbations which are closer to the physiological neutral posture of the wrist ($0°, \mp 5°, \mp 20°$). For large PS perturbations ($\mp 45°$), the distributions were mainly centered around zero *error bias*, indicating a better matching performance of the proprioceptive target. As for the FE task, the results were similar, although characterized by a less distinct, behaviour: for both the

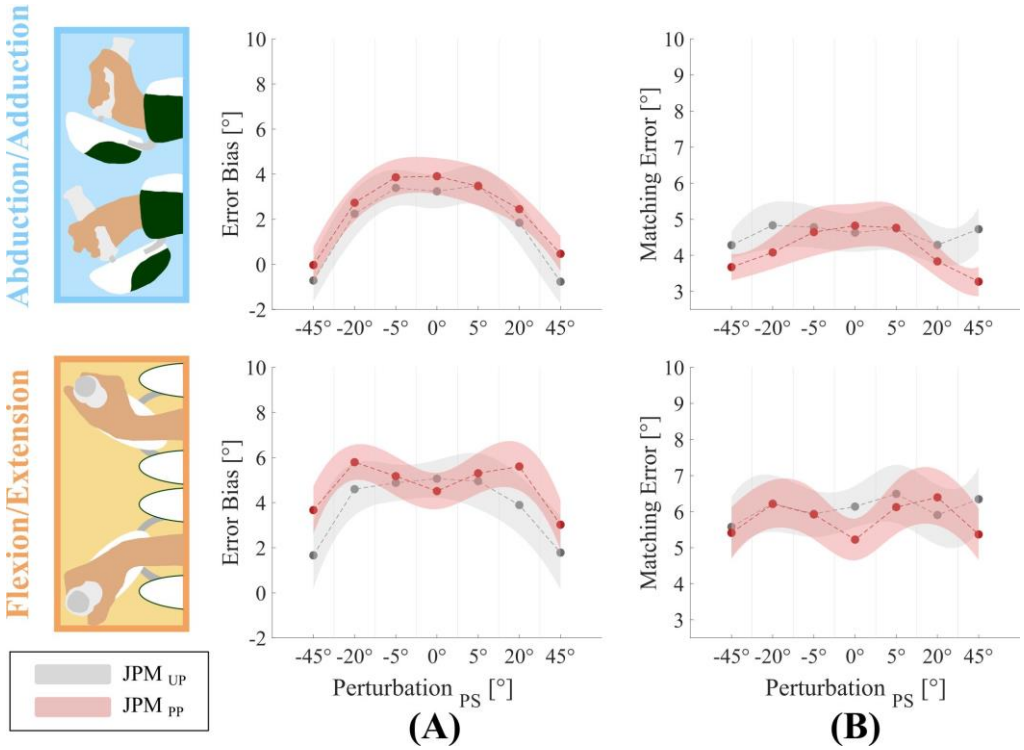

Figure 15: Outcome measures relative to the two DoFs: AA on the top and FE on the bottom for JPM_{UP} (grey) and JPM_{PP} (magenta) conditions. First column represents the *Error Bias* (**A**). Second column is relative to the *Matching Error* (**B**). On the x-axis is evidenced the amount of angular perturbation provided along the PS axis (-45°, -20°, -5°, 0°, 5°, 20°, 45°) during the experiment.

target presentation conditions (Figure 14C-D) subjects tended to overshoot the proprioceptive targets, but with a more accurate matching for those perturbations at the boundaries of the workspace ($\mp$45°), rather than in configurations (0°, $\mp$5°, $\mp$20°) close to the neutral position of wrist.

The aforementioned differences related to *Error Bias* were confirmed by the rANOVA highlighting a significant effect of the PS perturbation ($F=22.939$, $p<0.001$), and DoF ($F=37.199$, $p<0.001$), but not their interaction effect ('PS perturbation* DoF' effect $F=1.198$, $p=0.312$).

We statistically inferred the role of PS perturbation amplitude by a paired t-test post-hoc analysis for the *Error Bias,* and it revealed multiple significant differences (see Table 2). In particular, for all perturbations' amplitudes with the exception of the case related to the DoF FE and the condition JPM_{PP}, we found an overshoot inversely proportional to the PS amplitude as visible by a bell shape graph (Figure 15A).

At last, a post-hoc analysis between the two tested DoFs, is reported in Table 3 for the *Error Bias* outcome: we found a significant difference between FE and AA for all the perturbations except for the condition JPM_{PP} at 0° of PS. In particular, subjects presented a larger overshoot along the FE DoF, for all the perturbations and conditions.

Proprioceptive anisotropy related to the perturbation amplitude

In order to explore the distribution of proprioceptive acuity over the different PS perturbation amplitudes and across the two DoFs, we analyzed the *Matching Error* trend (Figure 15B).

The rANOVA showed on *Matching Error* showed a significant main effect of the DoF (FE Vs AA) ($F=44.695$, $p<0.001$) as well as of the PS perturbation amplitude ($F=3.025$, $p=0.008$). Detailed numerical outcomes of the post-hoc analysis across the two DoFs are reported in Table 4.

Again, on the *Matching Error*, a significant difference between FE and AA was found for almost all the perturbations with the exception of 0° for the JPM_{PP} and -45° for the JPM_{UP}. In particular, for both the conditions JPM_{UP} and JPM_{PP} and for all the PS amplitudes, subjects showed a larger *Matching Error* along the FE than the AA (Table 4), indicating an anisotropy of proprioceptive acuity across two DoFs which persists independently on the provided perturbations.

The post-hoc analysis between PS amplitudes for the *Matching Error* are reported in Table 5 and highlighted significant differences for the JPM_{PP} and the AA DoF. For all perturbations' amplitudes, we found a proprioceptive error inversely proportional to the PS amplitude as visible by a bell shape graph, Figure 15B. For large PS perturbations ($\mp 45°$), results show a better matching performance of the proprioceptive target.

		JPM_{UP}		JPM_{PP}	
PS [°]		**p (AA)**	**p (FE)**	**p (AA)**	**p (FE)**
45					
	20	<0.001*	0.007*	<0.001*	<0.001*
	5	<0.001*	<0.001*	<0.001*	0.003*
	0	<0.001*	<0.001*	<0.001*	0.008*
	-45	0.558	0.877	0.389	0.532
	-20	<0.001*	0.012*	0.002*	0.002*
	-5	<0.001*	0.001*	<0.001*	0.001*
20					
	5	0.007*	0.026*	0.015*	0.636
	0	0.011*	0.015*	<0.001*	0.200
	-45	<0.001*	0.013*	<0.001*	0.001*
	-20	0.721	0.614	0.884	0.355
	-5	0.011*	0.169	0.001*	0.838
5					
	0	0.569	0.430	0.245	0.171
	-45	<0.001*	<0.001*	<0.001*	0.01*
	-20	0.043*	0.284	0.186	0.734
	-5	0.796	0.909	0.213	0.855
0					
	-45	<0.001*	<0.001*	<0.001*	0.017*
	-20	0.05	0.155	0.020*	0.270
	-5	0.705	0.426	0.863	0.136
-45					
	-20	<0.001*	<0.001*	0.001*	0.002*
	-5	<0.001*	0.001*	<0.001*	0.006*
-20					
	-5	0.016*	0.620	0.005*	0.891

Table 2: Statistical p-values for the error bias across the seven perturbations.

	UP		PP	
PS [°]	**Mean ± SD [°]**	**p**	**Mean ± SD [°]**	**p**
-45	**-0.72±4.09**	0.016*	**0.39±3.06**	<0.001*
	1.66±6.21		3.76±4.55	
-20	**2.24±4.40**	0.002*	**3.31±3.06**	0.002*
	4.59±4.92		5.84±3.19	
-5	**3.39±3.42**	0.004*	**3.51±3.18**	0.035*
	4.88±3.45		5.05±3.65	
0	**3.24±3.22**	<0.001*	**3.65±3.32**	0.197
	5.06±3.54		4.51±3.42	
5	**3.50±3.67**	0.034*	**3.26±3.55**	0.010*
	4.95±5.23		5.30±3.85	
20	**1.84±4.05**	0.013*	**2.36±3.17**	<0.001*
	3.89±5.56		5.33±4.28	
45	**-0.77±4.10**	0.018*	**0.76±3.03**	0.007*
	1.78±6.90		3.02±4.74	

Table 3: Statistical p-values for the error bias between the two DoFs (AA/FE).

	UP		PP	
PS [°]	**Mean ± SD [°]**	**p**	**Mean ± SD [°]**	**p**
-45	**4.81±2.65**	0.053	**3.67±1.55**	0.001*
	5.95±4.00		5.68±3.10	
-20	**4.83±2.72**	0.012*	**4.18±1.97**	<0.001*
	6.45±3.55		6.73±3.05	
-5	**4.78±2.42**	0.014*	**4.64±2.79**	0.008*
	5.94±2.73		6.14±3.11	
0	**4.63±2.80**	<0.001*	**4.82±2.56**	0.128
	6.50±3.54		5.59±2.83	
5	**4.75±2.59**	0.005*	**4.76±2.63**	0.002*
	6.49±3.44		6.62±3.47	
20	**4.53±2.64**	0.022*	**3.75±1.86**	<0.001*
	5.91±3.52		6.15±3.03	
45	**4.13±2.04**	0.005*	**3.36±1.74**	<0.001*
	6.22±3.73		5.84±3.31	

Table 4: Statistical p-values for the matching error between the two DoFs.

		JPM_{UP}		JPM_{PP}	
PS [°]		**p (AA)**	**p (FE)**	**p (AA)**	**p (FE)**
45					
	20	0.377	0.473	0.145	0.114
	5	0.296	0.813	0.023*	0.152
	0	0.351	0.987	0.008*	0.860
	-45	0.409	0.323	0.478	0.810
	-20	0.312	0.863	0.061	0.160
	-5	0.318	0.522	<0.019*	0.246
20					
	5	0.666	0.198	0.020*	0.963
	0	0.724	0.300	0.002*	0.120
	-45	0.828	0.770	0.766	0.099
	-20	0.526	0.513	0.456	0.711
	-5	0.527	0.946	0.027	0.741
5					
	0	0.754	0.802	0.854	0.09
	-45	0.458	0.245	0.031	0.058
	-20	0.866	0.635	0.182	0.975
	-5	0.926	0.194	0.947	0.793
0					
	-45	0.483	0.577	0.028	0.805
	-20	0.620	0.977	0.067	0.104
	-5	0.613	0.332	0.804	0.083
-45					
	-20	0.328	0.245	0.200	0.074
	-5	0.350	0.692	0.069	0.131
-20					
	-5	0.883	0.483	0.157	0.861

Table 5: Statistical p-values for the matching error across the seven perturbations.

3.2.5. Discussions and Conclusions

Understanding how proprioceptive information is encoded at distal joints, has multiple intersections across different fields involving physiology, motor learning, sensorimotor recovery as well as those applications in haptics where proprioception is predominantly involved in a robot mediated manipulation. In rehabilitation practice, it is a common opinion among clinicians that current proprioceptive assessment fails in providing a reliable and quantitative information which would allow to compare motor and sensory deficits, known to be complementary information to a comprehensive diagnosis of the recovery process. However, authors usually focus on motor recovery (Soekadar et al., 2019) while not many evidences can be found in literature on the physiology of proprioception involving distal joints at the level of hand and wrist, despite they are anatomical districts covering an essential role in manual handling, and being the joints mostly involved in fine manipulation and exploitation of human dexterity, which is still unmatched in nature among species (Hoseini et al., 2015; Moser et al., 2020). With this in mind, we wanted to provide further evidence that using haptics, proprioceptive acuity can be accurately and geometrically characterized across the wrist's DoFs, synergistically involved during motor coordinated activities.

Hence, we decided to investigate if perturbations along one wrist joint (PS), can significantly alter the mechanism underlying perception of proprioceptive information on the adjacent DoFs (FE and AA). Outcomes revealed multiple aspects, which, to our knowledge have never been reported in previously published contributions, for the reason that most of the literature on proprioception primarily focused on proximal joints – shoulder and elbow – and privileged research on influence and role of multisensory integration in goal directed movements. Another reason for such lack of results, is the affordability of complex haptic devices, which not only assume operators able to skillfully program and run specific tailored physiological tests, but also they must be designed in such a way to provide robust and accurate position/force rendering and at the same time perform as reliable measurement systems.

By introducing a different order of presentation of the proprioceptive targets and disturbance input, we tried to understand if proprioceptive information is stored by the central nervous system in an absolute or relative coordinates frame. In our hypothesis the rotation of the reference system during or after the presentation of a target could have affected the final performance. Results clearly highlighted that mechanisms underlying the

encoding of a proprioceptive target does not depend on the temporal order of the superimposed geometrical conditions; subjects are, in fact, able to store sequence of joints' configurations and to replicate, with the same accuracy, a previously experienced proprioceptive target independently on the initial conditions in which the target is presented and encoded.

We also found that proprioceptive acuity varies across DoFs: previously published works (Cappello et al., 2015; Marini et al., 2016a) experimentally demonstrated the existence of wrist proprioceptive anisotropy among its DoFs. Marini et al. (Marini et al., 2016a) provided a map of the wrist position sense across each DoF, by means of the same robotic device used in our study, observing that wrist AA has a higher proprioceptive acuity respect to the remaining DoFs. Our results are in accordance, but also provide a wider perspective, reporting evidence that proprioception at the distal and multi-joint level, might be highly influenced by the mutual configuration between the DoFs composing the wrist anatomical joint, when the provided proprioceptive targets differ in amplitude across each DoF.

In details, the quantification of wrist anisotropy across its workspace and the dependence on initial posture, demonstrate that our peripheral sensory system tunes its sensitivity depending on geometric conditions and independently from the order of their presentation. Results clearly show a higher proprioceptive acuity for large perturbation amplitude, when the pronation supination (PS) was rotated $\mp 45°$. We found the lowest value of the *Matching Error* for both AA and FE when the maximum wrist PS perturbation of $\mp 45°$ was applied, unexpectedly meaning that the neutral physiological posture of the forearm (zero rotation of the PS) is not a configuration which enables the best proprioceptive sensitivity. This effect finds its explanation when considering the mutual relationship between the activation of the mechanoreceptors, the anatomical structures of the muscular and connective tissues that are instrumental in proprioceptive coding (van der Wal, 2009). The aforementioned parts cannot be divided into either joint receptors or muscle receptors when muscular and connective tissues work in series to maintain joint integrity and stability: this happens at the boundary of their workspace.

It is known that joint receptors are highly reactive at the extremes of joint workspace (Ferrell et al., 1987), when the joint capsule is significantly stressed (McCloskey, 1978b), for example (in our experiment) when the wrist is rotated at $\mp 45°$ along PS axis. The activation of the joint receptors, induced by the connective tissues after

the changes in muscle tension, occurs at the limits of wrist' range of motion (van der Wal, 2009), and it might be responsible for the high proprioceptive acuity.

In our study there are anyway limitations: the first concerns the small sample of subjects included in our experimental sessions. Another limitation mostly refers to the number of trials provided for each DoF, which has been limited in order to avoid longer sessions with consequent loss of attention from the subjects. In order to deeply correlate joint- and mechano-receptor activation, proprioceptive acuity and perturbations, other measurements, such as surface electromyography (Mugnosso et al., 2018), could have been included in order to highlight the physiological aspects in terms of bio signals and not merely relying on kinematic data extracted by the haptic device. At last, since the current study investigates the influence of static wrist posture variation on proprioceptive acuity, future research could explore how sensory information is coded when time-variable dynamic conditions are provided.

We also mentioned in the introduction the possible application of the proposed paradigm for clinical settings: we believe that using a neuroergonomic haptic technology for quantification of sensory impairment is a viable option. Our approach was meant to analyze the proprioceptive anisotropy across the different DoFs of the wrist workspace, in particular for healthy subjects. Yet the methodological approach must be tailored in such a way to design a more compact test which can be dispensed on patients where physiological conditions are unpredictably variable and heterogeneous.

Conclusions: This study aims at providing a wider and more comprehensive view on the physiological aspects influencing proprioception in the complex multi-joint articulation of the human wrist by means of a neuroergonomic robotic technology.

The outcomes are of interest for multiple disciplines: in neuroergonomics and medicine, for instance, the tests assessing sensory system's integrity, must be performed considering that different postural conditions may alter proprioceptive acuity. Testing patients' proprioception in a configuration which is close to the joints' physiological workspace limits, may increase mechanoreceptors excitation and provide a fine measurement of sensory acuity.

In haptics, especially for those applications where telemanipulation of real or virtual objects are mediated by robotic devices (robot aided surgical intervention), small movement of the master can be better perceived and controlled by the operator if her/his

proprioception is set to a high sensitivity level and therefore in a posture with is proximal to the physiological boundaries of the joints' workspace.

3.3. Three-Dimensional Assessment of Upper Limb Proprioception via a Wearable Exoskeleton[3]

3.3.1. Introduction

Proprioception can be defined as the awareness of body segment positions and movements in the surrounding space (McCloskey, 1978a). Any change regarding a body district's configuration activates mechanoreceptors located in joints, muscles, and tendons (Riemann and Lephart, 2002b). A key role in providing proprioceptive signals is played by the muscle spindles, the Golgi tendon organs, and the stretch receptors (Proske and Gandevia, 2012). All the proprioceptive processes that promote awareness of body segment's position are critical for the control of complex movement as well as posture (Schmidt, 1988).

Neurological injuries can significantly alter or deprive the central nervous system of peripheral sensory information (Langhorne et al., 2009), leading to a deterioration of the body awareness (Debert et al., 2012) and of the capacity to perform even a simple movement (Mochizuki et al., 2019). With neuropathies, despite gross motor functions are preserved (Schabrun and Hillier, 2009), yet considerable sensorimotor deficits can persist (Goble, 2010).

In regular clinical practice, proprioceptive impairments receive less attention than motor deficits (Findlater et al., 2019), and are usually quantified through clinical scales (Fugl-Meyer Assessment Scale (Gladstone et al., 2002) and Nottingham Sensory Assessment scale (Lincoln et al., 1998)), lacking in accuracy, precision, and reliability (Lincoln et al., 1991; Connell and Tyson, 2012), and leading to incongruences and low agreement with clinical results obtained from imaging studies (Findlater et al., 2019).
Scientific literature reports several attempts to provide quantitative measurements of proprioception (Fuentes and Bastian, 2010; Wilson et al., 2010; Cressman and Henriques, 2011; Kenzie et al., 2017; Mrotek et al., 2017): Dukelow et al. adopted a planar robotic exoskeletal arm to quantify proprioception after stroke in a *bidimensional workspace* (2D) by means of a classic position matching task paradigm (Dukelow et al., 2009, 2012). They

[3] The whole content of this Chapter has been published on *Applied Sciences* as: E. Galofaro*, E. D'Antonio*, F. Patané, M. Casadio and L. Masia. "*Three-dimensional Assessment of Upper Limb Proprioception via a Wearable Exoskeleton"* (2021).

passively moved the patients´ impaired arm towards a target position, and successively asked them to mirror with the contralateral arm. Results provided evidence that proprioceptive sensitivity depends on both the arm's configuration and the movement direction. Other contributions (Bergenheim et al., 2000; Roll et al., 2000; Jones et al., 2001) found that muscle spindles are sensitive to movements in different directions which are highly specific: each muscle shows a maximum sensitivity to a particular movement direction, i.e., the preferred sensory direction.

Further studies have shown that the central nervous system programs movements considering the gravity acting on the limb: arm kinematics changes for movements performed across different directions along the *vertical axis* (i.e., going upward or downward), coherently with the optimization of both inertial and gravitational forces (Papaxanthis et al., 2003; Le Seac'h and McIntyre, 2007; Berret et al., 2008). Hence, in a three-dimensional workspace, proprioceptive sensitivity could be modulated by gravity's effects on the arm configuration.

Sketch et al. (Sketch et al., 2018) used a planar robotic arm to analyse proprioceptive acuity in single-joint and multi-joint tasks, focusing on the elbow, shoulder, and hand, still limited to a 2D planar workspace.

Only recently, authors started to treat the evaluation of proprioception across a three-dimensional (3D) space: Marini et al. (Marini et al., 2016a) characterized the wrist proprioception by considering each of the three degrees of freedom (DoFs), showing changes in proprioceptive acuity across different directions. Similarly, other researchers (Klein et al., 2018; Valdés et al., 2019, 2020; D'Antonio et al., 2021) started investigating how proprioception varies when single or multiple joints are involved in a motion task. However, in the latter cases, their evaluation was only conducted by analyzing the final arm position, by means of end-effector devices.

Recent advancements in exoskeleton's design provide the possibility of implementing proprioceptive paradigms involving a full-human range of motion, complementing with many DoFs to precisely determine the joint position (Fitle et al., 2015; Blumenschein et al., 2017; Sui et al., 2017; Gupta et al., 2020). Exoskeletons exhibit numerous advantages compared to the end-effector robots, in particular for upper limb proprioceptive assessment: they offer the possibility of implementing three-dimensional tasks, following the arm's natural workspace, and enabling for independent or simultaneous movement of the shoulder, elbow, and wrist joints.

Based on the references above, it is a consolidated opinion that proprioception is fed back considering both direction of motion and final arm configuration, and given the lack of studies that evaluate proprioceptive acuity along every single arm joint in a 3D-workspace, we decided to develop a spatial task for the assessment of proprioception, using a 6 DoFs bimanual exoskeleton, ALEx-RS (Pirondini et al., 2016; Frisoli, 2018). Our protocol enables quantifying single and multi-joint position sense, involving an active matching movement of each upper limb.

The purpose of this study was to evaluate the *sensorimotor* contribution in single- or multi-joint arm movements (*shoulder abduction/adduction*, *shoulder flexion/extension,* and *elbow flexion/extension)* in healthy subjects, using an ipsilateral joint position matching (JPM) test. We aim at understanding (i) how proprioceptive acuity changes along the arm moving from proximal body joints to the distal ones; (ii) how the human nervous system decodes the simultaneous activation of more than one body joint (multi-joint).

3.3.2. Experimental Setup, Task and Participants

A group of eighteen healthy and right-handed subjects (8 females and 10 males, 27.94±3.83 (mean ± std) years old, range: 22-33 years) participated in this study. In the group, there was no significant difference in the age distribution between males and females. For all subjects, we evaluated the handedness through the Edinburgh Handedness Questionnaire (Oldfield, 1971) (Laterality score (LS) = 81.89 ± 13.07 (mean ± std), right-handed if LS > 60). All participants provided their informed consent. The experimental protocol was approved by the Heidelberg University Institutional Review Board (S-287/2020), and the study was conducted in accordance with the ethical standards of the Declaration of Helsinki. Experiments were carried out at the Aries Lab (Assistive Robotics and Interactive Exosuits) of the University of Heidelberg, Germany. Subjects self-reported no evidence or known history of neurological diseases and exhibited a normal joint range of motion and muscle strength.

The experimental design involved a task where subjects worn the bimanual Arm Light Exoskeleton Rehab Station ALEx-RS (Pirondini et al., 2016; Frisoli, 2018), shown in Figure 16A. An initial phase was run before starting the experiment to allow participants to familiarize with the device and its dynamics. Subjects wore a mask over their eyes to occlude vision during the whole experiment.

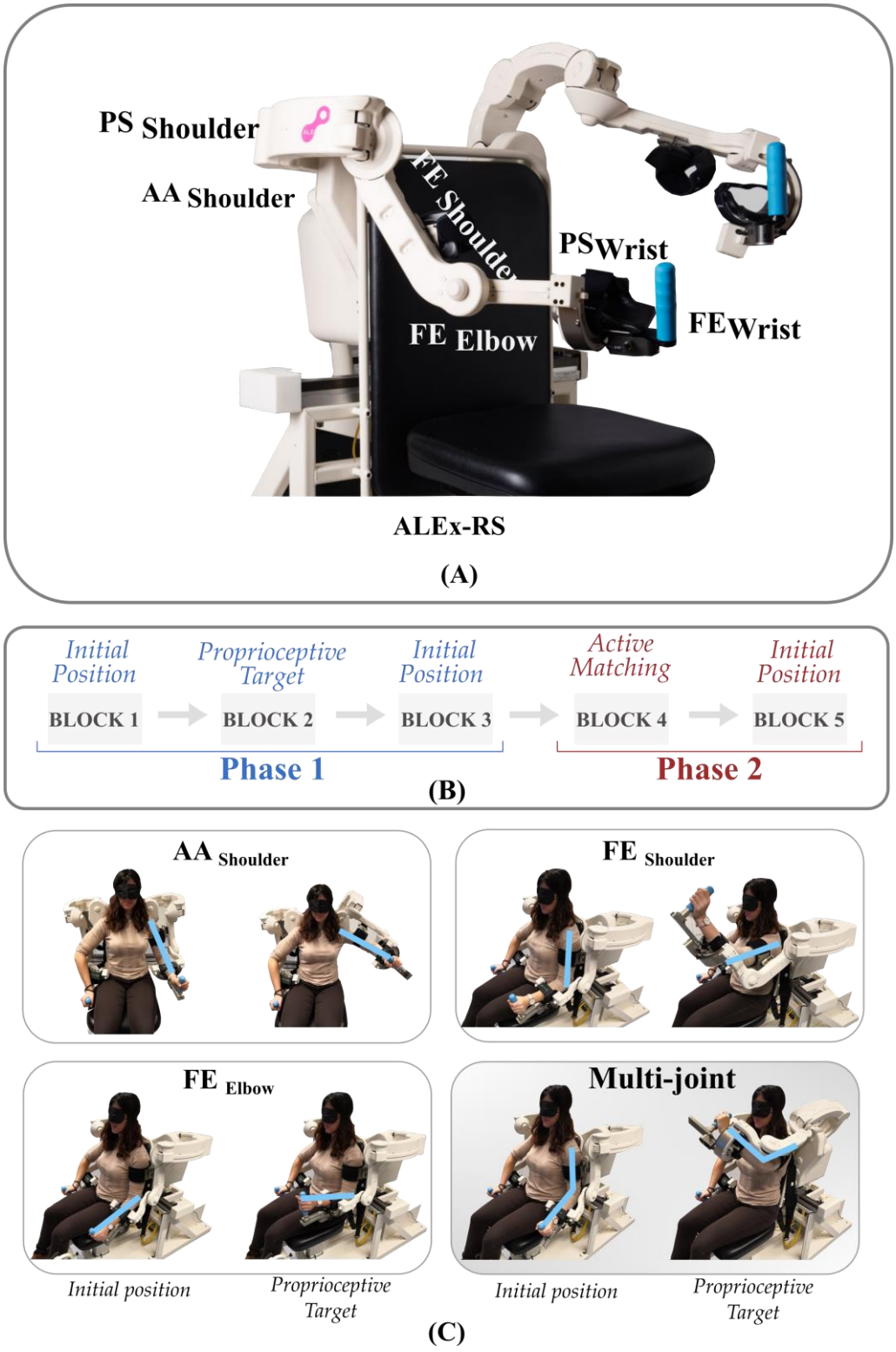

Figure 16: (**A**) Bimanual ALEx-RS device. (**B**) Block sequence presented to the participants during the ipsilateral JPM task. (**C**) Task representation: participants sat on the workstation chair wearing one of the robotic exoskeletons, depending on the tested body side. They were requested to grasp a pressure-sensitive handle of the contralateral exoskeleton (non-tested side). On the top left is illustrated the single joint (*SJ*) condition for the $AA_{Shoulder}$, on the top right for the $FE_{Shoulder}$, on the bottom left for the FE_{Elbow}. On the bottom right is illustrated the multi-joint (*MJ*) condition. For all conditions is shown the *Initial Position* on the left and the *Proprioceptive Target* position on the right.

The device consists of two identical robotic exoskeletons with 6-DoFs for each side. Four DoFs are sensorized and actuated: shoulder abduction/adduction ($AA_{Shoulder}$), shoulder pronation/supination ($PS_{Shoulder}$), shoulder flexion/extension ($FE_{Shoulder}$) and elbow flexion/extension (FE_{Elbow}); the other two DoFs are only sensorized: wrist pronation/supination (PS_{Wrist}) and wrist flexion/extension (FE_{Wrist}). The latter was blocked during the experiment to avoid uncontrolled movements.

The range of motion (ROM) of each exoskeleton can approximately cover 92% of the upper limb workspace: the system is powered by a tendon-driven transmission system with low inertia and makes the overall structure highly transparent. Four brushless motors provided maximum torque values of 35 Nm for both $AA_{Shoulder}$ and $PS_{Shoulder}$, 25 Nm for $FE_{Shoulder,}$ and 20 Nm for FE_{Elbow}.

The controller of the device includes the possibility to use the workstation in 3 modalities: i) *passive*, in which the subject individually moves her/his arms in a back driveable dynamic mode, ii) *assistive*, in which the robot drives the upper limbs during the task execution, and iii) *"assisted-when-needed*", in which the robot guides the user's arm when she/he is not able to initiate movements exceeding a time threshold. In all modalities, the exoskeletons provide gravity and friction compensation, and the inertia is mostly cancelled by an inverse dynamic model running during operation and perceiving the user´s motion by the absorbed currents from the motors In the framework of the current contribution, an impedance control has been adopted to allow the user to actively match the imposed target and being passively guided by the robot during the target presentation as described in the following section.

During the experiment, participants sat on the workstation chair wearing one of the robotic exoskeletons, depending on the tested body side. They were requested to grasp a pressure-sensitive handle of the contralateral exoskeleton (non-tested side). Arms and forearms were firmly strapped to ensure arm positioning's repeatability and limit inter-trial variability and undesired relative movements during the experiment.

The proprioceptive test consisted of an ipsilateral JPM task (Goble, 2010), involving a single trial with two main phases (Figure 16B):

1. *Phase 1* or "Stimuli Presentation" in which the blindfolded user 'arm was passively moved by the exoskeleton from an *Initial Position* ($AA_{Shoulder}$: 10°, $FE_{Shoulder}$: 5° and FE_{Elbow}: -40°) to a *Proprioceptive Target* ($AA_{Shoulder}$: 60°, $FE_{Shoulder}$: 80° and FE_{Elbow}: -10°). An auditory cue (high-frequency beep) was provided when the robot

reached the *Proprioceptive Target.* Successively, after the target presentation, the robot moves back the users´ arm to the initial posture (block 3).

2. *Phase 2* or "Active Matching" initiated by a sound and required the subjects to match, as accurately as possible, the previously experienced stimuli by actively moving her/his arm: this was possible because the exoskeleton was set in a transparent modality, i.e., without applying any force. Participants could stop the trial when matched position by squeezing the handle held in the contralateral hand (*Block* 4). After each trial's completion, the robot drove back the subject*'*s arm to the initial position before initiating the next trial (*Block* 5*),* Figure 16B.

We tested the proprioceptive acuity in two different modalities:

- *Single Joint* (*SJ*): only one of the three examined degrees of freedom was independently tested for JPM task ($AA_{Shoulder}$ or $FE_{Shoulder}$ or FE_{Elbow}) (Figure 16C top).
- *Multiple Joints* (*MJ*): proprioceptive targets were presented by moving all the three degrees of freedom in a multi-joint fashion ($AA_{Shoulder}$ + $FE_{Shoulder}$ + FE_{Elbow}) (Figure 16C bottom).

The whole experimental session included four target sets *(*3 *SJ* and 1 *MJ)* for both left and right arms, which were pseudo-randomly distributed across participants in order to avoid possible target sequence effects. Each target sets counted 10 proprioceptive target presentations and the relative matching tasks. A total of 80 trials (30 *SJ* +10 *MJ* distributed on the two arms) were administered to each subject, with a 5-minute break between each target set, for a total duration of about 1 hour for the whole experiment.

3.3.3. Data Analysis and Outcome Measures

Data were saved at 100 Hz frequency. Recorded joints´ positions were offline filtered using a 3rd order Savitzky–Golay low-pass filter (cut-off frequency of 10 Hz).

Proprioceptive performance was computed by using three kinematic indicators evaluated on the N repetition across each experimental condition (*SJ* and *MJ*):

- The *Matching Error*, which analyses performance accuracy, by computing the average of the absolute error between the proprioceptive target position ϑ_{target} and the arm configuration ϑ_i:

$$Matching\ Error = \frac{\sum_{i=1}^{N} |\vartheta_i - \vartheta_{target}|}{N}. \quad (8)$$

- The *Error Bias* (Schmidt, 1988) evaluates the overshoot and undershoot during the matching task by considering the signed error between the presented proprioceptive target location (ϑ_{target}) and the final position (ϑ_i) at the end of each trial (Galofaro et al., 2019):

$$Error\ Bias_{\ OS} = \text{sign}(\vartheta_{target}) * \frac{\sum_{i=1}^{N} (\vartheta_i - \vartheta_{target})}{N}. \quad (9)$$

Both metrics have been expressed as percentage (%) of the distance between the *Initial Position* and the *Proprioceptive Target* which varied for each DoF considered ($\Delta\vartheta\Delta\vartheta$=50° for $AA_{Shoulder}$, $\Delta\vartheta\Delta\vartheta$=75° for $FE_{Shoulder}$ and $\Delta\vartheta\Delta\vartheta$=30° for FE_{Elbow}). The target amplitudes were chosen to reproduce in the MJ condition a typical functional gesture of daily activities, maintaining a percentage of about 30% of the total functional ROM for each DoF.

Statistical Analysis. Data normality was evaluated using the Shapiro-Wilk test, and sphericity condition for repeated measures analyses of variance (rANOVA) was assessed using the Mauchly test. The rANOVA test was used to examine the effects of the upper limb condition, the DoF, and the body's side on the dependent variables (*Error Bias*, *Matching Error*). We considered three within-subject factors: (i) 'condition' (2 levels: *SJ* and *MJ*), (ii) 'DoF' (4 levels: $AA_{Shoulder}$, $FE_{Shoulder}$, FE_{Elbow}, and *MJ*), (iii) 'Side' (2 levels: left and right) and their interaction. A post-hoc analysis was performed using the paired t-tests to evaluate the significant pairwise differences between each perturbation, DoF, and condition. For all the tests, the statistical significance level was set at 0.05, except for post-hoc analysis, where the significance level was reduced to 0.004 for Bonferroni corrections. Statistical analysis was conducted by using IBM SPSS Statistics 23.

3.3.4. Results

Multi-Joint condition leads to a decrease of proprioceptive acuity resulting in an underestimation of the matching target.

All participants were able to perform the experiments involving the two conditions and the multiple target sets.

Yet, performance was significantly different when considering the DoFs and the testing modality. In detail, Figure 17 illustrates the comparison between the two conditions (*SJ* versus *MJ*) for both the *Error Bias* (A) and the *Matching Error* (B): two main different behaviours were found between the *SJ* and *MJ* tests.

All subjects showed a tendency to overshoot the *Proprioceptive Target* when requested to perform the matching task in *SJ* condition with the elbow FE_{Elbow}.

Contrarily, the same joint (FE_{Elbow}) undershot when the *MJ* condition was presented for both left and right arms.

Furthermore, a significant deterioration of proprioceptive acuity was also inferred in multiarticular complex movements (*MJ*) rather than in single joint (*SJ*): this was true

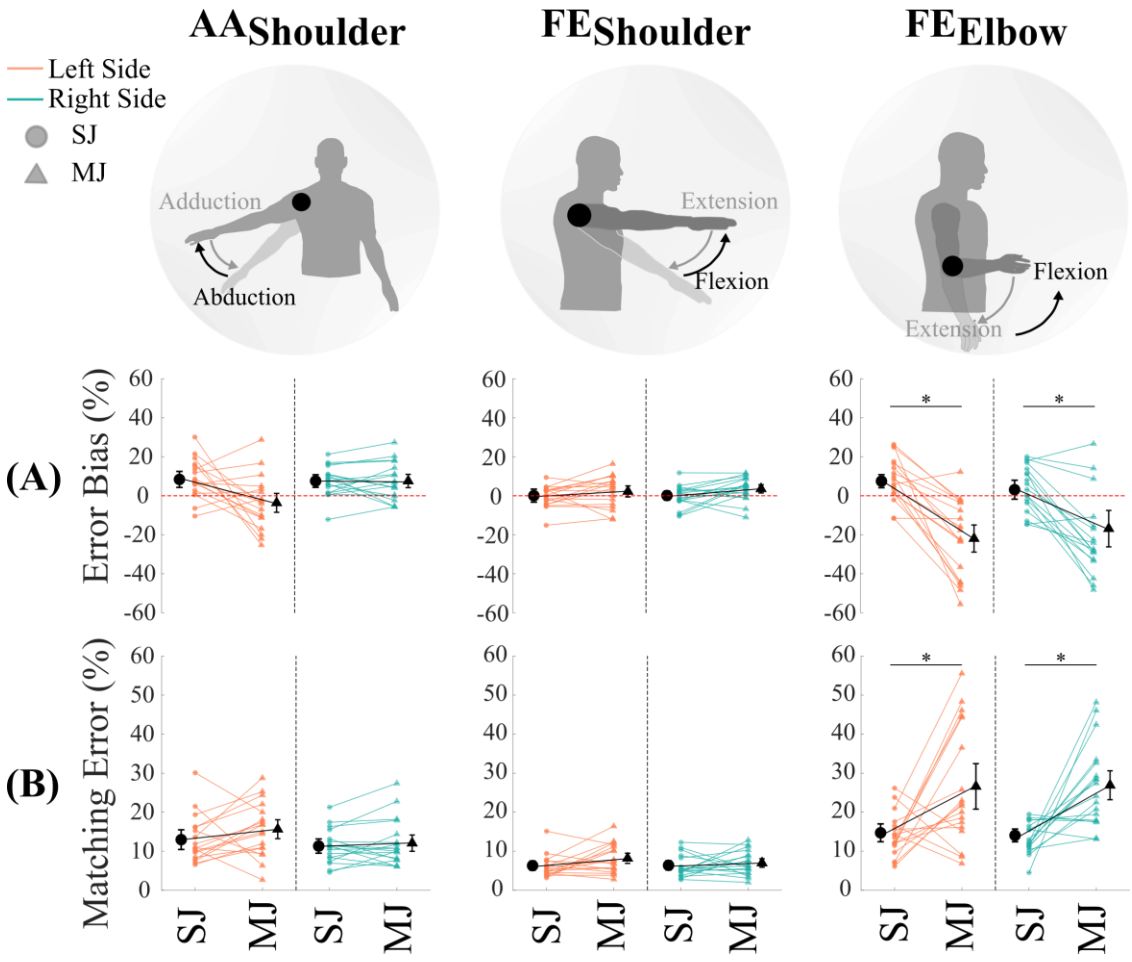

Figure 17: Outcome measures relative to the *Error Bias* and the *Matching Error*. In each graph, the orange colour represents the left body side, while the green colour represents the right one. The single-joint condition (*SJ*, which could be: $AA_{Shoulder}$ or $FE_{Shoulder}$ or FE_{Elbow}) is represented by a round marker, while a triangular marker represents the multi-joint condition (*MJ*). Black markers denote the averaged value between the subjects for each condition; the coloured ones represent the mean value for each participant across the trials. Each column represents one DoF ($AA_{Shoulder}$, $FE_{Shoulder}$, and FE_{Elbow}). **(A)** *Error bias*. **(B)** *Matching error*.

only for the distal joint of the arm FE_{Elbow}, while the proximal anatomical district AA/FE shoulder, provided similar results independently on the testing modality (*SJ* Vs *MJ*).

The aforementioned differences were confirmed by rANOVA test, highlighting a significant condition (*SJ* Vs *MJ*) effect ('condition': *Error Bias:* $F(1,18)=33.5$, $p<0.001$; *Matching Error:* $F(1,18)=30.5$, $p<0.001$).

Ultimately, we statistically inferred across the two conditions, by a paired t-test post-hoc analysis, different behaviour of each tested DoF, and it has been found that only FE_{Elbow} DoF presents statistically significant differences (see Table 6 and Table 7). Contrarily the other tested limb´s joint, the shoulder, maintains statistically similar performance independently on the condition.

Body Side	DoF	*Error Bias*		*Matching Error*	
		SJ	***MJ***	***SJ***	***MJ***
Right	FE_{Elbow}	3.97 ± 2.75	-16.89 ± 6.26	13.24 ± 0.93	26.80 ± 2.49
	$FE_{Shoulder}$	0.37 ± 1.31	3.54 ± 1.42	6.12 ± 0.66	6.95 ± 3.12
	$AA_{Shoulder}$	7.53 ± 1.82	7.13 ± 2.28	11.21 ± 1.03	12.10 ± 1.40
Left	FE_{Elbow}	8.21± 2.67	-21.96 ± 4.67	14.01 ± 1.29	26.64 ± 3.59
	$FE_{Shoulder}$	-0.47 ± 1.29	2.31 ± 1.91	6.04 ± 0.66	8.08 ± 0.87
	$AA_{Shoulder}$	8.73 ± 2.32	-3.76 ± 3.26	12.94 ± 1.43	15.56 ± 1.63

Table 6: Mean values and standard errors (%) for the *Error Bias* and *Matching Error*. Highlighted rows denote the significant outcomes between *SJ* and *MJ* conditions, as specified in Table 7.

Body Side	Condition		*Error Bias*			*Matching Error*		
			FE_{Elbow}	$FE_{Shoulder}$	$AA_{Shoulder}$	FE_{Elbow}	$FE_{Shoulder}$	$AA_{Shoulder}$
Right	***SJ***							
		MJ	0.002*	0.029	0.825	<0.001*	0.379	0.335
Left	***SJ***							
		MJ	<0.001*	0.112	0.012	0.002*	0.051	0.172

Table 7: Statistical p-values for the *Error Bias* and *Matching Error* between conditions. * represents significant differences.

Proprioceptive Error across body joints.

We investigated another aspect involving the proprioceptive performance across the different body segments and how their distal and proximal positions influence such performance in the body.

As depicted in Figure 17B, illustrating the *Matching Error*, for all conditions, it has been found a lower proprioceptive acuity for the distal body joint (elbow) than for the proximal one (shoulder).

The rANOVA test (Table 8), performed on the *Error Bias* and the *Matching Error*, highlighted a significant effect of the DoF (*Error Bias*: F (2,18) = 8.6, p = 0.001; *Matching Error:* F (2,18) = 73.0, p < 0.001) and an interaction effect between the conditions and the DoFs (*Error Bias*: F (2,18) = 29.7, p < 0.001; *Matching Error*: F (2,18) =17.2, p < 0.001). No significant difference has been found between the body sides (Error Bias: F (2,18)=1.7, p=0.213; *Matching Error*: F (2,18) = 1.5, p = 0.246). The post-hoc analysis between the DoFs for the *Error Bias* and the *Matching Error* is reported in Table 8. The proprioceptive error resulted significantly larger for the distal joint than the proximal one, considering the same DoF (FE).

Body Side	DoF		*Error Bias*		*Matching Error*	
			SJ	***MJ***	***SJ***	***MJ***
Right	FE_{Elbow}					
		$FE_{Shoulder}$	0.173	0.014	<0.001*	<0.001*
		$AA_{Shoulder}$	0.289	0.006	0.197	0.002*
	$FE_{Shoulder}$					
		$AA_{Shoulder}$	0.002*	0.082	<0.001*	<0.001*
Left	FE_{Elbow}					
		$FE_{Shoulder}$	0.002*	0.001*	<0.001*	<0.001*
		$AA_{Shoulder}$	0.836	0.006	0.445	0.008
	$FE_{Shoulder}$					
		$AA_{Shoulder}$	0.001*	0.127	0.001*	<0.001*

Table 8: Statistical p-values for the ***Error Bias*** and ***Matching Error*** between the joints. * represents significant differences.

3.3.5. Discussions and Conclusions

Despite the paramount importance of proprioception in sensorimotor control, studies investigating proprioceptive acuity in coordinated multi-joint setups are still limited to single-joint or confined in the execution of tests involving planar workspace. Furthermore, not much evidence can be found in the literature on experimentally assessed physiological aspects that stem from the interconnection between distal and proximal joints in the perception of proprioceptive targets. With this in mind, we aim at providing insights into

how proprioceptive acuity is encoded at the multi-joint level by means of a novel experimental paradigm involving proprioceptive assessment via a robotic device.

We developed a protocol to compare *single-* versus *multi-joint* position matching in order to assess how perception of a proprioceptive target changes when multiple sensory information is encoded from the different sources or joints involved in the task.

We used a robotic setup to overcome previous limitations of planar setups and test subjects' acuity of joints position across a 3D space.

The proposed paradigm aims at not only extending proprioceptive assessment to a multidimensional manifold, hence replicating complex arm configurations, but also provided the unprecedented possibility of studying in detail the interconnection between those anatomical joints responsible for covering the whole arm workspace. To the best of our knowledge, there are no previous studies investigating such aspects involving robotic technology to increase measurement accuracy as well as contemplating a 3D testing paradigm.

It has been observed that proprioceptive performance is influenced by the number of joints involved in the task as well as by the anatomical configuration of the tested degrees of freedom (Dukelow et al., 2009; Rincon-Gonzalez et al., 2011a; Sketch et al., 2018).

Proprioceptive Acuity differences between single- and multi-joint tasks

As evidenced by the performance indicators, the *multi-joint* condition leads to a decrease of proprioceptive acuity for the distal joint.

We want to support our results by the following considerations: (i) since *MJ* movements generally involve several processes required for stability, coordination, and neuromuscular control (Kraemer and Ratamess, 2004; Schwellnus, 2009), their execution results more complex than *SJ* ones; (ii) during the *single-joint* condition, the mechanoreceptors stimulation and the arising sensory information are better encoded by the central nervous system rather than when multiple information comes from different joints (*MJ*). In *SJ* condition, muscle spindles can work along their preferred direction by conveying their afferent information to the brain resulting in a population code representing the joint position (Bergenheim et al., 2000; Roll et al., 2000; Jones et al., 2001).

Moreover, our results have been extracted from an experimental setup involving a 3D-workspace and combining information arising from multiple peripersonal spatial components (Noel et al., 2018), and therefore introducing multiple factors: i.e., the gravity

perception, which was involved in the dynamics of the task, and hence introducing extra-information in the sensory channel that complicates feedback integration when a *MJ* movement is required (Papaxanthis et al., 2003; Le Seac'h and McIntyre, 2007; Berret et al., 2008). In contrast, Sketch et al. (Sketch et al., 2018), who implemented a 2D-task, obtained a reverse result, evidencing that the *MJ* condition leads to lower matching errors than the *SJ* one. They justified their result, highlighting how *MJ* movements are more relevant from a "*biological*" point of view, i.e., they are closest to our routines compared to the *SJ* ones. However, the possibility to implement a 3D-scenario allowed us to cover the whole arm movement. In our study, subjects' performance was compared across different workspaces, overcoming issues about how movements observed at the single-joint can be compared with their projection at the end-effector even though they have different metrics and dimensionality (Hansen et al., 2015).

Proprioceptive Error across Upper Limb Joints

As previously discussed, our results highlighted a significant difference in proprioceptive acuity between the tested joints: in particular, regardless of experimental conditions (*SJ* or *MJ*), the largest matching error has been found in the distal district of the arm, the elbow. Our outcomes are consistent with the hypothesis that proprioceptive signals are differently encoded if they originate from proximal or distal segments. Brinkman and Kuypers (Brinkman and Kuypers, 1973) in a study on primates, highlighted the aspect mentioned above by experimentally demonstrating that the contralateral motor cortex is responsible for mediating distal movements, while motor commands related to proximal districts involve a neural activity from both the ipsilateral and contralateral motor cortex. Different neural pathways generate diverse motor behaviours as well as sensory processing between distal and proximal limbs, resulting in a significantly different performance between joints of the same limb. There is evidence (Rincon-Gonzalez et al., 2011a) further demonstrating that in a 2D proprioceptive assessment, subjects' performance was not isotropically distributed over the task workspace, but the largest errors have been found for more distal configurations of the limb.

Other studies confirmed that proprioceptive acuity is highly influenced by the configuration of the tested limb: performance in joint position matching tasks is worse for targets located in a distal portion of the arm workspace (Adamo and Martin, 2009; Wilson et al., 2010; Iandolo et al., 2015; Galofaro et al., 2019) rather than for those tested in

proximal configurations (Janwantanakul et al., 2001; Tripp et al., 2006; Fuentes and Bastian, 2010).

Limitations: The current work explores a unique multi-joint (*MJ*) configuration. The implementation of further *MJ* movements would help understand the proprioceptive mechanisms involved in a 3D-workspace to be included in a proprioceptive assessment protocol. Our findings provide the first proof of concept that can be considered to develop *evaluation protocols* and *ad-hoc rehabilitative interventions* for somatosensory retraining as published in recent works (Elangovan et al., 2017; Wang et al., 2021), also providing real-time feedback of the proprioceptive errors.

Conclusions: This study proposes a new paradigm using a robotic device for quantitively assessing upper limb proprioception during a three-dimensional Joint Position Matching task.

The main finding can be summarized as the presence of a dissimilar proprioceptive acuity between joints of the same upper limb. In particular, the elbow and shoulder behave differently depending on the experimental condition and the arm configuration over the workspace.

The same robot-aided paradigm might be used in clinical settings. In fact, standard proprioceptive tests in medical practice provide assessments that are manually dispensed by the therapists, resulting in a qualitative low-resolution observation. Our findings may suggest that the use of robotic technology, which is rapidly and progressively spreading in hospitals and rehabilitation structures, might help clinicians in effectively evaluating proprioceptive deficits in a multi-joint fashion, thus drastically improving measurement accuracy and reliability. We hope that despite our investigation involves only an unimpaired sample population, it may arouse clinicians' interest in the proposed paradigm in conjunction with the recent advancement in wearable technology and invite the medical community to further pursue the use of robotics for clinical assessment.

Part II

Position and force control in bimanual tasks

4. Position and force control in *bimanual tasks*

In the literature, several attempts propose methods for evaluating sensorimotor abilities in patients. However, most of these focused on the single anatomical district rather than on the general patient's current motor status. Many studies consider, for example, the single joint assessment without considering what happens when the patient is asked to perform a more complex task involving multiple joints as in several daily living activities.

Daily activities require an accurate internal model of the body and the world. A correct internal model allows for transforming motor commands into sensory consequences to produce calibrated movements. One of the critical aspects for developing these robust dynamical models relies on *proprioceptive feedback*.

Neurological pathologies can permanently exclude the brain of its primary sources of information from skin and muscles, leading to a compromised coding of the proprioceptive information, with negative consequences in motor control and the associated recovery progress. Accurate assessment and quantification of proprioceptive function become an essential factor in diagnosing and treating neurological diseases.

The proprioception includes the sense of position, the sense of effort, and their interaction. Furthermore, in many of life's everyday actions, we are dealing with movements that require perfect coordination between the two sides of our body, and therefore the interaction between the two cerebral hemispheres. The performance of motor action in the space around us also requires recruitment of the whole kinematic system - multi-joint - and not only of the single joint.

Therefore, the second part of this thesis reports methods for investigating proprioception in a *bimanual* context. First, with a low-cost device designed and developed during my research path, BisBox V1.0, I investigated the accuracy in replicating bimanual object orientation in a "coupled" configuration, where one hand perceives the other manipulating the same object. Second, I assessed the modulation of force in a different configuration, i.e., the "non-coupled" one, to study the effects of age on final performance. Finally, thanks to the use of multiple degrees of freedom robotic exoskeleton, ALEx-RS, I studied how the haptic feedback could be influenced by the features of the material composing the object (stiffness) during manipulation tasks in space.

4.1. Assessment of bimanual proprioception during an orientation matching task with a physically coupled object [4]

4.1.1. Introduction

In the recent decades, robotic neurorehabilitation is becoming popular for facilitating sensory motor learning (Prange et al., 2006; Veerbeek et al., 2017) Clinical evidence suggests that rehabilitation therapy for upper limb through robotic assistant results at least as effective as traditional treatment (Lum et al., 2002; Kwakkel et al., 2008). However, despite its importance, technological *assessment tools* for objective evaluation of sensorimotor impairments are less explored. Somatosensory deficits in neurological diseases, such as multiple sclerosis or stroke, compromise the ability to perform everyday activities and have an independent lifestyle. For example, impaired proprioception affects the control of posture, motion and forces (Jamali et al., 2017), and the loss of position and force sensing contributes to impaired control of reaching movements and stabilization behaviours (Scheidt and Stoeckmann, 2007).

Daily activities require an accurate internal model of the body and the world. A correct internal model allows for transforming motor commands into sensory consequences to produce calibrated movements (Shadmehr et al., 2010). This capacity depends on learning of an internal model of the musculoskeletal dynamics and of the external forces acting on the limb (Shadmehr and Mussa-Ivaldi, 1994b; Sainburg et al., 1999). One of the critical aspects for developing such robust dynamical models is intact proprioceptive feedback.

Intact proprioceptive feedback allows for performing bimanual activities that are very common in our daily life. Previous studies (Wenderoth et al., 2004; Janssen et al., 2009) investigated the importance of bimanual coordination while holding different orientations using two different objects. Another study adopted a device consisting of two not-coupled handles to evaluate the position and force sense in healthy subjects (Ponassi et al., 2018).

[4] The whole content of this Chapter has been published as*:* E. Galofaro, G. Ballardini, S. Boggini, F. Foti, I. Nisky and M. Casadio. *Assessment of bimanual proprioception during an orientation matching task with a physically coupled object*, ICORR 2019.

However, bimanual activities often involve a single object that is co-manipulated by both hands, and in these activities, it is important to keep the object in a specific orientation. A definition of a *coupled* object is provided by (Shirota et al., 2016), where they considered a task physically coupled when the movement from one limb must have an effect on the dynamics of the opposite limb. Coupled tasks have the advantage of providing additional sensorimotor information: each individual hand can sense the force generated by the other hand through coordinated interaction with the object (Mutalib et al., 2019). We wished to address the clinical need of objectively assessing proprioception with a coupled object that mimics daily activities.

In normal clinical practice there are three different methods that are used to assess bimanual proprioception: (i) threshold to detection of passive motion (TTDPM), (ii) joint position reproduction (JPR), and (iii) active movement extent discrimination (AMEDA) (Han et al., 2016). These methods usually can be performed subjectively in a clinical routine by a therapist (Suetterlin and Sayer, 2014), or objectively by adopting robotic devices (e.g. (Dukelow et al., 2012; Contu et al., 2017)). Here, we extend the new direction of using *physically coupled objects* and develop a novel low-cost device – a sensorized box – and a new method to assess bimanual proprioception in a way that mimics realistic daily activities. To validate our sensorized box for future applications in clinical contexts, we report results of an assessment of bimanual proprioception with healthy participants. We used our device to evaluate objectively: (i) proprioception in an orientation matching task, (ii) how fatigue affects proprioception in terms of matching orientations before and after the introduction of known weights.

4.1.2. Experimental Setup, Task and Participants

Twelve healthy young participants (24.0 ± 1.2 years (mean ± std), 6 females) were enrolled for this experiment. They did not have any evidence or known history of neurological diseases and exhibited normal joint range of motion and muscle strength. Participants were tested for the hand dominance based on the Edinburgh Handedness Inventory (LQ: 74.81±13.02) (Oldfield, 1971), and we verified if they played an instrument or practiced a sport requiring an extensive use of one arm with respect to the other. Eleven participants were right-handed. One participant was predominantly left-handed (Edinburgh Test Score: -57), and he was the only one practicing an asymmetric sport and playing an instrument (guitar); however, he performed these activities with the

right hand. Participants had also no problems of visual integrity that could not be corrected with glasses or contact lenses, i.e., they could clearly see the information that was displayed on the computer screen. The research conforms to the ethical principles of the 1964 Declaration of Helsinki, which protects research participants. Each participant signed a consent form that conforms to these guidelines to participate in the study and to publish individual data.

We designed a new low-cost instrumented device that had the shape of a rectangular box (Figure 18A). The production cost was below 200$. The dimensions of the box were 20×40×25 cm (height × width × depth). The participants held the device with the two hands placed on the two smaller faces (Figure 18B). The larger faces were built with only four polymeric rods to reduce the weight of the device. The 40 cm length was chosen to match the average inter-shoulder distance of the participants, and in the future, the rods could be easily changed to match different participants anthropometry. Each smaller face consisted of two rigid plates with inside three load cells (Micro Load Cell CZL635,

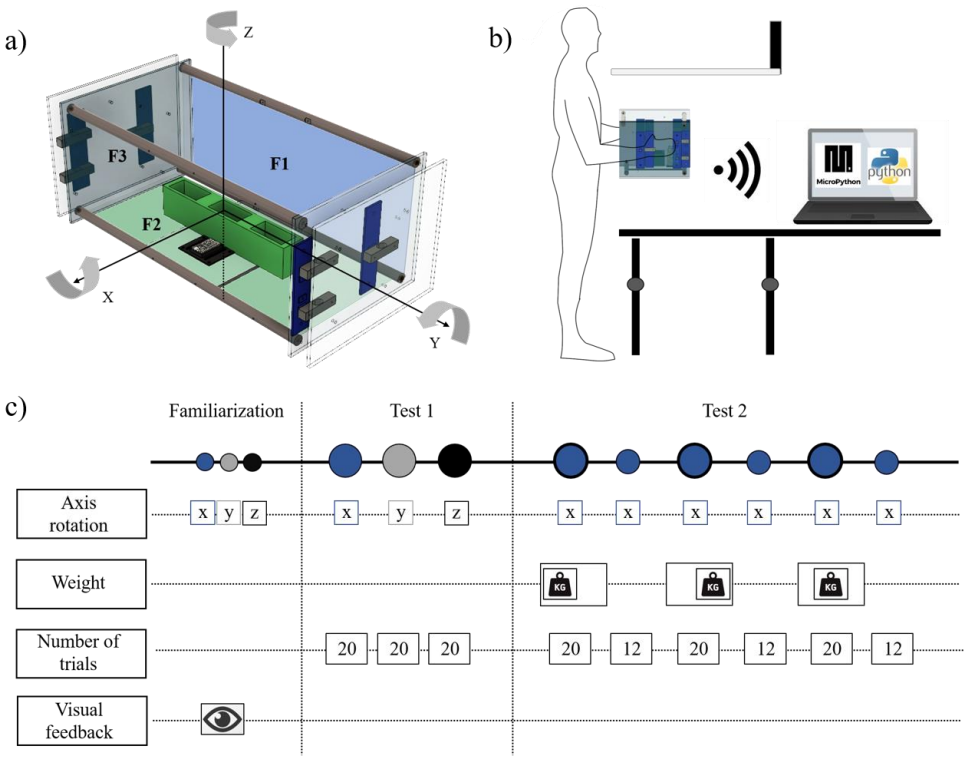

Figure 18: a) CAD Model (Fusion 360, Autodesk) of the *sensorized box device* used in the experiment, and the reference axes. The direction of the circular arrow denotes positive rotation. b) Task description. The participant is standing with the arms located in the starting position (forearms are parallel to the table). Arms are hidden by an opaque screen, and the participant can freely rotate the device, including about principal axes. In front of the participant up to opaque screen, there is the screen where visual information is displayed during the experiment. The device is Wi-Fi connected to the PC. c) Experimental protocol. Each color codes an orientation axis, and the dimensions of the circles code the number of trials performed during tests. Axis orientations during *Test 1* and weight locations (left, right or center) during *Test 2* are balanced between participants.

Phidgets, Canada) for measuring the force applied by each hand during the experiment. On the bottom of the box, there was an Inertial Measurement Unit (IMU ATBNO055-XPRO, Microchip, Italy) that allowed measuring the orientation of the box about the three principal axes, and a support for adding known weights in symmetric or asymmetric positions (Figure 18A). All the materials were selected to minimize the weight of the box that resulted in 1.5 kg before adding the weights.

The sensorized box could be used in a standalone mode with the data recorded on a memory card, or in combination with a laptop via wireless communication to provide instructions and feedback based on real-time monitoring of participants' actions. We used a WIPY 3.0 microcontroller development board that creates a Wi-Fi and Bluetooth network connection with a 1 Km range. The WIPY was programmed in MicroPython (Pymakr plug-in provided by Pycom).

We programmed the user interface in Python 2.7.9 with the open-source libraries OpenGl and Pygame. We implemented two different visual feedback modes: (1) a real-time representation of the orientation of the box in space and an indication of the forces applied by each hand on the lateral faces. If no force was applied the color of the corresponding face of the box was black. When participants applied force, a color appeared on the bottom of that face and its height increased proportionally with the applied force. This mode was used during the *Familiarization phase*, where participants could try all the different configurations and received a real-time feedback about the correct execution of the task. (2) Visual instruction of the target orientation that participants had to reach and written instructions. In this mode, no visual feedback about performance in terms of neither orientation nor forces was provided. This mode was used during the *Test 1* and *Test 2* phases of the experiment.

During the experiment, the participants stood in front of a 24" vertical monitor positioned 0.5 m away at eye level, and in front of a table of adjustable height. The box was located at a fixed starting position on the table with the face of 20×40 cm (F1) parallel to the participant frontal plane, and the face of 25×40 cm (F2) parallel to the floor (Figure 18B). We asked the participants to position each hand fully open on each of the lateral sides (25×20 cm) of the box (F3). We adjusted the table height so that when the participant grasped the device, the arms were extended along the body and forearms aligned to the table. Before the participants touched the device, the force signals from the load cells were recorded to remove their offsets. Then participants were required to lift the box, maintaining it parallel to the floor, at the level of their chest. This was the starting position

for each trial. The experimental session included three phases (Figure 18C). In all phases, a trial started with the box in the starting position, i.e. 0 deg rotation on each axis, to minimize proprioceptive drift (Paillard and Brouchon, 1968), (Wann and Ibrahim, 1992). Specifically, in this starting position the *z-axis* of the box was parallel and directs opposite with respect to the gravity force vector, the *x-axis* was directed toward the subject and the *y-axis* toward the right of the subject, completing the right-handed coordinate system, as depicted in Figure 18A.

Before each trial, we measured the orientation of the box and asked the participants to adjust the box if the orientation was not correct. Then we presented a 'go' message, and asked the participants to perform ballistic rotation, i.e. to reach the desired target orientation with one single fast movement. We also asked them to hold that final orientation for 2 seconds. In this study, we considered the average value of the orientation of the box during these final 2 seconds. In future studies, we also plan to dissociate the ballistic and feedback components of orientation control.

Phase 1 – Familiarization: throughout this phase, visual feedback about the actual orientation of the box and the forces that the participants applied was presented in real time. Moreover, to ensure the understanding of the task, participants received a visual feedback if they were able to match the target. Participants could hold and move the box freely for 3 minutes, while observing the graphical representation of the box. Then, we asked them to match four target orientations, +/- 30 and +/-60 deg, around each of the three principal axes of the device, resulting in 2×4×3=24 trials (Figure 18C).

Phase 2 - Test 1: throughout both test phases, participants did not receive visual feedback about the orientation of the box, the forces, their arm or the box itself. Only the target box orientation and written instructions were displayed on the screen. We asked participants to match the same four target orientations around each of the three principal axes of the device. Each target orientation was repeated 5 times for a total of 20 trials for each axis. Targets were presented in pseudorandom order: each target could take randomly one of the four possible values before the next four were presented, and the same target was never repeated sequentially. The order of the rotation axes was balanced among participants.

Phase 3 - Test 2: to test the effects of different loads of the box, we secured a weight of 1 kg in the centre of the box, or asymmetrically on the left or on the right side of the box (three loading conditions). Participants had no knowledge about the weight position (i.e. loading condition), and no visual feedback of their arms or box orientation. They were asked to reach the same four target orientations of the box, but only around the *x-axis*. For

each loading condition, they performed 20 trials, 5 for each target orientation. The order of presentation of the three loading conditions was balanced among participants. After each of the loading condition test, they also performed a set of 12 trials (three for each target orientation) without any weight. These trials were identical to those performed on the *Test 1* for the *x-axis*.

4.1.3. Data analysis and Outcome Measures

All signals, i.e., the forces recorded from the six load cells, as well as the angular rotations from the IMU were recorded at 30 Hz and filtered offline using a 4th order low-pass Butterworth filter with a 10 Hz cutoff. In the following we refer to the angular rotation (orientation) ϑ of the box around its principal axes.

For each trial, to measure the overall accuracy, we computed the absolute error (*AE),* defined as the absolute value of the difference between the measured value at the end of the trial (θ_i) and the desired target orientation (θ_{target}) averaged over the *N* repetitions of a same target:

$$AE = \frac{\sum_{i=1}^{N} \left| \theta_i - \theta_{target} \right|}{N} \tag{10}$$

Then, to measure the proprioceptive bias, i.e., a systematic overshoot or undershoot, we computed the constant error (*CE*): the signed difference between the measured and the target box orientation. For consistent interpretation, we transformed the signed *CE* to a measure of a signed overshoot, CE_{OS}:

$$CE_{OS} = sign\left(\theta_{target}\right) * \sum_{i=1}^{N} \frac{\left(\vartheta_i - \theta_{target}\right)}{N} \tag{11}$$

In this measure, negative values represent an undershoot and positive values represent an overshoot independently of the sign of the target rotation direction.

Finally, we evaluated the variable error (*VE*) as the standard deviation of the box orientations:

$$VE = \sqrt{\sum_{i=1}^{N} \frac{(\vartheta_i - \theta_M)^2}{N}}, \tag{12}$$

where θ_M is the average over all the measured box orientations for that target. This metric does not depend on the participants' accuracy, but it measures the repeatability of the participants' performance. All these parameters were evaluated for each orientation axis (*x*, *y*, *z*), and were averaged across participants.

To assess the forces that the participants applied on the box, for each trial, we considered the 2 seconds where participants held the final orientation statically. We computed (1) the *mean force*, i.e., the average value of the forces exerted during these 2 seconds, and (2) the *coefficient of variation* (*CV* (%)), assessing the magnitude of force variability, computed as the standard deviation of the applied force, normalized to the mean force value (×100). The *CV* was normalized to account for the dependence of force variability on the exerted force (Carlton and Newell, 1993),(Schmidt et al., 1979),(Slifkin and Newell, 1999). During these 2 seconds, the box was in a static condition, and both hands exerted the same force for rotations about the y and z axes. For the rotations about the *x-axis*, the two hands exerted the same force when they were at the same height with respect to the ground, i.e., the forces exerted at 60, 30, -30, -60 deg by the left hand corresponded to the force exerted in -60, -30, 30 and 60 by the right hand respectively. Therefore, we performed the statistical analysis and display the results only for one of the two hands, i.e., the right hand.

Statistical analysis. Normality was assessed using the Kolmogorov-Smirnov test, and sphericity condition for repeated measures ANOVA was assessed using the Mauchly test. The first was always verified. When the second was violated, we applied the Greenhouse-Geisser corrections. In *Test 1*, for all movement and force indicators, for each axis of rotation separately, we performed a repeated-measures ANOVA (rANOVA) with two within-participant factors: 'direction' (2 levels: clockwise – positive – and counterclockwise – negative – rotations), 'amplitude extent' (2 levels: 30 and 60 deg of rotation), and their interaction. In *Test 2*, we performed the same analysis, but we added two within-participant factors: 'presence of weight' (2 levels: weight, no-weight), and 'weight location' (3 levels: central, left, right). For each condition, axis of rotation, and participant, we considered the average value of the 3 repetitions. Finally, for rotations about the *x-axis*, we compared the force and position performance between initial and final testing, with a rANOVA with 3 within-participant factors: 'test' (2 levels: test 1 and test 2), 'direction', and 'amplitude extent'.

4.1.4. Results

We investigated the ability to match different orientations by rotating the sensorized box along its three principal axes with both hands. In the following, we report the results for the rotation around each axis:

Rotations about the X-axis. When rotating clockwise along the *x-axis* (i.e., -60/-30 deg), participants moved downward the right hand, and when rotating counter clockwise (i.e., 60/30 deg), they moved downward the left hand. For these rotations, the *absolute error* (Figure 19A) was 5.09 ± 0.78 (mean ± std) deg, without any significant difference for the extent and direction factors (p=0.536, p=0.817 respectively). Instead, we found a

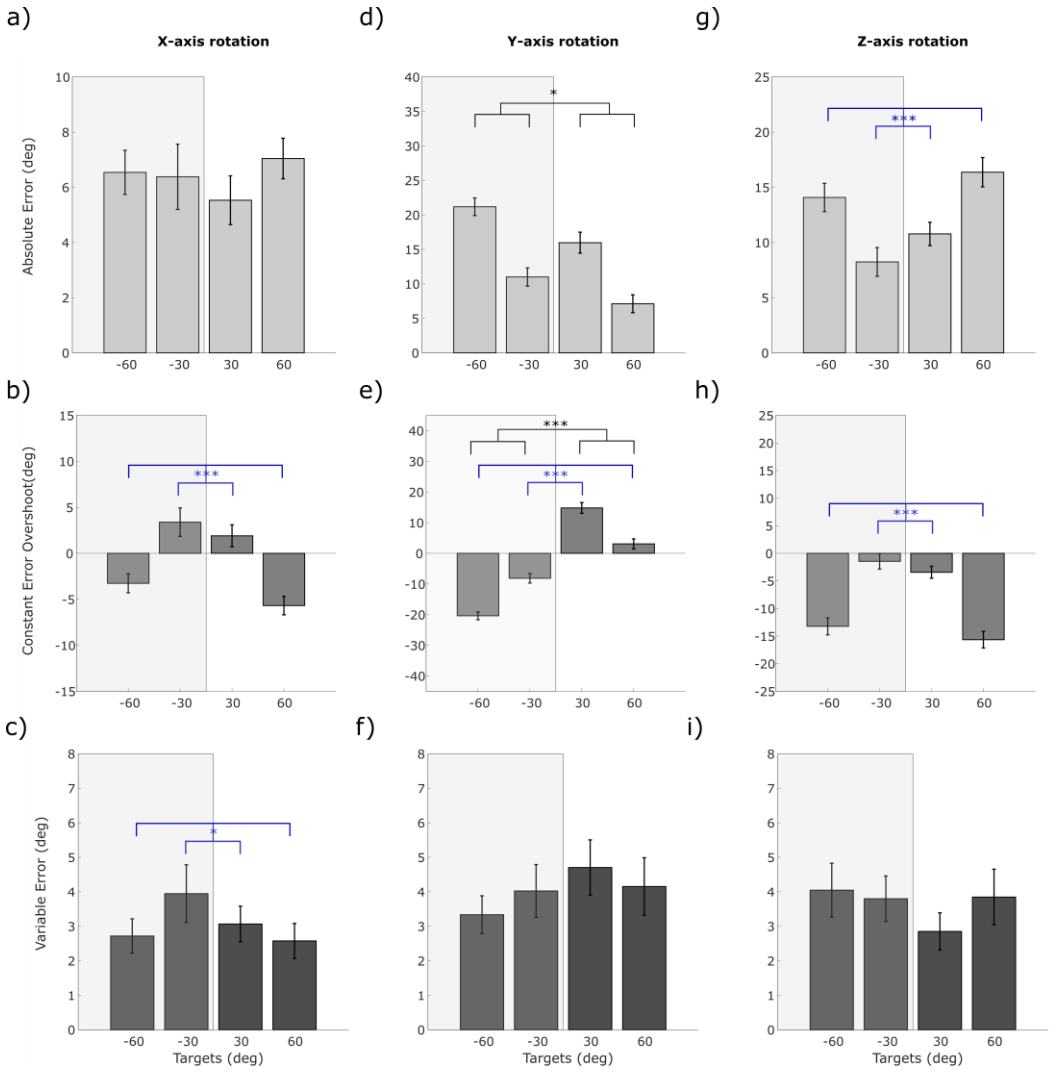

Figure 19: Results reported for the mean population data. *X-axis* Rotation: absolute **(A)**, constant **(B)**, and variable **(C)** errors and their standard error. *Y-axis* Rotation: absolute **(D)**, constant **(E)**, and variable **(F)** errors and their standard error. *Z-axis* Rotation: absolute **(G)**, constant **(H)**, and variable **(I)** errors and their standard error. In these panels, * means a significant difference with p<0.05, ** a significant difference with p<0.01 and *** if p < 0.001. Only significant main effects are marked in the panels, all significant interactions are described in the main text.

significant extent effect for the *constant error* (Figure 19B, $F(1,11)=37.63$, $p<0.001$): participants overshot the targets closer to the starting orientation (+/-30 deg), while they undershot the targets requiring the larger rotations, (+/-60 deg). Moreover, most participants rotated less the box in the clockwise than in the counter clockwise direction, but this trend did not reach the threshold for significance ($p=0.056$). For the *variable error* (Figure 19C), we found only a significant difference in the extent of rotations ($F(1,11)=9.35$, $p=0.011$), due to the fact the smaller target rotations were reached with more variable motor performance. For the force applied by each hand, as expected, the mean value changed both (1) with the direction of the rotations ($F(1,11)=226.56$, $p<0.001$); i.e., the lower hand exerted higher forces than the other, and (2) with the extent of the rotation, with larger rotations leading to higher errors for the counter-clockwise rotations, but not for the clockwise ('extent effect': $F(1,11)=8.55$, $p=0.013$; 'interaction effect' $F(1,11)=133.40$, $p<0.001$), Figure 21A. We did not find differences in the force variation coefficient ($p=0.818$), Figure 21B.

Rotation about the Y-axis. When rotating clockwise along the *y-axis*, participants moved toward targets away from the body, i.e., toward the distal targets: -30/-60 deg. When rotating counter clockwise, they moved toward the targets closer to the body, i.e., toward the proximal targets: 30/60 deg. For the *absolute error* (Figure 19D), rotating toward the body led to greater error than rotating in the opposite direction ('direction effect': $F(1,11)=5.58$, $p=0.038$). However, in the former case, the error increased with the extent of the required rotation, while in the latter the error decreased with it (direction × extent interaction: $F(1,11)=19.96$, $p<0.001$). More specifically, participants tended to undershoot the distal targets and to overshoot the proximal targets (*constant error*: 'direction effect': $F(1,11)=29.21$, $p<0.001$). The *constant error* (Figure 19E) for the +/-60 deg targets significantly changed with respect to the errors at +/-30 deg, increasing in the counter-clockwise direction ('extent effect': $F(1,11)=35.25$, $p<0.001$). This determined greater errors for the targets requiring 60 deg of rotation in the clockwise direction, and smaller error for those in opposite directions, with respect to the targets at 30 deg. The smaller errors in the 60 deg target could be due to the biomechanical limits of the wrist rotations preventing the participants to overshoot that target. For the *variable error* (Figure 19F), we did not find any significant difference among target rotations ($p=0.352$). For the *mean force* applied by each hand, we found a significant effect of the extent of rotation; i.e., the further were the rotations, the higher was the force applied ($F(1,11)=36.05$,

p<0.001), Figure 21A. The same effect was observable for the *coefficient of variation* ('extent effect': F(1,11)=12.36, p<0.01), Figure 21B. We did not find a significant 'direction effect' for the *mean force* or for its *coefficient of variation* (p=0.535, p=0.934). This makes sense in light of the symmetry of the directions of rotation about the *y-axis* with respect to gravitational and inertial forces.

Rotation about the Z-axis. When rotating clockwise along the *z-axis*, to reach the targets at -30/-60 deg, participants moved the right hand toward their body. When rotating counter clockwise along the *z-axis*, to reach the targets at 30/ 60 deg, participants moved the right hand away from their body. For the *absolute error* Figure 19G), we observed that smaller rotation corresponded to lower errors ('extent effect': F(1,11)=5.09, p=0.042). This behaviour was even more marked for the *constant error* ('extent effect': F(1,11) =68.05, p<0.001, Figure 19H). In addition, the latter indicator highlighted that participants undershot the targets for all desired orientations. No significant effects were found for both indicators with respect to direction (p=0.076, p=0.114). As for the *variable error* (Figure 19I), we did not find any significant difference (p=0.398, p=0.251). For the *mean force* applied by each hand, there was a significant extent effect; i.e., the further were the rotations, the higher was the force applied (F(1,11)=36.17, p<0.001), Figure 21A. We did not find significant 'direction effects' or significant differences for the *coefficient of variation*, Figure 21B. The absence of any significant 'direction effects' in rotations about the *z-axis* makes sense in light of its symmetry with respect to gravity, inertia, and distance from body. It also suggests that there are no laterality effects in bimanual manipulation of a coupled object.

Test 2. For all the movement indicators, we did not find any significant effects of the presence/absence of weights nor their locations. In contrast, when comparing the orientation-matching performance between *Test 1* and *Test 2*, for rotations around the *x-axis*, both in absence of additional weights, we found that at the end of the experiment, in *Test 2*, for all the target orientations, participants tended to undershoot the target angle compared to the beginning of the experiment, in *Test 1* (Figure 20A; 'testing condition effect' F(1,11)=7.87, p=0.017). No differences related to the two tests were found either related to main effects, or interaction effects for all the other motion and force indicators (Figure 20B). The significant differences related to the direction and extent factors were confirmed also in this analysis, in both *Test 1* and *Test 2*.

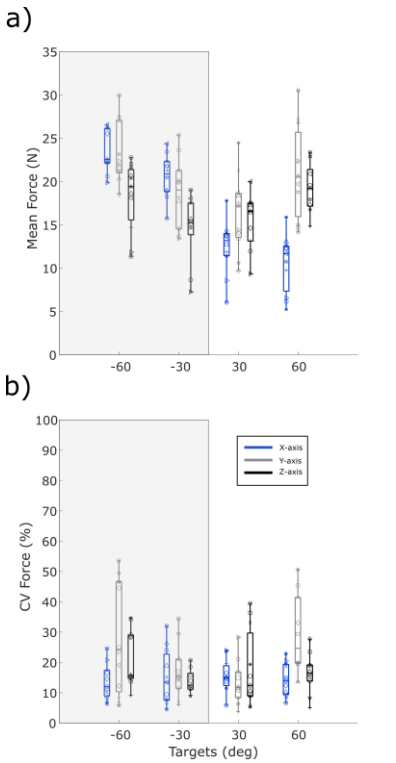

Figure 21: Results reported for force values relative to right hand for each orientation axis. **(A)** *Mean Force.* On each box, the central mark indicates the median, the bottom and top edges of the box indicate the 25th and 75th percentiles, respectively. Blue boxes are relative to rotations around *x-axis*, grey boxes for rotations around *y-axis* and black boxes for rotations around *z-axis*. **(B)** *CV Force.*

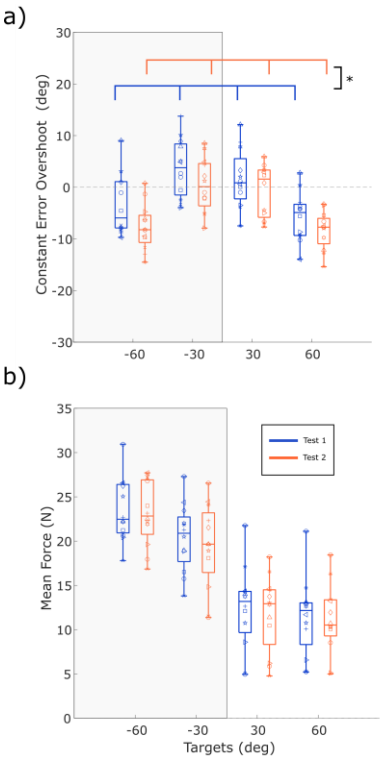

Figure 20: Comparison between between *Test 1* and *Test 2*. On each box, the central mark indicates the median, the bottom and top edges of the box indicate the 25th and 75th percentiles, respectively. Blue boxes depict $T1_x$, and orange boxes depict $T2_{xLRC}$. Individual markers depict the data of single subjects' performances. **(A)** *Constant error*. **(B)** *Mean force.*

4.1.5. Discussions and Conclusions

We investigated the ability to match a desired orientation when manipulating an object with both hands, by relying on proprioception, in absence of visual feedback.

We found significant differences between the directions of rotation only for axis *y*, where targets were proximal or distal with respect to the body. Specifically, participants underestimated angles for far from their body while they overestimated angles for near ones. This result is supported by several studies demonstrating that the proprioceptive acuity decreased for targets that are far from the body (Wilson et al., 2010), (Iandolo et al., 2015), (Adamo and Martin, 2009) or that required larger elbow extensions (Fuentes and Bastian, 2010). In this work, we found that similar conclusions hold for bimanual proprioception during an orientation-matching task with a physically coupled object.

This difference between proximal and distal targets may be also due to the limb or wrist configurations, i.e. may depend on difference in geometry, sensory noise and stretch of the muscles (Fuentes and Bastian, 2010; Wilson et al., 2010). However, we did not find any significant difference depending on the directions of rotation for other axes, where the role of the body is the same in both directions, while all these other factors might be different.

Moreover, by considering the *constant error*, we found significant differences between larger and smaller orientations angles for all the rotation axes. A recent study, focused on wrist joint proprioception, evidenced that joint position sense decreased in accuracy as the joint angle to be matched increased (Li et al., 2019). Here, we found similar results in terms of accuracy for *z-axis*, in particular we had higher errors for +/-60 deg compared to smaller error for +/-30 deg. However, for the *y-axis*, this result was confirmed only for the distal targets, as for the proximal targets the joint range was reduced, and subjects had more possibilities to make mistakes for smaller than for larger rotations. For the *x-axis* subjects overshoot the +/-30 deg targets and undershoot of the +/-60 deg targets.

Another interesting result is the effect of fatigue on proprioception in this orientation-matching task. Despite our limited number of participants, our comparisons between initial and final task without weight, seem to be stable in terms of the undershoot of the angle.

In conclusion, we developed a new low-cost and free-in-space device for the evaluation of bimanual proprioception and tested it on healthy participants. This device

and testing protocol, with proper changes, could be adopted in the future to assess proprioception in neurological diseases or as an early diagnosis tool.

4.2. Age-related changes evaluation of bimanual force sense in an uncoupled task [5]

4.2.1. Introduction

Several common daily activities performed with force and kinematics coupling between two hands, such as holding or moving a large box, or holding a can and simultaneously unscrewing its tap, require bimanual coordination (Swinnen and Wenderoth, 2004; Krishnan and Jaric, 2010). Although in these actions the temporal and spatial coordination between the two hands seems easy and natural, the central nervous system must deal with the complex upper limbs' mechanical properties, share control between arms, and integrate sensory feedback from both sides of the body (Córdova Bulens et al., 2018). Performing bimanual actions involves an extensive network of cortical and subcortical structures, including the primary sensorimotor, premotor, supplementary motor, parietal associative cortices, cerebellum and basal ganglia (Swinnen, 2002). During bimanual actions, the sensorimotor cortices have distinctive activity compared with unimanual tasks (Nair et al., 2003; Serrien et al., 2003; Long et al., 2016) and the corpus callosum has a crucial role in the interaction between the two hemispheres (Long et al., 2016). Neurological diseases such as stroke, Parkinson's disease and multiple sclerosis impact the ability to perform these bimanual actions (Gorniak et al., 2014; Kang and Cauraugh, 2014; Yan et al., 2015; Ballardini et al., 2019b). Also, aging affects bimanual coordination (Maes et al., 2017), both in motion (Lin et al., 2014) and force tasks (Jin et al., 2019b).

Deficits in bimanual force control tasks in older adults could be due both to changes in the structures and the physiology of the nervous system (Goble et al., 2010; Fjell et al., 2014) and to the diminished tactile sensibility (Thornbury and Mistretta, 1981; Bowden and McNulty, 2013). These changes determine weaker hand-grip strength, higher variability, and lower accuracy in isometric bimanual force matching task (Hu and Newell, 2011; Kubota et al., 2012; Lin et al., 2014, 2019; Jin et al., 2019b), increased reaction time

[5] The whole content of this Chapter is in preparation for full journal paper as*:* E. Galofaro, N. Valè, N. Smania, and M. Casadio*, "Effects of Aging on Bimanual Strategies During an Isometric Force Matching Task",*

(Fozard et al., 1994), decreased bimanual (Lin et al., 2014; Vieluf et al., 2015; Jin et al., 2019b) and impaired manipulation abilities (Sebastjan et al., 2017), compared to young adults.

Here, we focus on *bimanual isometric force tasks*. The ability to produce bilaterally isometric force has been studied mainly in tasks where subjects are required to produce maximal forces or match constant and time-variant force levels (Kang and Cauraugh, 2014; Lin et al., 2019). Most of these studies were limited to hand-grip (Jaric et al., 2005, 2006) or single-digit force (Kang and Cauraugh, 2014; Lin et al., 2014; Long et al., 2016; Patel et al., 2019), i.e., tasks where the force is due to distal muscles. Instead, several daily living activities as holding large objects also require the control of proximal muscles, i.e., upper arm and shoulders' muscles. Different muscle districts could significantly determine force control performance in terms of accuracy, variability, and bilateral asymmetries.

Moreover, in several studies often the two hands are evaluated separately, under the assumption of mutual single-hand independence, while bimanual control is characterized by specific and unique features, including between-hands interaction, that are poorly investigated (Morrison and Newell, 1998; Serrien and Wiesendanger, 2001; Kennedy et al., 2016; Jin et al., 2019a).

Most of the studies where the two hands are evaluated together focused their analysis on the overall performance of both hands (Ferrand and Jaric, 2006; Kang and Cauraugh, 2018), while only a few works investigated the strategies of each hand and their coupling, investigating asymmetries and differences due to the specialization of each hemisphere or to handedness (Hu et al., 2011; Jin et al., 2011). Therefore the knowledge about bilateral asymmetry when the hands' performance are evaluated simultaneously is still limited (Takagi et al., 2020).

Force control studies in healthy right-handed subjects, where the hands are tested sequentially or separately, found that the *right-dominant hand* tends to produce more force when matching the force previously produced by the other hand. This behavior was found for hand-grip (Lafargue et al., 2003; Mitchell et al., 2017) and isometric fingers force tasks (Henningsen et al., 1995). The reason for this behavior is that the *right-dominant hand* is usually stronger (Armstrong and Oldham, 1999; Incel et al., 2002), and less noisy in several motor tasks (Kubota et al., 2012). The right hand applied more force than the other hand also in the isometric concurrent tasks proposed by (Davis, 2007), where the force was applied by the fingers, involving distal muscles.

However, O'Sullivan et al. (O'Sullivan et al., 2009), focusing on a bilateral finger force control task, demonstrated that in bimanual tasks where the two hands act concurrently, the control responsibility is shared among the two sides: the brain decides the role of each hand based on its strength and variability. This evidence was confirmed by (Salimpour and Shadmehr, 2014), investigating a bimanual task in which people chose how much force to produce simultaneously with each arm so that their sum would equal a target. They applied forces toward eight different directions on two quasi-static handles, involving also proximal muscles. The *right-dominant hand* applied more force than the other one only in specific directions, and because it was less noisy, not stronger.
If the *right-dominant hand* is generally the strongest, the hand variability, instead, depends on several factors, including the proposed task, the muscles involved, and the population age, leading to different results in lateral asymmetries (Li and Wei, 2014).

Specifically, with age, the variability in task performance of the dominant right arm tends to increase (Vaillancourt and Newell, 2003). Several studies reported with age a loss of the advantage of this hand (e.g. (Vaillancourt and Newell, 2003; Kalisch et al., 2006)) due to its higher rate of decrease in performance. However, the literature results also provide conflicting or task-dependent evidence reporting an increase in *right-dominant hand* use (Weller and Latimer-Sayer, 1985) or not change (Cabeza, 2001; Hausmann et al., 2003).

The purpose of this study was to investigate task performance, bilateral coordination, and lateral asymmetries in *young* and *elderly healthy right-handed subjects* during *a bimanual isometric force task* requiring an essential contribution of the upper arm and shoulder muscles. Subjects were explicitly asked to simultaneously apply the same amount of isometric force pushing with the palm and fingers on two decoupled plates corresponding to a sensorized object's lateral faces and reaching three target forces, corresponding to 8 N, 20 N, 40 N applied by each arm.

The main hypothesis is that since in this task, subjects use three muscle groups - postural stabilizers, muscles supporting the execution of movement, and the muscles responsible for the execution of movement (forearm and hand) (Sebastjan et al., 2017) - strategies and performance in our task will differ from strategies and performance observed in power grip or the application of a force by single fingers: a higher level of proximal muscle recruitment could reflect different motor control strategies than those associated with distal muscle recruitment in fine movements.

4.2.2. Experimental Setup, Task and Participants

Thirty-one healthy volunteers participated in our study. The exclusion criteria were the presence of musculoskeletal injuries or any other neurological condition, history of surgery or pain affecting upper limbs, normal or corrected to normal visual and auditory abilities. To be included in the study, subjects had to be right-handed according to the Edinburgh Handedness Inventory (EHI score > 60) (Oldfield, 1971) and between 18 and 30 years old or between 65 and 85 years old. The two ranges corresponded to two different cohorts: sixteen participants (age = 24.65±1.32(std) years, 10 female, Edinburgh Test Score: 89.62±14.28) have been enrolled in the 'younger group' (YG) and the other fifteen (age = 76.66±6.61(std) years, 7 female, Edinburgh Test Score: 96.66±8.99) in the 'older group' (OG). We verified no statistically significant difference between the two groups in terms of gender (Chi-squared test p=0.15) and hand-dominance (t-test p=0.007).

This study was conformed to the ethical standards of the 1964 Declaration of Helsinki and all the study procedures and documents, including the consent form, were approved by Verona University Institutional Review Board (CARU n. 22/2019). All participants provided written informed consent to participate in the study and publish the results in the de-identified form.

The device used in this experiment, *Bisbox 2.0,* is a sensorized rectangular box, a new and lighter (0.8 kg) version of the prototype described in (Galofaro et al., 2019). The dimensions of the box were 15×35×25 cm (height × width × depth). The 35 cm length was chosen to match the participants' average inter-shoulder distance, who should hold the device with the two hands placed on the two smaller faces. These smaller faces consisted of a rigid plate mounted on top of three load cells (mod. CZL635, Phidgets Inc., Calgary, Canada; full-range scale of 5 kg; precision of 0.05% and linearity of 0.05% FS) for measuring the force applied during the experiment. The sensorized box could be used stand-alone, with a memory card for data recording, or, as in this experiment, connected to a laptop via wireless communication (Wi-Fi network connection through a WIPY 3.0 microcontroller, programming language: Python). The laptop ran the software that controlled the experiment and provided instructions and feedback to the participants on a screen. The user interface was developed in Python 2.7.9 with the open-source libraries OpenGl and Pygame.

In this experiment, the *Bisbox* was secured to the top of a table, to avoid any movement of the device and to decouple the force applied by the two hands on each of its

two lateral plates. Participants sat in an armless chair in front of a 24“ monitor placed ~ 0.5 m away from the subject's chest. The height of both table and chair was adjustable so that the forearms rested on the table with shoulders in ~20 deg flexion and elbows at ~110 deg flexion. The hands were positioned fully open on the lateral sides of the device. A schematic representation of the setup is shown in Figure 22A.

Subjects were asked to keep a cursor on top of the sides of an isosceles trapezoid, displayed on a computer screen (Figure 22A). The cursor was programmed to move horizontally from left to right with respect to the subject, at the constant speed of 0.85cm/s, regardless of the subjects' actions. The sum of the force applied by the participants' hands on the lateral plates of *Bisbox* controlled the height (i.e., the vertical displacement) of the cursor (1 N = 0.15 cm). When no forces were applied, the center of the cursor was on the lower side of the trapezoid, corresponding to his major base. Each trial consisted of four phases of equal duration (two constant and two time-variant, Figure 22B):

Phase 1) *Increment phase*, *I*, where the cursor should move upward along one leg of the trapezoid. In this phase, subjects had to gradually increase the applied force, starting from 0 N and reaching the maximum force level after 3.5s.

Phase 2 & 3) *Holding phases*, H_1 *and* H_2, where the cursor should stay at the same height, moving along the top side, i.e., the minor base of the trapezoid. Thus, subjects had to maintain the same maximum force for 7s. H_1 accounted for the first 3.5 s, and H_2, for the last 3.5s.

Phase 4) *Decrement phase*, D, where the cursor should move downward along the

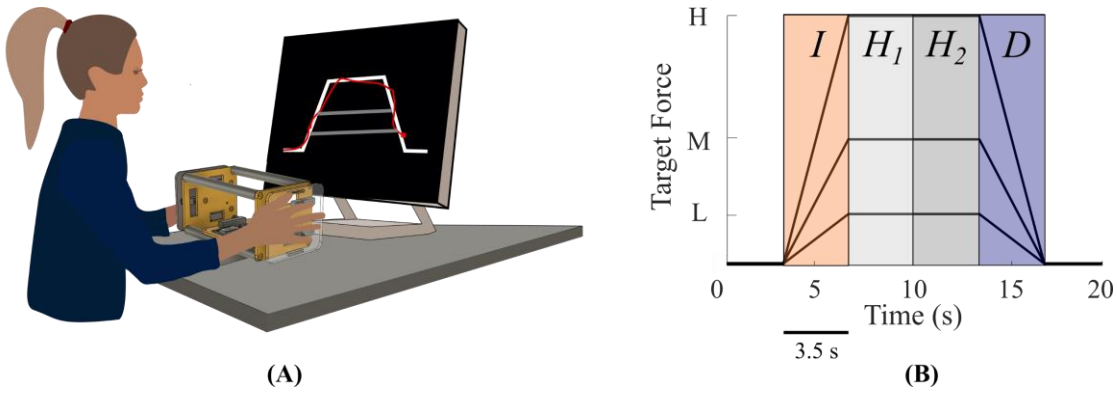

Figure 22. **(A)** Schematic representation of the setup. Subjects sat on an armless chair and pressed laterally the fixed device (designed with Fusion 360) following the visual cue on the screen (red cursor). All three trajectories (grey lines) were depicted on the screen and for each trial one of these was evidenced (continuous white line). **(B)** Ideal trajectories (L, M and H, evidenced on y-axis) that subjects had to follow. All the phases are evidenced by shaded areas: increasing phase (I, orange), holding phase 1 (H_1, light grey), holding phase 2 (H_2, dark grey) and decreasing phase (D, blue).

other leg of the trapezoid. In this phase, subjects had to gradually decrease the force reaching the 0 level in 3.5 seconds.

A trial lasted 14 seconds, and subjects paused for 6 seconds between trials.

In each trial, subjects had to reach with the *sum of the force* applied by the two hands one of the following three maximum force levels presented in random order: low (L=16 N), medium (M=40 N) and high (H=80 N). Three minor bases of the trapezoids corresponding to these three force levels were always displayed in grey on the screen, while for each trial, the sides of the trapezoidal shape to match were highlighted with a white line (thickness 0.8 cm) against a black background. The cursor was a red square of 0.4 cm side length.

The experimental session consisted of 30 trials, i.e., ten trials for each value of the maximal target force. An initial phase of familiarization was provided to explain the task sequence and how to perform it correctly.

4.2.3. Data Analysis and Outcome Measures

The raw force signals from the six load cells were recorded at 50 Hz and filtered using a 4th order low-pass Butterworth filter with a 10 Hz cutoff frequency before computing the performance metrics described in the following paragraph. Indicators were computed for each of the above-mentioned phases and for the entire trial. For each subject, we averaged the values obtained for the same target force.

Bimanual task performance.

We computed three parameters to evaluate the accuracy in controlling the total force applied by the two hands.

- ***Root-Mean-Squared Error (RMSE)*** measures the deviation of the participant's total force output from the target force trajectory (Lodha et al., 2010). Higher values for relative RMSE indicate less accuracy of total force output. It is defined as:

$$RMSE = \sqrt{\frac{1}{N}\sum_{i=1}^{N}(F_{Mi} - F_{Di})^2}, \tag{13}$$

where F_{Mi} is the *measured* total force at the sample *i* and F_{Di} the corresponding *desired* force. N is the total number of samples considered either on a single phase or on the entire trial.

- ***Bias Error (BE)***, the systematic component of the error, computed as the signed difference between the participant's total force output and the target force:

$$BE = \frac{1}{N}\sum_{i=1}^{N}(F_{Mi} - F_{Di}) \tag{14}$$

Positive values indicate an overshoot of the target force, negative values an undershoot (Schmidt et al., 1988; Marini et al., 2016b; Ballardini et al., 2019a).

- ***Coefficient of Variation (CV)****, a measure of* force variability (standard deviation) of the total force expressed as a percentage of the mean force output (Galganski et al., 1993):

$$CV(\%) = \frac{std\big(detrend(F_M)\big)}{|mean\ (F_M)|} * 100 \tag{15}$$

where F_M is the vector of the samples from force trajectory in each phase. We computed the standard deviation (std) of this signal after removing the best straight-fit line from the data (least-squares method, *Matlab* function detrend).

Differences between the force applied by each hand .

To determine the difference between the two hands while performing the bimanual task, we computed:

- ***Symmetry Index (SI)***, a measure of force symmetry between the two hands, computed as follow:

$$SI = \frac{1}{N}\sum_{i=1}^{N}\left(1 - \frac{|F_{MLi} - F_{MRi}|}{F_{Mi}}\right) * 100 \tag{16}$$

when the contribution % of the *right-dominant* (F_{MR}) and *left-non dominant* (F_{ML}) hands are equal, the symmetry index is 100, 0 instead indicated that the total force F_M is completely due only to one of the two hands. To remove contributions of noise, we computed this indicator on the average force profile (averaged over the 10 trial repetitions with equal target force) of each hand.

- ***Left Hand Force (LHF).*** This parameter indicated what % of the total force output (F_M) was applied by the *left – non dominant* hand (F_{ML})(Lodha et al., 2012):

$$LHF(\%) = \frac{1}{N}\sum_{i=1}^{N}\frac{F_{MLi}}{F_{Mi}} * 100 \tag{17}$$

- ***Correlation* between *right-dominant* and *left-non dominant* hand.** To estimates the coordination between the two hands, we evaluated the temporal correlation between left (F_{ML})- and right-hand force (F_{MR}) outputs within each trial by cross-correlating the forces applied by the two hands:

$$R_{xy}(\tau) = \int_{-\infty}^{\infty} {F_{ML}}^{*}(t)F_{MR}(t+\tau)\, d\tau \tag{18}$$

(* denotes complex conjugation) and we computed the maximum correlation Correlation = $\max_{\tau} R_{xy}(\tau)$ and the ***Time Delay*** between the two signals Lag= $\max_{\tau} R_{xy}(\tau)$.

- CV_H**.** This parameter assesses the force variation of each hand by considering, instead of the total force F_H, the force produced by each hand (H = L (*left-non dominant*) or R (*right-dominant*)). This outcome is similar to the CV(Equation 3) but defined for each hand force F_{MH} instead of the total one:

$$CV_H(\%) = \frac{std\,(detrend(F_H))}{|mean(F_H)|} * 100 \tag{19}$$

To further understand these results, we modelled the relationship between the parameter LHF and the parameter CV_L by mean of simple linear regression.

Statistical analysis. Normality was assessed by the Kolmogorov-Smirnov test, and sphericity condition for repeated measures ANOVA was assessed by the Mauchly test. These conditions were always verified. For all indicators, we performed a repeated-measures ANOVA (rANOVA) with one between-subjects factor: *'Group'* (2 levels: YG and OG) and two within-subjects factors: *'Target Force'* (3 levels: L, M and H) and *'Phase'* (4 levels: I, H_1, H_2 and D), and their interaction. Moreover, for the metrics CV_H we include a further within-subjects factor: 'Side' (2 levels: 'left-non dominant' and 'right-dominant').We also performed a post-hoc analysis (Fisher's LSD test) to investigate statistically significant main and interaction effects. The significance level was set at $p<0.05$. The p-values were reported with correction for multiple comparisons by the Bonferroni method (Hsu, 1996).

4.2.4. Results

The total force profiles applied by the two hands (Figure 23A) highlighted that the OG on average undershot the highest target level, while the two groups were more similar

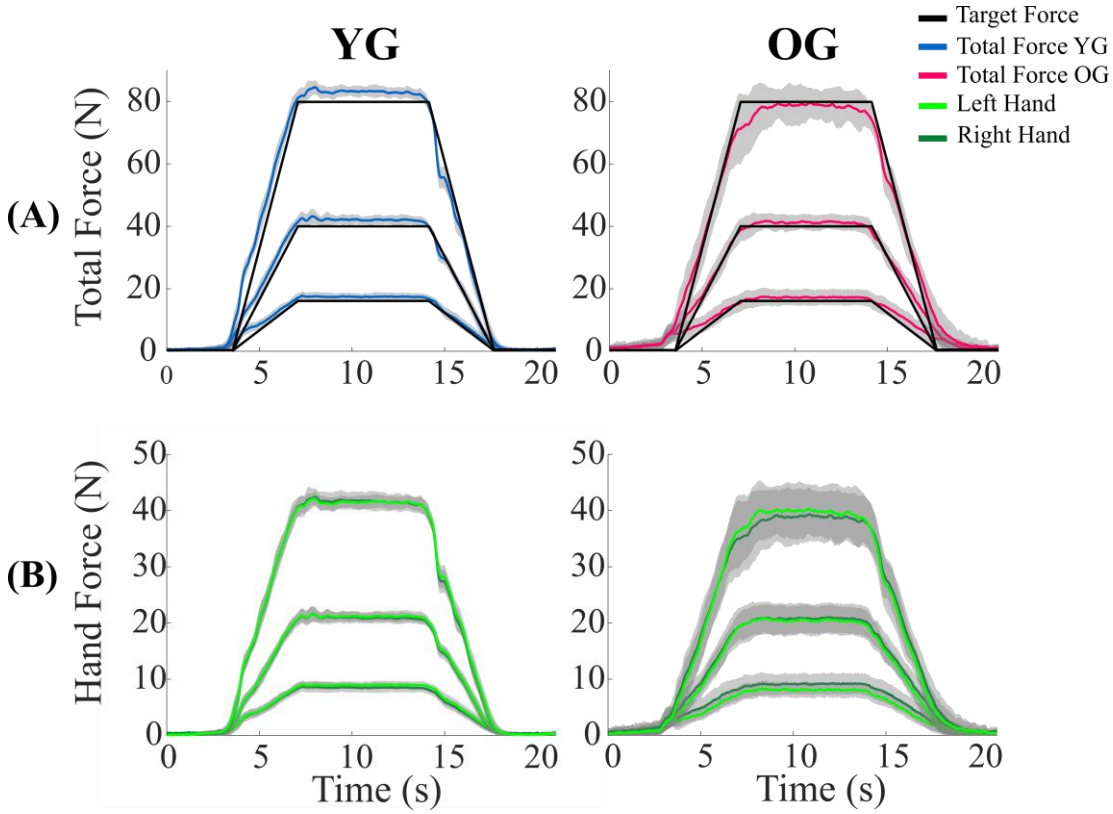

Figure 23: Trajectories (mean ± std) of each group for every target force, the first column is relative to the younger group (YG) while the second one is relative to the older group (OG). **(A)** Total Force: sum of the right-dominant and left-non dominant hand's forces: blue line indicates the YG while the magenta line denotes the OG. The black lines denote the desired target force. **(B)** Hand Force: force applied by each single hand; green lines indicate the left contribution while dark-green ones the right hand.

in terms of accuracy for the low and intermediate levels. By looking at the single force hand contribution (Figure 23B), younger subjects applied similar forces with both hands for all target levels. Instead, for most older subjects, each hand's contribution to the total force was more asymmetric, and the hand applying more force differed among subjects (high inter-subject variability) and depended on the force level. The analysis of these indicators confirmed and further extended these results.

In the following, we reported metrics computed for OG and YG groups related to each of the four phases (*I*, H_1, H_2, *D*) of the force profile separately and for the *overall* force profile (i.e., entire force profile: $I+H_1+H_2+D$ phases).

In all the related figures, we evidenced only the principal statistical effect (between-subjects factor: YG versus OG). The other effects (within-subject factor, interaction and post-hoc analysis) are described in the text. All values reported in the following text and in the figures are referred to (mean±SE).

Bimanual task performance

Older and younger participants had significantly different overall bimanual accuracy expressed in terms of RMSE (Figure 24A, 'Group' effect: $F(1, 32) = 91.68$, $p<0.001$), i.e., the younger subjects had lower RMSE in all phases for all the target forces. As expected, for both groups, the RMSE and the difference between the RMSE of the two groups increased with the target force ('Target Force' effect: $F(2,32)=189.48$, $p<0.001$, interaction effect: 'Group*Target Force': $F(2,32)=6.81$, $p<0.001$).

Finally, both groups had higher errors in the I and D phases (time-variant) than in the holding phases (H_1 and H_2) and evidenced higher errors in the first holding phase compared to the second one ('Phase' effect $F(3,32)=34.11$, $p<0.001$; 'Group*Phase' interaction effect: $F(3,32)=0.88$, $p=0.453$). The post-hoc analysis confirmed that errors in I and D were significantly higher compared to both H_1 and H_2 ($p<0.001$ for all comparisons). Also, comparing the two holding phases, the RMSE was slightly higher in the first than in the second ($p=0.01$); this difference was higher for the OG. Instead, the RMSE was not significantly different between I and D phases ($p=0.457$).

To further understand these results, we investigated the presence of a bias on the overall force exertion by computing the BE parameter (Figure 24B), whose positive and negative values indicate respectively a systematic tendency to overshoot and undershoot the required level of force. Also, in terms of force bias, the two groups were significantly different ('Group' effect: $F(1, 32)=11.24$, $p<0.001$). The difference depended on the target

level and the phase of the trial (interaction effects: 'Group*Target Force': $F(2,32)=9.56$, $p<0.001$ and 'Group*Phase': $F(3,32)=12.02$, $p<0.001$). We also found significant main effects of the 'Phase' factor ($F(3,32)=12.04$, $p<0.001$). Specifically, both groups had small bias errors at the lower target force (L) in all phases (YG: 0.45±0.43 N, OG: 0.60±0.67 N).

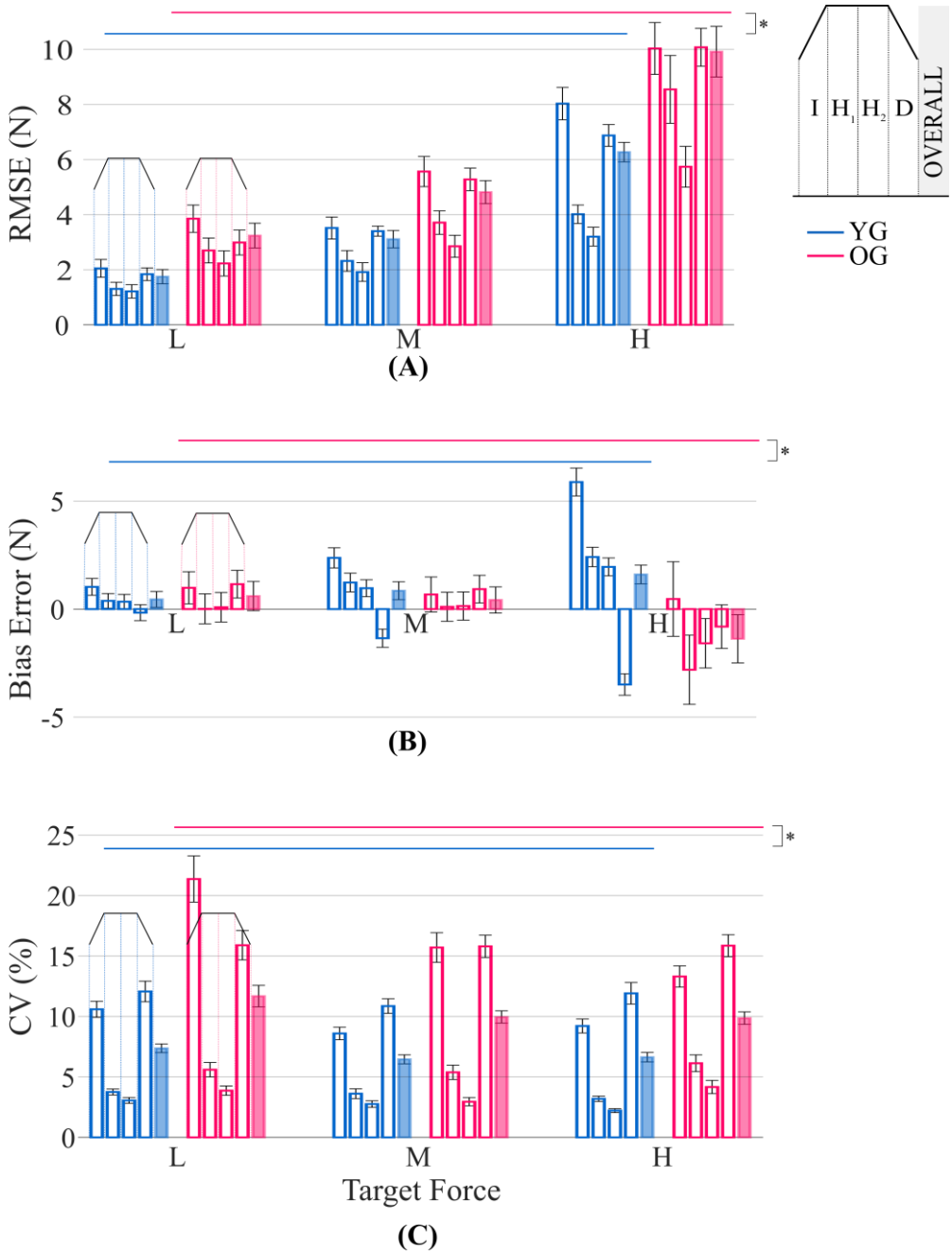

Figure 24: Bimanual performance metrics A) RMSE. B) BE. **C)** CV. Each metric is computed for the three force targets (L, M and H, as indicated in the x-axis). Blue colour denotes young adults (YG), magenta old adults (OG). As illustrated by the right-top legend, for each condition, each bar illustrates the parameter computed during one of the four phases, as indicated in the graph by the trapezoidal shape above them, while the right-ward fully coloured bar represents the metrics computed for the *overall* trajectory.

Then, for the intermediate target force (M), while the OG maintained similar performance compared to L, the YG group marginally worsened the performance (0.85±0.37 N), with a slightly higher undershoot in the descending phase and overshoot in all the other phases. Finally, for the highest target force (H), the bias error magnitude increased for both groups. However, while the YG overshoot the target force in all phases except the D phase, the OG, on average, undershoot the target force in all phases but in the I phase, having difficulties in reaching and maintaining the required maximum force.

As for the variability (CV, Figure 24C) of the overall applied force, the OG force was affected by higher variability than that of the YG ('Group' effect: $F(1,32)=144.79$, $p<0.001$). Both the variability factor and the difference in variability between groups depended on the phases ('Phase' effect: $F(3,32)=328.27$, $p<0.001$; interaction effect 'Group*Phase': $F(3,32)=20.53$, $p<0.001$). The CV was higher in the I and D phases for both groups and all target forces than in the holding phases (post-hoc: $p<0.001$, for all comparisons). Also, comparing the two holding phases, the CV was higher in the first than in the second (post-hoc: $p=0.006$), although this difference was higher for the OG. Instead, for both groups there was no statistical difference comparing the I and D phases (post-hoc: $p=0.523$). Finally, for the OG, the CV was on average higher for the lowest target force than for the intermediate and the highest target force ('Target Force' effect $F(2,32)=7.98$, $p=0.001$, post-hoc respectively $p=0.001$ and $p=0.002$) while there was no statistically significant difference between the two other levels ($p=0.993$).

Differences between the forces applied by the two hands.

We asked the subjects to control the cursor by applying the same amount of force with the two hands. OG applied forces less symmetrically than the YG (Figure 25A, 'Group' effect: $F(1, 32) = 56.78$, $p=0.02$). The SI increased with the target force amplitude ('Group*Target Force' interaction effect: $F(2,32)=15.38$, $p=0.004$, post-hoc 'Group' for all target force : $p<0.001$).

While the hand applying more force varied across subjects, for the lower target force, most of the participants belonging to the OG group relied more on the right-dominant hand, behaviour not observed in the younger group (LHF: 'Group*Target Force' interaction effect: $F(2,32)=156.78$, $p<0.001$, post-hoc between groups at the lower target force $p<0.001$).

The coefficients of variation of the left-non dominant and right-dominant hand ($CV_{H=L,R}$, Figure 25B) were similar for the YG. Instead, the OG had a higher CV for the

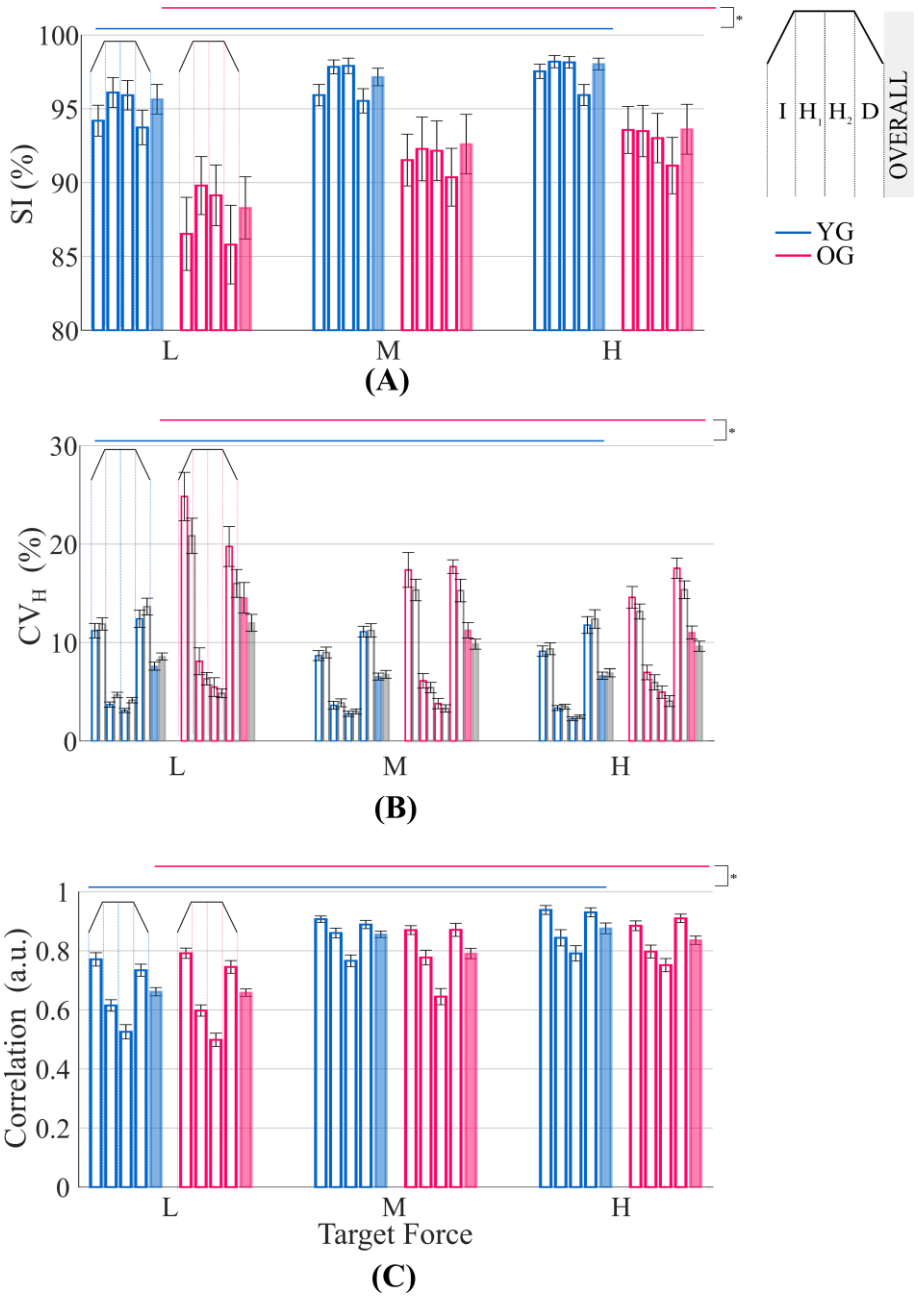

Figure 25: Single hand performance. Blue colour denotes young adults, magenta elderly adults As illustrated by the right-top legend, for each condition, each bar illustrates the parameter computed during one of the four phases, as indicated in the graph by the trapezoidal shape above them, while the right-ward fully coloured bar represents the metrics computed for the *overall* trajectory. Each metric shows the 3 levels of force that are evidenced on the x-axis (L, M and H). A) *Symmetry Index*. B) CV_H – Coefficient of Variation of the force produced by each hand (the pedix H denotes that the metrics is illustrated for both the left (coloured bar) and the right hand (grey bar)). C) *Correlation*.

left-non dominant than for the right-dominant arm ('Group*Side' effect: $F(1,32)=20.52$, $p<0.001$; post-hoc 'Side' YG: $p=0.476$, OG: $p<0.001$). This effect was observable for all target forces and in all phases, although it was more marked in the I and D phases.

Interestingly, the % of force applied by the left hand (LHF) for the lower target force (L), where we observed the higher differences between populations, significantly correlated with its coefficient of variation CV_L ($R^{\wedge 2}$=0.43, p<0.001): the higher CV_L, the lower the contribution of the left-non dominant hand. Interestingly the % of force applied by the left-non dominant hand had a similar correlation with CV_L /CV_R ($R^{\wedge 2}$=0.42, p<0.001), while a lower correlation was observed when considering the CV_R ($R^{\wedge 2}$=0.20, p=0.01). These correlations disappeared for the higher forces ($R^{\wedge 2}$ < 0.01 for both M and H targets force), Figure 26.

The two groups were also significantly different regarding the Correlation (Figure 25C) between the left-non dominant and the right-dominant hand forces profiles ('Group' effect: F(1,32)=19.41, p<0.001), but not in terms of Time Delay ('Group' effect: F(1,32)=1.54 p=0.215). The Correlation increased significantly with the increase of the target force for both groups targets ('Target Force' effect: F(2,32)=220.27, p<0.001), although in a different way for the two groups ('Target Force*Group' interaction effect: F(2,32)=4.82, p=0.009). In particular, the post-hoc analysis highlighted for the YG significant differences between the lowest level (L) and both the intermediate level (M) and the highest level (H) (post-hoc L-M and L-H: p<0.001 in both cases), but no difference between M and H target force levels (p=0.689). For the OG group, instead, we found

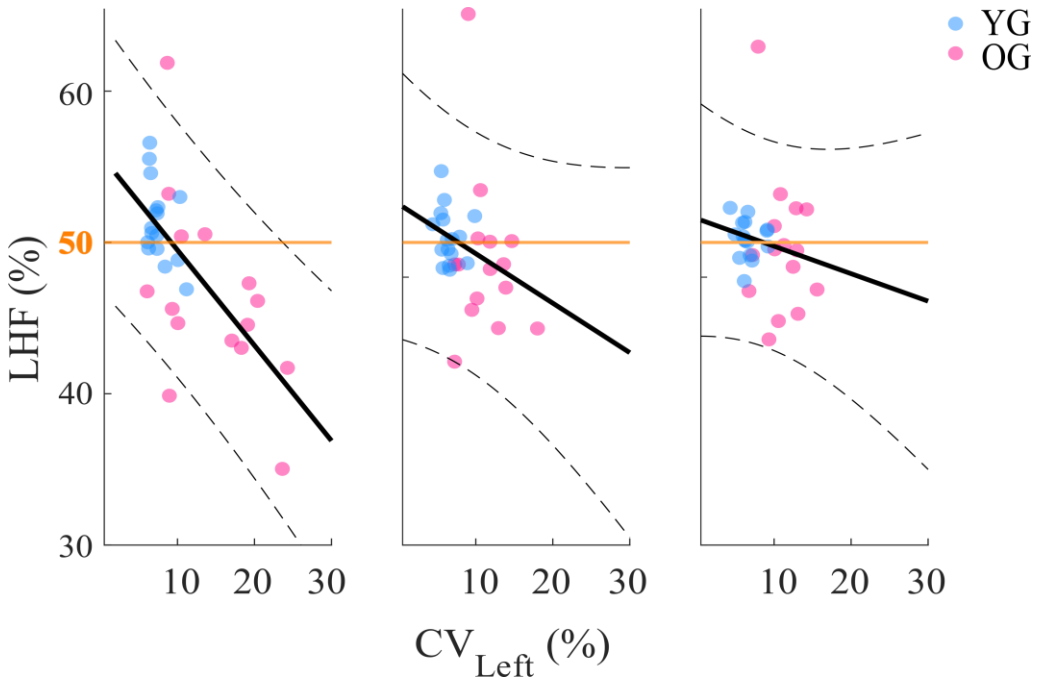

Figure 26: *LHF* versus CV_L – Left Hand Force versus Coefficient of Variation of the force produced by the *left-non dominant* hand. The dotted lines denote the confidence interval (95%), while the continuous line represents the regression line for each target force (left: Lower target force (L); middle: Medium target force (M); right: higher target force (H)) computed on both groups data.

significant differences between all levels (post-hoc: L-M and L-H $p<0.001$, M-H $p=0.02$). As expected, both groups had higher values of Correlation in the I and D phases than in the holding phases ('Phase' effect: $F(3,32)=127.81$, $p<0.001$; interaction effect 'Group*Phase': $F(3,32)=2.22$, $p=0.08$) and for the two higher target forces ('Target Force*Phase' interaction effect: $F(6,32)=5.03$, $p<0.001$). In the latter, the difference between force levels was mainly due to the holding phases. The post-hoc analysis evidenced higher values of Correlation in the I and D phases compared to the holding phases ($p<0.001$ for all comparisons) and significant differences between the two holding phases ($p<0.001$).

4.2.5. Discussions and Conclusions

From the first moment in which we are born, we interact with the outside world through touch, and haptic sensations allow us to understand the environment and to learn how plan and control our actions. We build and modify these abilities as we move through different stages of life, also adapting our motor skills to the changes in our brain and body.
The nerve fibers that are projected to the cerebral cortex through the corpus callosum are significantly reduced with aging, affecting the interhemispheric communication (Ota et al., 2006; Lin et al., 2014), increasing the difficulty to perform bimanual actions (Preilowski, 1972; Geschwind and Kaplan, 1998). The bimanual force control and its changes with age is mainly studied focusing on the pressure exerted by individual fingers without considering the joints complexity presented by the arms as a whole.
In this study, we investigated the performance and lateral asymmetries of younger and older subjects in a bimanual isometric force matching task, where subjects had to control the forces exerted by their hands against a sensorized object for matching constant and time-variant force profiles. Three different levels of maximum force were required: low, medium and high. To correctly solve the task, subjects had to satisfy three specific requirements: i) using both *distal* and *proximal* upper limb muscles; ii) simultaneously controlling the two arms to achieve a shared goal; iii) both arms acting symmetrically.
The older subjects significantly had lower accuracy and higher coefficients of force variation for both hands than younger subjects in all conditions. Interesting, for most of them, the *left-non dominant* hand was noisier than the other hand. Also, in the older participants, bilateral forces were more asymmetric, but with different hand preference/dominance among subjects. This asymmetry decreased with the higher target

levels. For the lower target force, where the asymmetries were more evident, subjects that exerted greater force with the *left-non dominant* hand were mainly those with lower *left-non dominant* hand variability. Conversely, subjects with higher *left-non dominant* hand variability relied more on the *right-dominant* hand to generate greater force.

As expected, we discovered significant differences concerning the different phases of the matched force profile: both groups showed lower accuracy (RMSE), higher variability (CV), and higher hands force correlation (*Correlation*) along with the *time-variant phases* compared to the *constant* ones; this result was more evident for the older group. Finally, we denoted lower accuracy, higher variability, and higher correlation, comparing the first holding phase with the second one.

In the following paragraphs, we discuss these findings in detail.

Older subjects had lower accuracy and more variable performance in all conditions. Aging is associated with a variation in the metabolic processes of the brain (Hyder and Rothman, 2012; Lin and Rothman, 2014) and with a degenerative process of the neuromuscular systems: the muscles fibers decrease together with the motor neuron number and firing rate, resulting in a reduced number of motor units (McNeil et al., 2005). This is combined with a reduced nerve conduction velocity (Norris et al., 1953; Jagga et al., 2011; Palve and Palve, 2018).

Several studies describe lower accuracy and higher variability while controlling force by older participants (Kapur et al., 2010), (Hu and Newell, 2011), (Lin et al., 2019), (Sosnoff and Newell, 2006), (Vaillancourt et al., 2003), (Lin et al., 2014). In our task, the reduced muscle strength (Rantanen et al., 1999; Kubota et al., 2012; Lin et al., 2019) and a faster fatigue onset (Hunter et al., 2016) for the older subjects could account for their undershooting the highest target force. Although we mitigated the last two factors by selecting three force levels that all our subjects were able to reach and we interspaced pauses among trials, the request of applying a force of 40 N repetitively with each hand could have been exceedingly challenging for the older subjects.

Along with the decrease in muscle strength and the acuity of the somatosensory feedback (Thornbury and Mistretta, 1981; Bowden and McNulty, 2013) aging is also associated with increased widespread cortical activity and reduced functional connectivity during the execution of motor tasks characterized by reduced interhemispheric inhibition (Goble et al., 2010; Fujiyama et al., 2016; Hermans et al., 2018; Monteiro et al., 2020). This increased activity has been referred to as either a compensatory phenomenon

reflecting higher cognitive demand for the elderly to accomplish the motor tasks or a differentiation deficit reflecting an impairment in recruiting specific and segregated cortical areas (Heuninckx et al., 2005), (Heuninckx et al., 2008), (Goble et al., 2010) and (Sala-Llonch et al., 2015). In line with this evidence, Vieluf et al. (Vieluf et al., 2018) found that during bimanual force matching tasks, a frontal activation shift compared with younger subjects, suggesting a more substantial use of cognitive resources like focused attention. These factors can account for an increase in force variability with age (Rudisch et al., 2020).

Older subjects had higher asymmetry between the two body' sides: the arm applying more force varied across subjects and depended on the force target. Recent findings shed new light on the phenomenon of hand dominance and preference, highlighting that it is significantly more complicated than it appeared. Several studies (Sainburg, 2002; Wang and Sainburg, 2007; Mutha et al., 2013) suggested that differences in the upper limbs motor performance could be interpreted as a consequence of upper limbs specialization, rather than a mere superiority of the dominant arm. Specifically, in reaching-to-target tasks, while the dominant upper limb maximized predictive control mechanisms that accounted for high precision in movement direction and trajectory, the non-dominant hand stabilizes the arm at the desired goal position by specifying the impedance around that position. This hypothesis was tested mainly in unimanual studies and/or by looking at the two hands' independent performance. Few studies focused on bimanual tasks where the two hands were physically coupled. Woytowicz et al. (Woytowicz et al., 2018) found a better stabilization performance of the *left-non dominant* hand in a task where the hands were coupled together by spring and had to reach a target position, moving one while holding steady the other. Instead, Takagi et al. (Takagi et al., 2020) found a more significant contribution -in terms of co-contraction- of the *right-dominant* arm investigating a task of hold and transport of a sizeable oscillating box. These two findings support the hypothesis that the *right - dominant* hand had a leading contribution in the bimanual stabilization task, while the *left–non dominant* one is 'only' better at compensating the *right-dominant* hand's interaction forces.

In our study the task was isometric, thus not influenced by the superiority in dynamic tasks of the right hand (Blakemore et al. 1998). The two arms performed a congruent task, as in (Takagi et al., 2020), but they were visually and not physically coupled, although they had to reach the same force goal. These isometric visually coupled

tasks were mainly investigated for fingers or hand-grip forces. In these cases, a higher force contribution of the strongest hand, i.e., the *right-dominant*, was found. However, the CNS is supposed to assign control authority based on each arm's strength and noise (O'Sullivan et al., 2009). While the strongest arm is usually the *right-dominant* arm, noise can depend on task requirements as the muscle districts involved or the specific target directions. In fact, in a task also involving proximal muscles (Salimpour and Shadmehr, 2014), a higher contribution of the *right-dominant* hand was found only for specific directions. Also, our task involves proximal muscles. As for the strength factor, lateralization is preserved in older subjects, although associated with a decreased asymmetry in between-hands dexterity (Teixeira, 2008) (Sale and Semmler, 2005). As for the noise factor, the somatosensory receptors can be affected by side-asymmetric changes with age (Iandolo et al., 2019), and this would increase the sensory feedback noise on one of the two sides of the body. These two findings could suggest that the control authority might vary individually, depending on sensorimotor noise. This evidence is confirmed by our data for the lower target force, requiring finer control and lower strength: there was a significant relationship between the relative amount of force exerted by the *left-non dominant* hand and the variability of such force. This relation was not observed for the higher forces when strength became more important for solving the task.

Both groups had more difficulty matching a time-variant than a constant force profile, and this difficulty was more remarkable for the older group. Both groups' performance was more accurate and affected by lower variability when maintaining a constant force level than when matching a *time-variant* force profile. This result was expected and supported by other literature results (Kubota et al., 2012). More interestingly, the elderly group's performance showed higher differences between *constant* and *variant - time* phases compared to young participants. The previous reporting suggested that aging is associated with an impaired ability to rapidly vary the force exerted (Kubota et al., 2012). In the study by Voelcker-Rehage et al. (Voelcker-Rehage and Alberts, 2005), the older adults performed as accurately as young subjects in static grasping force matching tasks, while their performance was significantly reduced in the time-variant tasks. Also, in our task, the two populations' force profiles highlighted the older subjects' more difficulty to change the control of the force from *time-variant* to *constan*t (this reflected on the higher error o the first constant phase with respect to the second). Several factors associated with the deterioration of the sensorimotor system could

account for this phenomenon. First, the cognitive demand could be more relevant when rapid changes are required (Goble et al., 2010). Second, the decline in the motor neuron firing rate and the number of motor units associated with aging could slow down the modulation rate of the force exerted (Kubota et al., 2012).

Both populations had higher hands force correlation in the time-variant phases compared to the constant ones. The bimanual coupling was investigated by computing the force profile cross-correlation (*Correlation*) between hands. We discovered that both groups evidenced higher Correlation along with the time-variant phases compared to the constant ones. Patel et al. (Patel et al., 2019) evidenced that higher correlation coefficients are associated with less accurate young and healthy adults' performances. The literature also emphasized the role of between-hands decoupling in the bimanual force control tasks as it could foster error compensation strategies (Patel et al., 2019), (Hu and Newell, 2011). Our data also support this result, finding higher hands force correlation (and lower accuracy) along with the *time-variant* phases compared to the *constant* ones.

Limitations

A limitation of our work was the absence of a concurrent muscle activity assessment that we plan to address it in a future study. This will allow us quantifying the contribution and the activation timing of both proximal and distal muscles involved in the task. This will also detect possible onset of fatigue that we tried to avoid interspacing resting phases between trials. Moreover, we made two protocol choices that could have determined the present results. First, we decided to select three-force levels equal for all subjects, not proportional to each individual’s maximum force, after verifying that the highest level, 40N for each hand, was a force level reachable by all participants. Second, we explicitly asked participants to apply equal force with the two hands, not allowing them to freely choose their strategy. It would be interesting to investigate if a different instruction would lead to equal or different results.

Conclusion

This study aims at delivering a general view on the age-related changes in the physiological aspects influencing the modulation of bimanual isometric force, involving, at the same time, both proximal and distal muscles. The results are promising, and the device

and the protocol could be integrated as assessment tool into clinical practice, while exploring its potential as rehabilitative instrument. Indeed, force modulation is crucial in multiple daily activities and the recovery of this ability is an import goal for several people suffering from different neurological diseases.

4.3. Exoskeleton-Based Haptic Interface for Bimanual Manipulation of Virtual Objects [6]

4.3.1. Introduction

Virtual reality (VR) employs interactive simulations to immerse users in an environment similar to the real-world (Tieri et al., 2018). The advantages of immersive and non-immersive VR for several applications, like entertainment, laparoscopic simulations, motor training as well as remote manipulation in industry settings, have been extensively validated (Schultheis and Rizzo, 2001; Saposnik et al., 2016; Laver et al., 2017; D'Antonio et al., 2020; Porcini et al., 2020). Presently, "immersive" systems usually deliver stereo images as a function of head-tracking such that the user can freely explore a virtual environment (VE) (Bohil et al., 2011). However, these sensorial channels alone are not sufficient when an interaction between the user's body and virtual objects is required. Indeed, in real life, the objects' manipulation involves a third sense, the so-called *haptic sense* (Garrington, 2010; Milstein et al., 2021).

Several authors (Panait et al., 2009; Overtoom et al., 2019) showed how the integration of force feedback in a simulated operative environment could drastically improve the training outcomes compared with performance obtained in the same task employing solely visual feedback (Maisto et al., 2017; Takahashi et al., 2020). In addition, Contu et al. (Contu et al., 2016) observed how bimanual performance improves when the haptic feedback is complemented by visual information using a bimanual wrist workstation. The importance of haptic contribution in interactive applications was also confirmed by Kuschel et al. (Kuschel et al., 2008), which compared the perception of virtual compliance when visual and haptic feedback were synchronously provided. A different study (Mugge et al., 2009) investigated human's ability to discriminate compliance in simulated haptic objects and how it is perceived in relation to the simulated objects' stiffness. Compliance perception is, however, subjective and it is not a process that can be described purely by haptics but rather involving psychophysics; furthermore,

[6] Part of this Chapter has been submitted as: E. D'Antonio*, E. Galofaro*, F. Patané, M. Casadio and L. Masia *Importance of Dynamic Features in Bimanual Haptic Interaction using a Dual Arm Exoskeleton*, IEEE/ASME International Conference on Advanced Intelligent Mechatronics 2021 and is in preparation for a full journal paper.

compliance perception integrates also a visual sensory component (Tiest and Kappers, 2009) that is deeply involved in the interpretation of virtual reality (VR) generated environment, and which plays an essential role in the motor learning process during interaction with simulated objects.

Nevertheless, the majority of the proposed haptic systems consist of end-effector or compact wearable devices with limited workspace and force ranges (Massie and Salisbury, 1994; Laycock and Day, 2003; Maisto et al., 2017; Sreelakshmi and Subash, 2017; Meli et al., 2018; Su et al., 2020) A full human range of motion and wide forces could be obtained through the new advancements in cooperative human-robot technology, overcoming the limitation due to the magnitude of the force that can be sent back to the user while maintaining system stability (Colgate and Brown, 1994; Adams and Hannaford, 1999). Furthermore, the generation of virtual surfaces in a simulated environment is still challenging due to actuators' limitations imposed by stability, which is the paramount requirement in haptics.

Haptic methods employ a representation of the device end-effector (EE) in the VE to compute in real-time the forces due to the interaction with virtual environmental objects. The “god-object method” is the classical paradigm of reference (Zilles and Salisbury, 1995): each EE is expressed in the VE by two spheres to implement an impedance control through the stiffness and damping parameters linking the two virtual counterparts. This interaction, named “virtual coupling”, modulates the force feedback to be sent to the user by means of the haptic device.

The most common Activities of Daily Living (ADLs) require coordinated use of both arms and the functional coordinated interaction between the two cerebral hemispheres to exploit the bimanual coordination. Each hand has its well-defined role: the non-dominant one stabilizes to steadily hold the object, while the dominant hand finely manipulates it and completes the aforementioned action. Most of the everyday situations require the recruitment of both arms, yet neural mechanisms underlying bimanual coordination are still a scientific debate, and the formalization of dynamic laws describing mutual interaction between limbs cannot be generalized across the vast manifold of human dexterity. Literature offers a noteworthy number of studies involving bimanual haptic settings targeting multiple purposes: from rehabilitation to general motor control and haptics. The aforementioned contributions and the employed setups have been compellingly summarized in a review paper by Talvas and colleagues (Talvas et al., 2014). However, they lack realistic scenarios involving multi-articular and complex movements.

Bimanual haptics specifically refers to a type of interaction taking place between the hands of the same person. In literature, such aspect is often categorized in two distinct types of approach: (i) *uncoupled independent control*, where hands separately act without a common objective and on separate workspaces, (ii) *coupled control* in which they mutually interact with a common purpose, i.e., by manipulating the same object simultaneously.

Mechanisms underlying the control of bimanual actions have been extensively investigated for *uncoupled* tasks (Tcheang et al., 2007; Nozaki and Scott, 2009; Casadio et al., 2010), while few contributions specifically focused on bimanual tasks in *coupled* settings (Johansson et al., 2006; Contu et al., 2016; Mutalib et al., 2019). Research mainly focuses on investigating *uncoupled schemes* regarding object manipulation subjected to gravity and various artificially generated force fields (Nozaki et al., 2006; Harley and Prilutsky, 2012; Hayashi and Nozaki, 2016).

The reduced number of investigations on *coupled bimanual* tasks followed a different approach by focusing on the brain's hemispheres and their specialization in motor control manifolds. In a study involving bimanual object manipulation through a dual-wrist robotic interface, Takagi et al. (Takagi et al., 2020), tried to characterize the role of each limb: conversely to the dynamic-dominance theory (Sainburg, 2002), whereby the non-dominant hand is specialized in the task stabilization, the authors found that subjects preferred to stabilize the manipulated object with the dominant hand.

There is a substantial difference between the two previously introduced conditions (*uncoupled Vs. coupled*), especially from a neurophysiological perspective: many studies on primates have highlighted how bimanual manipulation is computed in specifically dedicated brain areas where unique synapses develop (Donchin et al., 1998; Steinberg et al., 2002; Rokni et al., 2003; Ifft et al., 2013).

Two theories exist which describe the mechanisms underlying the interconnection of dominant and non-dominant hemispheres in processing sensorimotor information during bimanual manipulation: (i) the coordinated use of limbs is highly weighted by the dominance of one hemisphere over the other, with the dominant one primarily acting (imposing the task dynamics) and the other stabilizing the manipulation (Geschwind, 1975; Guiard, 1987; Viallet et al., 1992; Toga and Thompson, 2003); (ii) the remarkable dynamism and flexibility of the brain lead to switching the functional dominance of hands across various environmental constraints and task difficulties (Jiang and Kanwisher 2003; Johansson et al. 2006).

Considering the importance of *haptic feedback* and *coupled bimanual interaction* for practical applications and thanks to the currently available technologies, the purpose of our contribution is to provide evidence that our *haptic control* could be an available method in various fields. To this extent, our study is three folds: (i) to implement an exoskeleton-based haptic interface with virtual objects providing customized stimuli; (ii) to identify the strategies of motor control, i.e., the distribution of functional roles between the two limbs concurring in a bimanual coupled manipulation scenario; (iii) to characterize how subjects' performance change according to the perception of different simulated objects with variable compliances.

We designed a specific task where subjects performed a bimanual manipulation/reaching task employing a 6DoFs exoskeleton, named ALEx-RS: participants were requested to grab and lift a virtual object using two arms and move it across a 3D-workspace towards multiple targets. Different visuo-haptic feedback conditions were implemented to replicate objects of various dynamics and, therefore, compliances with the associated weight and inertia.

The central hypothesis is that an opportunely designed combination of haptic and visual feedbacks would differently affect manipulation strategy in a three-dimensional task; based on previous evidence (Joël Fagot, 1997), (Grouios, 2006), we hypothesize that hemispheric specialization might influence the bimanual coordination strategy during manipulation and target's reaching.

4.3.2. Experimental Setup, Task and Participants

Experiments have been carried out using the Arm Light Exoskeleton ALEx-RS (Ruffaldi et al., 2014; Pirondini et al., 2016; Frisoli, 2018) depicted in Figure 27A (see details in Paragraph 3.3.2).

In the framework of the current contribution, the robot has been wholly re-programmed in a new bimanual haptic modality able to provide torques at the joints computed from the virtual interaction in the environment with simulated objects. The controller will be deeply discussed in the next section providing information on how haptics has been computed.

The control architecture, designed to provide stable force feedback during the virtual objects' manipulation, included three main components (Figure 28): a ***Virtual Reality Unit*** (***VRU***), an ***Impedance Controller***, and a ***Torque Computation module***.

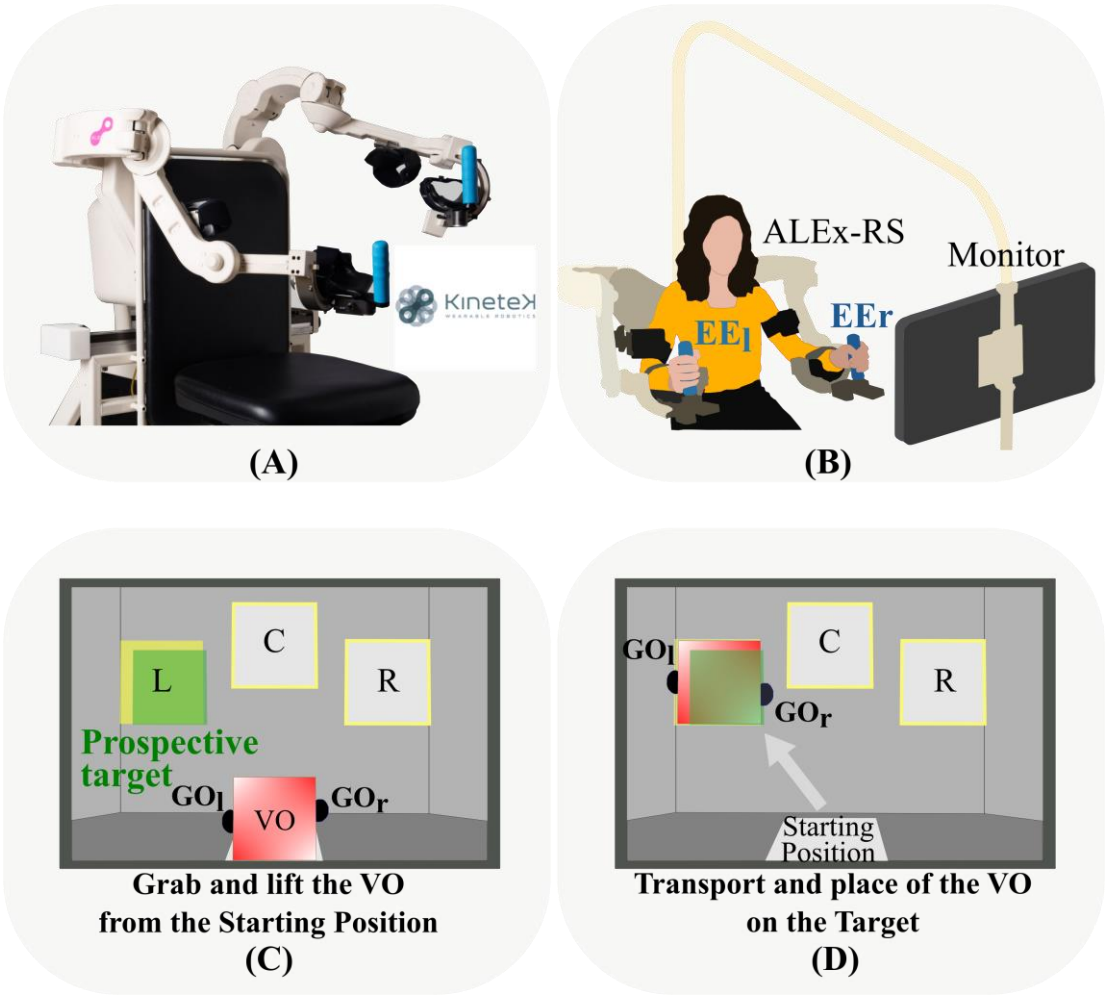

Figure 27: **(A)** ALEx-RS robotic device (http://www.wearable-robotics.com/kinetek/). **(B)** Subject is performing the experiment while wearing the exoskeletons. **(C)** Virtual scenario including the virtual object (VO, red cube) and the god-objects (GO_l and GO_r, black shapes) during the initial phase of the task. **(D)** Virtual scenario during the reaching of the left target (L).

The ***VRU*** (Figure 28B) provided the visual representation of the interactive scenario, and it computed the "physical-based" response to the user's movements in the virtual environment, generated by using Unity 3D ((Unity Technologies, 2018), version 2019.2.13f1). This module allows the collision detection between the virtual counterpart of the handles' device and the virtual environment: the resulting data is sent to the Impedance Controller at a frequency of 200 Hz to compute the haptic feedback (Figure 28C).

The scenario presented to the participants replicated a virtual room enclosed by four walls (3 walls and the floor) to allow users to visualize (i) the virtual object (VO) to manipulate, represented as a cube, (ii) the device end-effector positions (EEs), resembled as spheres and (iii) the targets, designed as square-shaped portion highlighted in the workspace.

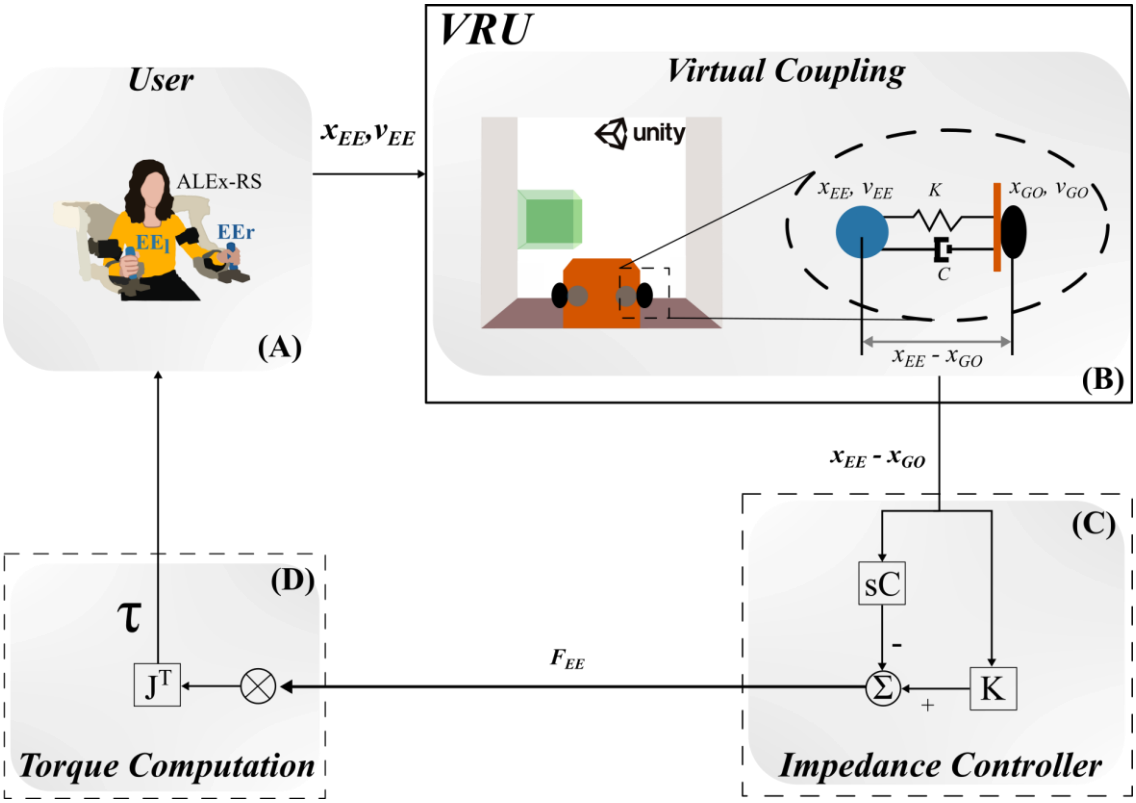

Figure 28: Control Architecture Scheme. (A) User. (B) Virtual Reality Unit (VRU). (C) Impedance Controller module. (D) Torque Computation module.

The task consisted of bimanually grabbing and lifting the VO, securing it in a stable interaction without exceeding force thresholds (Figure 27C), and successively delivering it to an indicated target position (Figure 27D).

The ***Impedance Controller*** module, running at 1kHz (Figure 28C), computed the haptic feedback by modulating the interaction force at each EE, whose position in the ***VRU*** was computed by means of the forward kinematics using the angular sensors integrated into the exoskeletons' joints. EEs coordinates (XYZ) were then converted into location in the virtual scenario by using linear scale mapping such that a 2 cm robot motion corresponds to a 1 cm in the virtual reality. Haptic rendering was implemented using the "*God-Object method*" with friction simulation (Ortega et al., 2007), which employs two representations of each end-effector to implement an impedance control rendering stiffness and damping effects perceived during interaction with a simulated object (***Impedance Controller*** module). Such interaction is called "Virtual Coupling": and it is exploited as force feedback which is rendered as a torque at the joints of the robotic device (Figure 28D), mediating the interaction between the user and the simulated environment.

In details, each hand position is represented in the ***VRU*** by two spheres respectively named End Effector (EE) and God Object (GO), as shown in Figure 29, and they are used for two different computations:

- a blue sphere (End Effector, EE), not visible to the user, represents the end point used to compute the haptics and corresponds to the real EE position in the robot workspace.
- a black sphere, named God Objects (GO), visible to the user, which feeds back the position and deformation due to contact with the VO. The GO is not used to compute the haptic forces but only the *visual feedback* to complement the *haptic feedback* (Contu et al., 2016). Yet, its shape factor, which is changed to visually provide contact (deformation), depends on the end effector's real position.

Considering Figure 29A, in the absence of contact between the EEs and the VO (or the room walls), the two spheres (blue and black) move synchronously, and no force is fed back to the user. The generation of haptic feedback and visual deformation is computed when the EE is in contact with the VO. The non-visible blue sphere EE (EE_l or EE_r for left or right end effectors) follows the actual position of the exoskeleton, which is penetrating the object, while the (black sphere) GO position (GO_l or GO_r) remains tangent to the object

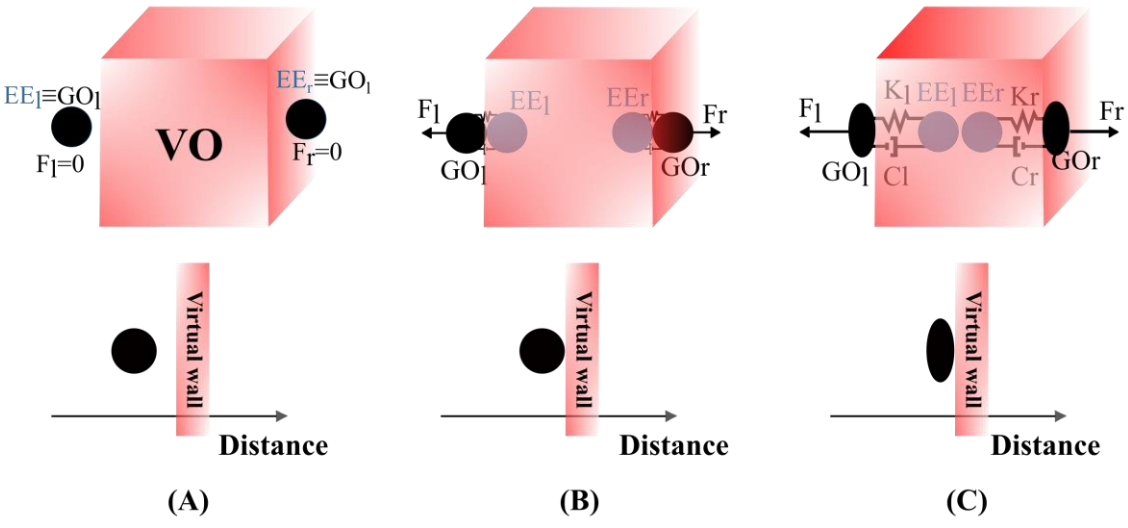

Figure 29: Principle of the *Virtual Coupling God-Object algorithm*: although the haptic EEs (blue spheres) penetrate the god-objects (GOs, black spheres) are constrained to remain on the surface of the obstacles. **(A)** Representation when the GOs and the EEs are in the surrounding space without touching obstacles, they are exactly overlapped, and no force is provided to the user. **(B)** Representation when the EEs compenetrate the VO and the GOs remain on the surface providing forces proportional to the distance between the GOs and the EEs. **(C)** Representation when the EEs deeply compenetrate the virtual object: more force is provided to the user and the GOs are squeezed. The bottom line simplifies the description by setting out in 2D what is represented in the line above.

and visible, Figure 29B. Generation of forces is progressively calculated, based on the penetration of the EE inside the VO, in the ***Impedance Controller*** module by means of elastic repulsive components proportional to the distance between the real sphere (EE_l or EE_r) and the God-Object (GO_l or GO_r), (Figure 28C). Simultaneously, a viscous term is provided by the mutual velocity between the two spheres during motion (Sankaranarayanan and Hannaford, 2006). To provide visual information of the contact force, the GOs are deformed by changing the form factor using the EE's penetration depth into the VO, Figure 29C. The spheres are squeezed on the object surface proportionally to the applied forces and, therefore, to the distance between EE and GO.

The haptic feedback to the user was provided for each EE by computing the interaction force $\overrightarrow{F_{EE}}$ along the three dimensions of motion:

$$\vec{F}_{EE} = \begin{pmatrix} 0 & -\overrightarrow{\Delta X} & -\overrightarrow{\Delta \dot{X}} \\ M/2 & 0 & 0 \\ 0 & 0 & 0 \end{pmatrix} \begin{pmatrix} g\vec{j} \\ k_0 \cdot (1-\varepsilon)\vec{i} \\ c\vec{i} \end{pmatrix} \qquad (20)$$

M is the mass of the virtual cube, $\vec{g}$ the gravity acceleration, $k_0 * (\mathbf{1} - \boldsymbol{\varepsilon})$ represents the object's stiffness where $\boldsymbol{\varepsilon}$ is the scale parameter for deforming the VO, c the damping factor of the viscous force, $\overrightarrow{\Delta X}$ the distance between the EE position (x_{EE}) and the GO position (x_{GO}), $\overrightarrow{\Delta \dot{X}}$ the mutual difference between the EE and the GO linear velocities obtained by discrete-time differentiation.

Since the task required to lift the VO using the two EEs, we also simulated the vertical static friction force (F_f) which assures contact between the EEs and the object preventing slippage by generating a minimum *contact force*. The dynamics of the VO, namely $\vec{F}_{cube}$, depends on the forces applied by the EEs during bimanual manipulation ($\overrightarrow{F_{EEr}}$ and $\overrightarrow{F_{EEl}}$), on the gravity force $M * \vec{g}$ and on the static friction ($\overrightarrow{F_f}$) and was described by the following equation:

$$\vec{F}_{cube} = \begin{pmatrix} 0 & 0 & 1 & 1 \\ M & 1 & 0 & 0 \\ 0 & 0 & 0 & 0 \end{pmatrix} \begin{pmatrix} g\vec{j} \\ F_f\vec{j} \\ F_{EEr}\vec{i} \\ F_{EEl}\vec{i} \end{pmatrix} \qquad (21)$$

VO parameters were chosen considering the haptic rendering capability of the device for not incurring in saturation during the task ($M = 0.2\ kg$, $c = 5\ Ns/m$, $k_0 = 150\ N/m, 0 \leq \boldsymbol{\varepsilon} \leq \mathbf{1}$) and preserving the device's *stability*.

To simplify the online computation of task dynamics and generate a stable interaction, the VO can be manipulated in a three and not six-dimensional manifold: linear movements along the orthonormal axes (XYZ) were allowed, but rotations (θ_X, θ_y, θ_z) were disabled. Constraining rotations was necessary due to the computational algorithm implemented to estimate the virtual interaction forces applied between the handles when in contact with the object, consequently feeding back the participants' resulting dynamics.

Forces and relative haptic feedback were computed using single interaction points between the object's surface and the EEs, which makes it impossible to balance rotations around the coordinated axes unless forces are directionally aligned and with opposite magnitude. Hence the VO can be moved along the coordinated axes but not rotated, providing across the workspace reaction forces generated by the interaction with the EEs.

The force values at each EE are then sent back to the device through a shared memory communication protocol, and then converted through the ***Torque Computation** module* (Figure 28D) in torque at the joints (τ), using the known jacobian transformation of the two exoskeletons:

$$\tau = J^T * F_{EE_{r/l}} \qquad (22)$$

The objects were implemented by modelling the following *virtual physical properties*, as depicted in Figure 30A:

1. *Stiffness* (k_i): ruled by the following relation:

$$k_i = k_0(1 - \varepsilon) \qquad (23)$$

2. *Breakage limit* (F_{break}): by varying the breaking point in terms of maximum force that the material could withstand without collapse and resulting in a failed trial.

During the pick and place task, an appropriate level of contact force between the *EEs* and the *VO* should be kept to prevent failure, which can occur when in two different ways: (i) when a sufficient level of *Contact Force* along the x-axis ($F_{contact}$) was not maintained

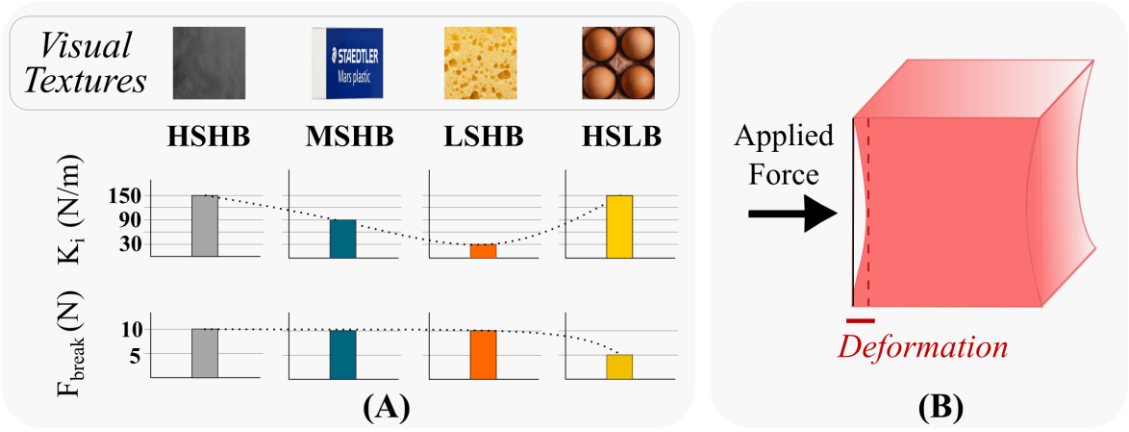

Figure 30: **(A)** Visual textures and physical features of the four virtual objects (VOs): **HSHB** (High Stiffness, High Breaking point), **MSHB** (Medium Stiffness, High Breaking point), **LSHB** (Low Stiffness, High Breaking point) and **HSLB** (High Stiffness, Low Breaking point). **(B)** Schematic description of the *Deformation* metrics: the red line evidences the effective measurement.

during grabbing the *VO* with the two *EEs* hence causing the object slippage and falling; (ii) when exceeding grabbing force ($> F_{break}$) causing the object breakage.

Objects' textures were chosen to provide users with visual information on the "material" to manipulate, as depicted in Figure 30A:

- "*HSHB – High Stiffness, High Breaking point"* in which subjects were provided with a rigid-looking object depicted with metallic surfaces, characterized haptically by high stiffness: the object was difficult to deform, presenting high rigidity, and the breakage limit was set high.

- "*MSHB - Medium Stiffness, High Breaking point*": subjects experience a compliant object which can be deformed yet presenting a medium/high stiffness. The visual texture resembled elastic components, and the breakage point was set high.

- "*LSHB – Low Stiffness High Breaking point*": the object was characterized by a very low stiffness, and therefore was highly deformable while the breaking threshold was set high. The visual texture resembled soft components.

- "*HSLB - High Stiffness, Low Breaking point*": this last haptic simulation aims at replicating a fragile object, as suggested by the visual texture. The stiffness was set

to high, and yet the breakage threshold was low. Subjects did not experience compliance.

The specifications of the four different VOs are presented in Table 9.

Table 9: Virtual Objects Properties.

Properties	**Virtual Objects**			
	HSHB	***MSHB***	***LSHB***	***HSLB***
F_{break} **(N)**	10	10	10	5
ε	0	0.4	0.8	0
$F_{contact}$ **(N)**	2	3	3	2
k_i **(N/m)**	150	90	30	150

A group of fifteen healthy young subjects (8 males and 7 females, 25.9 ± 3.5 (mean ± std) years old, range: 21-33 years), took part in the study. Within the group, there was no significant difference in the age distribution between males and females; all subjects were right-handed according to the Edinburgh Handedness Questionnaire (Oldfield, 1971) (Laterality score (LS) = 83.78 ± 15.91 (mean ± std)). All participants provided their informed consent before the experiment, and the experimental protocol was approved by Heidelberg University Institutional Review Board (S-287/2020): the study was conducted following the ethical standards of the 2013 Declaration of Helsinki. Experiments were carried out at the Aries Lab (Assistive Robotics and Interactive Exosuits) of the Heidelberg University. Subjects did not have any evidence or known history of neurological diseases and exhibited a normal joint range of motion and muscle strength.

Subjects were sitting on a comfortable seat equipped with adjustable footrests in front of a large screen (43 inches) on which the virtual scenarios were shown. The user's arms and forearms were secured by means of Velcro straps and safety belts on the exoskeletons, Figure 27B.

For every single trial, participants were requested to grab, lift, transport and place the object on the target (reach phase) from a predefined starting point.

Three target positions (left, L=-45°; centre, C=0°; right, R=45°) were presented in order to study and analyse the motor control strategies across different directions and the portion of the workspace, Figure 27C-D. Targets were placed along a semicircle, equally spaced from

the starting position (radius = 40 cm_{robot}, depth =15 cm_{robot}): each target was presented six times, obtaining a total of 18 repetitions for material condition. The targets were proposed as yellow squared shape pictures with the same VO dimensions along the x and y axes. A semi-transparent green squared shape was positioned in the same x and y coordinates of the target but at a distance equal to the size of the cube along the z-axis to help subjects understand the environment perspective since we represented a virtual 3D scenario on a 2D screen. No time constraints were imposed to avoid participants' anxiety and inability to complete the task.

Participants were instructed, by a familiarization phase, to maintain an appropriate level of contact force with the VO throughout all trials, to not incur in failure. In case of failure, an *auditory cue* was provided (a specific one for the breaking and another one for the falling condition) to inform subjects about the wrong task execution and return to the starting point for a new trial. If the movement was performed successfully, a further "success" *auditory cue* was provided, and subjects were asked to place their arms in a specific position to start with the new trial.

The experiment was organized in a single session. Four different conditions were randomly assigned to each subject, with a 5-mins rest break between different conditions for a total duration of the experiment of about 1 hour.

4.3.3. Data analysis and Outcome Measures

Forces and trajectories were recorded at 200 Hz and filtered using a 6^{th} order low-pass Butterworth filter with a 10 Hz cutoff frequency. We considered geometrical and kinematic factors to extract the participants' dynamics and extrapolate the indicators to characterize their performance.

The ***Deformation*** *(m)* of the VO (Figure 30B) during the interaction with the end-effectors of the dual exoskeletons was the primary data: defined as the difference between the VO initial width (before contact with the EEs) and the Euclidean distance (along the x-axis) computed between the EEs:

$$\boldsymbol{Deformation} = \frac{\text{VO initial width} - (\sqrt{EE_l - EE_r})}{2} \qquad (24)$$

For each target, data were collected and successively analyzed, considering both *successful trials* and *failure trials*. The *successful trials* were defined as the elapsing time

between the VO's last grab and the time in which it was successfully placed on the target, without any breakage or slippage. The *failure trials* were those where participants applied a too large grabbing force of undershooting the minimum contact force, provoking object slippage and consequent breakage.

We computed the following indicators using only *successful trials*, by post-processing the end-effector trajectories in both spatial and temporal domains.

The ***Dynamical Symmetry Index (DSI**, %)* (Contu et al., 2016), to evaluate temporal coordination during coupled bimanual manipulation tasks, and it is evaluated as the percentage difference between the trajectories of the two EEs across the trials:

$$\boldsymbol{DSI(t) = \frac{\Delta X_R(t) - \Delta X_L(t)}{\Delta X_R(t) + \Delta X_L(t))} * 100} \qquad (25)$$

where $\boldsymbol{\Delta X_R(t)}$ and $\boldsymbol{\Delta X_L(t)}$ are the distances between the initial grabbing point (computed as the point in which $F_x > minimum\ contact\ force$) and the instantaneous position of the dominant and non-dominant hand, respectively. This is an indicator of bimanual coordination in object manipulation. It ranges from -100% to 100%: positive values indicate that the right EE trajectory is longer than that of the left EE. In contrast, the DSI's negative signs describe an opposite situation in which the non-dominant EE traces a longer path than the dominant one. ***DSI*** values between ±5% indicate symmetry; larger values are considered to indicate asymmetry between the two limbs.

The ***Normalised Jerk (NJ)*** (Teulings et al., 1997) has been considered as an indicator of movement smoothness, and it is calculated by the following expression:

$$\boldsymbol{NJ = ln\left(\sqrt{\frac{T^5}{2L^2}\int_0^T j(t)^2\,dt}\right)} \qquad (26)$$

where ***T*** is the execution time for a single trial, ***L*** is the Path length and ***j(t)*** is the jerk index equal to the time derivative of acceleration (***j(t)*** $= \boldsymbol{\delta^3 x/\delta t^3}$, ***x*** = EE trajectory), that is minimised in the presence of smooth movements. ***NJ*** is normalized with respect to execution time and path length such that trajectories of different duration and sizes can be compared.

To observe the change in manipulation strategies across subjects, we evaluate the ***Force Profile*** shapes resulting from the haptic interaction between the end effectors $\boldsymbol{EE_{r/l}}$ and the ***VO***, given by the equation (20). In particular, we focused such analysis on the

interlimb differences of forces applied by the $\boldsymbol{EE_{r/l}}$, which indicates the variation of coordination between the two hands (Lai et al., 2019). We normalized the ***Force Profile*** with respect to the total length of the trajectory performed from the initial grab of the ***VO*** to the successfully reaching of the target.

The following metrics are extracted from data referred to both the *successful* and *failure trials.*

Force Percentage Break (FPB**, %)*, computed as the ratio between the force applied on the $\boldsymbol{EE_l}$ ($\boldsymbol{F_l}$) and the sum of the force on both the ***EEs ($\boldsymbol{F_r}$ and $\boldsymbol{F_l}$) in the instant in which subjects exceeded F_{break}:

$$\boldsymbol{FPB = \frac{F_L}{F_L + F_R} * 100} \qquad (27)$$

This is an indicator of the hand responsible for breaking the ***VO***. It ranges from 0% to 100%: values between 0% and 50% indicate that the dominant hand exceeded the imposed force limits, while values between 50% and 100% describe an opposite situation in which the non-dominant hand exceeded the force limits.

The ***Execution Time*** *(s)* is defined as the amount of time taken to successfully move the object from the starting position to the target, including the failure trials.

Finally, the ***Maximum Failures (MF) is*** computed as the maximum times of the ***VO*** breaking event during all the experiments for every condition.

Statistical Analysis. The metrics ***Deformation***, ***DSI***, ***NJ***, ***Force Profile,*** and ***FPB*** were averaged over time. We used a repeated-measures analysis of variance (rANOVA) on the dependent variables. We considered as within-subjects factors: '*Target*' (Right (R), Central (C), Left (L)), '*Material*' (HSHB, MSHB, LSHB, and HSLB) and '*Hand*' (left hand (LH), right hand (RH)) for the metrics ***Force Profile*** and ***FPB***; regarding instead the metrics ***DSI***, ***NJ***, ***Execution Time***, and ***MF*** we considered as within-subjects factors only '*Target*' and '*Material*'; finally we included only *'Material*' factor for the ***Deformation*** metrics.

Data normality was evaluated using the Shapiro-Wilk test, and the sphericity condition was assessed using the Mauchly test. Statistical significance was considered for p-values lower than 0,05. Post-hoc analysis on significant main effects and interaction was performed using Bonferroni corrected paired t-tests (n = 24 (2×4×3, 'Hand'×'Material'×'Target'), $p<0.0021$). Statistical analysis was conducted by using IBM SPSS Statistics 23 (IBM, Armonk, New York, USA).

4.3.4. Results

Discrimination between the implemented virtual objects

We analysed the ***Deformation*** parameter for each simulated object to have a preliminary view of the manipulation strategies across the different conditions and across multiple trials. The results are illustrated in Figure 31, which shows that higher deformation during manipulation happens for softer materials, as expected. From the statistical analysis with rANOVA we highlighted the material's effect ('Material' effect: $F=380.42$, $p<0.001$). From a further post-hoc analysis, we found a significant difference between all the implemented haptic features (post-hoc: $p<0.001$ for all the comparisons).

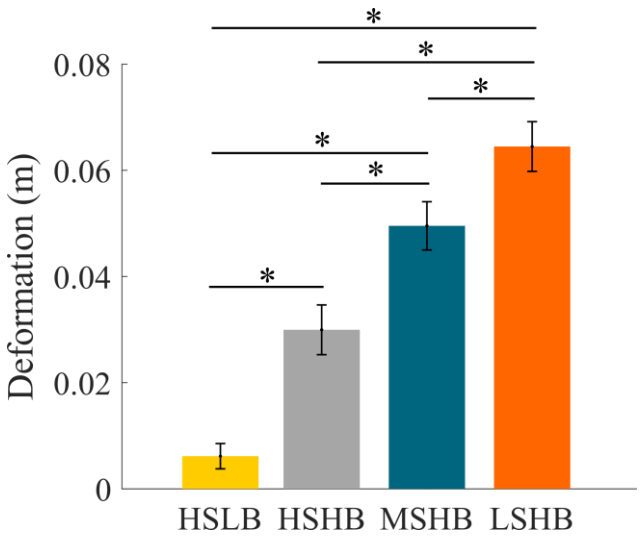

Figure 31: Deformation metrics for the four implemented virtual objects on ALEx RS. Each bar represents the mean value and the respective SE.

Dynamic manipulation strategies depend on the leading hand across the workspace

Figure 32A depicts the ***force profiles*** averaged across all the subjects for each condition, showing each hand contribution (left- and right- hand forces) for the left (L), centre (C) and right (R) portions of the workspace where the targets were placed.

They all resembled a bell-shaped, with an initial raising force, a single peak of maximum force and a decrease of force, which are applied to grab, lift and transport the object, respectively. Yet evident differences across simulated materials can be qualitatively observed at first glance, which also seems to change trend depending on the portion of the

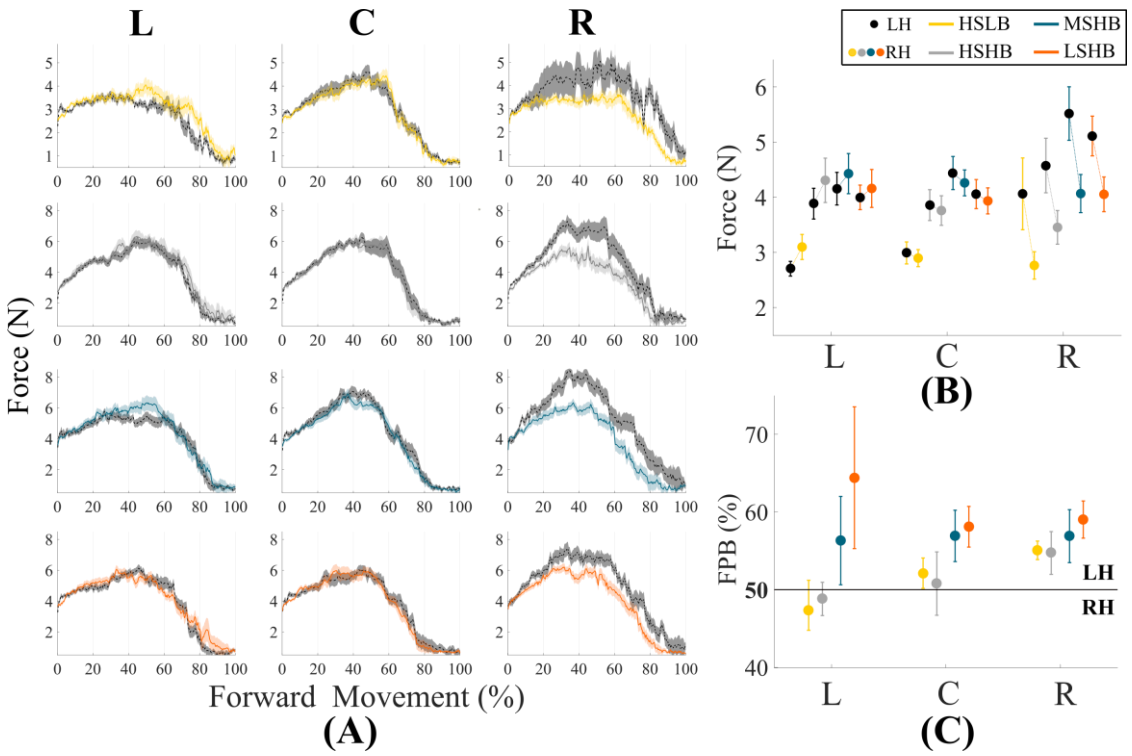

Figure 32: **(A)** Normalized force profile trajectories (mean ± SE) relative to the *left hand* (dashed black line) and the *right hand* (coloured line) depicted for each material (HSLB, HSHB, MSHB and LSHB - rows) and for each target direction (L, C and R - columns). On the x-axis is represented the percentage of movement during the forward movement (from the grasping phase until the object is released on the target). **(B) A**veraged Force computed across subjects. Mean and SE are highlighted for each material and for each side (*left hand*: black marker, *right hand:* coloured marker). **(C)** Force Percentage Break – FPB: mean and SE are highlighted for each virtual object. Values over the black line (FPB > 50 %) highlight that subjects exceed the maximal force (F_{break}) and thus broke the object with the *left hand* (LH), vice versa for values under the black line (RH).

workspace and the direction of motion across trials. Hence, we ran a statistical analysis of the mean force (Figure 32B), finding a significant difference between the materials ('*Material*' effect: F=30.72, p<0.001), the direction of movement ('*Target*' effect: F=7.30, p=0.003), the employed hand ('*Hand*' effect: F=28.18, p<0.001), and the target interaction with the hand ('*Target*Hand*' effect: F=47.55, p<0.001).

For targets towards the right direction the leading hand is the left one, vice versa for targets towards the left direction the leading hand is the right one. In fact, the post-hoc analysis between the hands showed larger values of force applied with the left hand only for the right target (post-hoc analysis: p<0.001 for all materials, Table 10). Conversely, for the other two target directions (L and C), the post-hoc analysis did not show statistical differences between the two hands (p>0.011 for all materials). When the non-dominant hand plays the leading hand's role, i.e., in movements directed to the right, it cannot modulate the force correctly and then is inclined to exert more force than the strictly necessary.

		RH			LH		
		FORCE [N] (Mean ± SD)			**FORCE [N] (Mean ± SD)**		
VIRTUAL OBJECT		**L**	**C**	**R**	**L**	**C**	**R**
HSHB		**4.31 ± 0.98**	**3.75 ± 0.66**	**3.45 ± 0.75**	**3.88 ± 0.68**	**3.86 ± 0.69**	**4.57 ± 1.21**
	MSHB	4.27 ± 0.89 (p = 0.557)	4.26 ± 0.57 (p = 0.008)	4.07 ± 0.85 (p = 0.027)	4.16 ± 0.72 (p = 0.211)	4.44 ± 0.73 (p = 0.008)	5.52 ± 1.19 (p =0.032)
	LSHB	4.15 ± 0.84 (p = 0.540)	3.93 ± 0.58 (p = 0.425)	4.05 ± 0.77 (p = 0.015)	4.00 ± 0.54 (p = 0.511)	4.06 ± 0.64 (p = 0.305)	5.11 ± 0.88 (p = 0.104)
	HSLB	3.10 ± 0.56 (p<0.001*)	2.90 ± 0.38 (p<0.001*)	2.76 ± 0.61 p=0.001*	2.70 ± 0.33 (p<0.001*)	2.99 ± 0.49 (p = 0.001*)	4.06 ± 1.59 (p = 0.242)
MSHB		**4.27 ± 0.89**	**4.26 ± 0.57**	**4.07 ± 0.85**	**4.16 ± 0.72**	**4.44 ± 0.73**	**5.52 ± 1.19**
	LSHB	4.15 ± 0.84 (p= 0.135)	3.93 ± 0.58 p=0.039	4.05 ± 0.77 p = 0.938	4.00 ± 0.54 (p = 0.427)	4.06 ± 0.64 (p = 0.049)	5.11 ± 0.88 (p = 0.058)
	HSLB	3.10 ± 0.56 (p<0.001*)	2.90 ± 0.38 (p<0.001*)	2.76 ± 0.61 (p<0.001*)	2.70 ± 0.33 (p<0.001*)	2.99 ± 0.49 (p<0.001*)	4.06 ± 1.59 (p = 0.003)
LSHB		**4.15 ± 0.84**	**3.93 ± 0.58**	**4.05 ± 0.77**	**4.00 ± 0.54**	**4.06 ± 0.64**	**5.11 ± 0.88**
	HSLB	3.10 ± 0.56 (p<0.001*)	2.90 ± 0.38 (p<0.001*)	2.76 ± 0.61 (p<0.001*)	2.70 ± 0.33 (p<0.001*)	2.99 ± 0.49 (p<0.001*)	4.06 ± 1.59 (p = 0.011)

Table 10: Mean Force and statistical p-values between the four virtual objects

This result was also evidenced by the post-hoc analysis performed among the targets, which revealed that the mean force applied by the *left hand* was significantly larger for the right target than for the left and central ones, only in the case of the softer materials (MSHB and LSHB: $p<0.001$). No differences were showed between C and L target and for LSHB and HSHB materials ($p>0.003$). The same analysis was conducted for the right hand: target direction had no effects on the force applied during manipulation of the VO ($p>0.006$), since the dominant hand modulates the force application correctly.

The switch of the functional hands' roles depending on the movement direction was further highlighted by the significant differences founded between the four analyzed materials. While for the *right hand*, for all target positions, the force' analysis showed a higher mean force in HSHB, MSHB, LSHB materials than HSLB material, for the *left hand* no significant differences were found when subjects were moving towards the right target (see Table 10). This result means that the non-dominant hand, which assumes the leading role in the right direction, lacks the ability to discriminate and therefore, to modulate the force when materials of different physics properties are manipulated.

In addition to the analysis carried out when the task was successful, i.e., when the subject reached the target, we evaluated what happened if participants overcame the force

and broke the object through the ***Force Percentage Break – FPB***. These further results confirmed the inability of the non-dominant hand to modulate the force. On average, we found that regardless of direction, the hand that exceeded the force limit was the left one (LH). This evidence was valid for all materials except for HSLB and HSHB (rigid materials without compliance) along the left direction (L), Figure 32C. For this metric, it was not possible to perform a statistical analysis since the number of repetitions was not consistent (not all subjects exceeded the required force).

Characterization of movement symmetry and smoothness

The results related to the ***Dynamical Symmetry Index – DSI*** - indicated that the movement direction influenced the motor control of bimanual action, generating different asymmetries between the two hands.

The ***DSI*** trend, depicted in Figure 33A for a single subject and in Figure 33B for the population, was highly influenced by the target position and the VO's typology. When moving towards the left portion of the workspace (L), subjects performed a longer path with the right hand (***DSI*** values between 10 and 20 %) for HSHB, MSHB, and LSHB materials, meaning that the right hand was leading the movement. Instead, for the HSLB material, subjects showed an initial negative peak of ***DSI***, for a movement percentage between 0 and 20 % before stabilizing around zero throughout the following movement phase. When the target was presented on the right (R), for all materials, subjects performed a longer path with the left hand (***DSI*** values between -10 and -20 %), meaning that the left hand was leading the movement. Finally, for the central target (C) subjects showed a symmetric behaviour for all the materials and the whole movement phase.

The statistical analysis confirmed the previous highlights, showing a significant difference between the targets ('*Target*' effect: $F=111.08$, $p<0.001$) and an interaction effect ('*Material * Target*': $F=9.77$, $p<0.001$). From the post-hoc analysis, we found significant differences between the HSLB and all the other materials for the left target (post-hoc analysis: $p<0.001$), Figure 33C. No statistical differences between materials were found for the central and right target ($p>0.03$).

We evaluated the smoothness of the trajectory employing the ***Normalised Jerk - NJ***. We found lower values and thus a good smoothness, for the central target (C), only for the medium stiffness VO (MSHB) that results in an optimal ratio between amplitude and frequency of deformation oscillations. The statistical analysis evidenced an effect of the direction ('*Target*': $F=17.00$, $p<0.001$) and an effect of the hand ('*Hand*': $F=14.72$,

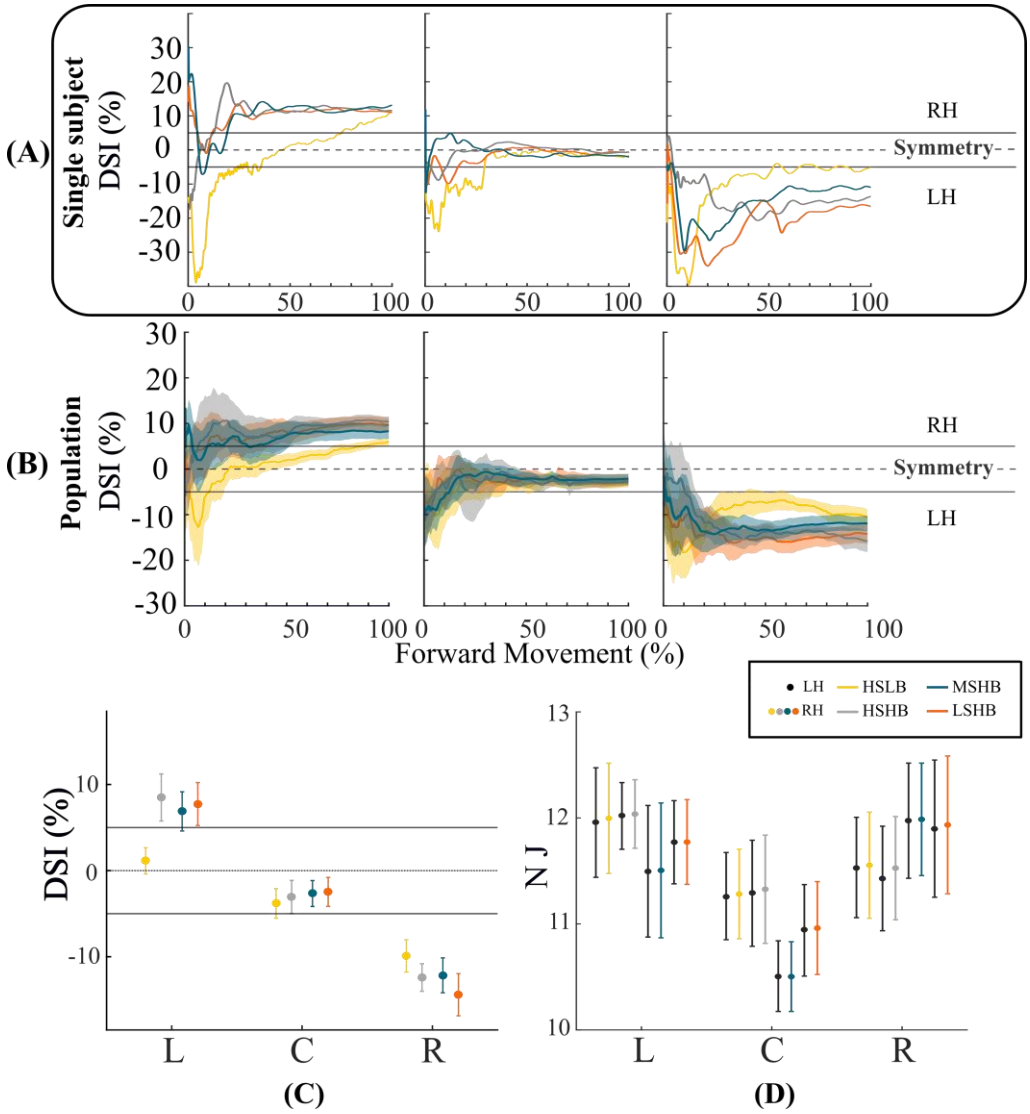

Figure 33: **(A)** Dynamical Symmetry Index – DSI – profiles from a single participant (L, C and R). **(B)** Dynamical Symmetry Index – DSI- shapes averaged across subjects (L, C and R). On the x-axis is represented the percentage of movement during the forward movement (from the grasping phase until the object is released on the target). **(C)** Mean and SE values of DSI computed during forward movement. **(D)** Normalised Jerk -NJ- Mean and SE values. Every metrics is represented across the three different targets and for each simulated virtual object.

p=0.002). We also obtained two interaction effects (*'Material*Target'*: F=2.50, p=0.028, *'Material*Hand'*: F=3.14, p=0.035) that allowed us to establish that the direction of movement and the body' side had an effect dependent on the VO proprieties.

In particular, we found a significant difference between targets only for the MSHB for both the right hand (p=0.001, C (10.51±0.82N) versus R (11.99±1.30N)) and the left hand (p=0.001: C (10.51±0.8N) versus R (11.97±1.33N); p=0.002: C (10.51±0.8N) versus L (11.50±1.52N). For all other materials, no significant differences were found (p>0.003). Furthermore, we found significant differences between hands only for the HSHB along

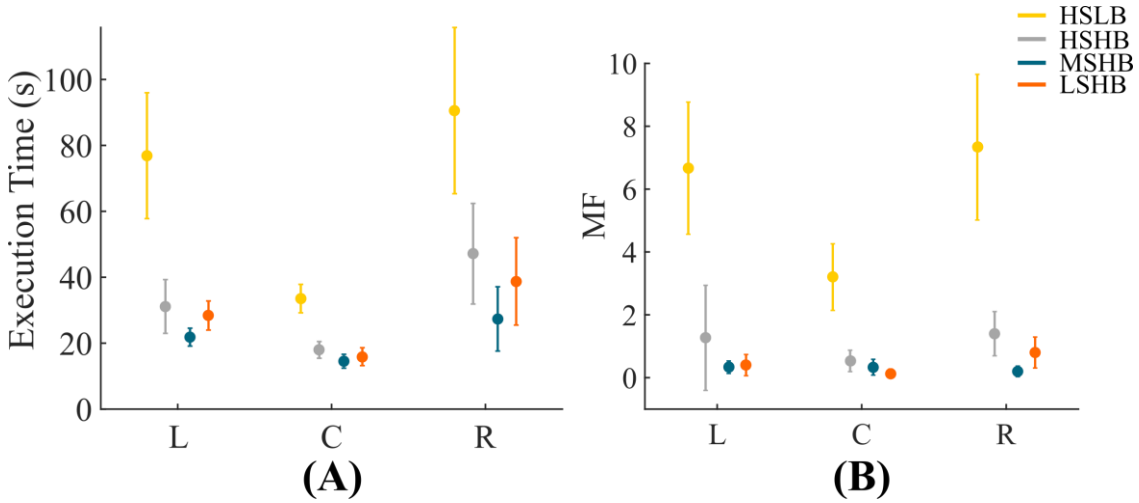

Figure 34: **(A)** Execution Time. **(B)** Max Failure – MF. Each parameter is represented for each material and for each target with mean and SE values.

with the right target ($p<0.001$) Figure 33D. No statistical differences between materials were found ($p>0.213$).

The low breakage point highly influences execution time and failures

As expected, and thanks to the quality of the simulation, the more fragile material was handled with care, and therefore participants needed a longer execution time to succeed. In fact, the statistical analysis on the ***Execution Time*** parameter, showed a significant difference between materials ('*Material*' effect: $F=22.40$, $p<0.001$), targets ('Target' effect: $F=10.53$, $p<0.001$), and their interaction ('*Material*Target'* effect: $F=4.20$, $p=0.001$).

The post-hoc analysis revealed a significant difference between the HSLB material and all other materials by analysing each direction individually (L direction: $p=0.003$ for the comparison HSLB versus HSHB and $p=0.001$ for the comparison HSLB versus MSHB and HSLB versus MSHB; C direction: $p<0.001$ for all; R direction: $p=0.003$ for the comparison HSLB versus HSHB, $p<0.001$ for HSLB versus MSHB and $p=0.003$ for HSLB versus LSHB).

Although the HSLB consisted of high stiffness, the low breakage point led subjects to perform the task slowly and carefully, with subsequent larger ***Execution Time***, as showed in Figure 34A.

The Bonferroni corrected t-tests showed also statistical differences between the targets, highlighting how the direction of movement influenced the motor control in

bimanual actions, modulating the ***Execution Time*** which resulted larger towards the right direction for most of the VOs: HSLB (L versus C: $p=0.002$), MSHB (L versus C: $p<0.001$) and LSHB (L versus C: $p<0.001$).

Finally, the difficulties in performing the task for a given type of simulated VO were analysed by the ***Max Failure - MF*** - parameter. This latter considered the number of times in which subjects exceeded the maximum force allowed. We had significant differences between materials ('*Material*' effect: $F=31.73$, $p<0.001$), targets ('*Target*' effect: $F=4.45$, $p=0.021$) and between their interactions (*'Material*Target'* effect: $F=2.64$, $p=0.021$). We found that the difficulties in performing the task increased when the compliance and the force necessary to break the VO decreased: a significant difference between the HSLB material and all other materials has been found by analysing each direction individually (L direction: $p<0.001$ for the comparison HSLB versus MSHB and HSLB versus LSHB; C direction: $p=0.001$ for the comparison HSLB versus HSHB and HSLB versus MSHB, $p<0.001$ for HSLB versus LSHB; R direction: $p=0.001$ for the comparison HSLB versus HSHB and $p<0.001$ for HSLB versus MSHB and HSLB versus LSHB), Figure 34B. No statistical differences were found between target directions ($p>0.03$).

4.3.5. Discussions and Conclusions

The coordinated coupled cooperation among upper limbs to achieve a common motor goal is a distinctive feature of human behaviours, since individuals use both hands to haptically explore and manipulate the objects in daily actions. In the last decades, bimanual coordination has been the key point of intensive investigation concerning how information from the proprioceptive and tactile senses is integrated (Talvas et al., 2014). However, very little is known about how the hemispheric specialization allocates different functional roles to the hands when directional changes occur between body and goal positions. Previous evidence was obtained without the employment of the recent haptics and robotics technologies which provide a broader context to test multiple conditions and simulate various tasks with a high degree of reliability for studying human bimanual manipulation.

Today, the dynamic process involving the use of the two hands can be described by two theories: (i) the coordinated use of limbs is ruled by the dominance of one hemisphere over the other, with the dominant hand primarily acting and the other stabilizing the manipulation (Geschwind, 1975; Guiard, 1987; Viallet et al., 1992; Toga and Thompson, 2003); (ii) the notable dynamism and flexibility of the brain lead to switching the

functional hands' roles across various environmental constraints (Jiang and Kanwisher, 2003; Johansson et al., 2006). With this in mind, we wanted to provide further evidence that, by using haptics, the bimanual coordination can be accurately characterized across the human workspace during motor coupled activities.

Hence, we decided to investigate how sensory information is processed by the dominant and non-dominant hand during a coupled bimanual 3D task in which participants manipulated a virtual object with four different *haptic features*. To this end, a bimanual reaching task has been developed through robotic exoskeletons integrated with VR and haptic interfaces, in which subjects handled the object and moved it across a 3D-workspace towards different targets (left-center-right).

Outcomes revealed multiple aspects, which, to our knowledge, have never been reported in previously published contributions, for the reason that most of the literature on bimanual actions primarily focused on *uncoupled* tasks (Casadio et al., 2010), (Tcheang et al., 2007), and (Nozaki and Scott, 2009), while few contributions specifically focused on bimanual tasks in *coupled* settings (Johansson et al., 2006; Mutalib et al., 2019). Another reason for such lack of results is the affordability of complex haptic devices, which must be designed in such a way as to provide robust and accurate force feedback in a three-dimensional workspace and to involve the whole upper limbs.

Functional hands' roles depend on movement direction

The study's central finding was related to the primary acting hand involved in the bimanual object manipulation. We identified a significant effect of the movement directionality concerning the utilization between the two hands. We detected a predominance of the non-dominant hand for movements towards the right direction. This outcome confirms the hypothesis that our brain, while manipulating objects, can switch the primary actor role, even in a task where symmetry between the hands is required for success (Johansson et al., 2006).

Therefore, the choice of the *acting hand* is related to the type of the investigated task and the movement's desired direction. Contu et al. (Contu et al., 2016) showed that depending on the direction of action of the movement, for the target towards right the leading hand is the non-dominant one, vice versa for target towards the left direction the leading hand is the dominant one.

The outcomes confirmed this feature, highlighting a significant asymmetry between hands only for movements towards the right way. The explanation can be found in the concept of "*Direction-dependent leading hand*". For clarity, the basis of this phenomenon can be investigated by merely considering right-handed subjects. When movements to the left are required, the leading hand is the dominant one, which in healthy subjects is the one normally used to fine control movements. Vice versa, when dealing with right directions, the guide's role is inverted and transferred on the hand that generally has the function to stabilize, namely the non-dominant one. For this reason, we identified a significant asymmetry: the non-dominant hand, when it plays the role of the leading hand, i.e., in movements directed to the right, it is not able to modulate the force correctly and is inclined to exert more force than the strictly necessary.

The present finding is consistent with the previous studies, which showed that direction is a primary movement parameter coded in various brain structures during unilateral upper limb movements (Caminiti et al., 1990; Prud'Homme and Kalaska, 1994). The production of bimanual action involves the activation of two neural populations, one for each hemisphere, which are combined as a function of the movement direction (Swinnen et al., 2001). The two cerebral hemispheres could be differentially adapted for processing bimanual movements with the lead arm depending on the movement direction when both hands move towards the same target (Franz et al., 2002).

When participants moved towards central targets, subjects showed symmetric behavior between the dominant and non-dominant hands. Among the multiple theories of motor control, the internal model theory (Yokoi et al., 2011) is aligned with our outcomes. According to this theory, during bimanual movement, the brain represents each arm in a model that integrates (i) arms kinematics information, (ii) the movement directions of both arms and (iii) the motor or cognitive constraints imposed by the task and the environment (Diedrichsen and Gush, 2009; Shea et al., 2016). The integration between the environment and the task constraints into the internal brain model can affect motor coordination during bimanual manipulation.

Compliance perception affects motor performance

Motor performance is influenced by the materials' compliance haptically rendered. Information from different senses is separately processed and converges into a unique environment so that the perception is the best possible estimation (Ernst and Bülthoff, 2004). According to Hooke's law, compliance is the combination of position and force

information. Since position information is provided from the *haptic* and *visual* modalities, subjects showed the highest performances for the more compliant materials. Indeed, as expected, the time necessary to successfully achieve the task was significantly higher for the material with the lower breakage point, meaning that it was handled with more care.

Conclusions

This study aims to provide a broader and more comprehensive view of the motor control strategies in bimanual coupled manipulation across a three-dimensional workspace through a new-designed exoskeleton, ALEx-RS.

Such a device, which provides multimodal sensory feedback, showed that haptic and visual feedback might influence the lateralization of dominant and non-dominant hands during the dynamic coupled bimanual task. Results also indicated that manipulating an object with higher compliance improves task performance.

Our outcomes on healthy subjects show the potentialities of the implemented haptic interface since the designed control represents a starting point for a fully customized and measurable haptic environment. The current experiment results could have implications for several teleoperated applications, complementing stable haptic feedback involving the whole upper limbs and could allow performance of activities of daily living in a safe and robot-mediated virtual environment in which progress of rehabilitation is monitored.

5. Discussion and Conclusion

5.1. General Discussion

This dissertation presents research conducted in both the context of *proprioceptive assessment tasks* and *haptic interfaces*. The signals involved in these two contexts, namely self-position and tactile contact, interact with each other, both perceptually and physiologically, in a way that complicates and, at the same time, renders the understanding of such processes interesting (Rincon-Gonzalez et al., 2011b).

This work exposed the design and the development of various testing setups implemented on sensorized technologies and robotic devices to objectively *assess proprioception,* conceived as a set of somatosensory afferents (position & force). Such technologies allowed to study motor control mechanisms that occur in healthy human subjects even during a simulated bimanual manipulation task in which *haptic feedback* is provided.

The various implemented experimental setups could offer an objective platform to evaluate the potential and the motor outcomes contributed by each one. Basically, they differed in the type of technology used and the body districts involved, the sensory afferents provided or removed, and the analysed body side.

The ***first study*** proposed a solution for evaluating force control mechanisms when the single right-dominant arm, acting against the handle of a planar manipulandum (Casadio et al., 2006), received or not feedback regarding the same-arm position information. In this application, the *single right-dominant arm* only was considered. This setup made it possible to investigate the mechanisms that coordinate the human sense of force and position in daily living activities. Commonly, the force needed to act is opportunely calibrated by our nervous system to complete it, even when *disturbing external elements* are present (Kawato, 1999). Objects' interaction involves variable impedances that require the estimation of their mechanical properties to handle them correctly (Gurari et al., 2012). To implement such a task, in which participants were asked to learn to modulate a force applied against a robot-simulated virtual spring, the situation mentioned above was partially replicated. In fact, the implementation of *variable* stiffness (the amount of spring displacement was independent with the applied force) or *constant* stiffness (the amount of spring displacement was always correlated with the applied force)

allowed investigating how much reliance on *position* sense could influence *force* control. The results showed that subjects who in the variable stiffness condition could either rely on a pure sense of force or perform some average estimate of the breakpoint location learned more slowly than those operating in the constant stiffness condition, which provided them with reliable and stable position information. However, the formers could generalize their learning even when using a different arm configuration, likely a side effect of more extensive statistical inference. Subjects who relied on *position* sense (*constant stiffness*), learned faster but could not generalize their learning when using a different arm configuration. This insight reflects the notion that our nervous system is capable of adapt to environmental uncertainties (*variable stiffness*) and exploits the sense of effort as a robust sensory afferent, likely as a consequence of the reliable signal that muscle spindles derive from the contracting muscle (Proske and Allen, 2019). Moreover, it has been pointed out that, when subjects failed the trial exerting more force than the set target force, they encountered the event where the force feedback was suddenly removed and experienced this as a *failure*. As a consequence of this, the comparison of performance immediately after failure with the performance immediately preceding shows a consistent increase of error corresponding to the adoption of a more prudent behavior at the expenses of a reduced but safer performance. Importantly, such catastrophic failures do not interrupt the progression of learning. They do slow down the progression of learning consistent with observations of (Herzfeld et al., 2014) who demonstrated that rapidly switching environments reduce the effectiveness of error-dependent learning.

The ***second study*** has highlighted the importance of *multi-joint* movements at the distal limb segments (wrist), still considering the *single right-dominant arm* only. A testing paradigm was implemented for assessing proprioception during coordinated wrist movements and in the presence of kinaesthetic perturbations through a 3DoFs robotic device, the WristBot (Masia et al., 2009). Human wrist proprioception is particularly important due to its role in daily living activities (ADLs) (Hoseini et al., 2015). Although it has been demonstrated that proprioception is involved in fine manipulation, few studies have been focused on distal joints, with particular emphasis on the wrist's proprioceptive functions (Basteris et al., 2018; Marini et al., 2018). With this setup, healthy subjects' ability to match proprioceptive targets along with two of the three wrist's degrees of freedom, flexion/extension, and abduction/adduction by introducing an *external kinaesthetic disturbance* along the pronation/supination axis was studied. In particular, two experimental conditions were provided that differed in *temporal* presentation of the

perturbations respect to the sequence of motions during the joint position matching test. Outcomes reported evidence that the order of disturbance presentation does not influences proprioceptive acuity. Moreover, a further phenomenon has been observed: proprioception is highly anisotropic and dependent on the perturbation amplitude. In particular, the findings evidenced a higher proprioceptive sensitivity for large pronation/supination perturbation amplitude. This finding may suggest applications in multiple areas: from general *haptics* where, knowing how wrist configuration influences proprioception, might suggest new solutions in device design, to *clinical evaluation* after neurological diseases, where accurately assessing proprioceptive deficits can complement regular therapy for a better prediction of the recovery path.

The ***third application*** comprised the *multi-articular complex full arm movements*: from proximal to distal joints (shoulder-elbow). The implemented design provides a paradigm for assessing ipsilateral proprioception during *single-* and *multi-joint* matching tasks in a three-dimensional workspace employing a dual-arm robotic exoskeleton, the Alex-RS device (Pirondini et al., 2016; Micera et al., 2020). Since daily compound activities require *multi-joint* movements, which involve more muscle mass and require more balance, coordination, and neuromuscular control than *single-joint* exercises, a consistent comprehension of proprioception mechanisms is necessary to facilitate the recovery in neurological patients. The proposed paradigm aimed at extending proprioceptive assessment tests to a multidimensional manifold by replicating complex arm configurations and providing the unprecedented possibility of studying in detail the interconnection between anatomical joints. To the best of my knowledge, no previous studies are investigating such aspects involving robotic technology to increase measurement accuracy and contemplate a 3D testing paradigm. Results provided evidence that proprioceptive performance is influenced by (i) the number of joints involved in the task as well as by (ii) the anatomical configuration of the tested degrees of freedom (Dukelow et al., 2009; Rincon-Gonzalez et al., 2011a; Sketch et al., 2018). Compared to the single-joint evaluation, the multi-joint condition leads to a decrease of proprioceptive acuity for the distal joint. This insight could find support in: (i) since *multi-joint* movements generally involve multiple processes (Kraemer and Ratamess, 2004; Schwellnus, 2009), their execution results more complex than *single-joint* ones; (ii) during the *single-joint* condition, the mechanoreceptors stimulation and the arising sensory information are better encoded by the central nervous system rather than when multiple information comes from different joints (Bergenheim et al., 2000; Roll et al., 2000; Jones

et al., 2001). Moreover, a proprioceptive error distribution across upper limb joints was inferred: the largest matching error has been found in the distal, namely in the elbow. This outcome is consistent with the hypothesis that proprioceptive signals are differently encoded if they originate from proximal or distal segments. Different neural pathways generate diverse motor behaviors as well as sensory processing between distal and proximal limbs, resulting in a significantly different performance between joints of the same limb (Brinkman and Kuypers, 1973). Even this robot-aided paradigm might be used in clinical settings.

The ***second part*** of this manuscript described the implemented setups that exploited the *dual-arm* configuration, both in *coupled* and *uncoupled* approaches. Since many daily tasks require bimanual manipulation of objects, but the state of the art methods for the proprioceptive assessment are far away from bimanual activities and instead evaluate sensorimotor integrity in oversimplified and often unimanual goal-directed tasks, in the ***first study*** (please refer to paragraph 4.1), I aimed at assessing proprioception adopting a *coupled* sensorized device. I developed a new low-cost device (*BiSBox* – Bimanual Sensorized Box - Version 1.0) and method to assess proprioception and force production by simulating a realistic bimanual human behavior.

This device's design was born from the need to quantitatively measure multiple aspects of proprioception by manipulating an object that somehow resembled an everyday object, such as a box. The development of a device wholly portable and, at the same time, able to measure and give real-time feedback has allowed developing two setups that in the future could be adapted to neurological patients.

During the first experiment, participants held the physically coupled object – *BiSBox* (Galofaro et al., 2019) – and matched target orientations about the three principal axes. The principal insight regards significant differences between rotation directions along the *y-axis*, where targets were *proximal* or *distal* concerning the body' participant. Specifically, subjects underestimated angles far from their bodies while they overestimated angles for near ones. This result is supported by several studies demonstrating that the proprioceptive acuity decreased for targets far from the body (Adamo and Martin, 2009; Wilson et al., 2010; Iandolo et al., 2015) or that required larger elbow extensions (Fuentes and Bastian, 2010). Since bimanual evaluation is essential for the correct recovery of somatosensory functions, this tool could be quickly adopted in clinics.

Then, I was interested in evaluating the effects of *aging* on force bimanual strategies. In particular, I focused my study on poorly investigated domains regarding

bimanual isometric force tasks involving both *distal* and *proximal* muscles. The ability to produce bilaterally isometric force has been studied mainly in tasks where subjects were required to produce maximal forces or match constant and time-variant force levels (Kang and Cauraugh, 2014; Lin et al., 2019). However, most of these studies were limited to *hand-grip* (Jaric et al., 2005, 2006) or *single-digit force* (Kang and Cauraugh, 2014; Lin et al., 2014; Long et al., 2016; Patel et al., 2019), i.e., tasks where the force is due to exclusively distal muscles. Instead, several daily living activities like holding large objects also require the control of *proximal muscles*, i.e., upper arm and shoulders' muscles. Different muscle districts could significantly determine force control performance in terms of accuracy, variability, and bilateral asymmetries. For this purpose, in the ***second study*** of this part, task performance, bilateral coordination, and lateral asymmetries were investigated in *young* and *elderly healthy right-handed subjects* during *a bimanual isometric force task* requiring an essential contribution of the upper arm and shoulder muscles while pushing hands against the customized device. Subjects were asked to simultaneously apply the same amount of isometric force pushing with the palm and fingers on the two *BiSBox uncoupled* plates and reaching three target forces. Results showed that *older subjects* had higher errors and more variable force profiles, and most of them undershot the highest force level. Several studies support lower accuracy and higher variability while controlling force by older participants (Vaillancourt et al., 2003; Sosnoff and Newell, 2006; Kapur et al., 2010; Hu and Newell, 2011; Lin et al., 2014, 2019). The increased variability observed in older subjects could be associate with the decrease of the acuity of the somatosensory feedback (Thornbury and Mistretta, 1981; Bowden and McNulty, 2013) and with increased widespread cortical activity and reduced functional connectivity during the execution of motor tasks characterized by reduced interhemispheric inhibition (Goble et al., 2010; Fujiyama et al., 2016; Hermans et al., 2018; Monteiro et al., 2020). Moreover, they also had more *asymmetric* performance between the two hands, although the hand applying more forces varied across subjects and depended on the target force. Interestingly, regarding the *lower target force,* the percentage of force applied by the left non-dominant hand correlated with its variability for our subject population. This insight shows that such evaluation, which recruits full arm, may be considered even in clinical practice to evidence motor strategies in an objective way.

Finally, in the ***last study*** of this thesis, a customize *haptic interface* was designed and implemented. The new technologies currently available allow simulating, if properly programmed, various feedback typologies (Skorina et al., 2018; Zhu et al., 2020). I was

interested in evaluating how during complex *multi-joint* manipulation of virtual objects with different impedance, subjects modify their motor control strategies. In the last decades, bimanual coordination has been the critical planer of intensive investigation concerning how information from the *proprioceptive* and *tactile senses* is integrated (Talvas et al., 2014). However, little is known about how the hemispheric specialization allocates different functional roles to the hands when directional changes occur between body and goal positions. Previous evidence was obtained without the employment of the recent haptics and robotics technologies which provide a broader context to test multiple conditions and simulate various tasks with a high degree of reliability. Today, the dynamic process involving the use of the two hands can be described by two theories: (i) the coordinated use of limbs is ruled by the dominance of one hemisphere over the other, with the dominant hand primarily acting and the other stabilizing the manipulation (Geschwind, 1975; Guiard, 1987; Viallet et al., 1992; Toga and Thompson, 2003); (ii) the remarkable dynamism and flexibility of the brain lead to switching the functional hands' roles across various environmental constraints (Jiang and Kanwisher 2003; Johansson et al. 2006). With recent robotic technologies, bimanual coordination can be accurately characterized across the human workspace. In this study, I investigated how sensory information is processed by the right-dominant and left non-dominant hand during a *coupled* bimanual 3D task in which participants manipulated a virtual object with four different haptic features. A bimanual robotic exoskeleton, ALEx-RS, integrated with VR and opportunely programmed to provide customized haptic feedback, was adopted. Subjects grabbed the object and moved it across a 3D-workspace towards different target locations across the workspace. Outcomes revealed exciting aspects, which, to my knowledge, have never been reported in previously published contributions, for the reason that most of the literature on bimanual actions primarily focused on *uncoupled* tasks (Tcheang et al., 2007; Nozaki and Scott, 2009; Casadio et al., 2010). The principal result regards a significant effect of the movement directionality concerning the utilization between the two hands. In particular, a predominance of the left non-dominant hand for movements towards the right direction was found in terms of applied force. This outcome confirms the hypothesis that our brain, while manipulating objects, can switch the primary actor role, even in a task where symmetry between the hands is required for success (Johansson et al., 2006).

5.2. Conclusion

This work aimed to provide objective methods to assess force and position senses. These methods gradually increased their complexity from evaluating single-arm proprioception and then progressively including bimanual and multiple joints movements until considering variable haptic feedback during bimanual coupled manipulation across a three-dimensional workspace.

The presented outcomes on healthy subjects show the potentialities of techniques that could be used for the motor rehabilitation of patients with neurological diseases. Both *proprioceptive assessment tasks* and *haptic interfaces* could be adopted through a fully customized and measurable programming environment. The patients' plan for recovery of upper limbs' motor control should exploit the possibility to manipulate virtual objects' physical properties: ad-hoc haptic sensory feedback could improve the motor retraining (Takai et al., 2018; Missiroli et al., 2019). Finally, the insights gained through this work may offer solutions for clinical sensorimotor evaluation and treatment after neurological disease to improve recovery path and complement the traditional rehabilitation therapies.

5.3. Open Questions and future development

This thesis's research project left some open questions, which would be addressed in the short-term future studies.

First, regarding the technologies adopted, particularly the WristBot and the BiSBox device, I would like to investigate their benefit in a realistic clinical scenario, particularly for their diagnostic capabilities on a stroke patients' population with distal upper limb motor and proprioceptive impairments. I would like to find evidence on how such instruments can positively impact the efficacy of current clinical diagnostic protocols, with particular focus on proprioceptive functions in both single-arm and bimanual configuration, respectively.

Moreover, a future development regards implementing an admittance control on the WristBot device by integrating a 6-Axis force-torque sensor on the handle. This improvement will allow the implementation of the note modality "assisted-when-needed", in which the device guides the user's wrist when she/he is not able to initiate movements after exceeding a pre-set force threshold while providing gravity and friction compensation.

The bimanual haptic interface here developed, which allowed users to move both hands inside the *Virtual Environment* and across a 3D-workspace, is still limited to a 2D visual feedback in which the user cannot perceive a fully ‘immersive experience’ as it would be expected in the real world. The addition of a 3D visor for *Virtual Reality* could allow users to elicit realistic perceptions and reactions involving different sensory and motor channels. Immersive applications are beneficial for the rehabilitation of cognitive and motor aspects of neurological patients.

Moreover, the *haptic interface* consisted of a simple grab-and-place task, but it could also be tested on different interactive scenarios. Currently, the ALEx-RS lacks a full-hand grasping detection system, such as a hand-exoskeleton; only a sensorized handle is integrated on it. Grasping devices like instrumented gloves or actuated hand-exoskeletons could be integrated into the existing haptic device to provide additional and realistic sensorimotor feedback.

In the future, I aim to investigate the potentiality of such a customized haptic interface in the medical field for motor rehabilitation of patients with neurological diseases. Such a device could also be used to deliver and modify treatment interventions based on the monitored progress in motor recovery, increasing training efficiency, and reducing individual attention needed from the clinician.

References

Abdollahi, F., Corrigan, M., Lazzaro, E. D. C., Kenyon, R. V, and Patton, J. L. (2018). Error-augmented bimanual therapy for stroke survivors. *NeuroRehabilitation* 43, 51–61.

Adamo, D. E., and Martin, B. J. (2009). Position sense asymmetry. *Exp. brain Res.* 192, 87–95.

Adams, R. J., and Hannaford, B. (1999). Stable haptic interaction with virtual environments. *IEEE Trans. Robot. Autom.* 15, 465–474.

Aman, J. E., Elangovan, N., Yeh, I., and Konczak, J. (2015). The effectiveness of proprioceptive training for improving motor function : a systematic review. *Front. Hum. Neurosci.* 8, 1–18. doi:10.3389/fnhum.2014.01075.

Anderson, R. (2006). *The aftermath of stroke: the experience of patients and their families*. Cambridge University Press.

Andres, F. G., Mima, T., Schulman, A. E., Dichgans, J., Hallett, M., and Gerloff, C. (1999). Functional coupling of human cortical sensorimotor areas during bimanual skill acquisition. *Brain* 122, 855–870.

Antfolk, C., D'Alonzo, M., Rosén, B., Lundborg, G., Sebelius, F., and Cipriani, C. (2013). Sensory feedback in upper limb prosthetics. *Expert Rev. Med. Devices* 10, 45–54. doi:10.1586/erd.12.68.

Armstrong, C. A., and Oldham, J. A. (1999). A comparison of dominant and non-dominant hand strengths. *J. Hand Surg. Br. Eur. Vol.* 24, 421–425.

Babin-Ratté, S., Sirigu, A., Gilles, M., and Wing, A. (1999). Impaired anticipatory finger grip-force adjustments in a case of cerebellar degeneration. *Exp. Brain Res.* 128, 81–85.

Bailey, R. R., Klaesner, J. W., and Lang, C. E. (2015). Quantifying real-world upper-limb activity in nondisabled adults and adults with chronic stroke. *Neurorehabil. Neural Repair* 29, 969–978.

Ballardini, G., Ponassi, V., Galofaro, E., Carlini, G., Marini, F., Pellegrino, L., et al. (2019a). Interaction between position sense and force control in bimanual tasks. *J. Neuroeng. Rehabil.* 16, 1–13.

Ballardini, G., Ponassi, V., Galofaro, E., Pellegrino, L., Solaro, C., Muller, M., et al. (2019b). Bimanual control of position and force in people with multiple sclerosis:

preliminary results. in *2019 IEEE 16th International Conference on Rehabilitation Robotics (ICORR)* (IEEE), 1147–1152.

Basteris, A., Contu, S., Plunkett, T. K., Kuah, C. W. K., Konczak, I. J., Chua, K. S., et al. (2018). Robot-aided bimanual assessment of wrist proprioception in people with acute stroke. in *2018 7th IEEE International Conference on Biomedical Robotics and Biomechatronics (Biorob)* (IEEE), 473–478.

Basteris, A., Nijenhuis, S. M., Stienen, A. H. A., Buurke, J. H., Prange, G. B., and Amirabdollahian, F. (2014). Training modalities in robot-mediated upper limb rehabilitation in stroke: a framework for classification based on a systematic review. *J. Neuroeng. Rehabil.* 11, 111.

Bastian, H. C. (1887). The "muscular sense"; its nature and cortical localisation. *Brain* 10, 1–89.

Bell, C. (1826). XII. On the nervous circle which connects the voluntary muscles with the brain. *Philos. Trans. R. Soc. London*, 163–173.

Bergenheim, M., Ribot-Ciscar, E., and Roll, J.-P. (2000). Proprioceptive population coding of two-dimensional limb movements in humans: I. Muscle spindle feedback during spatially oriented movements. *Exp. brain Res.* 134, 301–310.

Berret, B., Darlot, C., Jean, F., Pozzo, T., Papaxanthis, C., and Gauthier, J. P. (2008). The inactivation principle: mathematical solutions minimizing the absolute work and biological implications for the planning of arm movements. *PLoS Comput Biol* 4, e1000194.

Blakemore, S. J., Frith, C. D., and Wolpert, D. M. (2001). The cerebellum is involved in predicting the sensory consequences of action. *Neuroreport* 12, 1879–1884. doi:10.1097/00001756-200107030-00023.

Blumenschein, L. H., McDonald, C. G., and O'Malley, M. K. (2017). A cable-based series elastic actuator with conduit sensor for wearable exoskeletons. in *2017 IEEE International Conference on Robotics and Automation (ICRA)*, 6687–6693. doi:10.1109/ICRA.2017.7989790.

Bohil, C. J., Alicea, B., and Biocca, F. A. (2011). Virtual reality in neuroscience research and therapy. *Nat. Rev. Neurosci.* 12, 752–762.

Bowden, J. L., and McNulty, P. A. (2013). Age-related changes in cutaneous sensation in the healthy human hand. *Age (Omaha).* 35, 1077–1089.

Brihmat, N., Loubinoux, I., Castel-Lacanal, E., Marque, P., and Gasq, D. (2020). Kinematic parameters obtained with the ArmeoSpring for upper-limb assessment after

stroke: a reliability and learning effect study for guiding parameter use. *J. Neuroeng. Rehabil.* 17, 1–12.

Brinkman, J., and Kuypers, H. (1973). Cerebral control of contralateral and ipsilateral arm, hand and finger movements in the split-brain rhesus monkey. *Brain* 96, 653–674.

Brisben, A. J., Hsiao, S. S., and Johnson, K. O. (1999). Detection of vibration transmitted through an object grasped in the hand. *J. Neurophysiol.* 81, 1548–1558.

Cabeza, R. (2001). Functional neuroimaging of cognitive aging. in *HANDBOOK OF FUNCTIONAL NEUROIMAGING OF COGNITION*. (Citeseer).

Caminiti, R., Johnson, P. B., and Urbano, A. (1990). Making arm movements within different parts of space: dynamic aspects in the primate motor cortex. *J. Neurosci.* 10, 2039–2058.

Cappello, L., Elangovan, N., Contu, S., Khosravani, S., Konczak, J., and Masia, L. (2015). Robot-aided assessment of wrist proprioception. *Front. Hum. Neurosci.* 9, 198.

Carey, L. M. (1995). Somatosensory loss after stroke. *Crit. Rev. Phys. Rehabil. Med.* 7.

Carignan, C. R., and Cleary, K. R. (2000). Closed-loop force control for haptic simulation of virtual environments.

Carlton, L. G., and Newell, K. M. (1993). Force variability and characteristics of force production. *Var. Mot. Control*, 15–36.

Casadio, M., Iandolo, R., Nataletti, S., Marini, F., Morasso, P., Ponassi, V., et al. (2018). "Robotic techniques for the assessment of proprioceptive deficits and for proprioceptive training," in *Rehabilitation Robotics* (Elsevier), 289–303.

Casadio, M., Sanguineti, V., Morasso, P. G., and Arrichiello, V. (2006). Braccio di Ferro: a new haptic workstation for neuromotor rehabilitation. *Technol. Health Care* 14, 123–42. Available at: http://www.ncbi.nlm.nih.gov/pubmed/16971753.

Casadio, M., Sanguineti, V., Squeri, V., Masia, L., and Morasso, P. (2010). Inter-limb interference during bimanual adaptation to dynamic environments. *Exp. brain Res.* 202, 693–707.

Castel-Lacanal, E., Marque, P., Tardy, J., de Boissezon, X., Guiraud, V., Chollet, F., et al. (2009). Induction of cortical plastic changes in wrist muscles by paired associative stimulation in the recovery phase of stroke patients. *Neurorehabil. Neural Repair* 23, 366–372.

Cauraugh, J. H., and Summers, J. J. (2005). Neural plasticity and bilateral movements: a rehabilitation approach for chronic stroke. *Prog. Neurobiol.* 75, 309–320.

Cavdan, M., Doerschner, K., and Drewing, K. (2019). The many dimensions underlying

perceived softness: How exploratory procedures are influenced by material and the perceptual task. in *2019 IEEE World Haptics Conference (WHC)* (IEEE), 437–442.

Chen, P., Kwong, P. W. H., Lai, C. K. Y., and Ng, S. S. M. (2019). Comparison of bilateral and unilateral upper limb training in people with stroke: A systematic review and meta-analysis. *PLoS One* 14, e0216357.

Choi, I., Hawkes, E. W., Christensen, D. L., Ploch, C. J., and Follmer, S. (2016). Wolverine: A wearable haptic interface for grasping in virtual reality. in *2016 IEEE/RSJ International Conference on Intelligent Robots and Systems (IROS)* (IEEE), 986–993.

Colby, C. L. (1998). Action-oriented spatial reference frames in cortex. *Neuron* 20, 15–24.

Colgate, J. E., and Brown, J. M. (1994). Factors affecting the z-width of a haptic display. in *Proceedings of the 1994 IEEE International Conference on Robotics and Automation* (IEEE), 3205–3210.

Colgate, J. E., Stanley, M. C., and Brown, J. M. (1995). Issues in the haptic display of tool use. in *Proceedings 1995 IEEE/RSJ International Conference on Intelligent Robots and Systems. Human Robot Interaction and Cooperative Robots* (IEEE), 140–145.

Collins, D. F., and Prochazka, A. (1996). Movement illusions evoked by ensemble cutaneous input from the dorsum of the human hand. *J. Physiol.* 496, 857–871.

Collins, D. F., Refshauge, K. M., and Gandevia, S. C. (2000). Sensory integration in the perception of movements at the human metacarpophalangeal joint. *J. Physiol.* 529, 505–515.

Connell, L. A., and Tyson, S. F. (2012). Measures of sensation in neurological conditions: a systematic review. *Clin. Rehabil.* 26, 68–80.

Contu, S., Hughes, C. M. L., and Masia, L. (2016). The role of visual and haptic feedback during dynamically coupled bimanual manipulation. *IEEE Trans. Haptics* 9, 536–547.

Contu, S., Hussain, A., Kager, S., Budhota, A., Deshmukh, V. A., Kuah, C. W. K., et al. (2017). Proprioceptive assessment in clinical settings: Evaluation of joint position sense in upper limb post-stroke using a robotic manipulator. *PLoS One*. doi:10.1371/journal.pone.0183257.

Córdova Bulens, D., Crevecoeur, F., Thonnard, J.-L., and Lefèvre, P. (2018). Optimal use of limb mechanics distributes control during bimanual tasks. *J. Neurophysiol.* 119, 921–932.

Corrêa, C. G., Nunes, F. L. S., Ranzini, E., Nakamura, R., and Tori, R. (2019). Haptic interaction for needle insertion training in medical applications: The state-of-the-art.

Med. Eng. Phys. 63, 6–25.

Cressman, E. K., and Henriques, D. Y. P. (2011). "Motor adaptation and proprioceptive recalibration," in *Progress in brain research* (Elsevier), 91–99.

D'Antonio, E., Galofaro, E., Zenzeri, J., Patané, F., Konczak, J., Casadio, M., et al. (2021). Robotic Assessment of Wrist Proprioception During Kinaesthetic Perturbations: A Neuroergonomic Approach. *Front. Neurorobot.* 15, 19.

D'Antonio, E., Tieri, G., Patané, F., Morone, G., and Iosa, M. (2020). Stable or able? Effect of virtual reality stimulation on static balance of post-stroke patients and healthy subjects. *Hum. Mov. Sci.* 70. doi:10.1016/j.humov.2020.102569.

Davis, N. J. (2007). Memory and coordination in bimanual isometric finger force production. *Exp. Brain Res.* 182, 137–142.

De Santis, D., Zenzeri, J., Casadio, M., Masia, L., Riva, A., Morasso, P., et al. (2015). Robot-assisted training of the kinesthetic sense: enhancing proprioception after stroke. *Front. Hum. Neurosci.* 8, 1037.

Debert, C. T., Herter, T. M., Scott, S. H., and Dukelow, S. (2012). Robotic assessment of sensorimotor deficits after traumatic brain injury. *J. Neurol. Phys. Ther.* 36, 58–67.

Deblock-Bellamy, A., Batcho, C. S., Mercier, C., and Blanchette, A. K. (2018). Quantification of upper limb position sense using an exoskeleton and a virtual reality display. *J. Neuroeng. Rehabil.* 15, 24.

Diedrichsen, J., and Gush, S. (2009). Reversal of bimanual feedback responses with changes in task goal. *J. Neurophysiol.* 101, 283–288. doi:10.1152/jn.90887.2008.

Donchin, O., Gribova, A., Steinberg, O., Bergman, H., and Vaadia, E. (1998). Primary motor cortex is involved in bimanual coordination. *Nature* 395, 274–278.

Dosen, S., Markovic, M., Strbac, M., Belić, M., Kojić, V., Bijelić, G., et al. (2016). Multichannel electrotactile feedback with spatial and mixed coding for closed-loop control of grasping force in hand prostheses. *IEEE Trans. Neural Syst. Rehabil. Eng.* 25, 183–195.

Dover, G., and Powers, M. E. (2003). Reliability of Joint Position Sense and Force-Reproduction Measures During Internal and External Rotation of the Shoulder. *J. Athl. Train.* 38, 304–310. Available at: https://pubmed.ncbi.nlm.nih.gov/14737211.

Dukelow, S. P., Herter, T. M., Bagg, S. D., and Scott, S. H. (2012). The independence of deficits in position sense and visually guided reaching following stroke. *J. Neuroeng. Rehabil.* 9, 72.

Dukelow, S. P., Herter, T. M., Moore, K. D., Demers, M. J., Glasgow, J. I., Bagg, S. D., et

al. (2009). Quantitative Assessment of Limb Position Sense Following Stroke. *Neurorehabil. Neural Repair* 24, 178–187. doi:10.1177/1545968309345267.

Edin, B. B., and Johansson, N. (1995). Skin strain patterns provide kinaesthetic information to the human central nervous system. *J. Physiol.* 487, 243–251.

Elangovan, N., Cappello, L., Masia, L., Aman, J., and Konczak, J. (2017). A robot-aided visuo-motor training that improves proprioception and spatial accuracy of untrained movement. *Sci. Rep.* 7, 1–10.

Ernst, M. O., and Bülthoff, H. H. (2004). Merging the senses into a robust percept. *Trends Cogn. Sci.* 8, 162–169.

Evarts, E. V (1981). Sherrington's concept of proprioception. *Trends Neurosci.* 4, 44–46.

Fallon, J. B., and Macefield, V. G. (2007). Vibration sensitivity of human muscle spindles and Golgi tendon organs. *Muscle Nerve Off. J. Am. Assoc. Electrodiagn. Med.* 36, 21–29.

Farajian, M., Leib, R., Kossowsky, H., and Nisky, I. (2021). Visual Feedback Weakens the Augmentation of Perceived Stiffness by Artificial Skin Stretch. *IEEE Trans. Haptics*.

Farajian, M., Leib, R., Kossowsky, H., Zaidenberg, T., Mussa-Ivaldi, F. A., and Nisky, I. (2020). Stretching the skin immediately enhances perceived stiffness and gradually enhances the predictive control of grip force. *Elife* 9, e52653.

Ferrand, L., and Jaric, S. (2006). Force coordination in static bimanual manipulation: Effect of handedness. *Motor Control* 10, 359–370.

Ferrell, W. R., Gandevia, S. C., and McCloskey, D. I. (1987). The role of joint receptors in human kinaesthesia when intramuscular receptors cannot contribute. *J. Physiol.* 386, 63–71. doi:10.1113/jphysiol.1987.sp016522.

Findlater, S. E., Mazerolle, E. L., Pike, G. B., and Dukelow, S. P. (2019). Proprioception and motor performance after stroke: An examination of diffusion properties in sensory and motor pathways. *Hum. Brain Mapp.* 40, 2995–3009.

Fitle, K. D., Pehlivan, A. U., and O'Malley, M. K. (2015). A robotic exoskeleton for rehabilitation and assessment of the upper limb following incomplete spinal cord injury. in *2015 IEEE International Conference on Robotics and Automation (ICRA)* (IEEE), 4960–4966.

Fjell, A. M., McEvoy, L., Holland, D., Dale, A. M., Walhovd, K. B., and Initiative, A. D. N. (2014). What is normal in normal aging? Effects of aging, amyloid and Alzheimer's disease on the cerebral cortex and the hippocampus. *Prog. Neurobiol.* 117, 20–40.

Flament, D., Ellermann, J. M., Kim, S. G., Uğurbil, K., & Ebner, T. J. (1996). Functional magnetic resonance imaging of cerebellar activation during the learning of a visuomotor dissociation task. *Hum. Brain Mapp.* 4(3), 210–226.

Flanders, M., and Soechting, J. F. (1995). Frames of reference for hand orientation. *J. Cogn. Neurosci.* 7, 182–195.

Fozard, J. L., Vercruyssen, M., Reynolds, S. L., Hancock, P. A., and Quilter, R. E. (1994). Age differences and changes in reaction time: the Baltimore Longitudinal Study of Aging. *J. Gerontol.* 49, P179–P189.

Franz, E. A., Rowse, A., and Ballantine, B. (2002). Does handedness determine which hand leads in a bimanual task? *J. Mot. Behav.* 34, 402–412.

Freeman, A. W., and Johnson, K. O. (1982). Cutaneous mechanoreceptors in macaque monkey: temporal discharge patterns evoked by vibration, and a receptor model. *J. Physiol.* 323, 21–41.

Frisoli, A. (2018). "Exoskeletons for upper limb rehabilitation," in *Rehabilitation Robotics* (Elsevier), 75–87.

Fuentes, C. T., and Bastian, A. J. (2010). Where is your arm? Variations in proprioception across space and tasks. *J. Neurophysiol.* 103, 164–171.

Fujiyama, H., Van Soom, J., Rens, G., Gooijers, J., Leunissen, I., Levin, O., et al. (2016). Age-related changes in frontal network structural and functional connectivity in relation to bimanual movement control. *J. Neurosci.* 36, 1808–1822.

Gabardi, M., Solazzi, M., Leonardis, D., and Frisoli, A. (2016). A new wearable fingertip haptic interface for the rendering of virtual shapes and surface features. in *2016 IEEE Haptics Symposium (HAPTICS)*, 140–146. doi:10.1109/HAPTICS.2016.7463168.

Galganski, M. E., Fuglevand, A. J., and Enoka, R. M. (1993). Reduced control of motor output in a human hand muscle of elderly subjects during submaximal contractions. *J. Neurophysiol.* 69, 2108–2115.

Galofaro, E., Ballardini, G., Boggini, S., Foti, F., Nisky, I., and Casadio, M. (2019). Assessment of bimanual proprioception during an orientation matching task with a physically coupled object. in *2019 IEEE 16th International Conference on Rehabilitation Robotics (ICORR)* (IEEE), 101–107.

Galofaro, E., Scheidt, R. A., Mussa-Ivaldi, F. A., and Casadio, M. (2018). Testing the ability to represent and control a contact force. in, International Conference on Neurorehabilitation (I.

Gandevia, S. C., and Kilbreath, S. L. (1990). Accuracy of weight estimation for weights

lifted by proximal and distal muscles of the human upper limb. *J. Physiol.* 423, 299–310.

Garrington, A. (2010). Touching texts: The haptic sense in modernist literature. *Lit. Compass* 7, 810–823.

Geldard, F. A., and Sherrick, C. E. (1972). The cutaneous" rabbit": a perceptual illusion. *Science (80-.).* 178, 178–179.

Gerloff, C., and Andres, F. G. (2002). Bimanual coordination and interhemispheric interaction. *Acta Psychol. (Amst).* 110, 161–186.

Geschwind, N. (1975). The apraxias: Neural mechanisms of disorders of learned movement: The anatomical organization of the language areas and motor systems of the human brain clarifies apraxic disorders and throws new light on cerebral dominance. *Am. Sci.* 63, 188–195.

Geschwind, N., and Kaplan, E. (1998). A human cerebral deconnection syndrome: A preliminary report. *Neurology* 50, 1201.

Gibson, J. J. (1966). The senses considered as perceptual systems.

Gladstone, D. J., Danells, C. J., and Black, S. E. (2002). The Fugl-Meyer assessment of motor recovery after stroke: a critical review of its measurement properties. *Neurorehabil. Neural Repair* 16, 232–240.

Goble, D. J. (2010). Proprioceptive acuity assessment via joint position matching: from basic science to general practice. *Phys. Ther.* 90, 1176–1184.

Goble, D. J., and Brown, S. H. (2009). Dynamic proprioceptive target matching behavior in the upper limb: effects of speed, task difficulty and arm/hemisphere asymmetries. *Behav. Brain Res.* 200, 7–14.

Goble, D. J., Coxon, J. P., Van Impe, A., De Vos, J., Wenderoth, N., and Swinnen, S. P. (2010). The neural control of bimanual movements in the elderly: Brain regions exhibiting age-related increases in activity, frequency-induced neural modulation, and task-specific compensatory recruitment. *Hum. Brain Mapp.* 31, 1281–1295.

Goble, D. J., Lewis, C. A., Hurvitz, E. A., and Brown, S. H. (2005). Development of upper limb proprioceptive accuracy in children and adolescents. *Hum. Mov. Sci.* 24, 155–170.

Goldscheider, A. (1898). *Physiologie des Muskelsinnes*. Barth.

Goodwin, A. W., and Wheat, H. E. (1999). Effects of nonuniform fiber sensitivity, innervation geometry, and noise on information relayed by a population of slowly adapting type I primary afferents from the fingerpad. *J. Neurosci.* 19, 8057–8070.

Gorniak, S. L., Plow, M., McDaniel, C., and Alberts, J. L. (2014). Impaired object handling during bimanual task performance in multiple sclerosis. *Mult. Scler. Int.* 2014.

Grouios, G. (2006). Right hand advantage in visually guided reaching and aiming movements: brief review and comments. *Ergonomics* 49, 1013–1017.

Guiard, Y. (1987). Asymmetric division of labor in human skilled bimanual action: The kinematic chain as a model. *J. Mot. Behav.* 19, 486–517.

Guo, S., Yu, M., Song, Y., and Zhang, L. (2017). The virtual reality simulator-based catheter training system with haptic feedback. in *2017 IEEE International Conference on Mechatronics and Automation (ICMA)*, 922–926. doi:10.1109/ICMA.2017.8015939.

Gupta, A., Singh, A., Verma, V., Mondal, A. K., and Gupta, M. K. (2020). Developments and clinical evaluations of robotic exoskeleton technology for human upper-limb rehabilitation. *Adv. Robot.* 34, 1023–1040.

Gurari, N., Kuchenbecker, K. J., and Okamura, A. M. (2012). Perception of springs with visual and proprioceptive motion cues: Implications for prosthetics. *IEEE Trans. Human-Machine Syst.* 43, 102–114.

Haaland, Kathleen Y., Deborah L. Harrington, and R. T. K. (2000). Neural representations of skilled movement. *Brain* 123(11), 2306–2313.

Haggard, P., and Flanagan, J. R. (1996). *Hand and brain: the neurophysiology and psychology of hand movements*. Elsevier.

Han, J., Waddington, G., Adams, R., Anson, J., and Liu, Y. (2016). Assessing proprioception: A critical review of methods. *J. Sport Heal. Sci.* doi:10.1016/j.jshs.2014.10.004.

Hansen, E., Grimme, B., Reimann, H., and Schöner, G. (2015). Carry-over coarticulation in joint angles. *Exp. Brain Res.* 233, 2555–2569. doi:10.1007/s00221-015-4327-4.

Harley, L. R., and Prilutsky, B. I. (2012). Transfer of learning between the arms during bimanual reaching. in *2012 Annual International Conference of the IEEE Engineering in Medicine and Biology Society*, 6785–6788. doi:10.1109/EMBC.2012.6347552.

Haryani, H., Fetzer, S. J., Wu, C.-L., and Hsu, Y.-Y. (2017). Chemotherapy-Induced Peripheral Neuropathy Assessment Tools: A Systematic Review. in *Oncology nursing forum*.

Hauser, S. C., and Gerling, G. J. (2017). Force-rate cues reduce object deformation necessary to discriminate compliances harder than the skin. *IEEE Trans. Haptics* 11,

232–240.

Hausmann, M., GuÈntuÈrkuÈn, O., and Corballis, M. (2003). Age-related changes in hemispheric asymmetry depend on sex. *Laterality Asymmetries body, brain Cogn.* 8, 277–290.

Hayashi, T., and Nozaki, D. (2016). Improving a Bimanual Motor Skill Through Unimanual Training . *Front. Integr. Neurosci.* 10, 25.

Henningsen, H., Ende-Henningsen, B., and Gordon, A. M. (1995). Asymmetric control of bilateral isometric finger forces. *Exp. brain Res.* 105, 304–311.

Hermans, L., Levin, O., Maes, C., Van Ruitenbeek, P., Heise, K.-F., Edden, R. A. E., et al. (2018). GABA levels and measures of intracortical and interhemispheric excitability in healthy young and older adults: an MRS-TMS study. *Neurobiol. Aging* 65, 168–177.

Herzfeld, D. J., Vaswani, P. A., Marko, M. K., and Shadmehr, R. (2014). A memory of errors in sensorimotor learning. *Science (80-.).* 345, 1349–1353.

Heuninckx, S., Wenderoth, N., Debaere, F., Peeters, R., and Swinnen, S. P. (2005). Neural basis of aging: the penetration of cognition into action control. *J. Neurosci.* 25, 6787–6796.

Heuninckx, S., Wenderoth, N., and Swinnen, S. P. (2008). Systems neuroplasticity in the aging brain: recruiting additional neural resources for successful motor performance in elderly persons. *J. Neurosci.* 28, 91–99.

Hogan, N., Bizzi, E., Mussa-Ivaldi, F. A., and Flash, T. (1987). Controlling multijoint motor behavior. *Exerc. Sport Sci. Rev.* 15, 153–190.

Hoseini, N., Sexton, B. M., Kurtz, K., Liu, Y., and Block, H. J. (2015). Adaptive staircase measurement of hand proprioception. *PLoS One* 10.

Hsu, J. (1996). *Multiple comparisons: theory and methods*. CRC Press.

Hu, X., Loncharich, M., and Newell, K. M. (2011). Visual information interacts with neuromuscular factors in the coordination of bimanual isometric force. *Exp. brain Res.* 209, 129–138.

Hu, X., and Newell, K. M. (2010). Adaptation to selective visual scaling of short time scale processes in isometric force. *Neurosci. Lett.* 469, 131–134.

Hu, X., and Newell, K. M. (2011). Aging, visual information, and adaptation to task asymmetry in bimanual force coordination. *J. Appl. Physiol.* 111, 1671–1680.

Hunter, S. K., Pereira, H. M., and Keenan, K. G. (2016). The aging neuromuscular system and motor performance. *J. Appl. Physiol.* 121, 982–995.

Hyder, F., and Rothman, D. L. (2012). Quantitative fMRI and oxidative neuroenergetics. *Neuroimage* 62, 985–994.

Iandolo, R., Carè, M., Shah, V. A., Schiavi, S., Bommarito, G., Boffa, G., et al. (2019). A two alternative forced choice method for assessing vibrotactile discrimination thresholds in the lower limb. *Somatosens. Mot. Res.* 36, 162–170.

Iandolo, R., Squeri, V., De Santis, D., Giannoni, P., Morasso, P., and Casadio, M. (2015). Proprioceptive bimanual test in intrinsic and extrinsic coordinates. *Front. Hum. Neurosci.* 9, 1–11. doi:10.3389/fnhum.2015.00072.

Ifft, P. J., Shokur, S., Li, Z., Lebedev, M. A., and Nicolelis, M. A. L. (2013). A brain-machine interface enables bimanual arm movements in monkeys. *Sci. Transl. Med.* 5, 210ra154-210ra154.

Imamizu, H., et al. (2000). Human cerebellar activity reflecting an acquired internal model of a new tool. *Nature* Imamizu, H, 192.

Incel, N. A., Ceceli, E., Durukan, P. B., Erdem, H. R., and Yorgancioglu, Z. R. (2002). Grip strength: effect of hand dominance. *Singapore Med. J.* 43, 234–237.

Itkonen, M., Costa, Á., Yamasaki, H., Okajima, S., Alnajjar, F., Kumada, T., et al. (2019). Influence of bimanual exercise on muscle activation in post-stroke patients. *ROBOMECH J.* 6, 1–11.

Jagga, M., Lehri, A., and Verma, S. K. (2011). Effect of aging and anthropometric measurements on nerve conduction properties-A review. *J. Exerc. Sci. Physiother.* 7, 1.

Jamali, A., Sadeghi-Demneh, E., Fereshtenajad, N., and Hillier, S. (2017). Somatosensory impairment and its association with balance limitation in people with multiple sclerosis. *Gait Posture*. doi:10.1016/j.gaitpost.2017.06.020.

Janssen, L., Beuting, M., Meulenbroek, R., and Steenbergen, B. (2009). Combined effects of planning and execution constraints on bimanual task performance. *Exp. Brain Res.* doi:10.1007/s00221-008-1554-y.

Janwantanakul, P., Magarey, M. E., Jones, M. A., and Dansie, B. R. (2001). Variation in shoulder position sense at mid and extreme range of motion. *Arch. Phys. Med. Rehabil.* 82, 840–844.

Jaric, S., Collins, J. J., Marwaha, R., and Russell, E. (2006). Interlimb and within limb force coordination in static bimanual manipulation task. *Exp. brain Res.* 168, 88–97.

Jaric, S., Knight, C. A., Collins, J. J., and Marwaha, R. (2005). Evaluation of a method for bimanual testing coordination of hand grip and load forces under isometric

conditions. *J. Electromyogr. Kinesiol.* 15, 556–563.

Jenkins, I. H., Brooks, D. J., Frackowiak, R. S. J., and Passingham, F. E. (1994). Motor Sequence Tomography Learning : A Study with Positron. 14.

Jiang, Y., and Kanwisher, N. (2003). Common neural substrates for response selection across modalities and mapping paradigms. *J. Cogn. Neurosci.* 15, 1080–1094.

Jin, X., Uygur, M., Getchell, N., Hall, S. J., and Jaric, S. (2011). The effects of instruction and hand dominance on grip-to-load force coordination in manipulation tasks. *Neurosci. Lett.* 504, 330–335.

Jin, Y., Kim, M., Oh, S., and Yoon, B. (2019a). Motor control strategies during bimanual isometric force control among healthy individuals. *Adapt. Behav.* 27, 127–136.

Jin, Y., Seong, J., Cho, Y., and Yoon, B. (2019b). Effects of aging on motor control strategies during bimanual isometric force control. *Adapt. Behav.* 27, 267–275.

Joël Fagot, A. L. (1997). Role of sensory and post-sensory factors on hemispheric asymmetries in tactual perception. *Cereb. asymmetries Sens. Percept. Process.*, 469.

Johansen-Berg, H., Rushworth, M. F. S., Bogdanovic, M. D., Kischka, U., Wimalaratna, S., and Matthews, P. M. (2002). The role of ipsilateral premotor cortex in hand movement after stroke. *Proc. Natl. Acad. Sci.* 99, 14518–14523.

Johansson, R. S. (1996). "Sensory control of dexterous manipulation in humans," in *Hand and brain* (Elsevier), 381–414.

Johansson, R. S., Theorin, A., Westling, G., Andersson, M., Ohki, Y., and Nyberg, L. (2006). How a lateralized brain supports symmetrical bimanual tasks. *PLoS Biol* 4, e158.

Johnson, K. O. (2001). The roles and functions of cutaneous mechanoreceptors. *Curr. Opin. Neurobiol.* 11, 455–461.

Johnson, K. O., Yoshioka, T., and Vega–Bermudez, F. (2000). Tactile functions of mechanoreceptive afferents innervating the hand. *J. Clin. Neurophysiol.* 17, 539–558.

Jones, K. E., Wessberg, J., and Vallbo, Å. B. (2001). Directional tuning of human forearm muscle afferents during voluntary wrist movements. *J. Physiol.* 536, 635–647.

Jones, L. A. (1989). Matching forces: constant errors and differential thresholds. *Perception* 18, 681–687.

Jones, L. A. (1994). Peripheral mechanisms of touch and proprioception. *Can. J. Physiol. Pharmacol.* 72, 484–487.

Kalisch, T., Wilimzig, C., Kleibel, N., Tegenthoff, M., and Dinse, H. R. (2006). Age-related attenuation of dominant hand superiority. *PLoS One* 1, e90.

Kandel, E. R., Schwartz, J. H., and Jessell, T. M. (2000). *Principles of neural science*. 4th ed. New York: McGraw-Hill, Health Professions Division.

Kane, P. M., Vopat, B. G., Got, C., Mansuripur, K., and Akelman, E. (2014). The effect of supination and pronation on wrist range of motion. *J. Wrist Surg.* 3, 187–191.

Kang, N., and Cauraugh, J. H. (2014). Bimanual force variability and chronic stroke: asymmetrical hand control. *PLoS One* 9.

Kang, N., and Cauraugh, J. H. (2018). Coherence and interlimb force control: effects of visual gain. *Neurosci. Lett.* 668, 86–91.

Kantak, S. S., Sullivan, K. J., Fisher, B. E., Knowlton, B. J., and Winstein, C. J. (2010). Neural substrates of motor memory consolidation depend on practice structure. *Nat. Neurosci.* 13, 923–925.

Kapur, S., Zatsiorsky, V. M., and Latash, M. L. (2010). Age-related changes in the control of finger force vectors. *J. Appl. Physiol.* 109, 1827–1841.

Kawato, M. (1999). Internal models for motor control and trajectory planning. *Curr. Opin. Neurobiol.* 9, 718–727.

Kelso, J. A. (1984). Phase transitions and critical behavior in human bimanual coordination. *Am. J. Physiol. Integr. Comp. Physiol.* 246, R1000–R1004.

Kennedy, D. M., Boyle, J. B., Wang, C., and Shea, C. H. (2016). Bimanual force control: cooperation and interference? *Psychol. Res.* 80, 34–54.

Kenzie, J. M., Findlater, S. E., Pittman, D. J., Goodyear, B. G., and Dukelow, S. P. (2019). Errors in proprioceptive matching post-stroke are associated with impaired recruitment of parietal, supplementary motor, and temporal cortices. *Brain Imaging Behav.* 13, 1635–1649.

Kenzie, J. M., Semrau, J. A., Hill, M. D., Scott, S. H., and Dukelow, S. P. (2017). A composite robotic-based measure of upper limb proprioception. *J. Neuroeng. Rehabil.* 14, 114.

Kilbreath, S. L., and Heard, R. C. (2005). Frequency of hand use in healthy older persons. *Aust. J. Physiother.* 51, 119–122.

Kim, H., Miller, L. M., Fedulow, I., Simkins, M., Abrams, G. M., Byl, N., et al. (2013). Kinematic Data Analysis for Post-Stroke Patients Following Bilateral Versus Unilateral Rehabilitation With an Upper Limb Wearable Robotic System. *IEEE Trans. Neural Syst. Rehabil. Eng.* 21, 153–164. doi:10.1109/TNSRE.2012.2207462.

Kim, T. S., Park, D. D. H., Lee, Y. B., Han, D. G., su Shim, J., Lee, Y. J., et al. (2014). A study on the measurement of wrist motion range using the iPhone 4 gyroscope

application. *Ann. Plast. Surg.* 73, 215–218.

Klein, J., Whitsell, B., Artemiadis, P. K., and Buneo, C. A. (2018). Perception of arm position in three-dimensional space. *Front. Hum. Neurosci.* 12, 331.

Konczak, J., Sciutti, A., Avanzino, L., Squeri, V., Gori, M., Masia, L., et al. (2012). Parkinson's disease accelerates age-related decline in haptic perception by altering somatosensory integration. *Brain* 135, 3371–3379.

Kossowsky, H., Farajian, M., Milstein, A., and Nisky, I. (2021). The Effect of Variability in Stiffness on Perception and Grip Force Adjustment. *IEEE Trans. Haptics*.

Kraemer, W. J., and Ratamess, N. A. (2004). Fundamentals of resistance training: progression and exercise prescription. *Med. Sci. Sport. Exerc.* 36, 674–688.

Krebs, H. I., Hogan, N., Aisen, M. L., and Volpe, B. T. (1998). Robot-aided neurorehabilitation. *IEEE Trans. Rehabil. Eng.* 6, 75–87.

Krishnan, V., and Jaric, S. (2010). Effects of task complexity on coordination of inter-limb and within-limb forces in static bimanual manipulation. *Motor Control* 14, 528–544.

Kubota, H., Demura, S., and Kawabata, H. (2012). Laterality and age-level differences between young women and elderly women in controlled force exertion (CFE). *Arch. Gerontol. Geriatr.* 54, e68–e72.

Kuschel, M., Buss, M., Freyberger, F., Farber, B., and Klatzky, R. L. (2008). Visual-haptic perception of compliance: fusion of visual and haptic information. in *2008 Symposium on Haptic Interfaces for Virtual Environment and Teleoperator Systems* (IEEE), 79–86.

Kwakkel, G., Kollen, B. J., and Krebs, H. I. (2008). Effects of Robot-Assisted Therapy on Upper Limb Recovery After Stroke: A Systematic Review. *Neurorehabil. Neural Repair*. doi:10.1177/1545968307305457.

Lackner, J. R., and Dizio, P. (1994). Rapid adaptation to Coriolis force perturbations of arm trajectory. *J. Neurophysiol.* 72(1), 299–313.

Lafargue, G., Paillard, J., Lamarre, Y., and Sirigu, A. (2003). Production and perception of grip force without proprioception: is there a sense of effort in deafferented subjects? *Eur. J. Neurosci.* 17, 2741–2749.

Lai, C.-H., Sung, W.-H., Chiang, S.-L., Lu, L.-H., Lin, C.-H., Tung, Y.-C., et al. (2019). Bimanual coordination deficits in hands following stroke and their relationship with motor and functional performance. *J. Neuroeng. Rehabil.* 16, 101. doi:10.1186/s12984-019-0570-4.

Langhorne, P., Coupar, F., and Pollock, A. (2009). Motor recovery after stroke: a

systematic review. *Lancet Neurol.* 8, 741–754.

Laufer, Y., and Elboim-Gabyzon, M. (2011). Does sensory transcutaneous electrical stimulation enhance motor recovery following a stroke? A systematic review. *Neurorehabil. Neural Repair* 25, 799–809.

Laver, K. E., Lange, B., George, S., Deutsch, J. E., Saposnik, G., and Crotty, M. (2017). Virtual reality for stroke rehabilitation. *Cochrane database Syst. Rev.*

Laycock, S. D., and Day, A. M. (2003). Recent Developments and Applications of Haptic Devices. *Comput. Graph. Forum* 22, 117–132. doi:https://doi.org/10.1111/1467-8659.00654.

Le Seac'h, A. B., and McIntyre, J. (2007). Multimodal reference frame for the planning of vertical arms movements. *Neurosci. Lett.* 423, 211–215.

Lee, M.-J., Lee, J.-H., Koo, H.-M., and Lee, S.-M. (2017). Effectiveness of bilateral arm training for improving extremity function and activities of daily living performance in hemiplegic patients. *J. Stroke Cerebrovasc. Dis.* 26, 1020–1025.

Leib, R., Karniel, A., and Nisky, I. (2015). The effect of force feedback delay on stiffness perception and grip force modulation during tool-mediated interaction with elastic force fields. *J. Neurophysiol.* 113, 3076–3089.

Leib, R., Rubin, I., and Nisky, I. (2018). Force feedback delay affects perception of stiffness but not action, and the effect depends on the hand used but not on the handedness. *J. Neurophysiol.* 120, 781–794.

Lewis, G. N., and Perreault, E. J. (2009). An assessment of robot-assisted bimanual movements on upper limb motor coordination following stroke. *IEEE Trans. Neural Syst. Rehabil. Eng.* 17, 595–604.

Li, K., and Wei, N. (2014). Fingertip force variability on the left and right hand during low-level sustained precision pinch. in *2014 7th International Conference on Biomedical Engineering and Informatics* (IEEE), 302–306.

Li, L., Li, S., and Li, Y. (2019). Wrist joint proprioceptive acuity assessment using inertial and magnetic measurement systems. *Int. J. Distrib. Sens. Networks* 15, 1550147719845548.

Li, X., Yi, W., Chi, H.-L., Wang, X., and Chan, A. P. C. (2018). A critical review of virtual and augmented reality (VR/AR) applications in construction safety. *Autom. Constr.* 86, 150–162.

Lin, A.-L., and Rothman, D. L. (2014). What have novel imaging techniques revealed about metabolism in the aging brain? *Future Neurol.* 9, 341–354.

Lin, C.-H., Chou, L.-W., Wei, S.-H., Lieu, F.-K., Chiang, S.-L., and Sung, W.-H. (2014). Influence of aging on bimanual coordination control. *Exp. Gerontol.* 53, 40–47.

Lin, C.-H., Sung, W.-H., Chiang, S.-L., Lee, S.-C., Lu, L.-H., Wang, P.-C., et al. (2019). Influence of aging and visual feedback on the stability of hand grip control in elderly adults. *Exp. Gerontol.* 119, 74–81.

Lin, K., Chen, Y., Chen, C., Wu, C., and Chang, Y. (2010). The effects of bilateral arm training on motor control and functional performance in chronic stroke: a randomized controlled study. *Neurorehabil. Neural Repair* 24, 42–51.

Lincoln, N. B., Crow, J. L., Jackson, J. M., Waters, G. R., Adams, S. A., and Hodgson, P. (1991). The unreliability of sensory assessments. *Clin. Rehabil.* 5, 273–282. doi:10.1177/026921559100500403.

Lincoln, N. B., Jackson, J. M., and Adams, S. A. (1998). Reliability and revision of the Nottingham Sensory Assessment for stroke patients. *Physiotherapy* 84, 358–365.

Loch, F., Ziegler, U., and Vogel-Heuser, B. (2018). Integrating haptic interaction into a virtual training system for manual procedures in industrial environments. *IFAC-PapersOnLine* 51, 60–65.

Lodha, N., Coombes, S. A., and Cauraugh, J. H. (2012). Bimanual isometric force control: Asymmetry and coordination evidence post stroke. *Clin. Neurophysiol.* doi:10.1016/j.clinph.2011.08.014.

Lodha, N., Naik, S. K., Coombes, S. A., and Cauraugh, J. H. (2010). Force control and degree of motor impairments in chronic stroke. *Clin. Neurophysiol.* 121, 1952–1961.

Long, J., Tazoe, T., Soteropoulos, D. S., and Perez, M. A. (2016). Interhemispheric connectivity during bimanual isometric force generation. *J. Neurophysiol.* 115, 1196–1207.

Lum, P. S., Burgar, C. G., Shor, P. C., and Majmundar, M. (2002). Robot-Assisted Movement Training Compared With Conventional Therapy Techniques for the Rehabilitation of Upper-Limb Motor Function After Stroke. *Arch Phys Med Rehabil Vol* 83, 952–959. doi:10.1053/apmr.2001.33101.

Macefield, V. G., Häger-Ross, C., and Johansson, R. S. (1996). Control of grip force during restraint of an object held between finger and thumb: responses of cutaneous afferents from the digits. *Exp. Brain Res.* 108, 155–171.

Macefield, V. G., and Knellwolf, T. P. (2018). Functional properties of human muscle spindles. *J. Neurophysiol.* 120, 452–467.

Maes, C., Gooijers, J., de Xivry, J.-J. O., Swinnen, S. P., and Boisgontier, M. P. (2017).

Two hands, one brain, and aging. *Neurosci. Biobehav. Rev.* 75, 234–256.

Maisto, M., Pacchierotti, C., Chinello, F., Salvietti, G., Luca, A. De, and Prattichizzo, D. (2017). Evaluation of Wearable Haptic Systems for the Fingers in Augmented Reality Applications. *IEEE Trans. Haptics* 10, 511–522. doi:10.1109/TOH.2017.2691328.

Marchal-Crespo, L., and Reinkensmeyer, D. J. (2009). Review of control strategies for robotic movement training after neurologic injury. *J. Neuroeng. Rehabil.* 6, 20. doi:10.1186/1743-0003-6-20.

Marini, F., Ferrantino, M., and Zenzeri, J. (2018). Proprioceptive identification of joint position versus kinaesthetic movement reproduction. *Hum. Mov. Sci.* 62, 1–13.

Marini, F., Squeri, V., Morasso, P., Campus, C., Konczak, J., and Masia, L. (2017). Robot-aided developmental assessment of wrist proprioception in children. *J. Neuroeng. Rehabil.* 14, 3.

Marini, F., Squeri, V., Morasso, P., Konczak, J., and Masia, L. (2016a). Robot-aided mapping of wrist proprioceptive acuity across a 3D workspace. *PLoS One* 11, e0161155.

Marini, F., Squeri, V., Morasso, P., and Masia, L. (2016b). Wrist proprioception: amplitude or position coding? *Front. Neurorobot.* 10, 13.

Masia, L., Casadio, M., Sandini, G., and Morasso, P. (2009). Eye-hand coordination during dynamic visuomotor rotations. *PLoS One* 4.

Massie, T. H., and Salisbury, J. K. (1994). The phantom haptic interface: A device for probing virtual objects. in *Proceedings of the ASME winter annual meeting, symposium on haptic interfaces for virtual environment and teleoperator systems* (Chicago, IL), 295–300.

McCloskey, D. I. (1978a). Kinesthetic sensibility. *Physiol. Rev.* 58, 763–820.

McCloskey, D. I. (1978b). Kinesthetic sensibility. *Physiol. Rev.* 58, 763–820. doi:10.1152/physrev.1978.58.4.763.

McNeil, C. J., Doherty, T. J., Stashuk, D. W., and Rice, C. L. (2005). Motor unit number estimates in the tibialis anterior muscle of young, old, and very old men. *Muscle Nerve Off. J. Am. Assoc. Electrodiagn. Med.* 31, 461–467.

Meli, L., Hussain, I., Aurilio, M., Malvezzi, M., O'Malley, M. K., and Prattichizzo, D. (2018). The hBracelet: A Wearable Haptic Device for the Distributed Mechanotactile Stimulation of the Upper Limb. *IEEE Robot. Autom. Lett.* 3, 2198–2205. doi:10.1109/LRA.2018.2810958.

Micera, S., Caleo, M., Chisari, C., Hummel, F. C., and Pedrocchi, A. (2020). Advanced

Neurotechnologies for the Restoration of Motor Function. *Neuron* 105, 604–620. doi:https://doi.org/10.1016/j.neuron.2020.01.039.

Milstein, A., Alyagon, L., and Nisky, I. (2021). Grip Force Control During Virtual Interaction with Deformable and Rigid Objects via a Haptic Gripper. *IEEE Trans. Haptics*.

Missiroli, F., Barsotti, M., Leonardis, D., Gabardi, M., Rosati, G., and Frisoli, A. (2019). Haptic Stimulation for Improving Training of a Motor Imagery BCI Developed for a Hand-Exoskeleton in Rehabilitation. in *2019 IEEE 16th International Conference on Rehabilitation Robotics (ICORR)*, 1127–1132. doi:10.1109/ICORR.2019.8779370.

Mitchell, M., Martin, B. J., and Adamo, D. E. (2017). Upper limb asymmetry in the sense of effort is dependent on force level. *Front. Psychol.* 8, 643.

Mochizuki, G., Centen, A., Resnick, M., Lowrey, C., Dukelow, S. P., and Scott, S. H. (2019). Movement kinematics and proprioception in post-stroke spasticity: assessment using the Kinarm robotic exoskeleton. *J. Neuroeng. Rehabil.* 16, 146.

Molnar, C., and Gair, J. (2013). 17.2 Somatosensation. *Concepts Biol. Can. Ed.*

Monteiro, T. S., Zivari Adab, H., Chalavi, S., Gooijers, J., King, B. (Bradley) R., Cuypers, K., et al. (2020). Reduced Modulation of Task-Related Connectivity Mediates Age-Related Declines in Bimanual Performance. *Cereb. Cortex* 30, 4346–4360.

Morrison, S., and Newell, K. M. (1998). Interlimb coordination as a function of isometric force output. *J. Mot. Behav.* 30, 323–342.

Moser, N., O'Malley, M. K., and Erwin, A. (2020). Importance of Wrist Movement Direction in Performing Activities of Daily Living Efficiently. in *2020 42nd Annual International Conference of the IEEE Engineering in Medicine & Biology Society (EMBC)* (IEEE), 3174–3177.

Mrotek, L. A., Bengtson, M., Stoeckmann, T., Botzer, L., Ghez, C. P., McGuire, J., et al. (2017). The Arm Movement Detection (AMD) test: a fast robotic test of proprioceptive acuity in the arm. *J. Neuroeng. Rehabil.* 14, 64.

Mugge, W., Schuurmans, J., Schouten, A. C., and van der Helm, F. C. T. (2009). Sensory weighting of force and position feedback in human motor control tasks. *J. Neurosci.* 29, 5476–5482.

Mugnosso, M., Marini, F., Holmes, M., Morasso, P., and Zenzeri, J. (2018). Muscle fatigue assessment during robot-mediated movements. *J. Neuroeng. Rehabil.* 15, 119.

Murphy, M. A., Willén, C., and Sunnerhagen, K. S. (2011). Kinematic variables quantifying upper-extremity performance after stroke during reaching and drinking

from a glass. *Neurorehabil. Neural Repair* 25, 71–80.

Mutalib, S. A., Mace, M., and Burdet, E. (2019). Bimanual coordination during a physically coupled task in unilateral spastic cerebral palsy children. *J. Neuroeng. Rehabil.* 16, 1.

Mutha, P. K., Haaland, K. Y., and Sainburg, R. L. (2013). Rethinking motor lateralization: specialized but complementary mechanisms for motor control of each arm. *PLoS One* 8, e58582.

Nair, D. G., Purcott, K. L., Fuchs, A., Steinberg, F., and Kelso, J. A. S. (2003). Cortical and cerebellar activity of the human brain during imagined and executed unimanual and bimanual action sequences: a functional MRI study. *Cogn. brain Res.* 15, 250–260.

Newell, K. M., and McDonald, P. V. (1994). Information, coordination modes and control in a prehensile force task. *Hum. Mov. Sci.* 13, 375–391.

Niespodziński, B., Kochanowicz, A., Mieszkowski, J., Piskorska, E., and Żychowska, M. (2018). Relationship between Joint Position Sense, Force Sense, and Muscle Strength and the Impact of Gymnastic Training on Proprioception. *Biomed Res. Int.* 2018, 5353242. doi:10.1155/2018/5353242.

Nisky, I., Baraduc, P., and Karniel, A. (2010). Proximodistal gradient in the perception of delayed stiffness. *J. Neurophysiol.* 103, 3017–3026.

Nisky, I., Leib, R., Milstein, A., and Karniel, A. (2014). "Perception of stiffness with force feedback delay," in *Multisensory Softness* (Springer), 167–185.

Nisky, I., Mussa-Ivaldi, F. A., and Karniel, A. (2008). A regression and boundary-crossing-based model for the perception of delayed stiffness. *IEEE Trans. Haptics* 1, 73–82.

Noel, J.-P., Samad, M., Doxon, A., Clark, J., Keller, S., and Di Luca, M. (2018). Peri-personal space as a prior in coupling visual and proprioceptive signals. *Sci. Rep.* 8, 1–15.

Norman, J. F., Norman, H. F., Clayton, A. M., Lianekhammy, J., and Zielke, G. (2004). The visual and haptic perception of natural object shape. *Percept. Psychophys.* 66, 342–351.

Norouzi-Gheidari, N., Archambault, P. S., and Fung, J. (2012). Effects of robot-assisted therapy on stroke rehabilitation in upper limbs: systematic review and meta-analysis of the literature. *J. Rehabil. Res. Dev.* 49, 479.

Norris, A. H., Shock, N. W., and Wagman, I. H. (1953). Age changes in the maximum

conduction velocity of motor fibers of human ulnar nerves. *J. Appl. Physiol.* 5, 589–593.

Nowak, D. A., Glasauer, S., and Hermsdörfer, J. (2004). How predictive is grip force control in the complete absence of somatosensory feedback? *Brain* 127, 182–192.

Nowak, D. A., Hermsdörfer, J., Marquardt, C., and Fuchs, H.-H. (2002). Grip and load force coupling during discrete vertical arm movements with a grasped object in cerebellar atrophy. *Exp. brain Res.* 145, 28–39.

Nozaki, D., Kurtzer, I., and Scott, S. H. (2006). Limited transfer of learning between unimanual and bimanual skills within the same limb. *Nat. Neurosci.* 9, 1364–1366.

Nozaki, D., and Scott, S. H. (2009). Multi-compartment model can explain partial transfer of learning within the same limb between unimanual and bimanual reaching. *Exp. brain Res.* 194, 451–463.

O'malley, M. K., and Gupta, A. (2008). Haptic interfaces. *HCI beyond GUI Des. Haptic, Speech, Olfactory, other Nontradit. Interfaces*, 25–64.

O'Sullivan, I., Burdet, E., and Diedrichsen, J. (2009). Dissociating variability and effort as determinants of coordination. *PLoS Comput Biol* 5, e1000345.

Oblak, J., Cikajlo, I., and Matjačić, Z. (2010). Universal Haptic Drive: A Robot for Arm and Wrist Rehabilitation. *IEEE Trans. Neural Syst. Rehabil. Eng.* 18, 293–302. doi:10.1109/TNSRE.2009.2034162.

Ohnishi, H., and Mochizuki, K. (2007). Effect of delay of feedback force on perception of elastic force: a psychophysical approach. *IEICE Trans. Commun.* 90, 12–20.

Olausson, H., Wessberg, J., and Kakuda, N. (2000). Tactile directional sensibility: peripheral neural mechanisms in man. *Brain Res.* 866, 178–187.

Oldfield, R. C. (1971). The assessment and analysis of handedness: The Edinburgh inventory. *Neuropsychologia*, 97–113. doi:10.1016/0028-3932(71)90067-4.

Ortega, M., Redon, S., and Coquillart, S. (2007). A six degree-of-freedom god-object method for haptic display of rigid bodies with surface properties. *IEEE Trans. Vis. Comput. Graph.* 13, 458–469.

Ota, M., Obata, T., Akine, Y., Ito, H., Ikehira, H., Asada, T., et al. (2006). Age-related degeneration of corpus callosum measured with diffusion tensor imaging. *Neuroimage* 31, 1445–1452.

Overtoom, E. M., Horeman, T., Jansen, F.-W., Dankelman, J., and Schreuder, H. W. R. (2019). Haptic feedback, force feedback, and force-sensing in simulation training for laparoscopy: A systematic overview. *J. Surg. Educ.* 76, 242–261.

Ozkul, F., Barkana, D. E., Demirbas, S. B., and Inal, S. (2011). Evaluation of proprioceptive sense of the elbow joint with RehabRoby. in *2011 IEEE International Conference on Rehabilitation Robotics* (IEEE), 1–6.

Paillard, J., and Brouchon, M. (1968). Active and passive movements in the calibration of position sense. *Neuropsychol. Spat. oriented Behav.* 11, 37–55.

Palve, S. S., and Palve, S. B. (2018). Impact of aging on nerve conduction velocities and late responses in healthy individuals. *J. Neurosci. Rural Pract.* 9, 112.

Panait, L., Akkary, E., Bell, R. L., Roberts, K. E., Dudrick, S. J., and Duffy, A. J. (2009). The role of haptic feedback in laparoscopic simulation training. *J. Surg. Res.* 156, 312–316.

Papaxanthis, C., Pozzo, T., and Schieppati, M. (2003). Trajectories of arm pointing movements on the sagittal plane vary with both direction and speed. *Exp. brain Res.* 148, 498–503.

Papini, G. P. R., Fontana, M., and Bergamasco, M. (2016). Desktop Haptic Interface for Simulation of Hand-Tremor. *IEEE Trans. Haptics* 9, 33–42. doi:10.1109/TOH.2015.2504971.

Patel, P., Zablocki, V., and Lodha, N. (2019). Bimanual force control differs between increment and decrement. *Neurosci. Lett.* 701, 218–225.

Pirondini, E., Coscia, M., Marcheschi, S., Roas, G., Salsedo, F., Frisoli, A., et al. (2016). Evaluation of the effects of the Arm Light Exoskeleton on movement execution and muscle activities : a pilot study on healthy subjects. *J. Neuroeng. Rehabil.* 13.1, 1–21. doi:10.1186/s12984-016-0117-x.

Ponassi, V., Galofaro, E., Ballardini, G., Carlini, G., Pellegrino, L., Marini, F., et al. (2018). The interaction between position sense and force control. in *The interaction between position sense and force control*, International Conference on Neurorehabilitation.

Porcini, F., Chiaradia, D., Marcheschi, S., Solazzi, M., and Frisoli, A. (2020). Evaluation of an Exoskeleton-based Bimanual Teleoperation Architecture with Independently Passivated Slave Devices. in *2020 IEEE International Conference on Robotics and Automation (ICRA)*, 10205–10211. doi:10.1109/ICRA40945.2020.9197079.

Prange, G. B., Jannink, M. J. A., Groothuis-Oudshoorn, C. G. M., Hermens, H. J., and IJzerman, M. J. (2006). Systematic review of the effect of robot-aided therapy on recovery of the hemiparetic arm after stroke. *J. Rehabil. Res. Dev.* doi:10.1682/JRRD.2005.04.0076.

Preilowski, B. F. B. (1972). Possible contribution of the anterior forebrain commissures to bilateral motor coordination. *Neuropsychologia* 10, 267–277.

Pressman, A., Welty, L. J., Karniel, A., and Mussa-Ivaldi, F. A. (2007). Perception of delayed stiffness. *Int. J. Rob. Res.* 26, 1191–1203.

Proske, U. (2006). Kinesthesia: the role of muscle receptors. *Muscle Nerve Off. J. Am. Assoc. Electrodiagn. Med.* 34, 545–558.

Proske, U., and Allen, T. (2019). The neural basis of the senses of effort, force and heaviness. *Exp. Brain Res.* 237, 589–599. doi:10.1007/s00221-018-5460-7.

Proske, U., and Gandevia, S. C. (2009). The kinaesthetic senses. *J. Physiol.* 587, 4139–4146.

Proske, U., and Gandevia, S. C. (2012). The proprioceptive senses: their roles in signaling body shape, body position and movement, and muscle force. *Physiol. Rev.* 92, 1651–1697.

Prud'Homme, M. J., and Kalaska, J. F. (1994). Proprioceptive activity in primate primary somatosensory cortex during active arm reaching movements. *J. Neurophysiol.* 72, 2280–2301.

Quaney, B. M., Perera, S., Maletsky, R., Luchies, C. W., and Nudo, R. J. (2005). Impaired grip force modulation in the ipsilesional hand after unilateral middle cerebral artery stroke. *Neurorehabil. Neural Repair* 19, 338–349.

Radianti, J., Majchrzak, T. A., Fromm, J., and Wohlgenannt, I. (2020). A systematic review of immersive virtual reality applications for higher education: Design elements, lessons learned, and research agenda. *Comput. Educ.* 147, 103778.

Rantanen, T., Guralnik, J. M., Foley, D., Masaki, K., Leveille, S., Curb, J. D., et al. (1999). Midlife hand grip strength as a predictor of old age disability. *Jama* 281, 558–560.

Raspopovic, S., Capogrosso, M., Petrini, F. M., Bonizzato, M., Rigosa, J., Di Pino, G., et al. (2014). Restoring natural sensory feedback in real-time bidirectional hand prostheses. *Sci. Transl. Med.* 6, 222ra19-222ra19.

Riemann, B. L., and Lephart, S. M. (2002a). The sensorimotor system, part I: the physiologic basis of functional joint stability. *J. Athl. Train.* 37, 71.

Riemann, B. L., and Lephart, S. M. (2002b). The sensorimotor system, part II: the role of proprioception in motor control and functional joint stability. *J. Athl. Train.* 37, 80.

Rincon-Gonzalez, L., Buneo, C. A., and Tillery, S. I. H. (2011a). The proprioceptive map of the arm is systematic and stable, but idiosyncratic. *PLoS One* 6, e25214.

Rincon-Gonzalez, L., Warren, J. P., Meller, D. M., and Tillery, S. H. (2011b). Haptic

interaction of touch and proprioception: implications for neuroprosthetics. *IEEE Trans. Neural Syst. Rehabil. Eng.* 19, 490–500.

Rinderknecht, M. D., Lambercy, O., Raible, V., Büsching, I., Sehle, A., Liepert, J., et al. (2018). Reliability, validity, and clinical feasibility of a rapid and objective assessment of post-stroke deficits in hand proprioception. *J. Neuroeng. Rehabil.* 15, 47.

Rokni, U., Steinberg, O., Vaadia, E., and Sompolinsky, H. (2003). Cortical representation of bimanual movements. *J. Neurosci.* 23, 11577–11586.

Roll, J.-P., Bergenheim, M., and Ribot-Ciscar, E. (2000). Proprioceptive population coding of two-dimensional limb movements in humans: II. Muscle-spindle feedback during" drawing-like" movements. *Exp. brain Res.* 134, 311–321.

Rose, C. G., Pezent, E., Kann, C. K., Deshpande, A. D., and O'Malley, M. K. (2018a). Assessing Wrist Movement With Robotic Devices. *IEEE Trans. Neural Syst. Rehabil. Eng.* 26, 1585–1595. doi:10.1109/TNSRE.2018.2853143.

Rose, D. K., and Winstein, C. J. (2004). Bimanual training after stroke: are two hands better than one? *Top. Stroke Rehabil.* 11, 20–30.

Rose, T., Nam, C. S., and Chen, K. B. (2018b). Immersion of virtual reality for rehabilitation-Review. *Appl. Ergon.* 69, 153–161.

Rudisch, J., Müller, K., Kutz, D. F., Brich, L., Sleimen-Malkoun, R., and Voelcker-Rehage, C. (2020). How age, cognitive function and gender affect bimanual force control. *Front. Physiol.* 11, 245.

Ruffaldi, E., Barsotti, M., Leonardis, D., Bassani, G., Frisoli, A., and Bergamasco, M. (2014). Evaluating virtual embodiment with the alex exoskeleton. in *International Conference on Human Haptic Sensing and Touch Enabled Computer Applications* (Springer), 133–140.

Ruspini, D. C., Kolarov, K., and Khatib, O. (1997). The haptic display of complex graphical environments. in *Proceedings of the 24th annual conference on Computer graphics and interactive techniques*, 345–352.

Sacks, R., Perlman, A., and Barak, R. (2013). Construction safety training using immersive virtual reality. *Constr. Manag. Econ.* 31, 1005–1017.

Sagastegui Alva, P. G., Muceli, S., Farokh Atashzar, S., William, L., and Farina, D. (2020). Wearable multichannel haptic device for encoding proprioception in the upper limb. *J. Neural Eng.* 17, 56035. doi:10.1088/1741-2552/aba6da.

Sainburg, R. L. (2002). Evidence for a dynamic-dominance hypothesis of handedness. *Exp.*

brain Res. 142, 241–258.

Sainburg, R. L., Ghez, C., and Kalakanis, D. (1999). Intersegmental Dynamics Are Controlled by Sequential Anticipatory, Error Correction, and Postural Mechanisms. *J. Neurophysiol.* doi:10.1152/jn.1999.81.3.1045.

Sala-Llonch, R., Bartrés-Faz, D., and Junqué, C. (2015). Reorganization of brain networks in aging: a review of functional connectivity studies. *Front. Psychol.* 6, 663.

Sale, M. V, and Semmler, J. G. (2005). Age-related differences in corticospinal control during functional isometric contractions in left and right hands. *J. Appl. Physiol.* 99, 1483–1493.

Salimpour, Y., and Shadmehr, R. (2014). Motor costs and the coordination of the two arms. *J. Neurosci.* 34, 1806–1818.

San Vito, P. D. C., Shakeri, G., Brewster, S. A., Pollick, F. E., Brown, E., Skrypchuk, L., et al. (2019). Haptic Navigation Cues on the Steering Wheel. in *CHI*, 210.

Sankaranarayanan, G., and Hannaford, B. (2006). Virtual coupling schemes for position coherency in networked haptic environments. in *The First IEEE/RAS-EMBS International Conference on Biomedical Robotics and Biomechatronics, 2006. BioRob 2006.* (IEEE), 853–858.

Saposnik, G., Cohen, L. G., Mamdani, M., Pooyania, S., Ploughman, M., Cheung, D., et al. (2016). Efficacy and safety of non-immersive virtual reality exercising in stroke rehabilitation (EVREST): a randomised, multicentre, single-blind, controlled trial. *Lancet Neurol.* 15, 1019–1027.

Sarlegna, F. R., and Sainburg, R. L. (2007). The effect of target modality on visual and proprioceptive contributions to the control of movement distance. *Exp. Brain Res.* 176, 267–280.

Schabrun, S. M., and Hillier, S. (2009). Evidence for the retraining of sensation after stroke: a systematic review. *Clin. Rehabil.* 23, 27–39.

Scheidt, R. A., and Stoeckmann, T. (2007). Reach Adaptation and Final Position Control Amid Environmental Uncertainty After Stroke. *J. Neurophysiol.* doi:10.1152/jn.00870.2006.

Schmidt, R. A. (1988). *Motor Control and Learning: A Behavioral Emphasis, 2nd Edn.* USA: Human Kinetics Publishers.

Schmidt, R. A., Lee, T. D., Winstein, C., Wulf, G., and Zelaznik, H. N. (1988). *Motor control and learning: A behavioral emphasis*. Human kinetics.

Schmidt, R. A., Zelaznik, H., Hawkins, B., Frank, J. S., and Quinn Jr, J. T. (1979). Motor-

output variability: a theory for the accuracy of rapid motor acts. *Psychol. Rev.* 86, 415.

Schultheis, M. T., and Rizzo, A. A. (2001). The application of virtual reality technology in rehabilitation. *Rehabil. Psychol.* 46, 296.

Schwellnus, M. P. (2009). *The Olympic textbook of medicine in sport*. John Wiley & Sons.

Sebastjan, A., Skrzek, A., Ignasiak, Z., and Sławińska, T. (2017). Age-related changes in hand dominance and functional asymmetry in older adults. *PLoS One* 12, e0177845.

Serrien, D. J., Cassidy, M. J., and Brown, P. (2003). The importance of the dominant hemisphere in the organization of bimanual movements. *Hum. Brain Mapp.* 18, 296–305.

Serrien, D. J., and Wiesendanger, M. (2001). Dissociation of grip/load-force coupling during a bimanual manipulative assignment. *Exp. brain Res.* 136, 417–420.

Shadmehr, R., and Mussa-Ivaldi, F. (1994a). Adaptive representation of dynamics during learning of a motor task. *J. Neurosci.* doi:10.1523/JNEUROSCI.14-05-03208.1994.

Shadmehr, R., and Mussa-Ivaldi, F. A. (1994b). Adaptive Representation of Dynamics during Learning of a Motor Task. *J. Neurosci. May 1994*, *14 3208-3224*.

Shadmehr, R., Smith, M. A., and Krakauer, J. W. (2010). Error correction, sensory prediction, and adaptation in motor control. *Annu. Rev. Neurosci.* 33, 89–108.

Shakeri, G., Williamson, J. H., and Brewster, S. (2018). May the force be with you: Ultrasound haptic feedback for mid-air gesture interaction in cars. in *Proceedings of the 10th International Conference on Automotive User Interfaces and Interactive Vehicular Applications*, 1–10.

Shea, C. H., Buchanan, J. J., and Kennedy, D. M. (2016). Perception and action influences on discrete and reciprocal bimanual coordination. *Psychon. Bull. Rev.* 23, 361–386. doi:10.3758/s13423-015-0915-3.

Sherrington, C. (1952). *The integrative action of the nervous system*. CUP Archive.

Sherrington, C. S. (1907). On the proprioceptive system, especially its reflex aspect. *Brain* 29, 467–482.

Shirota, C., Jansa, J., Diaz, J., Balasubramanian, S., Mazzoleni, S., Borghese, N. A., et al. (2016). On the assessment of coordination between upper extremities: Towards a common language between rehabilitation engineers, clinicians and neuroscientists. *J. Neuroeng. Rehabil.* doi:10.1186/s12984-016-0186-x.

Shmuelof, L., and Krakauer, J. W. (2011). Are we ready for a natural history of motor learning? *Neuron* 72, 469–476.

Shmuelof, L., Krakauer, J. W., and Mazzoni, P. (2012). How is a motor skill learned? Change and invariance at the levels of task success and trajectory control. *J. Neurophysiol.* 108, 578–594.

Simo, L., Botzer, L., Ghez, C., and Scheidt, R. A. (2014). A robotic test of proprioception within the hemiparetic arm post-stroke. *J. Neuroeng. Rehabil.* 11, 77.

Sisti, H. M., Geurts, M., Clerckx, R., Gooijers, J., Coxon, J. P., Heitger, M. H., et al. (2011). Testing multiple coordination constraints with a novel bimanual visuomotor task. *PLoS One* 6, e23619.

Sketch, S. M., Bastian, A. J., and Okamura, A. M. (2018). Comparing proprioceptive acuity in the arm between joint space and task space. in *2018 IEEE Haptics Symposium (HAPTICS)* (IEEE), 125–132.

Skorina, E. H., Luo, M., and Onal, C. D. (2018). A soft robotic wearable wrist device for kinesthetic haptic feedback. *Front. Robot. AI* 5, 83.

Sleimen-Malkoun, R., Temprado, J.-J., Thefenne, L., and Berton, E. (2011). Bimanual training in stroke: How do coupling and symmetry-breaking matter? *BMC Neurol.* 11, 1–9.

Slifkin, A. B., and Newell, K. M. (1999). Noise, information transmission, and force variability. *J. Exp. Psychol. Hum. Percept. Perform.* 25, 837.

Slifkin, A. B., Vaillancourt, D. E., and Newell, K. M. (2000). Intermittency in the control of continuous force production. *J. Neurophysiol.* 84, 1708–1718.

Snyder, L. H., Grieve, K. L., Brotchie, P., and Andersen, R. A. (1998). Separate body-and world-referenced representations of visual space in parietal cortex. *Nature* 394, 887–891.

Soekadar, S. R., Nann, M., Crea, S., Trigili, E., Gómez, C., Opisso, E., et al. (2019). "Restoration of Finger and Arm Movements Using Hybrid Brain/Neural Assistive Technology in Everyday Life Environments," in *Brain-Computer Interface Research* (Springer), 53–61.

Sosnoff, J. J., and Newell, K. M. (2006). Are age-related increases in force variability due to decrements in strength? *Exp. Brain Res.* 174, 86.

Sreelakshmi, M., and Subash, T. D. (2017). Haptic Technology: A comprehensive review on its applications and future prospects. *Mater. Today Proc.* 4, 4182–4187.

Steinberg, O., Donchin, O., Gribova, A., De Oliveira, S. C., Bergman, H., and Vaadia, E. (2002). Neuronal populations in primary motor cortex encode bimanual arm movements. *Eur. J. Neurosci.* 15, 1371–1380.

Stephens-Fripp, B., Alici, G., and Mutlu, R. (2018). A review of non-invasive sensory feedback methods for transradial prosthetic hands. *IEEE Access* 6, 6878–6899.

Stevens, J. C., and Cain, W. S. (1970). Effort in isometric muscular contractions related to force level and duration. *Percept. Psychophys.* 8, 240–244.

Stillman, B. C. (2002). Making sense of proprioception: the meaning of proprioception, kinaesthesia and related terms. *Physiotherapy* 88, 667–676.

Su, Y.-H., Munawar, A., Deguet, A., Lewis, A., Lindgren, K., Li, Y., et al. (2020). Collaborative Robotics Toolkit (CRTK): Open Software Framework for Surgical Robotics Research. in *2020 Fourth IEEE International Conference on Robotic Computing (IRC)*, 48–55. doi:10.1109/IRC.2020.00014.

Suetterlin, K. J., and Sayer, A. A. (2014). Proprioception: Where are we now? A commentary on clinical assessment, changes across the life course, functional implications and future interventions. *Age Ageing*. doi:10.1093/ageing/aft174.

Sui, D., Fan, J., Jin, H., Cai, X., Zhao, J., and Zhu, Y. (2017). Design of a wearable upper-limb exoskeleton for activities assistance of daily living. in *2017 IEEE International Conference on Advanced Intelligent Mechatronics (AIM)*, 845–850. doi:10.1109/AIM.2017.8014123.

Swanik, C. B., Lephart, S. M., and Rubash, H. E. (2004). Proprioception, kinesthesia, and balance after total knee arthroplasty with cruciate-retaining and posterior stabilized prostheses. *JBJS* 86, 328–334.

Swanik, K. A., Lephart, S. M., Swanik, C. B., Lephart, S. P., Stone, D. A., and Fu, F. H. (2002). The effects of shoulder plyometric training on proprioception and selected muscle performance characteristics. *J. shoulder Elb. Surg.* 11, 579–586.

Swinnen, S. P. (2002). Intermanual coordination: from behavioural principles to neural-network interactions. *Nat. Rev. Neurosci.* 3, 348–359.

Swinnen, S. P., Dounskaia, N., Levin, O., and Duysens, J. (2001). Constraints during bimanual coordination: the role of direction in relation to amplitude and force requirements. *Behav. Brain Res.* 123, 201–218.

Swinnen, S. P., and Wenderoth, N. (2004). Two hands, one brain: cognitive neuroscience of bimanual skill. *Trends Cogn. Sci.* 8, 18–25.

Takagi, A., Maxwell, S., Melendez-Calderon, A., and Burdet, E. (2020). The dominant limb preferentially stabilizes posture in a bimanual task with physical coupling. *J. Neurophysiol.* 123, 2154–2160.

Takahashi, N., Furuya, S., and Koike, H. (2020). Soft Exoskeleton Glove with Human

Anatomical Architecture: Production of Dexterous Finger Movements and Skillful Piano Performance. *IEEE Trans. Haptics* 13, 679–690. doi:10.1109/TOH.2020.2993445.

Takai, A., Rivela, D., Lisi, G., Noda, T., Teramae, T., Imamizu, H., et al. (2018). Investigation on the Neural Correlates of Haptic Training. in *2018 IEEE International Conference on Systems, Man, and Cybernetics (SMC)*, 519–523. doi:10.1109/SMC.2018.00098.

Talvas, A., Marchal, M., and Lécuyer, A. (2014). A survey on bimanual haptic interaction. *IEEE Trans. Haptics* 7, 285–300.

Tcheang, L., Bays, P. M., Ingram, J. N., and Wolpert, D. M. (2007). Simultaneous bimanual dynamics are learned without interference. *Exp. brain Res.* 183, 17–25.

Teixeira, L. A. (2008). Categories of manual asymmetry and their variation with advancing age. *Cortex* 44, 707–716. doi:https://doi.org/10.1016/j.cortex.2006.10.002.

Teulings, H.-L., Contreras-Vidal, J. L., Stelmach, G. E., and Adler, C. H. (1997). Parkinsonism reduces coordination of fingers, wrist, and arm in fine motor control. *Exp. Neurol.* 146, 159–170.

Thornbury, J. M., and Mistretta, C. M. (1981). Tactile sensitivity as a function of age. *J. Gerontol.* 36, 34–39.

Tieri, G., Morone, G., Paolucci, S., and Iosa, M. (2018). Virtual reality in cognitive and motor rehabilitation: facts, fiction and fallacies. *Expert Rev. Med. Devices* 15, 107–117. doi:10.1080/17434440.2018.1425613.

Tiest, W. M. B., and Kappers, A. M. L. (2009). Cues for Haptic Perception of Compliance. *IEEE Trans. Haptics* 2, 189–199. doi:10.1109/TOH.2009.16.

Toga, A. W., and Thompson, P. M. (2003). Mapping brain asymmetry. *Nat. Rev. Neurosci.* 4, 37–48.

Tripp, B. L., Uhl, T. L., Mattacola, C. G., Srinivasan, C., and Shapiro, R. (2006). A comparison of individual joint contributions to multijoint position reproduction acuity in overhead-throwing athletes. *Clin. Biomech.* 21, 466–473.

Trousset, K., Phillips, D., and Karduna, A. (2018). An investigation into force sense at the shoulder. *Motor Control* 22, 462–471.

Unity Technologies (2018). *SteamVR*.

Vaillancourt, D. E., Larsson, L., and Newell, K. M. (2003). Effects of aging on force variability, single motor unit discharge patterns, and the structure of 10, 20, and 40 Hz EMG activity. *Neurobiol. Aging* 24, 25–35.

Vaillancourt, D. E., and Newell, K. M. (2003). Aging and the time and frequency structure of force output variability. *J. Appl. Physiol.* 94, 903–912.

Valdés, B. A., Khoshnam, M., Neva, J. L., and Menon, C. (2019). Robot-Aided Upper-limb Proprioceptive Training in Three-Dimensional Space. in *2019 IEEE 16th International Conference on Rehabilitation Robotics (ICORR)* (IEEE), 121–126.

Valdés, B. A., Khoshnam, M., Neva, J. L., and Menon, C. (2020). Robotics-assisted visual-motor training influences arm position sense in three-dimensional space. *J. Neuroeng. Rehabil.* 17, 1–11.

van Delden, A. E. Q., Peper, C. E., Nienhuys, K. N., Zijp, N. I., Beek, P. J., and Kwakkel, G. (2013). Unilateral versus bilateral upper limb training after stroke: the Upper Limb Training After Stroke clinical trial. *Stroke* 44, 2613–2616.

van der Wal, J. (2009). The architecture of the connective tissue in the musculoskeletal system-an often overlooked functional parameter as to proprioception in the locomotor apparatus. *Int. J. Ther. Massage Bodywork* 2, 9–23. doi:10.3822/ijtmb.v2i4.62.

Veerbeek, J. M., Langbroek-Amersfoort, A. C., van Wegen, E. E. H., Meskers, C. G. M., and Kwakkel, G. (2017). Effects of Robot-Assisted Therapy for the Upper Limb After StrokeStroke: A Systematic Review and Meta-analysis. *Neurorehabil. Neural Repair*. doi:10.1177/1545968316666957.

Viallet, F., Massion, J., Massarino, R., and Khalil, R. (1992). Coordination between posture and movement in a bimanual load lifting task: putative role of a medial frontal region including the supplementary motor area. *Exp. brain Res.* 88, 674–684.

Vieluf, S., Godde, B., Reuter, E.-M., Temprado, J.-J., and Voelcker-Rehage, C. (2015). Practice effects in bimanual force control: Does age matter? *J. Mot. Behav.* 47, 57–72.

Vieluf, S., Mora, K., Gölz, C., Reuter, E.-M., Godde, B., Dellnitz, M., et al. (2018). Age- and expertise-related differences of sensorimotor network dynamics during force control. *Neuroscience* 388, 203–213.

Virani, S. S., Alonso, A., Benjamin, E. J., Bittencourt, M. S., Callaway, C. W., Carson, A. P., et al. (2020). Heart disease and stroke statistics—2020 update: a report from the American Heart Association. *Circulation*, E139–E596.

Virzi, R. A. (1992). Refining the Test Phase of Usability Evaluation: How Many Subjects Is Enough? *Hum. Factors* 34, 457–468. doi:10.1177/001872089203400407.

Voelcker-Rehage, C., and Alberts, J. L. (2005). Age-related changes in grasping force modulation. *Exp. brain Res.* 166, 61–70.

von Holst, E. (1954). Relations between the central Nervous System and the peripheral organs. *Br. J. Anim. Behav.* 2, 89–94. doi:https://doi.org/10.1016/S0950-5601(54)80044-X.

Voutsakelis, G., Kokkonis, G., and Kontogiannis, S. (2020). Haptic Applications for People with Limited Motor Skills. in *2020 3rd World Symposium on Communication Engineering (WSCE)* (IEEE), 1–6.

Wang, J., and Sainburg, R. L. (2007). The dominant and nondominant arms are specialized for stabilizing different features of task performance. *Exp. Brain Res.* 178, 565–570.

Wang, Y., Zhu, H., Elangovan, N., Cappello, L., Sandini, G., Masia, L., et al. (2021). A robot-aided visuomotor wrist training induces gains in proprioceptive and movement accuracy in the contralateral wrist. *Sci. Rep.* 11, 5281. doi:10.1038/s41598-021-84767-9.

Wann, J. P., and Ibrahim, S. F. (1992). Does limb proprioception drift? *Exp. Brain Res.* 91, 162–166.

Weber, A. I., Saal, H. P., Lieber, J. D., Cheng, J.-W., Manfredi, L. R., Dammann, J. F., et al. (2013). Spatial and temporal codes mediate the tactile perception of natural textures. *Proc. Natl. Acad. Sci.* 110, 17107–17112.

Weiss, S. J. (2005). Haptic perception and the psychosocial functioning of preterm, low birth weight infants. *Infant Behav. Dev.* 28, 329–359.

Weller, M. P. I., and Latimer-Sayer, D. T. (1985). Increasing right hand dominance with age on a motor skill task. *Psychol. Med.* 15, 867–872.

Wenderoth, N., Debaere, F., Sunaert, S., Van Hecke, P., and Swinnen, S. P. (2004). Parieto-premotor areas mediate directional interference during bimanual movements. *Cereb. Cortex*. doi:10.1093/cercor/bhh075.

Whitall, J., Waller, S. M., Sorkin, J. D., Forrester, L. W., Macko, R. F., Hanley, D. F., et al. (2011). Bilateral and unilateral arm training improve motor function through differing neuroplastic mechanisms: a single-blinded randomized controlled trial. *Neurorehabil. Neural Repair* 25, 118–129.

Willingham, D. B. (1998). A neuropsychological theory of motor skill learning. *Psychol. Rev.* 105, 558.

Wilson, E. T., Wong, J., and Gribble, P. L. (2010). Mapping proprioception across a 2D horizontal workspace. *PLoS One* 5, e11851.

Wingert, J. R., Burton, H., Sinclair, R. J., Brunstrom, J. E., and Damiano, D. L. (2009). Joint-position sense and kinesthesia in cerebral palsy. *Arch. Phys. Med. Rehabil.* 90,

447–453.

Wolf, S. L., Winstein, C. J., Miller, J. P., Taub, E., Uswatte, G., Morris, D., et al. (2006). Effect of constraint-induced movement therapy on upper extremity function 3 to 9 months after stroke: the EXCITE randomized clinical trial. *Jama* 296, 2095–2104.

Wolpert, D. M., and Flanagan, J. R. (2001). Motor prediction. *Curr. Biol.* 11, R729–R732.

Wolpert, D. M., and Kawato, M. (1998). Multiple paired forward and inverse models for motor control. *Neural networks* 11(7–8), 1317–1329.

Woytowicz, E. J., Westlake, K. P., Whitall, J., and Sainburg, R. L. (2018). Handedness results from complementary hemispheric dominance, not global hemispheric dominance: evidence from mechanically coupled bilateral movements. *J. Neurophysiol.* 120, 729–740.

Wu, C., Yang, C., Lin, K., and Wu, L. (2013). Unilateral versus bilateral robot-assisted rehabilitation on arm-trunk control and functions post stroke: a randomized controlled trial. *J. Neuroeng. Rehabil.* 10, 35.

Xu, C., He, H., Hauser, S. C., and Gerling, G. J. (2019). Tactile exploration strategies with natural compliant objects elicit virtual stiffness cues. *IEEE Trans. Haptics* 13, 4–10.

Xu, D., Loeb, G. E., and Fishel, J. A. (2013). Tactile identification of objects using Bayesian exploration. in *2013 IEEE International Conference on Robotics and Automation* (IEEE), 3056–3061.

Yan, L., Wu, Y., Zeng, X., and Gao, L. (2015). Dysfunctional putamen modulation during bimanual finger-to-thumb movement in patients with Parkinson's disease. *Front. Hum. Neurosci.* 9, 516.

Yeong, C. F., Melendez-Calderon, A., Gassert, R., and Burdet, E. (2009). ReachMAN: a personal robot to train reaching and manipulation. in *2009 IEEE/RSJ International Conference on Intelligent Robots and Systems*, 4080–4085. doi:10.1109/IROS.2009.5354837.

Yokoi, A., Hirashima, M., and Nozaki, D. (2011). Gain Field Encoding of the Kinematics of Both Arms in the Internal Model Enables Flexible Bimanual Action. *J. Neurosci.* 31, 17058 LP – 17068. doi:10.1523/JNEUROSCI.2982-11.2011.

Yu, N., Xu, C., Li, H., Wang, K., Wang, L., and Liu, J. (2016). Fusion of haptic and gesture sensors for rehabilitation of bimanual coordination and dexterous manipulation. *Sensors* 16, 395.

Zeitlin, S. B., Lane, R. D., O'Leary, D. S., and Schrift, M. J. (1989). Interhemispheric transfer deficit and alexithymia. *Am. J. Psychiatry*.

Zhao, L., Wang, Y., Jia, Y., Zhong, S., Sun, Y., Qi, Z., et al. (2017). Altered interhemispheric functional connectivity in remitted bipolar disorder: A Resting State fMRI Study. *Sci. Rep.* 7, 1–8.

Zhu, M., Sun, Z., Zhang, Z., Shi, Q., He, T., Liu, H., et al. (2020). Haptic-feedback smart glove as a creative human-machine interface (HMI) for virtual/augmented reality applications. *Sci. Adv.* 6, eaaz8693.

Zilles, C. B., and Salisbury, J. K. (1995). A constraint-based god-object method for haptic display. in *Proceedings 1995 ieee/rsj international conference on intelligent robots and systems. Human robot interaction and cooperative robots* (IEEE), 146–151.

Zujevs, A., Osadcuks, V., and Ahrendt, P. (2015). Trends in robotic sensor technologies for fruit harvesting: 2010-2015. *Procedia Comput. Sci.* 77, 227–233.

6. Appendix A

6.1. List of Publications

Journal Paper

- C. Pierella*, **E. Galofaro***, A. De Luca, L. Losio, S. Gamba, A. Massone, F. Mussa-Ivaldi and M. Casadio. "*Recovery of distal arm movements in spinal cord injured patients with a body-machine interface: a proof of concept study"*, Sensors (2021).

- **E. Galofaro***, E. D'Antonio*, F. Patané, M. Casadio and L. Masia. ***"****Three-Dimensional Assessment of Upper Limb Proprioception via a Wearable Exoskeleton",* Applied Sciences (2021).

- E. D'Antonio*, **E. Galofaro***, J. Zenzeri, F. Patané, J. Konczak, M. Casadio and L. Masia. "*Robotic Assessment of Wrist Proprioception During Kinaesthetic Perturbations: A Neuroergonomic Approach*", Frontiers in Neurorobotics (2021).

- N. Lotti, M. Xiloyannis, G. Durandau, **E. Galofaro**, V. Sanguineti, L. Masia and M. Sartori, "*Adaptive model-based myoelectric control for a soft wearable arm exosuit*", IEEE Robotics and Automation Magazine (2020).

- G. Ballardini*, V. Ponassi*, **E. Galofaro**, G. Carlini, F. Marini, L. Pellegrino, P. Morasso and M. Casadio, "*Interaction between position sense and force control in bimanual tasks*", Journal of NeuroEngineering and Rehabilitation (2019).

Conference Proceedings (peer-reviewed)

- **E. Galofaro**, G. Ballardini, S. Boggini, F. Foti, I. Nisky and M. Casadio. "*Assessment of bimanual proprioception during an orientation matching task with a physically coupled object*", International Conference on Rehabilitation Robotics (ICORR 2019), Toronto, Canada, (2019).

- F. Rizzoglio, F. Sciandra, **E. Galofaro**, L. Losio, E. Quinland, C. Leoncini, A. Massone, F.A. Mussa-Ivaldi and M.Casadio, "*A Myoelectric Computer Interface for Reducing Abnormal Muscle Activations after Spinal Cord Injury*", International Conference on Rehabilitation Robotics (ICORR 2019), Toronto, Canada (2019).

- G. Ballardini, V. Ponassi, **E. Galofaro**, L. Pellegrino, C. Solaro, I. Muller & M. Casadio, "*Bimanual control of position and force in people with multiple sclerosis: preliminary results*". International Conference on Rehabilitation Robotics (ICORR 2019), Toronto, Canada, (2019).

- **E. Galofaro**, R.A. Scheidt, F.A. Mussa-Ivaldi and M. Casadio, "*Testing the ability to represent and control a contact force"*, International conference on Neurorehabilitation (ICNR 2018), Pisa, Italy, (2018).

- V. Ponassi, **E. Galofaro**, G. Ballardini, G. Carlini, L. Pellegrino, F. Marini, P. Morasso and M. Casadio, "*The interaction between position sense and force control*", International conference on Neurorehabilitation (ICNR 2018) Pisa, Italy, (2018).

Conference Abstract

- **E. Galofaro**, A. De Luca, E. Tasso, F. Cervetto, S. Gamba, L. Losio, A. Venegoni, S. Mandraccia, I. Muller, E. Quinland, A. Massone, F.A.Mussa-Ivaldi, M. Casadio and C. Pierella, "*Functional evaluation of cervical spinal cord injury survivors after training with a body-Machine interface"*, National Congress of Bioengineering (GNB 2018), Milan, Italy, (2018).

- **E. Galofaro**, R.A. Scheidt, F.A. Mussa-Ivaldi and M. Casadio, "*Force can be represented independently of position and impedance in a contact task"*, Abstract & Oral Presentation, (BioRob 2018, Workshop "Assistive user interfaces and control strategies for adaptive human-robot interaction", Organizers: Francesca cordella, Loredana Zollo and Surjo Soekadar), Enschede, The Netherland, (2018).

7. Appendix B

7.1. *Side Project*: Recovery of distal arm movements in spinal cord injured patients with a body-machine interface: a proof of concept study[7]

7.1.1. Introduction

Spinal Cord Injury (SCI) results in deep and devastating life changes connected to the loss of motor and/or sensory functions below the level of the lesion (Post et al., 2004; Jazayeri et al., 2015). This condition is not only physically but also psychologically challenging for SCI people because one of the main and impacting consequences is the loss of functional independence in activities of daily living (ADLs), making its recovery a priority for SCI individuals (Jazayeri et al., 2015; Lynch and Cahalan, 2017). To this aim, physical rehabilitation continues to remain a mainstay in the treatment of SCI because so far no curative treatments exist and only limited spontaneous recovery attributed to the natural and intrinsic neural plasticity of the remaining intact fibers happens after the lesion occurrence (Curt et al., 2008; Jazayeri et al., 2015; Lynch and Cahalan, 2017). Commonly, the rehabilitation treatments, administered manually by the therapist, depend on the injury level and can follow diversified approaches based on each individual's needs (Field-Fote, 2000; Lim and Tow, 2007; Dietz and Fouad, 2014). They are not fully resolutive and are focused on maximizing residual motor skills or overcoming inabilities by teaching compensatory strategies or using assistive devices (Field-Fote, 2000; Curt et al., 2008; Murray and Goldfarb, 2012).

In the last decade, robotic devices and other technologies have been integrated into training programs of people with neuromotor disabilities, like SCI, with promising results (Kamper, 2016; Mekki et al., 2018; Dunkelberger et al., 2020). In parallel with the

[7] The whole content of this Chapter has been published as: C. Pierella*, E. Galofaro*, A. De Luca, L. Losio, S. Gamba, A. Massone, F. Mussa-Ivaldi and M. Casadio *Recovery of distal arm movements in spinal cord injured patients with a body-machine interface: a proof of concept study*, Sensors (2021).

development of robots and their introduction into clinical practice, there has also been fast progress in advancing body-machine interfaces (BoMIs). Such interfaces transform user' body movements to control signals for external assistive devices (Miehlbradt et al., 2018; Ranganathan et al., 2019; Rizzoglio et al., 2020), and have been considered as a safe means for achieving rehabilitative goals (Pierella et al., 2017a, 2017b). A BoMI normally requires the application of surface sensors to different parts of the body that the user is still capable to move or that need to be treated in a therapeutic intervention. The general BoMI goal is to allow the user to control, through active movements external devices such as personal computers, wheelchairs, and assistive manipulators. Typically, the BoMI exploits two key features of the motor control system: redundancy and plasticity. Redundancy, as suggested by Bernstein (Bernstein, 1967), can be employed by the BoMIs in two manners: (a) to explore an overabundant number of body signals for extracting the best signal subspace, and (b) to find new natural subsets of solutions, either when the users' ability decreases for the progression of a related pathology, or as it increases as a consequence of the treatment or of motor learning. Neural plasticity refers to the reorganization of connections within the central nervous system allowing the assignment of new functions to the available capacity for movement's control. The exploitation of redundancy also requires a reorganization, or remapping, of the residual ability to control body motions. When subjects use movements of the eye (Barea et al., 2002; Philips et al., 2007), head (Craig and Nguyen, 2006; Aspelund et al., 2020), shoulders (Casadio et al., 2010, 2011; Thorp et al., 2016), or tongue (Huo et al., 2008; Kim et al., 2013) for driving a wheelchair or piloting a robotic arm, they associate controlling these parts of the body with functions that before the injury were performed by other parts.

Earlier studies tested the efficacy of a new generation of BoMI harnessing the spared abilities of the upper body after a cervical spinal cord injury (cSCI) (Seáñez-González et al., 2016; Thorp et al., 2016; Abdollahi et al., 2017; Pierella et al., 2017a). In particular, such studies exploit small shoulder residual movements to control a power wheelchair (Thorp et al., 2016), or low-cost BoMI in which patients can receive personalized therapy, even within the home environment, with sensors placed exclusively on shoulders and arms (Seáñez-González et al., 2016; Abdollahi et al., 2017; Pierella et al., 2017a).

Depending on the severity of injury, survivors of spinal cord injury, retain some movement, which can be used to control assistive devices such as power wheelchairs or a computer. These studies, mapping shoulder movements onto control signals for computers or virtual and power wheelchairs, demonstrated that a BoMI based on inertial measurement

units (IMUs) capturing natural movements facilitates the exploration of new motor patterns by recognizing silent or weak abilities and targeting them with specific exercises. The combination of assistive and rehabilitative functions (Pierella et al., 2015, 2017a, 2017b) could result in complementary benefits for the Bo-MI users: the motor skills that are partially recovered through training can be reprocessed and included in the control of the same interface, making it continuously customized and calibrated on the evolving abilities of its user.

In this study, the BoMI sensors were placed on both arms and forearms, as op-posed to shoulders and arms like in previous studies, with the rationale that more distal limb regions are more challenging for people with cSCI to control. The objective was to do a retrospective study on the efficacy of the BoMI in the clinical practice as an instrument for physical therapists (PTs) to lead high-level cSCI subjects toward their rehabilitative goals. In particular, we aimed at quantifying: (i) the effects of using the BoMI to recover distal body movements in cSCI patients; (ii) the possible motor changes that occurred after the training with the BoMI; (iii) the effects of the BoMI supported training with an analysis of the cSCI subjects' movement recorded at the beginning, at the end, and one month after the end of the training.

Our results shown that with the current BoMI, we were able to tailor personalized rehabilitative interventions increasing the use of the distal parts of the upper body and motivating the subjects to explore a larger range of movement.

7.1.2. Experimental setup and protocol

In this study, we used four wireless and low-cost inertial measurement units (IMUs) (Yei Technology, 3-Space Sensor™ Wireless) placed on a garment attached by Velcro™ strips to the upper arms and forearms. The sensors were positioned on the distal portions of the upper body as shown in Figure 1A: sensor 1 on the left forearm, sensor 2 on the left arm, sensor 3 on the right arm and sensor 4 on the right forearm.

Each IMU, combining the information of a triaxial gyroscope, accelerometer and compass sensors embedded in the IMU, in conjunction with on-board filtering algorithms, provided in real-time pitch and roll angles. For this reason, the system generated, at every instant n, an 8-dimensional signal vector $\boldsymbol{q}^{(n)} = [{q_1}^{(n)}, {q_2}^{(n)}, \cdots, {q_8}^{(n)}]^{T}$ containing the output (pitch, roll) of all sensors. During the calibration phase, at the beginning of the first

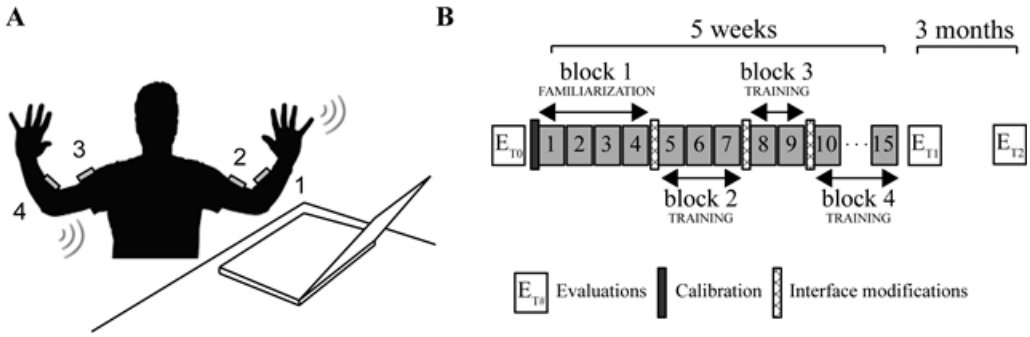

Figure 1: Experimental setup and protocol. **(A):** The subject sits in front of a computer wearing four IMUs that communicate wireless with the computer. With upper body movements the user is controlling the movements of a virtual cursor. **(B):** The subject had evaluation sessions before (ET0), at the end (ET1) and three months after the end of the training with the BoMI (ET2). The practice with the BoMI consisted of 15 sessions with increasing difficulty, which can be grouped into four main blocks (block1: familiarization and blocks 2-4: training blocks), in which subjects performed a set of different tasks.

session, each subject was instructed to perform self-directed and self-paced upper-body motions – described as a free body-dance - for 1 minute. In this phase, the IMU's signals were continuously recorded. Then, through principal component analysis (PCA), we identified the plane of maximum body mobility embedded within the space of the IMU signals, taking the first two eigenvectors, $\boldsymbol{h}_1 = [h_{1,1}, h_{1,2}, \cdots, h_{1,8}]^T$ and $\boldsymbol{h}_2 = [h_{2,1}, h_{2,2}, \cdots, h_{2,8}]^T$, of the covariance matrix and combining them in a matrix H that generated the linear mapping from body to cursor vectors:

$$\boldsymbol{p}^{(n)} = \begin{bmatrix} h_{1,1} & \cdots & h_{1,8} \\ h_{2,1} & \cdots & h_{2,8} \end{bmatrix} \cdot \boldsymbol{q}^{(n)} = H \cdot \boldsymbol{q}^{(n)} \quad (1)$$

where $\boldsymbol{q}^{(n)}$ is the 8-dimensional "body vector" and $\boldsymbol{p}^{(n)}$ the 2-dimensional control vector encoding the position of a computer cursor. More details of this procedure are in (Farshchiansadegh et al., 2014). By establishing a correspondence of the task space - the space of cursor's positions - with this plane, we associated the control variables with the degrees of freedom that the impaired subjects spontaneously used with the greatest ease.

The training protocol (Figure 1B) consisted of 15 sessions of practice with the BoMI of about 45 minutes that were repeated for 5 weeks. The sessions were organized in four main blocks of increasing difficulty: 1 block of familiarization and 3 blocks of training.

Through these, the user completed a series of different tasks, already adopted in (Pierella et al., 2017a, 2017b):

- ***Reaching***. Subjects, starting from the center of the screen, had to reach for three times eight external targets equally spaced in eight directions (0°, 45°, 90°, 135°, 180°, 225°, 270°, 315°), for a total of 24 center-out reaching movements. The external target was positioned at 8.5 cm from the center and appeared randomly in each of the eight directions. Subjects were to reach the external target before it changed color from green to red and then to come back to the central one. This color change happened 1 second after the external target appeared. The target was considered acquired when the cursor remained inside it for 500 ms. The reaching task was performed at the beginning (named 1st Reaching) and at the end (named 2nd Reaching) of each session.
- ***Vertical pong*** simulation. The subjects, by controlling the x and y coordinate of a paddle, were asked to hit a ball moving in the 2-d space of the game field. The prevalent motion of the ball was along the vertical direction (up/down). Subjects obtained a point for every hit, sending the ball to bounce off the top wall. During each session subjects played five epochs of pong, each lasting 2.5 minutes.
- ***Horizontal pong*** simulation. This task was the same as the vertical pong, but the movement of the ball was mostly horizontal (left/right) and the target wall was along the right side of the screen.
- ***Flash games***. The BoMI had a library of flash games that the subjects could choose (e.g. Solitaire, Uno or Arkanoid).

In the first block (familiarization block), the subjects began practicing and became acquainted with the BoMI. From session 5 the PT, thanks to a graphical user interface, introduced the modifications intended to encourage the cSCI subjects to recruit movement combinations that were more difficult to execute. The modifications consisted of:

i) changing the contributions that each sensor gave to the movement of the cursor, by modifying the elements of the matrix H through the multiplication with the matrix D. D is a 2x8 matrix whose first row $\boldsymbol{d}_1 = [d_{1,1} \quad \dots \quad d_{1,8}]$ contains the contribution of each sensors' channel to the horizontal cursor movement, and the second row $\boldsymbol{d}_2 = [d_{2,1} \quad \dots \quad d_{2,8}]$ the contribution to the vertical movement. All its elements were initialized to 1, and to change, for example, the contribution of all

sensor channels to the horizontal movement it was sufficient to set the coefficients of $\boldsymbol{d}_1$ >1.

ii) changing the IMU signals by multiplying one or more IMUs by the gains contained in the matrix S, an 8x8 diagonal matrix. All the elements s_i were initialized to 1, if then s_i was set to be >1the correspondent body signal q_i increased.

These operations are already described in (Pierella et al., 2014, 2015), are expressed as:

$$H_{change} = H \circ (D \cdot S)$$

where D is 2x8, S 8x8 and $\circ$ the Hadamard product that operates a pairwise multiplication between the elements of the two matrices. The GUI, through few textboxes and written indications, was helping the PTs to insert the numbers in order to operate all the necessary modifications. The modifications were applied before starting session 5, session 8 and session 10. This was done to gradually increase the difficulty of the exercise, keeping the subjects motivated and engaged in the training.

For all subjects, the goal was to shift the control toward more distal regions, e.g., from the upper- to the forearms, and if needed to promote symmetry in the use of right and left body sides.

To evaluate the effectiveness of training with the BoMI, the upper limb mobility was evaluated with clinical tests and instrumental tests (see section *Data Analysis*) at different time points: before BoMI treatment (T0), at the end of the BoMI treatment (T1) and 3 months after the end of the treatment (T2).

7.1.3. Subjects

We analyzed retrospectively the data of the cSCI subjects who, within a period of one year, underwent a training with the BoMI focused on distal upper limbs rehabilitation at the Santa Corona Hospital, in Pietra Ligure, Italy.

Inclusion criteria were complete injuries at the C3-6 cervical level (American Spinal Injury Association, ASIA, grade A) or incomplete injuries in the cervical cord (ASIA B and C). They must be medically stable, able to see in adequate light, able to perform some shoulder and arm movements and able to follow simple instructions. Five subjects matched these criteria (see Table 1 for diagnostic and demographic information). All data were collected as part of routine diagnosis and treatment. The ASIA grade reported in Table1 was the result of the evaluation performed at the time of recruitment (1 week before

starting the BoMI training). cSCI subjects were treated according to the national guidelines and to the ethical standards of the 1964 Declaration of Helsinki and signed an informed consent to the analysis of their data for research purposes. cSCI subjects' data were compared with that of five unimpaired age and gender-matched adults with no history of neurological or muscular disorders. The study, the informed consent, and the publication of the results were approved by the local ethical committee (Comitato Etico Regione Liguria N.92366).

Table 1: cSCI subjects characteristics. The fourth column reports the level of lesion and the American Spinal Injury Association (ASIA) impairment scale (Roberts et al., 1999), indicating how much sensory or motor function is preserved. Grade A: Complete. No sensory or motor function preserved. Grade B: Incomplete. Sensory function preserved but no motor functions. Grade C: Motor Incomplete (less than half of the key muscle functions below the neurological level have a muscle grade ≥ 3). Grade D: Motor Incomplete (at least half or more of key muscle functions below the neurological level have a muscle grade ≥ 3). Grade E: Normal motor and sensory functions.

Subjects	Gender	Age	Level of Injury	Time after Injury
SCI 1	Male	21	C5 ASIA A	4 months
SCI 2	Male	19	C5 ASIA B	6 months
SCI 3	Male	20	C6 ASIA C	6 years
SCI 4	Female	29	C5 ASIA A	6 months
SCI 5	Female	28	C5 ASIA A	3 months

7.1.4. Data analysis

To investigate if the subjects became skilled at controlling the cursor, we focused our analysis on the center-out movements only in the Reaching and the Pong tasks per-formed during the first and last session of the familiarization phase, the sessions before and after each interface modification and the session at the end of the training. For the Reaching task we computed the following metrics:

- *Movement Time*, time elapsed as the cursor reaches a target since it left the starting position;
- *Linearity Index*, length of the cursor trajectory to the external target normalized by the distance between start and end points. A linearity index equal to 1 means that the cursor moved along a straight line;
- *Number of peaks in the velocity profile*. We considered every peak larger than 15% of the maximum speed of each trajectory (Krebs et al., 1999). This is a measure of smoothness.

Those are simple metrics commonly used to evaluate controllability and movement quality since they allow describing both spatial and temporal performance as well as

smoothness of the controlled effector (cursor). In the Pong game we calculated the hit rate as the number of hits divided by the duration of the pong session (2.5 minutes).

Symmetry and distal body recruitment indices in body-space and task-space while using the BoMI

To analyze the symmetry and distality of control, we isolated the contribution of the Left L and right R side of the body and the Proximal upper arm P and the Distal fore-arm D to the cursor movement. The IMU signals were partitioned into 4 components, depending on which side of the body (right/left, R/L) and which portion of the arm (proximal /distal, P/D) they referred to. Therefore, we rewrite q as the sum of 4 vectors:

$$\boldsymbol{q} = \boldsymbol{q}_{LD} + \boldsymbol{q}_{LP} + \boldsymbol{q}_{RP} + \boldsymbol{q}_{RD} \tag{2}$$

where each term is an 8-dimensional vector with only two non-zero elements obtained from the corresponding IMU (Figure 1A: LF=IMU1, LU=IMU2, RU=IMU3, RF=IMU4). Substituting this expression in Equation 1, we determine how each side and each part of the body contributed to the total movement of the cursor:

$$\boldsymbol{p} = H \cdot (\boldsymbol{q}_{LD} + \boldsymbol{q}_{LP} + \boldsymbol{q}_{RP} + \boldsymbol{q}_{RD}) = \boldsymbol{p}_{LD} + \boldsymbol{p}_{LP} + \boldsymbol{p}_{RP} + \boldsymbol{p}_{RD} = \boldsymbol{p}_{L} + \boldsymbol{p}_{R} \tag{3}$$

Then in the task space, we can compute the 2D trajectory derived only considering the signals of the sensors placed on the right body side (T_R) or on the left side (T_L). Defining PL as the operator that computes the path length of a trajectory, we can define the cursor contribution of the right body parts c_R and of the left body parts c_L as:

$$\frac{\boldsymbol{PL}(\mathbf{T}_{\boldsymbol{R}})}{\boldsymbol{PL}(\mathbf{T}_{\boldsymbol{R}})+\boldsymbol{PL}(\mathbf{T}_{\boldsymbol{L}})} + \frac{\boldsymbol{PL}(\mathbf{T}_{\boldsymbol{L}})}{\boldsymbol{PL}(\mathbf{T}_{\boldsymbol{R}})+\boldsymbol{PL}(\mathbf{T}_{\boldsymbol{L}})} = \boldsymbol{c_R} + \boldsymbol{c_L} = \mathbf{1} \tag{4}$$

We therefore calculated the symmetry index c_{sym} in order to evaluate if the subject is using left and right body sides in a similar way as:

$$\boldsymbol{c_{sym}} = (\mathbf{1} - |\boldsymbol{c_L} - \boldsymbol{c_R}|) \cdot \mathbf{100} \tag{5}$$

if c_{sym}~100 there is a symmetric condition in the cursor control. If $c_{sym} \rightarrow 0$ one of the sides is being used almost exclusively. In the same way, we computed the 2D trajectory derived considering the signals of the sensors placed on proximal portions of the

arms, upper arms (T_P) or on distal portions, the forearms (T_D) and calculated their contributions to cursor movement, respectively c_P and c_D as:

$$\frac{PL(T_P)}{PL(T_P)+PL(T_D)} + \frac{PL(T_D)}{PL(T_P)+PL(T_D)} = c_P + c_D = 1 \quad (6)$$

To determine whether subjects used more distal body parts, we considered the index c_{distal}:

$$c_{distal} = c_D \cdot 100 \quad (7)$$

if c_{distal} is increasing the subject was using more the distal part of the body.

The same approach was used in the body space to compute the relative contribution of each body side (b_L and b_R) and district (b_P and b_D) from the standard deviations (std) of the 2 channels (pitch and roll) of each IMU:

$$\frac{std_{pitch1}+std_{roll1}}{std_{tot}} + \frac{std_{pitch2}+std_{roll2}}{std_{tot}} + \frac{std_{pitch3}+std_{roll3}}{std_{tot}} + \frac{std_{pitch4}+std_{roll4}}{std_{tot}} \equiv b_{LD} + b_{LP} + b_{RP} + b_{RD} = b_L + b_R = 1 \quad (8)$$

with $std_{tot} = std_{pitch1} + std_{roll1} + std_{pitch2} + std_{roll2} + std_{pitch3} + std_{roll3} + std_{pitch4} + std_{roll4}$.

Similarly, as equation (5) and (7), we defined b_{sym} and b_{distal} as:

$$b_{sym} = (1 - |b_L - b_R|) \cdot 100 \quad (9)$$

$$b_{distal} = (b_{LD} + b_{RD}) \cdot 100 \quad (10)$$

Also in this case, with high symmetry we will have b_{sym}~100% and with a greater use of the distal body parts b_{distal}~100%. Differently from the indicators computed from the trajectories in the task space, the ones extracted directly from the IMUs output are not influenced by the BoMI mapping. Therefore, they account for the actual body movements. We should consider that the movements of the upper arm influence both readouts of the distal and proximal sensors. So, for example, in the arm kinematic chain a movement of the upper arm results also in a movement of the forearm. Thus, decoupled distal movement due to the elbow joint, that are the main target of the BoMI-based exercises proposed in this work, are related to symmetry values above the 50%.

We computed these indicators during two sessions: a) session 4, the last session of the *familiarization* phase, and b) session 15, the last session of the *training* phase.

Clinical evaluations

According to prevalent clinical practice we decided to use the Manual Muscle Test (MMT) (Hislop et al., 2007), performed by expert clinicians blind to the subject's training, to assess upper body strength. In particular, we focused on three upper body regions: scapulae, shoulders, and arms. See Table S1, for details on the tested movements. Each movement was evaluated with a number from 0 (no movement) to 5 (normal movement). The maximum achievable score for the scapula is 15, for the shoulder is 30, and for the arm is 10.

To assess upper body mobility, we measured the Range of Motion (ROM) of the shoulders and arms in all the possible directions using a goniometer, see Table S2 for more information. Since cSCI subjects were tested while sitting in their wheelchair, we did not include shoulder adduction and shoulder extension measures due to substantial range of motion limitations while being in this position.

Instrumented evaluation – stabilization task

We also evaluated using an instrumented test the BoMI training' effects on movement kinematic before (T0), at the end (T1), and 3 months after the end of training (T2). There were some missing data for the cSCI population: subject SCI2 did not perform the instrumented evaluation at T1, while subject SCI4 did not perform the instrumented evaluation at T2. The instrumented evaluation was selected from those presented in the Van Lieshout Test (VLT) Manual (Lieshout, 2003). The reason behind the choice of such task was that, differently from the tests usually adopted in the clinical practice, it involved

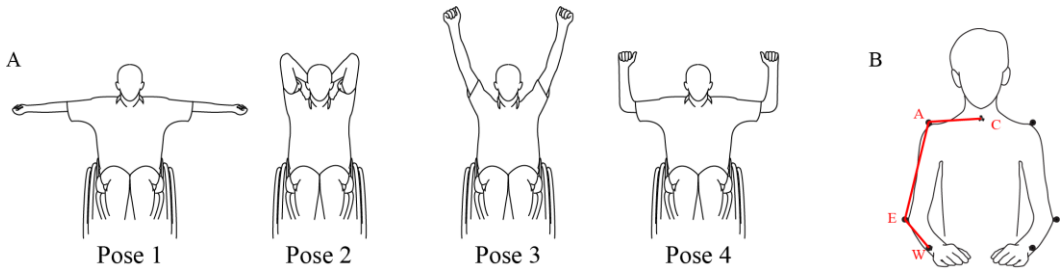

Figure 2: **(A):** The poses of the arm *stabilization task* from the VLT manual that were evaluated in this study, from the easiest (Pose 1) to the most difficult one (Pose 4). **(B):** Markers placement on the anatomical landmarks of acromion (A), elbow (E), wrist (W) and C7 (C) used in the kinematic analysis. The marker on C7 is displayed in the figure, despite the frontal view, to simplify the visualization.

both arms at the same time and required multi-joint coordinated movements in three-dimensional space. The clinical version of the VLT consists of 19 items divided into 5 areas of interest: arm ability to transfer the body, arm positioning and stabilizing, hand opening and closing, grasping and releasing, and manipulating. In particular, we chose the second area of interest, namely the stabilization, which is composed of a set of five poses (see Figure 2A) that assess the ability to freely stabilize the arms in space against gravity during five seconds for each pose. Every subject performed a session composed of six repetitions for each pose for a total of 30 movements. The poses were characterized by an increasing level of difficulty, from pose 1 to pose 5.

In the first pose, the arms were positioned horizontally in the lateral direction, and the elbows were completely extended while the thumbs pointed posteriorly. The second pose consisted of setting the elbow to point upward with hands that touched the neck and vertical forearms near the head. Pose 3 instead required to extend the arms over the head fully; they could be positioned slightly apart and not necessarily exactly vertically with the elbow fully extended. In the fourth pose, the arms were set horizontally in the lateral direction, with elbows flexed of 90 degrees in outward rotation. Finally, in pose 5, the arms were stabilized horizontally in the lateral direction with elbows fully extended, and the thumbs point downward. In this study, we excluded pose five from the task sequence because none of the subjects could perform this pose due to the level of their injury. For each pose, we could distinguish *an execution phase*, consisting in the time elapsing from the instant the subject left the starting position to the reach of the desired pose, and a *holding phase*, consisting in the 5 seconds during which the subject has to maintain the pose.

Kinematic recordings

During the execution of the stabilization task, the kinematics for the upper body was acquired. We used a motion capture system (SMART DX, BTS Bioengineering, Italy) with 8 infrared cameras and 2 video cameras (Vixta). The global reference of the system was located with the X-axis along the sagittal plane of the subject, the Y-axis along the vertical direction and the Z-axis along the frontal plane. To reduce the variability of the marker placement among sessions, the same person was in charge of placing markers. We located 13 markers (15 mm diameter) on anatomical landmarks ac-cording to the Davis protocol (Davis, 1988): head, 7th cervical vertebra, right scapula, left scapula, sternum, right acromion, left acromion, right elbow, left elbow, right wrist, left wrist, right

metacarpus, left metacarpus. The kinematic data were recorded at a sampling frequency of 100 Hz.

Visual analysis

A physical therapist evaluated the performance in the VLT by assigning a score to each pose's repetition by visual inspection of the recorded task. Then, for every pose, the scores obtained in each repetition were summed and normalized by the maximum value that could have been reached so as to have a range of values from 0 to 1.

Kinematic analysis

Movements were sampled at 100 Hz and smoothed by a 4th order Savitzky-Golay filter (cutoff: ~15 Hz), which was also used to estimate the subsequent time derivatives of the trajectory. For each pose, movement onset was defined as the first time instant when the speed of the marker placed on the wrist exceeded 10% of the peak speed in that phase. The movement end was defined as the last time sample the speed reached the minimum value. This allowed the inclusion of possible movement adjustments. Indicating as C, W, E, and A the locations of the markers placed respectively on C7, wrist, elbow, and acromion (Figure 2B) we also extracted the following parameters for right and left body side:

- Elbow Angle (EA). The angle $\widehat{(WEA)}$ formed by the segments WE and EA;
- Shoulder Angle on Frontal plane (SAF). The angle $\widehat{(CAE)}$ formed by the segments CA and AE projected on the frontal plane;
- Shoulder Angle on Sagittal/Transverse plane (SAST). The angle $\widehat{(CAE)}$ projected on the sagittal plane (for pose 2 and pose 3) or on the transverse plane (for pose 1 and pose 4);

It should be noted that this kinematic analysis is not complete in a geometrical and physiological sense as it does not consider for example rotations of the forearm along the elbow-wrist axis. *Kinematic Symmetry* (K_{sym}). This metric evaluates if the subject used left and right body side in a symmetric way while holding the different poses. It was computed by averaging together the symmetry indicator extracted from the three previously defined parameters:

$$\boldsymbol{K_{sym}} = \frac{\boldsymbol{EA_{sym}+SAF_{sym}+SAST_{sym}}}{\boldsymbol{3}} \tag{11}$$

where each kinematic measure of symmetry (EA_{sym}, SAF_{sym} and $SAST_{sym}$) is defined as the ratio of the indicator computed from data of the right side of the body to the indicator computed from data on the left.

Statistical analysis

The small sample size of our population did not allow for appropriate full statistical analysis of the data to assess the significance of the changes in the performance metrics during the BoMI training and during the instrumented evaluation. However, consistencies were tested using a Wilcoxon signed-rank test with 5 matched pairs (Wilcoxon, 1946; Chen et al., 2005) (Matlab function signrank). We acknowledge that because the small sample size the significance is debatable, but we still report the p-values in order to give an idea of the common trend, if any, of the population. The level of significance has been set as follows for the signed-rank test: p***=0.03 if all five differences were in the same directions, p**=0.06 if 4 out of 5 differences were in the same direction with the non-conforming difference being the smallest in magnitude, p*=0.09 if 4 out of 5 differences were in the same direction, with the non-conforming difference between the second smallest in magnitude.

A Wilcoxon signed-rank test was run on the learning metrics, regarding the Reaching task: we compared the session 1 of *reaching 1* with the last of *reaching 2*. We ran the Wilcoxon signed-rank test on the metrics describing the reorganization of body movement, symmetry (c_{sym} and b_{sym}) and body parts recruitment (c_{distal} and b_{distal}) on session 4 and session 15.

We also compared the MMT and ROM results obtained during T0 and T1 to check for changes due to the BoMI treatment and the ones obtained during T1 and T2 to evaluate if eventual positive changes were still maintained after 3 months.

For the analysis of the instrumented evaluation (*stabilization task*), for each parameter, we obtained a single indicator as the average of the four poses and we compared the performance of the 5 subjects pre and post treatment (T0 and T1) to check for changes due to BoMI training and we compared post-treatment and follow-up (T1 and T2) to verify if the performance were maintained after three months. For the kinematic parameters (*EA*, *SAF* and *SAST*), we removed the "normality" baseline (control group performance) from the cSCI population before running statistical tests.

7.2. *Results*

SCI subjects learned to use the interface

All cSCI subjects practiced for a long time and quickly learned to proficiently operate the interface also in this experiment, where the sensors were placed on more distal parts than in previous studies (Abdollahi et al., 2017; Pierella et al., 2017a), Figure 3. During the familiarization phase (block 1), they improved the cursor control skills in reaching tasks, becoming faster, and making straighter and smoother trajectories (Figure 3 A-C).

As expected, after modifying the BoMI map so to encourage the use of more distal segments and a similar involvement of right and left sides (beginning of blocks 2-4), the performance worsened. When the BoMI induced the subjects to generate more forearm movements, the cursor became more jittery as showed by the increase of our jerk index (the number of peaks in the velocity profile, Figure 3 C). However, at the end of training (end of block 4), the reaching metrics were comparable to the metrics at the end of the familiarization phase (end of block 1). Globally, all subjects improved their performance from beginning to end of the BoMI training in terms of the linearity index ($p=0.0312$), the movement time ($p=0.0312$), and the number of peaks ($p=0.0312$). Instead, in both pong games, three subjects increased the hits rate from the beginning to the end of the training, while one maintained constant performance and one showed a slight decrease ($p=0.2188$, vertical pong, $p=0.312$ horizontal pong).

Increased recruitment of distal regions of the arms

The training mostly focused on increasing the use of more distal parts and the symmetry of the right and left sides. The data presented in Figure 4 show that training

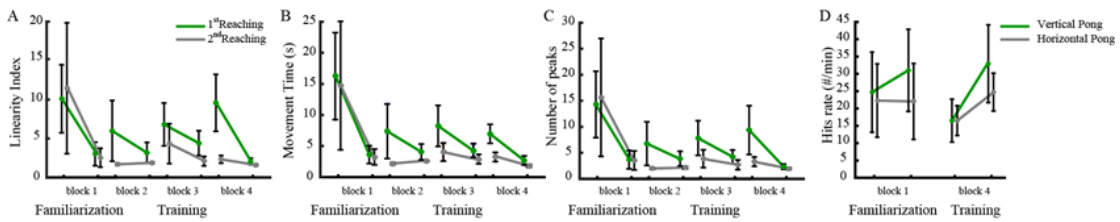

Figure 3: Performance metrics. Reaching tasks: linearity index **(A)**, movement time **(B)** and number of peaks in the velocity profile **(C)**. First and last sessions of the familiarization phase, first and last sessions after the 1st, 2nd and 3rd map modification of the training phase. Pong hits rate during vertical and horizontal pong **(D)**. For the Pong tasks we are reporting only values at the beginning (respectively session 3 for vertical pong and session 4 for the horizontal pong) and end of the familiarization and at the beginning and end of the last change of the interface. We reported the mean values and standard error of the subjects.

indeed influenced the recruitment of the upper limbs' distal parts. The subjects at the end of the *familiarization* contributed to the cursor control with high symmetry (above 80%, with 100% indicating perfect symmetry), but with different use of the upper arms and forearms (Figure 4 A), the same trend when looking at the total mobility of the upper body (Figure 4 B). In this case the goal was to encourage the use of the forearms and this objective was reached at the end of the training with the BoMI.

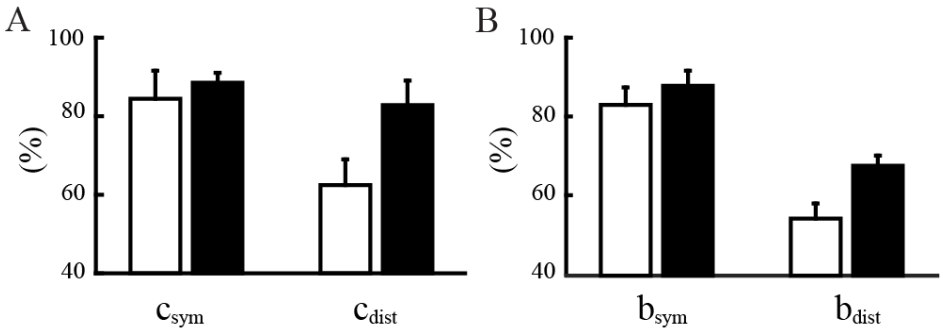

Figure 4: Symmetry and distality indices for body contribution to cursor movement **(A)** and for body mobility **(B)** at the end of the familiarization phase (white bars) and end of training (black bars). The indices are calculated for representing the symmetry between right and left upper body ($\boldsymbol{c_{sym}}$ and $\boldsymbol{b_{sym}}$) and for representing the usage of more distal body parts ($\boldsymbol{c_{dist}}$ and $\boldsymbol{b_{dist}}$).

All the subjects increased, in general, their mobility still maintaining symmetrical body recruitment, in fact c_{sym} and b_{sym} did not show differences at the end of the training with respect to the end of familiarization (respectively p=0.4062 and p=0.1562). Noticeably, when we compared the usage of the body parts that they had more difficulty controlling, in this case the forearms, all the users increased the percentage of the forearm recruitment contributing to cursor control (c_{dist}) at the end of the training, going from 61.63±7.38% on session 4 to 82.77±6.28% on the last session (p= 0.0312). Similarly, when looking at the mobility of the forearm, b_{dist}went from 54.46±3.29% to 61.94±2.99% (p= 0.0312). Note that values above the 50% indicate, as explained in the methods, a contribution of the distal (elbow) movements decupled from the proximal (shoulder) joint motions.

Improvements in the clinical evaluation tests

The clinical evaluation tests, MMT (Figure 5) and ROM (Figure 6) performed before, after and three months since the end of the training, showed a positive effect of the BoMI in SCI rehabilitation for all subjects. At training completion, all subjects had an increase of muscle strength (p= 0.0312 for the left body parts and p=0.0312 for the right of the entire population). The improvement was maintained at the follow-up (comparing the

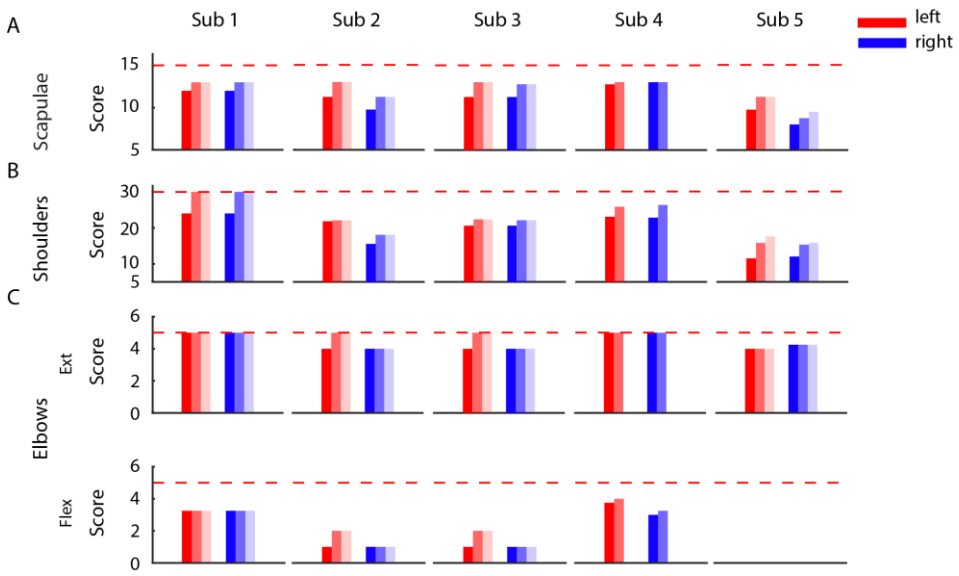

Figure 5: Manual muscle test. Each row presents the results of the MMT for the left (shades of red) and right (shades of blue) body parts of each of the 5 subjects recruited in the study performed before (dark shade), at end (medium shade) and 3 months after the end of the training (light shade). The scores are divided by body districts (rows) and the dashed horizontal red lines correspond to the maximum score that could be assigned to each district.

results for the left side and for the right side at the end of the training with the ones at the T2 we obtained no changes p= 0.5). The same trend was also evident in the outcomes of the ROM. All the subjects exhibited an increase in the range of movements of shoulders, arms and forearms ($p<0.001$); the only measure that did not change was elbow flexion because all subjects had a complete elbow flexion since the beginning.

There was no noticeable change between the end of training and the follow-up for the right side of the body (p=0.2318) while a change was still present for the left side (p=0.0139).

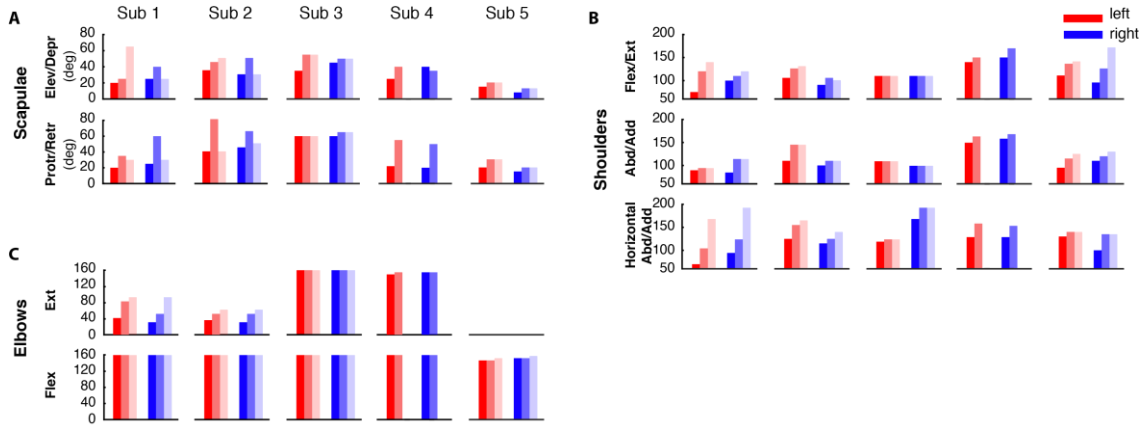

Figure 6. Range of motion. Results of the ROM for each subject before (dark shade), at the end (medium shade) and 3 months after the end of the training (light shade) for the left (shades of red) and right (shades of blue) body parts. The results are presented divided by upper-body districts: scapulae **(A)**, shoulders **(B)** and elbows **(C)**.

Kinematics for the stabilization task

Subjects' kinematic during the arm stabilization task was assessed in two ways: by a visual inspection of the video recordings and subsequent scoring of the performance, and by extracting significant parameters from the markers placed on the upper limbs. Figure 7 reports the mean scores given to all the poses performed by each subject at the different time points (T0, T1 and T2).

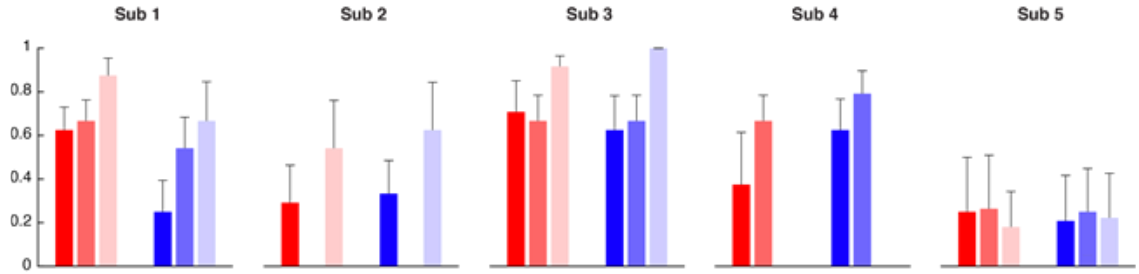

Figure7: Normalized scores assigned to each body side (right in blue and left in red) averaged across the four poses performed by each subject (columns). The evaluation was performed before the BoMI treatment (T0, dark shades), at the end of the BoMI treatment (T1, medium shades) and three months after (T2, light shades).

The entire SCI population showed an improvement in all the poses between T0 and T1, especially for the right side of the upper-limb ($p=0.0312$). Pose 1 was the one that all the subjects were able to perform almost from the beginning, for the other poses, there was a clear trend of improvement from T0 and T1. The improvement was also maintained at T2. Subject 5, being the one with the highest level of lesion and so more impaired, was the subject that obtained the lowest scores being not able to perform the pose 2 and 4 in none of the evaluation sessions and the pose 3 only at T1 and T2.

Figure 8 depicts the trend of all the three kinematic parameters EA, SAF and SAST computed for a representative subject (SCI1), respectively to evaluate distal movements (EA) and proximal movements (SAF and SAST) for both left and right body side. This subject showed a global improvement in EA, while the other two kinematic parameters improved only for pose 2 and 3.

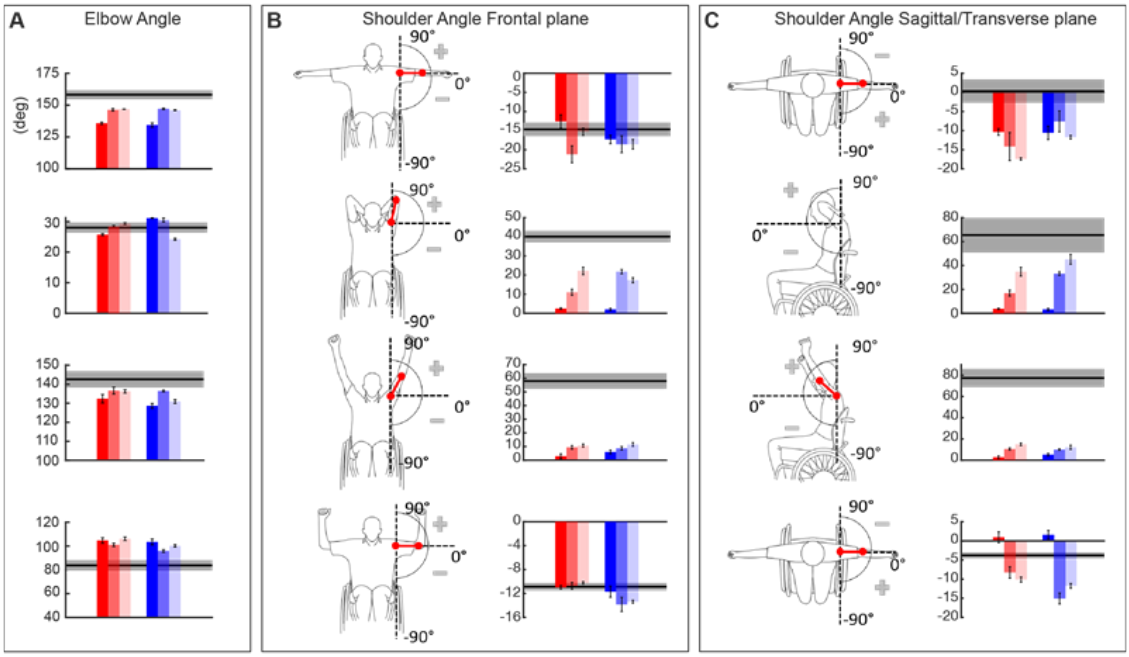

Figure 8: Kinematic parameters of the stabilization task for an example subject, SCI1. In each panel each row indicates the parameters relative to pose 1, pose 2, pose 3 and pose 4. In the shades of red the parameters extracted from the left body parts while in the shades of blue the one from the right body parts at T0 (dark shades), T1 (medium shades) and T2 (light shades). The grey area in each graph represents mean and standard error of each parameter for the control subjects (mean±SE). **(A)** Elbow Angle - EA. **(B)** On the left a schematic description, for each pose, of the computed angle and on the right the results of the Shoulder Angle on the Frontal plane - SAF. **(C)** Schematic description, for each pose, of the computed angle on the left side and Shoulder Angle on the Sagittal/Transverse plane -SAST- graphs on the right.

The kinematic performance of the entire cSCI population is reported in Figure 9 where *EA*, *SAF* and *SAST* metrics are displayed as distance from the control group values. Thus, the metrics close to zero indicated performance similar to the healthy ones, highlighting that subjects were able to correctly achieve the required postures. We found that after treatment (T0-T1), for all the poses, four out of five SCI subjects reported an improvement for the *EA* metrics (p** = 0.06 for both left and right body parts), and this improvement was maintained in the follow-up evaluation (T1-T2: p=0.875 for the right side and p=1 for the left side). This result supports the findings previously described after the BoMI training, and it is an additional proof that improving distal body parts movements with the BoMI training was actually achieved. Conversely, the two kinematic parameters related to the proximal movements, *SAF* and *SAST*, did not reveal an overall improvement for the cSCI subjects in both T0-T1 comparison (*SAF*: p=0.43 for right body parts, p=0.56 for left body parts; *SAST*: p=0.3125 for right, p=0.1857 for left) and T1-T2 comparison (*SAF* metrics: p=0.12 for both sides; *SAST*: p=0.75 for right side, p=1 for left side). As for the

Kinematic Symmetry (K_{sym}), this parameter (Figure 9) improved between T0 and T1 for all the poses for 4 subjects out of 5 (p**=0.0625). No differences were evidenced between T1 and T2 (p=1). Therefore, the performance achieved at the end of the training were maintained at follow-up.

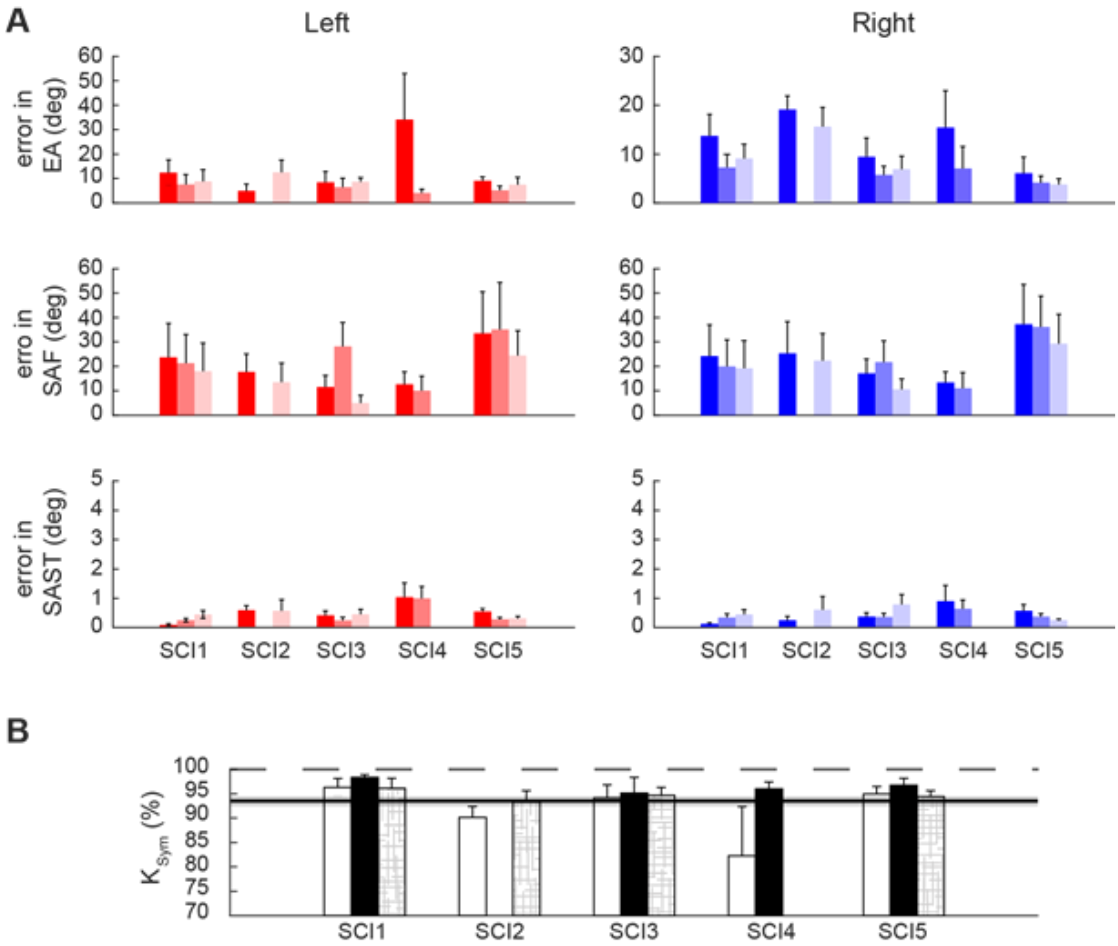

Figure 9: **(A)** Kinematic parameters of the stabilization task for the cSCI population normalized with respect to the control population. Elbow Angle, (EA, first row), Shoulder Angle on Frontal plane (SAF, second row) and on Sagittal/Transverse plane (SAST, third row) were averaged across poses for each subject, mean and standard error are reported in the figure. Shades of red represent the parameters extracted from the left body parts while in the shades of blue the ones from the right body parts at T0 (dark shades), T1 (medium shades) and T2 (light shades). **(B)** Overall kinematic symmetry parameter, K_{sym}, computed for each cSCI subject at T0 (white bars), T1 (black bars) and T2 (patterned bars).

7.3. *Discussions and conclusions*

The BoMI presented in this study is a rehabilitative tool tested in the clinical environment that provides therapists with a simple technology with a high potential to help the training and recovery of upper limb movements of acute cervical SCI subjects. In this

study, we described and quantified the efficacy of its use for distal movement skills recovery. Concurrently, we described the effects of the BoMI training not only based on clinical scales but also on an instrumented test that engaged the subjects in bilateral arms movements towards poses of increasing difficulties. In previous studies, a similar BoMI was tested, but these either focused on proving the BoMI as an assistive tool for operating a computer or a virtual and powered wheelchair (Thorp et al., 2016; Abdollahi et al., 2017) or they demonstrated the capability of the BoMI to operate both as an assistive and as a rehabilitative tool, always working with chronic cSCI subjects and with sensors placed on proximal regions, i.e., shoulders and upper arms (Pierella et al., 2015, 2017a). Here, we analyzed data of 5 cSCI subjects, in their acute phase with the only exception of SCI 3 that went through a period of training with the BoMI as part of their inpatient rehabilitation routine. Sensors were also moved in distal positions, being all of the cSCI subjects able to exert some kind of control on their forearms and not only on their arms. Despite these differences with previous works, all sub-jects while playing reaching and pong games had a final behavior and performance comparable to the one of the study where the sensors were involving upper arms (Pierella et al., 2017a), no longer only shoulder movements like in (Abdollahi et al., 2017). Specifically, in studies where the control involved more distal movements, either shoulders and arms or arms and forearms movements, the initial performance was worse than when the control involved only shoulder movements. However, de-spite this sensors' location, after a short period of four sessions, all the subjects became proficient in the control, with movement time and smoothness performance similar to those observed in previous studies, including the works based on shoulder movements.

From the BoMI data, we also extracted indicators regarding body movements and body contributions to cursor control, that allowed the PTs to modify the interface to reach the individual rehabilitation objectives included in the recovery plan of each cSCI subject. All of them at the end of the familiarization phase were using the BoMI with similar recruitment of right and left upper body, therefore for everyone, the main rehabilitative goal was to increment the movements of the forearms over the arms. Indeed, using the forearms for a cervical SCI subject is more challenging due to a reduced innervation of peripheral muscles because of the lesion location on the cervical tract of the spinal cord (Snoek, G. J., IJzerman, M. J., Hermens, H. J., Maxwell, D., & Biering-Sorensen, 2004; Spooren, A. I., Janssen-Potten, Y. J., Snoek, G. J., Ijzerman, M. J., Kerckhofs, E., & Seelen, 2008). The BoMI parameters' modifications succeeded in pushing the subjects to

increase forearm movements, still maintaining a symmetrical body use. This was also confirmed by the results obtained from the instrumented evaluation. All the standard clinical tests, MMT and ROM, for all the cSCI subjects improved between pre and post assessments (T0 vs T1). Also, the results of the stabilization task had the same trend both looking at the score provided by expert clinicians and at the kinematic data of the instrumented VLT. With training, all cSCI subjects improved and got closer to the posture assumed by the control subjects. The kinematic parameters that had the greatest improvement were the elbow angles, i.e., the main target of our new BoMI-based training. This finding confirms that this rehabilitation training aimed mainly to improve distal body parts' functionality, fundamental for several daily life tasks, lasted also at follow-up. The choice of use and instrument the VLT test, a test that has been proven to be valid, reliable and responsive (Post et al., 2006; Spooren et al., 2013), was motivated by the need of having a test that consisted of a bilateral task as support of the standard clinical tests, where each district is evaluated singularly. Moreover, we wanted to extract kinematic indicators that could help doctors and PTs to objectify progress during and after a rehabilitative program in a clinically meaningful way and to use these indicators together with standard MMT and ROM, which often lacks objectivity, to answer questions like: is this level of functioning a satisfying result in this phase of treatment? Is the current level of functioning the best that can be reached by the subject?

Our works' limitations mainly regard the sample size of cSCI subjects and the lack of a control cSCI group. It is worth noting that since the cSCI subjects, except SCI 3, were in the acute phase, the improvements might be at least partially due to the spontaneous recovery happening during this early stage of the injury. A control cSCI group would have allowed us to decouple the effects of spontaneous recovery, traditional rehabilitation training and BoMI-based treatment. However, the enhanced improvement in the kinematic parameters targeted by the BoMI suggests a positive synergy between these factors, to further investigate in a future study. An additional limit of this study is in the low number of cSCI subjects recruited. Cervical SCI is a relatively rare condition. Further studies including larger cohorts of participants will be necessary to draw more robust general conclusions. Finally, two subjects missed one of the three evaluation sessions. This was due to a personal impediment to participate in that particular session that the experimenter could not anticipate. This is not an uncommon occurrence in SCI subjects, who may experience sudden and unexpected medical problems or complications in the acute phase.

Conclusion: This study validated the feasibility of using BoMI as a complementary tool for SCI rehabilitation in the clinical environment. The functional evaluation protocol proposed and tested resulted easy to apply and well tolerated by people with cervical SCI. This protocol and selected indicators augmented the standard clinical evaluations and permitted to quantify with mode details the improvement brought by the BoMI training, combined with the standard rehabilitation treatment.

7.4. *References*

Abdollahi, F., Farshchiansadegh, A., Pierella, C., Seáñez-González, I., Thorp, E., Lee, M.-H., et al. (2017). Body-Machine Interface Enables People With Cervical Spinal Cord Injury to Control Devices With Available Body Movements: Proof of Concept. Neurorehabil. Neural Repair 31, 487–493. doi:10.1177/1545968317693111.

Aspelund, S., Patel, P., Lee, M.-H., Kagerer, F. A., Ranganathan, R., and Mukherjee, R. (2020). Controlling a robotic arm for functional tasks using a wireless head-joystick: A case study of a child with congenital absence of upper and lower limbs. PLoS One 15, e0226052. doi:10.1371/journal.pone.0226052.

Barea, R., Boquete, L., Mazo, M., and López, E. (2002). System for assisted mobility using eye movements based on electrooculography. IEEE Trans. neural Syst. Rehabil. Eng. 10, 209–218.

Bernstein, N. (1967). The coordination and regulation of movement. Oxford, New York: Pergamon Press.

Casadio, M., Pressman, A., Acosta, S., Danzinger, Z., Fishbach, A., Mussa-Ivaldi, F. A., et al. (2011). Body machine interface: Remapping motor skills after spinal cord injury. in 2011 IEEE International Conference on Rehabilitation Robotics (IEEE), 1–6.

Casadio, M., Pressman, A., Fishbach, A., Danziger, Z., Acosta, S., Chen, D., et al. (2010). Functional reorganization of upper-body movement after spinal cord injury. Exp. Brain Res. 207, 233–247.

Chen, G., Patten, C., Kothari, D. H., and Zajac, F. E. (2005). Gait differences between individuals with post-stroke hemiparesis and non-disabled controls at matched speeds. Gait Posture 22, 51–56. doi:10.1016/j.gaitpost.2004.06.009.

Craig, D. A., and Nguyen, H. T. (2006). Wireless real-time head movement system using a personal digital assistant (PDA) for control of a power wheelchair. in Engineering in Medicine and Biology Society, 2005. IEEE-EMBS 2005. 27th Annual International Conference of the (IEEE), 772–775.

Curt, A., Van Hedel, H. J. A., Klaus, D., and Dietz, V. (2008). Recovery from a spinal cord injury: Significance of compensation, neural plasticity, and repair. J. Neurotrauma 25, 677–685. doi:10.1089/neu.2007.0468.

Davis, R. B. (1988). Clinical gait analysis. IEEE Eng. Med. Biol. Mag. 7, 35–40.

Dietz, V., and Fouad, K. (2014). Restoration of sensorimotor functions after spinal cord injury. Brain 137, 654–667. doi:10.1093/brain/awt262.

Dunkelberger, N., Schearer, E. M., and O'Malley, M. K. (2020). A review of methods for achieving upper limb movement following spinal cord injury through hybrid muscle stimulation and robotic assistance. Exp. Neurol. 328, 113274. doi:10.1016/j.expneurol.2020.113274.

Farshchiansadegh, A., Abdollahi, F., Chen, D., Lee, M.-H., Pedersen, J., Pierella, C., et al. (2014). A body machine interface based on inertial sensors. in 2014 36th Annual International Conference of the IEEE Engineering in Medicine and Biology Society, EMBC 2014 doi:10.1109/EMBC.2014.6945026.

Field-Fote, E. C. (2000). Spinal cord control of movement: implications for locomotor rehabilitation following spinal cord injury. Phys Ther 80, 477–484.

Hislop, H., Avers, D., and Brown, M. (2007). Daniels and Worthingham's Muscle Testing: Techniques of Manual Examination and Performance Testing. 8th ed. Saunders.

Huo, X., Wang, J., and Ghovanloo, M. (2008). Introduction and preliminary evaluation of the Tongue Drive System: Wireless tongue-operated assistive technology for people with little or no upper-limb function. J. Rehabil. Res. Dev. 45, 921–930. doi:10.1682/JRRD.2007.06.0096.

Jazayeri, S. B., Beygi, S., Shokraneh, F., Hagen, E. M., and Rahimi-Movaghar, V. (2015). Incidence of traumatic spinal cord injury worldwide: a systematic review. Eur. spine J. 24, 905–918.

Kamper, D. G. (2016). "Restoration of hand function in stroke and spinal cord injury," in Neurorehabilitation technology (Springer), 311–331.

Kim, J., Park, H., Bruce, J., Sutton, E., Rowles, D., Pucci, D., et al. (2013). The tongue enables computer and wheelchair control for people with spinal cord injury. Sci Transl Med 5, 213ra166. doi:10.1126/scitranslmed.3006296.

Krebs, H. I., Aisen, M. L., Volpe, B. T., and Hogan, N. (1999). Quantization of continuous arm movements in humans with brain injury. Proc. Natl. Acad. Sci. U. S. A. 96, 4645–4649. doi:10.1073/pnas.96.8.4645.

Lieshout, G. V (2003). User manual Van Lieshout Test. Hoensbroek iRv.

Lim, P. A., and Tow, A. M. (2007). Recovery and regeneration after spinal cord injury: a review and summary of recent literature. Ann Acad Med Singapore 36, 49–57.

Lynch, J., and Cahalan, R. (2017). The impact of spinal cord injury on the quality of life of primary family caregivers: a literature review. Spinal Cord 55, 964–978.

Mekki, M., Delgado, A. D., Fry, A., Putrino, D., and Huang, V. (2018). Robotic Rehabilitation and Spinal Cord Injury: a Narrative Review. Neurotherapeutics 15, 604–617. doi:10.1007/s13311-018-0642-3.

Miehlbradt, J., Cherpillod, A., Mintchev, S., Coscia, M., Artoni, F., Floreano, D., et al. (2018). Data-driven body–machine interface for the accurate control of drones. Proc. Natl. Acad. Sci. Available at: http://www.pnas.org/content/early/2018/07/10/1718648115.abstract.

Murray, S., and Goldfarb, M. (2012). Towards the use of a lower limb exoskeleton for locomotion assistance in individuals with neuromuscular locomotor deficits. Conf Proc IEEE Eng Med Biol Soc 2012, 1912–1915. doi:10.1109/EMBC.2012.6346327.

Philips, G. R., Catellier, A. A., Barrett, S. F., and Wright, C. H. (2007). Electrooculogram wheelchair control. Biomed. Sci. Instrum. 43, 164–169.

Pierella, C., Abdollahi, F., Farshchiansadegh, A., Pedersen, J., Chen, D., Mussa-Ivaldi, F. A., et al. (2014). Body machine interfaces for neuromotor rehabilitation: a case study. Conf. Proc. Annu. Int. Conf. IEEE Eng. Med. Biol. Soc. IEEE Eng. Med. Biol. Soc. Annu. Conf. 2014. doi:10.1109/EMBC.2014.6943612.

Pierella, C., Abdollahi, F., Farshchiansadegh, A., Pedersen, J., Thorp, E. B., Mussa-Ivaldi, F. A., et al. (2015). Remapping residual coordination for controlling assistive devices and recovering motor functions. Neuropsychologia 79, 364–376. doi:10.1016/j.neuropsychologia.2015.08.024.

Pierella, C., Abdollahi, F., Thorp, E., Farshchiansadegh, A., Pedersen, J., Seáñez-González, I., et al. (2017a). Learning new movements after paralysis: Results from a home-based study. Sci. Rep. 7, 4779. doi:10.1038/s41598-017-04930-z.

Pierella, C., De Luca, A., Tasso, E., Cervetto, F., Gamba, S., Losio, L., et al. (2017b). Changes in neuromuscular activity during motor training with a body-machine interface after spinal cord injury. in IEEE International Conference on Rehabilitation Robotics doi:10.1109/ICORR.2017.8009396.

Post, M. W. M., Van Lieshout, G., Seelen, H. A. M., Snoek, G. J., Ijzerman, M. J., Pons, C., et al. (2004). Rehabilitation outcome of upper extremity skilled performance in persons with cervical spinal cord injuries. Spinal Cord 24(1), 294–301. doi:10.2340/16501977-0231.

Post, M. W. M., Van Lieshout, G., Seelen, H. A. M., Snoek, G. J., Ijzerman, M. J., and Pons, C. (2006). Measurement properties of the short version of the Van Lieshout test for arm/hand function of persons with tetraplegia after spinal cord injury. Spinal Cord 44, 763–771. doi:10.1038/sj.sc.3101937.

Ranganathan, R., Lee, M. H., Padmanabhan, M. R., Aspelund, S., Kagerer, F. A., and Mukherjee, R. (2019). Age-dependent differences in learning to control a robot arm using a body-machine interface. Sci. Rep. 9, 1–9. doi:10.1038/s41598-018-38092-3.

Rizzoglio, F., Pierella, C., De Santis, D., Mussa-Ivaldi, F., and Casadio, M. (2020). A hybrid Body-Machine Interface integrating signals from muscles and motions. J. Neural Eng. 17, 046004. doi:10.1088/1741-2552/ab9b6c.

Roberts, T. T., Leonard, G. R., and Cepela, D. J. (1999). IN BRIEF Classifications In Brief: American Spinal Injury Association (ASIA) Impairment Scale. Clin. Orthop. Relat. Res. 475. doi:10.1007/s11999-016-5133-4.

Seáñez-González, I., Pierella, C., Farshchiansadegh, A., Thorp, E. B., Wang, X., Parrish, T., et al. (2016). Body-machine interfaces after spinal cord injury: Rehabilitation and brain plasticity. Brain Sci. 6. doi:10.3390/brainsci6040061.

Snoek, G. J., IJzerman, M. J., Hermens, H. J., Maxwell, D., & Biering-Sorensen, F. (2004). Survey of the needs of patients with spinal cord injury: impact and priority for improvement in hand function in tetraplegics. Spinal Cord 42(9), 526–532. Available at: https://www.nature.com/articles/3101638 [Accessed August 6, 2020].

Spooren, A. I., Janssen-Potten, Y. J., Snoek, G. J., Ijzerman, M. J., Kerckhofs, E., & Seelen, H. A. (2008). Rehabilitation outcome of upper extremity skilled performance in persons with cervical spinal cord injuries. J. Rehabil. Med. 40(8), 637–644. doi:10.2340/16501977-0231.

Spooren, A. I. F., Arnould, C., Smeets, R. J. E. M., Bongers, H. M. H., and Seelen, H. A. M. (2013). Improvement of the Van Lieshout hand function test for Tetraplegia using a Rasch analysis. Spinal Cord 51, 739–744. doi:10.1038/sc.2013.54.

Thorp, E. B., Abdollahi, F., Chen, D., Farshchiansadegh, A., Lee, M.-H., Pedersen, J. P., et al. (2016). Upper Body-Based Power Wheelchair Control Interface for Individuals with Tetraplegia. IEEE Trans. Neural Syst. Rehabil. Eng. 24. doi:10.1109/TNSRE.2015.2439240.

Wilcoxon, F. (1946). Individual comparisons of grouped data by ranking methods. J. Econ. Entomol. 39, 269. doi:10.2307/3001968.